An Analytical Study on the Behavior of Reinforced Concrete Interior Beam-Column Joints

Chenxi Xing

Dissertation submitted to the faculty of the Virginia Polytechnic Institute and State University in partial fulfillment of the requirements for the degree of

Doctor of Philosophy
In
Civil Engineering

Roberto T. Leon, Chair

Ioannis Koutromanos, Co-Chair

Carin L. Roberts-Wollmann

Matthew R. Eatherton

May 10, 2019
Blacksburg, Virginia

Keywords: Interior Beam-Column Joint, Reinforced Concrete Structures, Nonlinear Finite Element Analysis, Bond-slip Behavior, Nonlinear Truss Model, ACI352

An Analytical Study on the Behavior of Reinforced Concrete Interior Beam-Column Joints

Chenxi Xing

ABSTRACT

Reinforced concrete (RC) moment frame structures make up a notable proportion of buildings in earthquake-prone regions in the United States and throughout the world. The beam-column (BC) joints are the most crucial regions in a RC moment frame structure as any deterioration of strength and/or stiffness in these areas can lead to global collapse of the structure. Thus, accurate simulations of the joint behavior are important for assessment of the local and global performance of both one-way and two-way interior BC joints. Such simulations can be used to study the flexural-shear-bond interaction, the failure modes, and sensitivity of various parameters on the performance of BC joints. Most of the existing analytical approaches for interior BC joints have either failed to account for the cyclic bond-slip behavior and the triaxial compressive state of confined concrete in the joint correctly or require so many calibrations on parameters as to render them impractical. The core motivation for this study is the need to develop robust models to test current design recommendations for 3D beam-column-slab subassemblies subjected to large drifts.

The present study aims to first evaluate the flexural-shear-bond interaction behavior of two-way beam-column-slab interior connections by both finite element and nonlinear truss methodologies. The local performance such as bond-slip and strain history of reinforcing bar are compared with the experimental results. The reliability of applied finite element approach is evaluated against a series of one-way interior BC joints and a two-way interior beam-column-slab joint. The accuracy and efficiency of the nonlinear truss methodology is also evaluated by comparisons to the same series of joints. Results show good agreement for the finite element method against both global and local response, including hysteretic curve, local bond-slip development and beam longitudinal bar stress/strain distributions. The nonlinear truss model is also capable in obtaining satisfactory global response, especially in capturing large shear cracks.

A parametric study is conducted on a prototype two-way interior beam-column-slab joint described in an example to ACI 352R-02. The objective is to investigate several issues

in the design of interior BC connections, such as the joint shear force subjected to bidirectional cyclic loading, the development of bond-slip behavior, and the failure modes of two-way interior joints with slab, for which non consensus exists in the design literature. Results from connections with different levels of joint shear force subjected to unidirectional loading show that meeting the requirements from ACI 352 is essential to maintain the force transfer mechanism and the integrity of the joint. The connections achieved satisfactory performance under unidirectional loading, while the bidirectional monotonic loading decreases the joint shear force calculated by ACI 352 by 10%~26% based on current results. Poorer performance is obtained for wider beams and connections fail by shear in the joint rather than bond-slip behavior when subjected to bidirectional cyclic loading. In general, the study indicates that the ACI352-02 design methodology generally results in satisfactory performance when applied to one-way joints (planar) joints. Less satisfactory performance was found for cases of two-way joints with slabs.

An Analytical Study on the Behavior of Reinforced Concrete Interior Beam-Column Joints

Chenxi Xing

GENERAL AUDIENCE ABSTRACT

Reinforced concrete (RC) moment frames are one of the most popular structure types because of their economical construction and adaptable spaces. Moment frames consist of grid-like assemblages of vertical columns and horizontal beams joined by cruciform connections commonly labelled as beam-column joints. Because of the regularity of the grid and the ability to have long column spacing, moment frames are easy to form and cast and result in wide open bays that can be adapted and readapted to many uses.

In RC structures, steel bars embedded in the concrete are used to take tensile forces, as concrete is relatively weak when loaded in tension. Forces are transferred between the steel and concrete components by so-called “bond” forces at the perimeter of the bars. The proper modeling of the behavior of bond forces inside the beam-column joints of reinforced concrete moment frames is the primary objective of this dissertation.

Reinforced concrete moment frames constitute a notable proportion of the existing buildings in earthquake-prone regions in the United States and throughout the world. The beam-column joints are the most crucial elements in a RC moment frame structure as any deterioration of strength and/or stiffness in these areas can lead to global collapse of the structure.

Physical experimentation is the most reliable means of studying the performance of beam-column joints. However, experimental tests are expensive and time-consuming. This is why computational simulation must always be used as a supplemental tool. Accurate simulations of the behavior of beam-column joints is important for assessment of the local and global behavior of beam-column joints. However, most of the existing analytical approaches for interior beam-column joints have either failed to account for the bond-slip behavior and the triaxial compressive state of confined concrete in the joint correctly or require so many calibration parameters as to render them impractical.

The present study aims to provide reliable numerical methods for evaluating the behavior of two-way beam-column-slab interior joints. Two methods are developed. The

first method is a complex finite element model in which the beam-column joint is subdivided into many small 3D parts with the geometrical and material characteristics of each part carefully defined. Since the number of parts may be in the hundreds of thousands and the geometry and material behavior highly non-linear, setting up the problem and its solution of this problem requires large effort on the part of the structural engineer and long computation times in supercomputers. Finite element models of this type are generally accurate and are used to calibrate simpler models.

The second method developed herein is a nonlinear truss analogy model. In this case the structure is modelled as nonlinear truss elements, or elements carrying only axial forces. When properly calibrated, this method can produce excellent results especially in capturing large shear cracks.

To evaluate the accuracy and to quantify the current seismic design procedure for beam-column joints, a prototype two-way interior beam-column-slab joint described in an example to ACI 352R-02, the current design guide used for these elements in the USA, is analytically studied by the finite element methodology. The study indicates that the ACI352-02 design methodology generally results in satisfactory performance when applied to one-way (planar) joints under monotonic and cyclic loads. Less satisfactory performance was found for cases of three-dimensional (3D) joints with slabs.

To My Family

Acknowledgements

The research presented in this dissertation was conducted under the supervision of Professors Roberto T. Leon and Ioannis Koutromanos at Virginia Polytechnic Institute and State University. I would like to acknowledge the Civil and Environmental Engineering department of Virginia Tech for supporting my research through graduate assistantship. I also wish to express my gratitude to Chinese Scholarship Council for partially supported my graduate studies at Virginia Tech.

I would like to thank the members of my committee, Professors Matthew R. Eatherton and Carin L. Roberts-Wollmann for providing precious feedbacks for the content of my dissertation and teaching me courses that are valuable for my research.

I wish to thank the support of the Advanced Research Computing (ARC) division of Virginia Tech and Dr. James McClure in conducting the simulations in the cluster Blueridge.

I am deeply grateful to Dr. Mohammadreza Moharrami Gargari and Jeremy T. Bowers from Simpson Gumpertz & Heger for sharing their invaluable experiences in establishing finite element and nonlinear truss models.

Special thanks are due to my friends and colleges from CEE department of VT, for spending memorable everyday together and enrich my life in Blacksburg.

I am most grateful to my mentor, Professor Roberto T. Leon, for his guidance, support and patience throughout all these years. He is as knowledgeable as a walking library which always reminds me that there is no boundary for learning. His accurate-to-hour everyday schedule teaches me professionalism, responsibility and meticulousness. His tolerance, understanding and gentleness show me great wisdom in life. As a famous Chinese proverb puts: An advisor for a day is a father for a lifetime. I am mostly grateful for having an opportunity to work with a scholar with his expertise and high moral standards.

I am also deeply grateful to my supervisor, Professor Ioannis Koutromanos, a sincere and forthright scholar with dreams in career, and an academic guide who devotes himself to lofty ideals in teaching and research. He doesn't have time for everyday lunch, but have a whole afternoon debugging codes with a student line by line. He has hundreds of answers and ideas in his mind but never tells you straightforwardly and enables you to enjoy the happiness after finding it out by yourself. He may expect you to achieve high requirements as what he does to himself, but also revise your writings word by word like to his own paper. I am deeply grateful to him giving me the chance to work with him.

Finally, I wish to thank my parents and my husband for their support throughout the duration of my graduate studies in Blacksburg, also my loveliest kids Caroline and Bryan for being the best gifts ever in my life! It is to them that I delicate this dissertation.

Table of Contents

List of Figures

List of Tables

List of Abbreviations

2D	:	Two-Dimensional
3D	:	Three-Dimensional
ACI 352	:	ACI 352R-02 Recommendations for Design of Beam-Column Connections in Monolithic Reinforced Concrete Structures
ACI	:	American Concrete Institution
ASCE	:	American Society of Civil Engineers
BCJ	:	Beam-to-Column Joints
BCJ2	:	Beam-Column Joint No.2 tested by Leon 1989
BCJ3	:	Beam-Column Joint No.3 tested by Leon 1989
BCJ4	:	Beam-Column Joint No.4 tested by Leon 1989
DMRFs	:	Ductile Moment-Resisting Frames
DCH	:	Ductility Class High
MCFT	:	Modified compression field theory
RC	:	Reinforced Concrete
URI	:	Uniform reduced integration
J2	:	Beam-Column Joint No.2 tested by Kurose et al. 1988
EW	:	East-West
NS	:	North-South
MYS	:	Modified Yield Surface

List of Symbols

Chapter 1

d_b	:	Nominal diameter of bar
u_b	:	The average bond stress
T_i	:	Tensile force at section i
ΔT	:	The change in bar tensile force
ΔL	:	Length of bar over which bond stress is computed

Chapter 2

A_c	:	Area of column core measured from outside edge to outside edge of either spiral or hoop reinforcement
A_g	:	Gross area of column section
A_s	:	The total sectional area of beam longitudinal reinforcement
A_s^*	:	The greater of the area of top or bottom beam reinforcement passing through the joint. It excludes bars in effective tension flanges
A_{ch}	:	The cross-sectional area of a member measured to the outside edges of transverse reinforcement
A_{sh}	:	The total cross-sectional area of all legs of hoop reinforcement including crossties, crossing a section having core dimension $b_c^{"}$
b_b	:	Web width of beam
$b_c^{"}$	:	Core dimension of tied column from outside to outside edge of transverse reinforcement bars, perpendicular to the transverse reinforcement area A_{sh} being designed
b_c	:	Width of column transverse to the direction of shear
b_j	:	Effective width of joint transverse to the direction of shear
b_o	:	Is the minimum dimension of the concrete core (to the centerline of the hoops)
d_b	:	Nominal diameter of bar
f_c'	:	Compressive strength of concrete
f_t	:	Tensile strength of concrete

f_y	:	Yield strength of reinforcement
f_{yh}	:	Yield stress of spiral, hoop, and crossties reinforcement
h_c	:	Full depth of column
s_h	:	Center to center spacing of hoops or hoops plus crossties
d	:	Distance from extreme compression fiber to centroid of tension reinforcement
m	:	Slope to define the effective width of joint transvers to the direction of shear
P_u	:	Factored axial force; to be taken as positive for compression and negative for tension, lb
V_n	:	Nominal shear strength of joint
V_u	:	Design shear force in joint
α	:	Stress multiplier for longitudinal reinforcement at joint-member interface
γ	:	Shear strength factor reflecting confinement of joint by lateral members
φ	:	Strength reduction factor

Chapter 3

$\hat{\varepsilon}_i$	:	i-component of principal strain vector
$\hat{\varepsilon}_{ini}$	:	Strain at onset of tensile softening
$\hat{\sigma}_i$	:	i-component of principal stress vector
τ_2	:	The tangential bond resistance along the axis of bar
τ_b	:	Full bearing resistances of an elastic bar subjected to monotonic pull out
τ_f	:	Full friction resistances of an elastic bar subjected to monotonic pull out
d_b	:	Nominal diameter of bar
$\hat{\sigma}$	:	Principal stress value
τ_{max}	:	Maximum bond strength
c_c	:	Uniaxial strength parameter in compressive region

c_c	:	is uniaxial compressive strength of the material
c_t	:	Uniaxial strength parameter in tensile region
d	:	A parameter increasing the ductility due to confinement
d_a	:	Maximum aggregate size in mm
e	:	Eccentricity
f_c	:	Uniaxial compressive strength
f_o	:	Compressive strength of material at first yielding
f_{res}	:	Residual compressive strength
f_t	:	Tensile strength of concrete
g_c	:	Total area under hardening-softening curve
G_c	:	Compressive fracture energy
G_t	:	Mode-I fracture energy
I_1	:	First invariant of stress tensor
J_2	:	Second deviatoric invariant of stress tensor
M	:	The ratio of residual tensile strength over tensile strength
p	:	Pressure
r	:	Weight factor
S_2	:	The tangential displacement along the axis of bar
S_{peak}	:	The amount of slip at maximum bond strength
S_R	:	The clear spacing between the ribs
w/c	:	Water/cement ratio
X	:	A material parameter to exclude confinement effect for uniaxial loading
α	:	Material parameter increasing the strength due to confinement
α_0	:	Aggregate type parameter
α_p	:	Dilatancy parameter
θ	:	Lode angle
κ	:	Hardening variable
λ_t	:	A parameter controlling the rate of tensile softening
$\rho_{b,c}$	:	Reduction factors based on the slip history to take the effect of cyclic

		bond deterioration on the bearing resistance
$\rho_{b,s}$	:	Reduction of bearing resistances due to the yield of reinforcement and are functions of bar strain
$\rho_{f,c}$	:	Reduction factors based on the slip history to take the effect of cyclic bond deterioration on the friction resistance
$\rho_{f,s}$	:	Reduction of friction resistances due to the yield of reinforcement and are functions of bar strain
ρ_n	:	Reduction factor accounting for splitting cracks in the concrete
a	:	Auxiliary material parameter
g	:	Plastic potential function

Chapter 4

h_b	:	Beam height
h_c	:	Full depth of column
A_{b1}	:	Sectional area of the top horizontal steel elements in the beam
A_{b2}	:	Sectional area of the bottom horizontal steel elements in the beam
A_{c1}	:	Sectional area of the left outermost vertical steel elements in the column
$A_{c2,tot}$	:	Sectional area of the total vertical steel elements in the middle in the column
A_{c3}	:	Sectional area of the right outermost vertical steel elements in the column
b_1	:	Cover of horizontal reinforcing bar at top of beam section
b_2	:	Cover of horizontal reinforcing bar at bottom of beam section
b_3	:	Spacing of horizontal reinforcing bar in the beam
b_w	:	Out-of-plane width of beam
c_1	:	Cover of vertical reinforcing bar at left end of column section
c_2	:	Cover of vertical reinforcing bar at right end of column section
c_3	:	Spacing of longitudinal reinforcing bar in the column
c_w	:	Out-of-plane depth of column
θ_d	:	The inclination angle of diagonal truss element
b_{eff}	:	Effective width of diagonal elements

d_{max}	:	Reloading stiffness of bond-stress constitutive curve
f'_c	:	Compressive strength of concrete
f_{cc}	:	Peak confined compressive strength of concrete
f_{cint}	:	Stress value of the intermediate user defined point in the uniaxial compressive stress-strain curve of unconfined concrete
f_{max}	:	Peak bond strength
f_{res}	:	Compressive residual stress of concrete
f_{sh1}	:	Stress of an arbitrary user defined intermediate node of monotonic constitutive curve of steel
f_{su}	:	Ultimate stress of monotonic constitutive curve of steel
f_t	:	Tensile strength of concrete
f_{tint}	:	Stress value of the intermediate point in the trilinear tensile region of the uniaxial stress-strain curve of concrete
f_{tres}	:	Stress at which the concrete completely loses tensile strength
f_y	:	Yield strength of reinforcement
k	:	Unloading stiffness of bond-stress constitutive curve
ε_{cc}	:	Strain value corresponding to the peak confined compressive strength of concrete
ε_{cint}	:	Strain value of the intermediate user defined point in the uniaxial compressive stress-strain curve of unconfined concrete
ε_{co}	:	Strain value corresponding to the peak unconfined compressive strength of concrete
ε_{cr}	:	Peak tensile strain of concrete
ε_{cu}	:	Ultimate compressive strain of confined concrete
ε_{res}	:	Compressive residual strain of concrete
ε_{sh}	:	Strain at the onset of strain hardening of reinforcing bar
ε_{sh1}	:	Strain of an arbitrary user defined intermediate node of monotonic constitutive curve of steel
ε_{su}	:	Ultimate strain of monotonic constitutive curve of steel
ε_{tint}	:	Strain value of the intermediate point in the trilinear tensile region of the uniaxial stress-strain curve of concrete

ε_{tres}	:	Strain at which the concrete completely loses tensile strength
ε_u	:	Ultimate compressive strain of unconfined concrete

Chapter 5

f_c':	:	Compressive strength of concrete
f_t	:	Tensile strength of concrete
f_y	:	Yield strength of reinforcement
d	:	Distance from extreme compression fiber to centroid of tension reinforcement
E	:	Young's modulus of steel
f_{res}	:	Compressive residual stress of concrete
f_u	:	Ultimate stress of reinforcement
M_n	:	Negative moment with beam end loading downward
M_p	:	Positive moment with beam end loading upward
ε_o	:	Strain value corresponding to the peak compressive strength of concrete
ε_{res}	:	Compressive residual strain of concrete
ε_{sh}	:	Strain at the onset of strain hardening of reinforcing bar
ε_u	:	Ultimate strain of reinforcement

Appendix A

A_c	:	Area of column core measured from outside edge to outside edge of either spiral or hoop reinforcement
A_g	:	Gross area of column section
A_{sh}	:	The total cross-sectional area of all legs of hoop reinforcement including crossties, crossing a section having core dimension $b_c^{"}$
$b_c^{"}$	:	Core dimension of tied column from outside to outside edge of transverse reinforcement bars, perpendicular to the transverse reinforcement area A_{sh} being designed
f_c':	:	Compressive strength of concrete
f_{yh}	:	Yield stress of spiral, hoop, and crossties reinforcement

A_{cc}	:	Area of concrete in the column section
A_{cs}	:	Total area of column longitudinal reinforcement
A_{s1}	:	Area of top beam longitudinal reinforcement
A_{s2}	:	Area of bottom beam longitudinal reinforcement
A_{slab}	:	Area of slab reinforcement within the effective width
b_e	:	Effective width of slab in calculating negative bending moment
C_{b2}	:	Compressive force from beam longitudinal reinforcement
C_c	:	Compressive force from concrete
C_{s4}	:	Compressive force from the fourth layer of column longitudinal reinforcement
d_b	:	Nominal diameter of bar
f_y	:	Yield strength of reinforcement
M_{pr1}	:	Positive bending moment of beam section
M_{pr2}	:	Negative bending moment of beam section
P	:	Axial force applied on column
P_0	:	The nominal axial strength of column section
s_h	:	Center to center spacing of hoops or hoops plus crossties
T_{b1}	:	Tensile force from beam longitudinal reinforcement
$T_{s,s1}$	:	Tensile force of the upper layer slab reinforcing bar
$T_{s,s2}$	:	Tensile force of the lower layer slab reinforcing bar
T_{s1}	:	Tensile force from the first layer of column longitudinal reinforcement
T_{s2}	:	Tensile force from the second layer of column longitudinal reinforcement
T_{s3}	:	Tensile force from the third layer of column longitudinal reinforcement
V_n	:	Required joint shear force
α	:	Stress multiplier for longitudinal reinforcement at joint-member interface
γ	:	Shear strength factor reflecting confinement of joint by lateral members
φ	:	Strength reduction factor

Chapter 1 Introduction

Reinforced concrete (RC) moment frames are a popular lateral-load-resisting system, ensuring a flexibility in terms of space configuration. Moment frames rely on the combined resistance of beams and columns to transfer lateral loads due to, e.g., earthquakes, safely to the ground. The frame action relies on force transfer in the beam-to-column connection regions, which are commonly referred to as beam-to-column joints. These regions must be designed to carry the most critical load combination of axial, bending, torsion, and shear forces prescribed by the applicable building code load combinations (ACI352R-02, 2002). Moment frames are detailed using capacity design principles, to ensure that inelastic deformations are concentrated in desired locations (plastic hinges), primarily at the beam ends, while preventing the occurrence of significant inelastic deformations in the columns and the strength degradation of the joint regions.

Before 1977, seismic design codes in the United States required that the BC joints are only designed for gravity and wind loads. Frame buildings designed prior to 1977 were expected to exhibit premature strength degradation, due to deterioration of the BC joints under cyclic deformations. This means that pre-1977 RC frames are expected to exhibit a non-ductile behavior, which can lead to a sudden collapse of full structure under strong seismic ground motions (Figure 1-1). The rather unsatisfactory performance of RC frames observed during the 1971 San Fernando Valley Earthquake motivated a significant number of experimental and analytical studies to assess the vulnerability of such structures (Bertero and Mahin, 1978). Much of the work aimed to develop new design procedures and detailing to improve the seismic design criteria of new BC joints to ensure adequate strength and ductility. The design of so-called ductile BC joints, emp hasizes the following aspects: a) shear capacity of the joint, b) moment capacity ratio between columns and beams, c) development length of beam and column reinforcement (Jirsa, 1991). The prevention of

joint or story mechanisms maximizes the amount of inelastic lateral deformations that a moment frame can safely develop, as explained in more detail in the latest edition of the ACI code ACI318-14 (ACI318-14, 2014).

Figure 1-1 Damaged BCJs in non-ductile RC frames (H. Sezen et al. 2000)

1.1 Behavior of Interior Beam-to-Column Joints

As the BC joints are a key component of RC moment frames, many collapses can be traced to the degradation or failure of BC joints. Figure 1-2(a) and (b) conceptually illustrate the overall deformation of a moment frame structure and the forces acting on one of its interior joints.

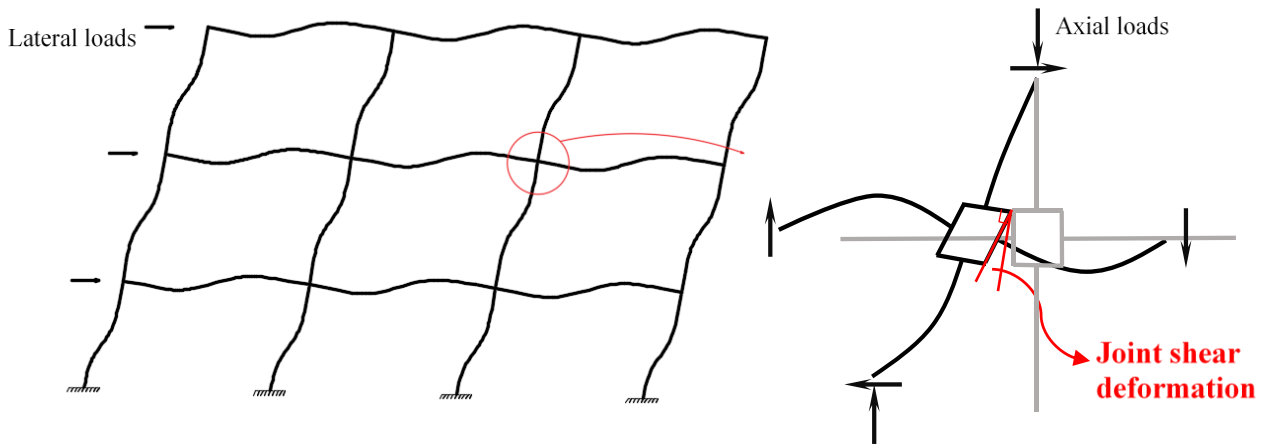

(a) Deformation of DMRF under lateral loads **(b) Deformation of an interior BC joint**

Figure 1-2 Deformation of a typical DMRF

Common types of BC joint damage observed after earthquakes include joint shear cracking, bond slip, and flexural and shear cracking of adjacent beams and column. The bond-slip behavior refers to the deterioration of cohesive stress and relative motion between reinforcing bar and concrete and is a primary topic for this dissertation. Shear cracking and bond slip in the BC joints are major contributors to drift of DMRFs for structures with both ductile and non-ductile BC joints.

1.1.1 Shear Failure

Common causes of extensive BC joint shear behavior include insufficient or lack of transverse confinement in and near the joint area, low ratio of column-to-beam flexural strength, strength deterioration of reinforced concrete materials, and insufficient development lengths of reinforcing bars. The shear forces in the joint, developing primarily from the flexural forces developed at beam plastic hinges (Figure 1-2(b)), result in the average shear stresses in the joint on the order of 15 to $20\sqrt{f_c'}$. This is several times the conventionally assumed shear resistance of concrete, which is taken as 2 to $3.5\sqrt{f_c'}$; the balance of the shear force must be taken by closely spaced ties. When this reinforcement is insufficient, large inclined shear cracks, concrete cover spalling and yielding of the reinforcement will occur, as shown in Figure 1-3(b) for joints with pre-1970s details.

Experimental and field research has demonstrated that the BC joints incorporating newer design criteria, i.e., with closely spaced ties and higher nominal shear will still exhibit inclined cracks under strong seismic loading (Figure 1-3(a)). Cracking in joints leads to a reduction in stiffness and may significantly affect the deformations of a frame structure (Shin and LaFave, 2004). Severe damage can also occur by concrete crushing in the joint and by reinforcing bar

buckling and rupture in the beam. The latter typically follows the occurrence of inelastic buckling of reinforcement (Kim and Koutromanos, 2016).

(a) Shear crack observed in 2011 Christchurch earthquakes (Leon et al. 2014);

(b) shear crack observed

Figure 1-3 Shear crack in BC joints

1.1.2 Bond-slip of Reinforcing bar

The formation of cracks in reinforced concrete is accompanied by the development of increased stresses in the reinforcing bars crossed by the crack. To take advantage of both materials in reinforced concrete member with steel bars carrying tensile forces and concrete resisting compressive stresses, a robust force transferring mechanism along the interface between the reinforcing bars and the surrounding concrete is an essential requirement. This force transfer is termed as bond of reinforcing bar, and is quantitatively described as a uniform stress, called bond stress, on the surface of an idealized, cylindrical bar geometry.

The significance of bond for allowing bars to carry tensile forces can be demonstrated by considering a reinforcing bar embedded in a concrete segment with a length equal to ΔL, as shown in Figure 1-4(a). The bar axial force has different values, T_1 and T_2, at the two ends of the segment. Axial force equilibrium for the reinforcing bar requires the development of a bond stress along the surface of the bar. Assuming that the bond stress has a constant value, equal to u_b, over the segment,

gives the following equation:

$$u_b = \frac{\Delta T}{\Delta L(\pi d_b)} \tag{1-1}$$

where ΔT is the tensile force change in the segment and d_b is the bar diameter.

If the required bond stress is higher than the provided value, permanent deformations, or slip, can occur. The deformability of RC components such as BC joints is significantly affected by the relation between bond stresses and slip in reinforcing bars. The latter relation is typically established based on pull-out experiments, where a bar is embedded in a concrete cylinder and is subsequently pulled out. Typical bond stress-versus-slip relations obtained from pullout tests are presented Figure 1-4(b). Severe bond stress demand occurs within the development length of reinforcing bar of BC joints which can be regarded as one-half of the dimension of column when they are subjected to large earthquake loads, as the axial forces in the beam longitudinal reinforcement are expected to go from tension to compression yielding across the joint. This is a large demand of bond stress and conventional development length equations would suggest 65 to 75 bar diameters to transfer similar forces, while the available development length is only around 20 bar diameters based on the dimension of column. Inadequate embedment length can lead to bond failures which may result in excessive drifts and will lead to structural collapse or second-order stability effects brought by inordinate residual deformations.

Theoretical results of RC elements behavior in the cracked state, under the hypothesis of full bond condition, can lead to a significant overestimation of up to 400% of the stiffness of the actual RC elements (Bartelletti et al., 2004). However, the bond slip behavior of reinforcement has not been accurately accounted for in the majority of finite element analysis of RC joints until quite recently because of the computational complexities involved.

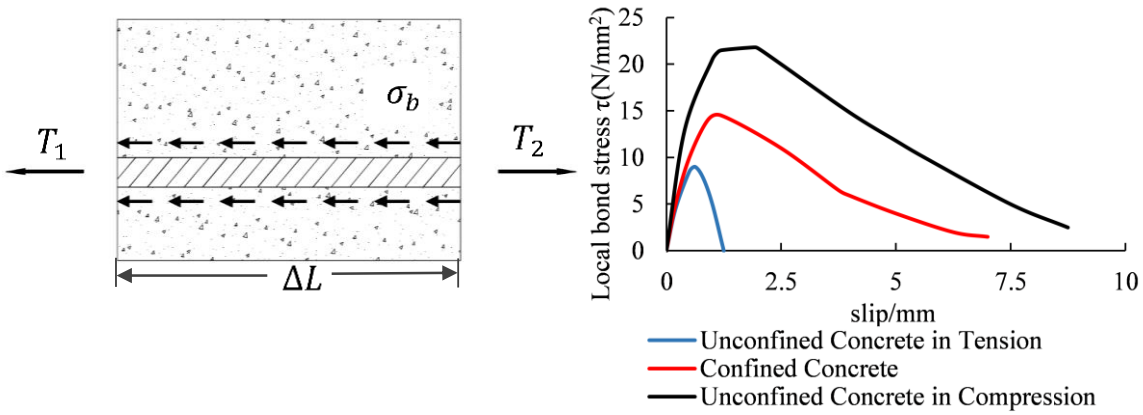

(a) Definition of bond stress

(b)Monotonic bond stress-slip curve for pull poll failure (Redrawn after Eligehausen et al., 1983)

Figure 1-4 Definition and simple bond stress-slip relation

1.2 Motivation of Research

Recommendations from the Joint ACI-ASCE Committee 352 (Joints and Connections in Monolithic Concrete Structures (ACI 352 for short) have identified several aspects of design which may require research, most notably it's not clear how conservative the currently adopted limit values of joint shear force is (ACI352R-02, 2002). Additionally, the behavior of connections with current design requirements prescribed by ACI Committee 318 (Building Code Requirement for Structural Concrete and Commentary, ACI318-14, 2014) and ACI 352 under bidirectional loading has not been fully evaluated.

Many previous experimental studies have provided information on the behavior and damage patterns of BC joints (Jirsa 1991, Kurose et al., 1988), and have supported the development of pertinent design procedures to ensure safe and economic structural configurations. After the pioneering experiments of Hanson and Conner (Hanson and Conner, 1967), there has been an ongoing effort in understanding the behavior of BC joints under seismic loads through progressively more sophisticated 2D and 3D testing (Viwathanatepa et al., 1979; Leon, 1984, 1989;

Kurose et al., 1988; Beres et al., 1996; Pagni and Lowes, 2004 and more, as summarized in Section 2.3).

Despite that experiments give the most authentic measured responses, they are mostly global results and even the most extensive experimental studies cannot fully capture the trends of the numerous parameters impacting the behavior of the BC joints. The numbers of full-scale experimental studies are limited by economic considerations and laboratory conditions. Thus, analytical simulation must supplement experimental tests to enable a complete understanding of the strength and damage patterns under a sufficiently wide range of structural configurations and loading scenarios. Based on the observed behavior and damage patterns of interior BC joints, the analysis should account for concrete cracking and its impact on the shear deformability of the joint, the bond-slip behavior between concrete and reinforcing bar, the rupture and buckling of reinforcing bar, confinement effect of concrete in the joint region, the crushing of concrete, and the spalling of concrete cover.

In the traditional analytical simulation of RC moment frames, BC joints are assumed to be rigid. The joint area is not explicitly modelled even though the BC joints undergo significant damage. The strength degradation due to bond deterioration is not accounted for. Within these assumptions, it is clearly impossible for the traditional analytical method of BC joints to capture complex nonlinear degrading performance. As a result, traditional analytical simulations heavily rely on the calibration with existing experiments, and cannot give reasonable predictions on BCJs that have not been tested. Establishing a robust analytical methodology, as developed in this dissertation. will also provide an approach for calibrating simplified analytical models, especially the BCJs in complicated loading circumstances.

Accompanying with more experimental supports, various numerical simulation methods have

been proposed to eliminate the drawbacks from traditional analytical simulations by simplified models (Alath 1995; Biddah and Ghobarah 1999; Youssef and Ghobarah 2001; Lowes and Altoontash 2003; Shin and LaFave 2004 etc.) and finite element models (Ngo and Scordelis, 1967; Eligehausen et al., 1982; Alath Vallenas et al., 1995; Noguchi et al., 2008; Panagiotou et al., 2012 and more, as summarized in Section 2.4). The simplified models, which are applying empirical based nonlinear springs in representing shear and bond-slip behavior based on the calibration from existing experiments, cannot predict the true mechanisms in the joint. The joint behavior plays a most significant role in a frame analysis. When involving the simplified joint model in a frame analysis, it is rarely proper to apply the response from experiments directly into the frame analyses since the joints are not exactly the same. What's more, simplified models are 2D only, which inherently neglect the bidirectional effect in perpendicular direction.

The finite element method is a powerful analytical tool which can be used to explore the behavior of BC joints under a variety of loading conditions if properly defined. Continuum-based, three-dimensional (3D) finite element analyses can provide insights on the stress and strain distributions in the interior of a joint, trace the damage accumulation, assess the efficiency of force transfer mechanisms and determine the levels of inelastic deformations that may cause deterioration of a joint. All these would be difficult to accomplish in an experiment. Moreover, establishing a reliable analytical methodology would be valuable when conducting experimental design, particularly for instrumentation and load history protocols, in order to simulate or exclude certain failure modes. In spite of the fact that there are various kinds analytical models accounting for shear deformations and bond slip behavior of BC joint, previously proposed finite element methods for the analysis of RC joints fail to get accurate results when modeling complex multiaxial stress states in the concrete under cyclic loading (Eligehausen et al., 2006; Deaton, 2013). In

addition, the behavior of interior BC joints with slabs under bidirectional loading is still not fully understood. Finally, there is no satisfactory model than can capture the local bond-slip behavior in 3D interior BC joint simulations under cyclic loading.

The aforementioned considerations indicate that there is still a need for computational simulation schemes for BC joints in RC frames, capable of capturing the salient aspects of material response, and enabling the rigorous parametric investigation of prototype BC joint configurations. The present study establishes such a methodology for the simulation of both one-way and two-way interior BC joint regions, including the effect of floor slabs. The method is evaluated through analyses of 2D and 3D interior BC joints that had been experimentally tested in the past. Then, analytical simulations of prototype interior BC joints based on the design requirements from ACI 352 will be carried out to evaluate the current design criteria and extended into a parametric study to explore how various factors influence the performance of interior BC joints. These factors include:

1. the effect of material properties such as compressive strength of concrete and yield strength of reinforcing bar,
2. the effect of development length of reinforcement and associated bond deterioration,
3. the effect of column axial load ratio on joint behavior,

Despite the availability and capabilities of continuum-based finite element models, the research and professional communities will most probably prefer to rely on simplified analytical tools for characterizing the cyclic behavior of BC joints. To address this need, a simplified analysis methodology for interior BC joints, based on the nonlinear truss analogy for reinforced concrete (Panagiotou et al., 2012; Lu and Panagiotou, 2014) is also developed. The nonlinear truss methodology (Panagiotou et al., 2012) has proven its accuracy and efficiency at simulating

interactive behavior of concrete structures such as walls (Lu and Panagiotou, 2014), floor slabs (Lu et al., 2016), and columns (Moharrami et al., 2015). However, local response of interior BC joints, such as the strain penetration and stress distribution of beam longitudinal reinforcement, as well as local bond-slip values, have only recently begun to be studied utilizing truss models. A more refined bond-slip model needs to be applied to accomplish local monitoring of interior BC joints, and also to have a better understanding of the global behavior such as hysteretic response and failure mode.

The objectives of this study are therefore to utilize advanced FE simulations to conduct parametric studies on BC joint behavior. The process can be summarized as:

1. Evaluation of a 3D finite element methodology against a series of one-way interior BC joints under cyclic loading tested by Leon (1989), including both global and local responses as affected by flexural-shear-bond interactions;
2. Further evaluation of the 3D finite element methodology through a two-way beam-column-slab interior joint subjected to bidirectional cyclic loading tested by Kurose et al. (1988), including hysteretic response on both directions, failure modes, and local strain history;
3. Evaluation of a nonlinear truss element methodology through the same specimens tested by Leon (1989) based primarily on global responses such as force-deformation curves;
4. Parametric study of a prototype interior beam-column-slab joint based on an ACI352 design criteria utilizing the 3D finite element methodology mentioned above.

The ultimate objective of the work is the development of two robust analyses methodologies, one based on 3D non-linear FE and one on truss methodology methods, that can be used to systematically study BC joint 3D behavior accurately and efficiently. This will lead to the

development of more efficient designs, reduce the number of experimental tests that need to be conducted and speed up the introduction of novel force transfer technologies.

The original work of the present study includes:

1. Finite element model:
    1) Set up an analytical scheme to capture the hysteretic behavior and failure of one-way and two-way interior beam-column joints;
    2) Evaluate the proposed FE scheme through both global and local results of previously conducted experimental tests on BC joints under cyclic loading;
    3) Carry out sensitivity analysis on critical parameters including both physical (material properties and bond-slip effect for example) and model (user inputs in the model for example) parameters of the proposed FE scheme;
2. Nonlinear truss model:
    1) Evaluate the applicability of the nonlinear truss analogy to a series of one-way interior beam-column joint;
    2) Evaluate its ability to capture shear failure in the joint and a good agreement with global response;
    3) Conclude that more proper bond-slip model is needed for a better result on bond-slip response.
3. Parametric study of prototype:
    1) Establish the analytical model for connections based on the an example calculation in ACI352R-02;
    2) Compare the performance of connections that comply with design recommendations to that of connections which do not comply;

3) Quantify the impact of bidirectional loading on the average shear stress in the joint.
4) Quantify the impact of bidirectional loading on the local bond-slip behavior;
5) Explain the global behavior by local responses and find out the relation between the global and local result;
6) Analytically study the influence of axial force of column on the performance of connection;
7) Trace the stress distribution of reinforcing bar around plastic hinge.

1.3 Outline of Dissertation

Chapter 2 presents a review of previous experimental and numerical investigations of interior BC joints. The capabilities and limitations of pertinent analytical methods are also discussed.

Chapter 3 introduces the proposed FE scheme first and then evaluates four one-way BC joint specimens through the proposed FE scheme. Global and local performance indices for the BC joints are compared with experimental data. The sensitivity of the analytical results to various parameters, such as reinforcement yield stress and peak bond strength, is investigated. The aforementioned analytical method is applied on simulating 3D two way RC interior BC-slab joints. Results will be compared with experimental responses in both global and local scale. Step by step outline of this 3D simulation will be provided.

Chapter 4 provides a method based on the nonlinear truss methodology for the analysis of the same specimens in Chapter 3. The procedure to determine the geometry of the truss elements is introduced, as well as the constitutive laws used for the materials. The method is validated using experimental test results on one-way BC joints.

Chapter 5 presents the step by step outline of parametric analysis of an example prototype

two-way BC connection with slab in ACI 352. The impact of joint shear force, bar embedment length and bidirectional loading on the performance is also studied through a parametric investigation. Parametric studies are performed to explore various factors on the performance of the two-way interior BC joint.

Chapter 6 summarizes the conclusions of this study and provides recommendations for future research.

Chapter 2 Background - Literature Review

This chapter provides the necessary conceptual background for the present study, together with a review of relevant literature. Section 2.1 summarizes the main resistance mechanisms for BC joints, while Section 2.2 summarizes the design criteria for seismic design of BC joints in different countries/regions. Sections 2.3 and 2.4 constitute a review of previous experimental and numerical investigations of interior BC joints. Sections 2.5 and 2.6 introduce the bond behavior of steel reinforcing bars and describe several existing analytical techniques to simulate the cyclic bond-slip behavior of the reinforcement in RC structures.

2.1 Force Transfer Mechanisms in Beam-to-Column Joints

A necessary first step to understand the force transfer mechanism in an interior beam-to-column joint is to draw a free-body diagram of the joint region, subjected to the forces and moments corresponding to the ends of the frame members, as shown in Figure 2-1. The member moments and axial forces are included through incorporation of the reinforcing bar tensile forces, T, and concrete compressive forces, C, as shown in the same figure. The shear force of each member is denoted as V, and axial force is denoted as P. Taking a horizontal section in the free-body diagram of the joint, as shown in Figure 2-1, and considering horizontal force equilibrium for, e.g., the piece of the joint above the section, leads to the conclusion that a horizontal shear force, V_j, must be developed in the interior of the joint to ensure equilibrium. To ensure a ductile response mechanism (dominated by inelastic flexural deformations occurring at the ends of members, primarily beams), the shear capacity of the joint must never be less than the value of V_j corresponding to the instant that the frame members develop their expected flexural strength.

The shear resistance in an interior BCJ can be attributed to a combination of two mechanisms,

namely, a strut mechanism and a panel zone mechanism, shown in Figure 2-2 (Leon, 1990). These mechanisms represent two possible extreme situations of joint behavior. The first possible mechanism involves the formation of a single diagonal concrete compressive strut (the blue shadow in Figure 2-2(a)).. This mechanism is controlled primarily by the compressive strength of the concrete, as well as the compressive resistance of the equilibrating compression blocks in the columns and beams. This strut mechanism assumes that large flexural cracks have formed at the joint interfaces between the beams and columns, but that the compression blocks are in contact because the bars have slipped through the joint. When the strut mechanism dominates, the equilibrating tensile forces will come from tension on the horizontal (beam) and vertical (column) reinforcing bars outside the joint. In this case, the required ties in the joint reduce to the amount necessary to properly confine the concrete.

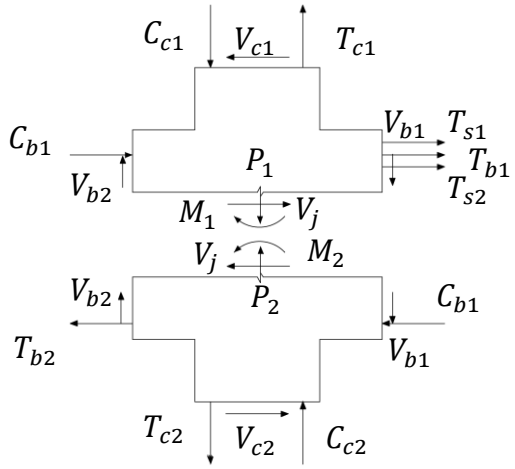

Figure 2-1 Free body diagram of interior BC joint

The second resistance mechanism is the so-called panel truss mechanism, wherein the horizontal ties in the joint region develop tensile forces, and a diagonal compression field forms by many smaller inclined compressive concrete struts between those ties in the joint (the blue shadow in Figure 2-2(b)). This mechanism depends on the strength of both the horizontal ties and

the vertical column reinforcement in the core to maintain the truss action. When the truss panel mechanism dominates, the reinforcement in the beam is assumed to have yielded under cyclic deformations, resulting in a large crack across the entire beam-joint interface that cannot fully close due to little or no slip in the reinforcing bar with good anchorage conditions in the joint. These good condition imply, in addition, that the shear forces are transferred into the core by the bond of steel reinforcing bars. The arrows with the same color represents the same kind of force in Figure 2-2 (a) and (b). Some forces that share the same names in two figures are not labeled for simplification.

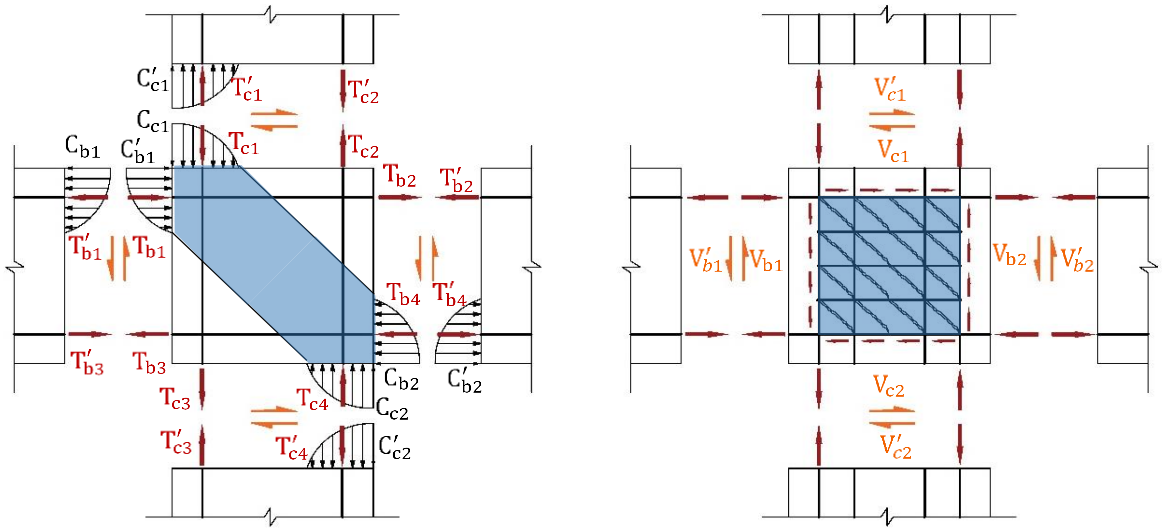

(a) Strut mechanism **(b)Panel zone mechanism**

Figure 2-2 Joint shear transfer mechanisms. (Leon, 1990)

When the interior BC joint is subjected to cyclic deformation, the behavior is typically characterized by the following sequence of events (Leon 1990):

1. Before the beam reinforcement yields, both mechanisms contribute to the shear resistance in the joint with the strut mechanism contributing more because strains in the tension members are not large enough to activate the panel truss mechanism.

2. There are two possibilities after the first yield of the beam reinforcement, which depends on the bond demands:

1) When the bond demands in the joint are low, as would be the case if the development length of the bars through the joint (which can be regarded equals to the dimension of the column) is at or above 24 bar diameters, the yielding of the reinforcement takes place at the joint face with no or little yield penetration (which represents the yield of reinforcing bar develops into the joint region due to the bond-slip behavior) into the joint. Under cyclic lateral deformations, the formation of a plastic hinge in the beam will lead to the complete separation of the joint from the beam, as the top and bottom beam flexural reinforcement have undergone large strains at the interface. This separation between the beam and column face eliminates the strut mechanism since compression forces are all transferred to the joint region through the bond stresses. A large volume of ties in the core, as well as long development lengths, are essential to maintain this mechanism through large inelastic cyclic excursions. In this case, a panel mechanism dominates (Figure 2-2(b)).

2) If the bond demands in the joint are essentially high, as would be the case if the development lengths are at or below 20 bar diameters, a completely different situation arises. The high demand in bond stresses will result in yield penetration into the joint and, under lateral loads, a rapid deterioration of the bond strength resulting in large bar slips. In this case the beam bars will be anchored in the beams at the opposite side of the joint, increasing the effectiveness of the strut mechanism through enlarging the size of the compressive blocks at the beam-column interfaces. The joint corners which are well confined by beams bring a more effective strut mechanism, although there

would be larger compressive strains and more shear crack in the joint. Large compressive strains may lead to losses of section in the corners of the column, which results in larger shear deformations and less energy dissipation capacity. In this case, a strut mechanism dominates (Figure 2-2(a)).

The descriptions herein have only dealt with the horizontal shear; equilibrium considerations for a joint free-body diagram lead to the conclusion that vertical shear forces must also be resisted by the joint. These forces are typically not explicitly addressed in design, because the large number of column longitudinal bars which are distributed in the joint region are expected to develop the required resistance for vertical shear.

The two force transfer mechanisms described above will be better captured by a triaxial concrete model and an accurate description of the confining effect of the ties in order to carry out realistic simulations. The model needs to account for multiaxial stress states in concrete and to capture both the compressive strength degradation due to crushing and the increased compressive strength and ductility under confining pressure. When subjected to cyclic loading, the concrete model is required to capture crack opening and closing, as well as element removal due to concrete cover spalling. In addition, the nonlinear bond deterioration needs to be considered, especially when the bond condition is poor and large cyclic deformations are imposed.

2.2 Design of BC Joints in RC Frames

The seismic design for BC joint regions in the United States is conducted in accordance with two documents, namely, the ACI-318 code (ACI318-14) and the latest edition of the recommendations by Committee 352 of (ACI352R-02), which will hereafter be referred to as the ACI 352 document. The majority part of the two documents are the same, except for that the

ACI318-14 includes the confinement effect duo to high axial pressure on the column when calculating transverse reinforcement amount and requires higher development length for reinforcing bar embedded in lightweight concrete.

The ACI 352 document differentiates between Type 1 (non-seismic) and Type 2 (seismic) joints. According to ACI 352, there are six aspects that significantly influence the performance of interior BC joint, namely: 1) column longitudinal reinforcement, 2) joint transverse reinforcement, 3) joint shear capacity, 4) flexural capacity of columns as compared to the corresponding capacity of the beams, 5) development length of reinforcement, and 6) the beam transverse reinforcement. From a design standpoint, these are addressed by requiring that:

1. For Type 2 connections, column longitudinal reinforcing bars must be uniformly distributed around the perimeter of the column core, with a relatively tight minimum spacing requirement. The intent is to improve confinement of the column core by ensuring a relative uniform distribution of the longitudinal bars in the column section of Type 2 connection. Extra ties should be provided if the bars are offset within the joint.

2. Adequate lateral confinement of the concrete in the joint is ensured by transverse reinforcement, to guarantee that the joint can safely resist the design forces. When rectangular hoop and crosstie horizontal transverse reinforcement is used, and the factored axial force $P_u \le 0.3A_g f_c^{'}$, $f_c^{'} \le 10000$ psi, the minimum total cross-sectional area of transverse reinforcement is calculated as:

$$A_{sh} = 0.3\frac{s_h b_c^{''} f_c^{'}}{f_{yh}}\left(\frac{A_g}{A_c} - 1\right) \tag{2-1}$$

but not less than

$$A_{sh} = 0.09 \frac{s_h b_c^{"} f_c^{'}}{f_{yh}} \tag{2-2}$$

where A_{sh} is the total cross-sectional area of transverse reinforcement; s_h is center-to-center spacing of the transverse reinforcement; f_{yh} is the yield strength of the transverse reinforcement; $b_c^{"}$ is core dimension of tied column from outside to outside edge of transverse reinforcement bars, which is perpendicular to the transverse reinforcement area A_{sh} that being designed; A_c is the area of column core and calculated by the product of $b_c^{"}$ from each side; A_g is the gross area of column section (Figure 2-3).

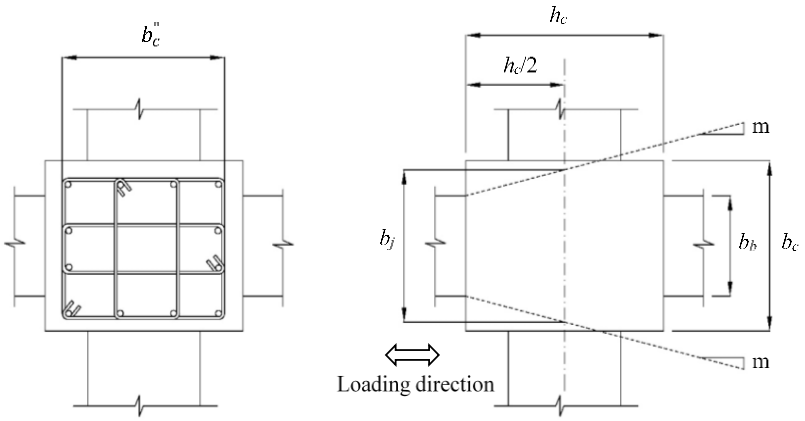

Figure 2-3 Example of the parameters' measurement (plan views)

As required by ACI 318-14, when the factored axial force $P_u > 0.3A_g f_c^{'}$ and $f_c^{'} > 10000\,\text{psi}$, A_{sh} should not be less than $0.2k_f k_n \frac{P_u}{f_{yt} A_{ch}}$ except for satisfying Equation (2-1 and (2-2. Where $k_f = \frac{f_c^{'}}{25000} + 0.6 \geq 1.0$, and $k_n = \frac{n_l}{n_l - 2}$; A_{ch} is the cross-sectional area of a member measured to the outside edges of transverse reinforcement.

The center-to-center spacing between layers of horizontal transverse reinforcement

(hoops or hoops and crossties), s_h, should not exceed the least of 1/4 of the minimum column dimension, six times the diameter of longitudinal column bars to be restrained, and 6 in. (150 mm).

3. The design procedure implicitly assumes an elliptical interaction relation of unidirectional response for the bidirectional loading, and requires the joint shear strength be evaluated in each direction independently. The nominal shear strength on the horizontal plane at the mid-height of a type 2 interior BC joint is given as:

$$V_u \le \varphi V_n = \varphi\gamma\sqrt{f_c'}\, b_j h_c \quad (psi) \tag{2-3}$$

where γ is a coefficient to account for the joint configuration, as schematically summarized in Figure 2-4. For the three-dimensional interior joints assumed herein, $\gamma = 20$ with $\varphi = 0.85$; b_j is the effective joint width, defined as follows:

$$b_j = \min\left\{\frac{b_b + b_c}{2},\ b_b + \sum\frac{mh_c}{2},\ b_c\right\} \tag{2-4}$$

where b_b is the width of the beam section; b_c is the width of the column section; h_c is the full depth of the column section in the direction of the joint shear force, m=0.5 for joints without eccentricity and the summation term should be applied on each side of the joint where the edge of column is wider than beam; the value of $mh_c/2$ should not be larger than the extension of the column beyond the beam edge. Thus the shear stress demand in the joint, taken as $\frac{v_u}{b_j h_c}$ must be smaller than $\phi 20\sqrt{f_c'}$ or $17\sqrt{f_c'}$ (Figure 2-3).

Tests indicated that by this level of nominal shear stresses, the inclined crack in a well-confined interior joint should be excessively wide. Note that it is assumed that the shear stress

is uniformly distributed and that stress concentrations do not exist; this is a convenient assumption for design but its validity for all configurations has not been properly assessed.

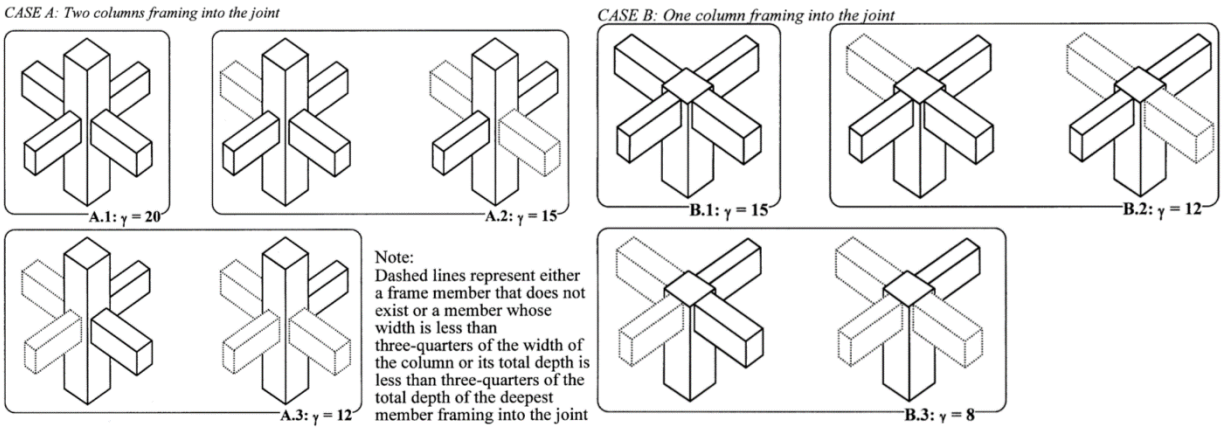

Figure 2-4 γ-values for Type 2 connections(ACI352R-02, 2002)

4. The ratio of the nominal moment of columns to beams which are calculated at the corresponding factored axial load should not be less than 1.2. This 1.2 factor cannot ensure the longitudinal reinforcement in the column will not yield, but a compromise between the need to protect column against hinging and the economical need of column sizes and reinforcement.

5. For Type 2 connections, the yield stress f_y of all straight beam and column bars passing through the joint should satisfy the following expressions:

$$\frac{h_{(column)}}{d_{b(beam\ bars)}} \geq 20\frac{f_y}{60000} \geq 20 \qquad (2\text{-}5)$$

$$\frac{h_{(beam)}}{d_{b(column\ bars)}} \geq 20\frac{f_y}{60000} \geq 20 \qquad (2\text{-}6)$$

The minimum development length required by ACI 352 is roughly one third of the development length required to properly develop a bar in a beam under static conditions, assuming that 40 d_b of development length required for tension and about 20 d_b required for

compression. ACI 381-14 requires the column dimension should be at least 26 times the diameter of the largest longitudinal bar for lightweight concrete.

6. For type 2 joints, beam transverse reinforcement should be provided within an enforced region at a maximum spacing value to provide enough shear strength for the potential plastic hinge zone in the beam.

For the DMRFs located in an area of high seismic demand, there is no international consensus in design codes as to the best design procedure for BC joints. The main discrepancies arise in the level of shear stress allowed in the joint, the development length requirement for beam and column reinforcement, and the transverse reinforcement requirement. These differences are reflected in Table 2-1, which compares several well-known codes from around the world.

Coefficients for the highest class of earthquake design is applied in Table 2-1. The definition of the "highest class" joint differs from code to code slightly, while all of them aim at forming plastic hinge in the beam at some distance away from the joint. In the design recommendation used in USA (ACI352R-02 2002), Type 2 is a connection with members required to dissipate energy through reversals of deformation into the inelastic range; In the design code used in New Zealand (NZS3101:Part1:2006), it refers to the BC joint subjected to forces arising from the formation of ductile plastic regions in the adjacent members where the required energy dissipation occurs; In the design code used in Europe (Eurocode8 2004), it refers to Ductility Class High (DCH) which ensures a stable and trustworthy model of absorbing energy in predicted critical areas and to provide higher security levels against local or total collapse under earthquakes greater than the design seismic action; In the design code used in China (GB50011-2010), RC frames are classified into class one to four based on the importance of the building, seismic precautionary intensity of the site and the building height. For example, a RC building higher than 24 meters located in an

area with the VIII degree of seismic precautionary intensity (with peak design acceleration of horizontal ground motion at 2.5 m/s^2) should apply the First Class criteria, which is also referred to in Table 2-1.

Table 2-1 Comparison of BC Joint Designing Code from Different Regions (With Normalized Design Axial Force in The Column Equals to $0.2P_o$, psi, in)

	USA[1]	New Zealand[2]	Europe[3]	China[4]
Joint shear stress[5]	$17\sqrt{f_c'}$	Smaller of $0.2f_c'$ and 1450	$\approx 0.37f_c'$	$\approx 0.44f_c'$
Development length[6]	$20d_b$	$28d_b$	$\approx \frac{0.24f_y}{f_t}d_b$	$\approx 0.16\frac{f_y}{f_t}d_b$
Moment ratio[7]	1.2	1.6-1.8	1.3	1.7,1.5,1.3,1.2[10]
Joint transverse Reinforcement[8]	$0.09\frac{s_h b_c'' f_c'}{f_{yh}}$	$1.68\frac{A_s^* f_y}{f_{yh}}$	$1.008\frac{A_s f_y}{f_{yh}}$	$0.1\frac{s_h b_c'' f_c'}{f_{yh}}$
Minimum tie spacing in the joint[9]	Least of $0.25h_c$, $6d_b$ and 6"	Smaller of $10d_b$ and 7.87"	Smaller of and $0.5b_o$, $8d_b$,6.89"	Smaller of $6d_b$ and 7.87"

[1]: ACI352R-02 2002: "Recommendations for Design of Beam-Column Connections in Monolithic Reinforced Concrete Structures" is referred to herein.

[2]: NZS3101:Part1:2006: "New Zealand Standard Concrete Structures Standard Part 1 The Design of Concrete Structures" is referred to herein.

[3]: BS EN 1998-1:2004 Eurocode8 "Design of structures for earthquake resistance" is referred to herein.

[4]: GB50011-2010: Code for seismic design of buildings (edition of 2016) is referred to herein.

[5]: The joint shear stress refers to the maximum shear stress allowed in the design.

[6]: The development length is the minimum value of the effective depth of column/beam divided by the ratio of reinforcing bar yield strength over 60 ksi.

[7]: The moment ratio refers to the ratio of the nominal moment strength of the columns to the beams.

[8]: Joint transverse reinforcement refers to the minimum total cross-sectional area of horizontal transverse reinforcement required in the joint.

[9]: The spacing in the joint refers to the minimum spacing of transverse reinforcement allowed in the joint area.

[10]: The four numbers corresponding to the moment ratio for the First, Second, Third and Fourth Class, respectively.

Table 2-1 reflects a large range of expected performance, from essentially no damage

expected in the design code in New Zealand to a moderate damage allowed in the ACI code of the USA. Thus, there is a need to conduct parametric studies to determine the best combinations of bounds of these parameters. It is clear that these studies cannot be experimental, as the large number of parameters and the full-scale needed for these tests, make such an approach impractical both from the technical and economic standpoint.

2.3 Experimental Investigation of Interior Beam Column Joints

The most reliable method for investigating the behavior of RC components and systems is through appropriately instrumented, large-scale, experimental tests. This section provides a summary of previous experimental studies, together with their principal findings and conclusions.

2.3.1 Experimental Studies on Non-Ductile Interior BC Joints

Understanding the behavior of non-ductile BCJs is a precondition for both improving joint performance in new DMRF and developing possible retrofits for older non-ductile moment frames. It has been widely accepted that improper BCJ details result in inevitable damage of the joint and the structure. Examples of poor detailing include (Beres et al., 1996):

1. Lapped splices that occur immediately above the floor level when the column longitudinal reinforcements ratio is less than 2%
2. Beam bottom reinforcement that is discontinuous and has an insufficient development length into the column
3. Little or no transverse reinforcement is present in the joint region
4. Insufficient transverse reinforcement spacing is present in the column

5. There is a low moment capacity ratio, and/or
6. Construction joints are present below and above the joint

The following subsections describe some relevant test series that have elucidated the damage mechanisms and their sequence; this knowledge is essential to develop robust models for simulation. In particular, attention will be placed on the interaction between key factors which influence the performance of both interior BCJ with newer design criteria and the retrofit of existing poorly constructed joints.

2.3.1.1 Observed Behavior in Non-Ductile Interior BC Joint Tests

Damage states observed in tests include flexural cracking at the beam-joint interface, cracking within the joint, yielding of longitudinal beam reinforcement, spalling of concrete at joint surface, deterioration of joint shear strength, extension of joint cracks into beam and/or column, concrete crushing in joint core and beam ends, buckling of column longitudinal reinforcement, loss of beam longitudinal reinforcement anchorage within the joint core, and pull-out of beam longitudinal reinforcing bar. Joint shear strength degradation was observed right after the spalling of cover concrete in the joint area. A simple failure mode sequence is shown in Figure 2-5.

2.3.1.2 Factors Influencing the Cyclic Response of Non-Ductile Interior BC Joint

Synthesis of BCJ experimental work show interests on the following aspects:

1. Nominal Joint Shear Strength:

   Higher joint shear stress demand results in an increased possibility of brittle failure (Meinheit and Jirsa, 1977; Durrani and Wight, 1982). Experimental research does not provide a clear trend to determine if larger compressive strength of concrete has no impact (Noguchi

and Kashiwazaki, 1992), proportional impact (Goto et al., 1996) or nonlinear impact (Oka and Shiohara, 1992) on joint shear strength. Current design equations assume that shear strength is proportional to $\sqrt{f_c'}$.

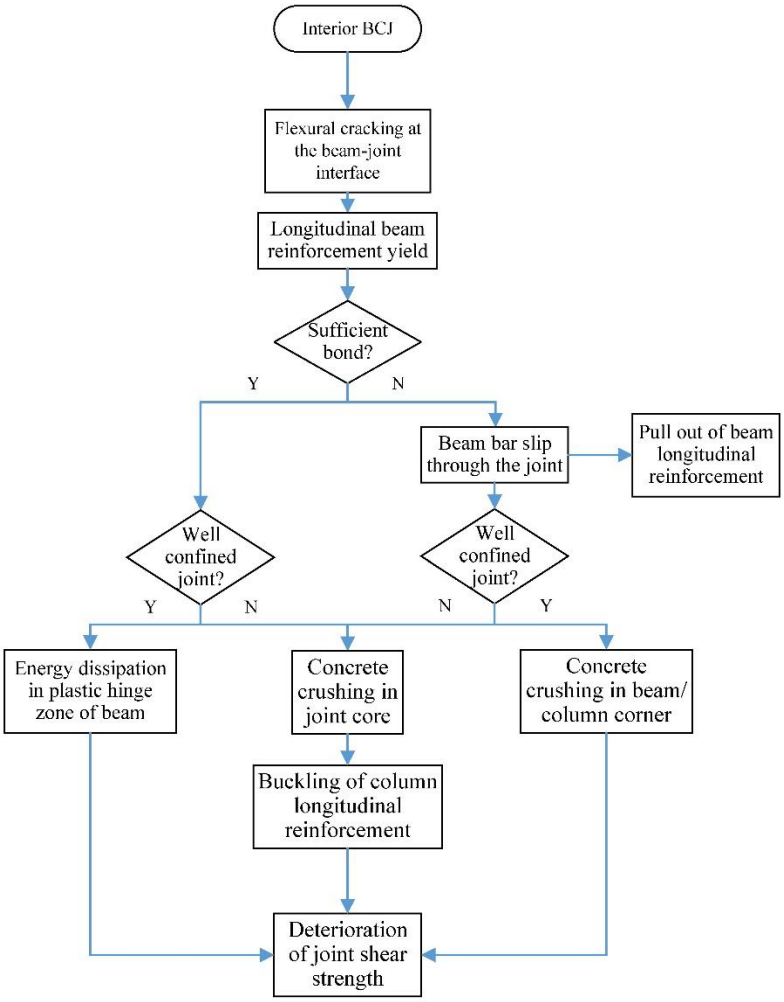

Figure 2-5 Failure mode sequence of interior BC joints

2. Bond strength:

The decreased area of longitudinal reinforcement after yield due to tensile elongation and associated crushing of the concrete at the top of the lugs brings large bond deterioration (Pagni and Lowes, 2004). Bond strength is tied to bar size, showing a definite size effect. For

conventional development lengths, ACI makes differentiation between larger bars and smaller bars. This step function is acknowledged to be a rough approximation to real performance. Bond performance of smaller bars is usually assumed to be better than that of larger bars.

3. Joint Transverse Steel Ratio:

The shear resistance mechanism is significantly influenced by the transverse reinforcement in the joint (Bonacci and Pantazopoulou, 1993). Increasing the joint transverse steel ratio does (Joh et al., 1991) or does not (Li et al., (2003) who concluded that bond condition depends mainly on the ratio of main bar diameter to the size of column/beam for beam-wide column joints) help to reduces slip of beam bars in the joint and delays failure (Hanson and Conner, 1967; Durrani and Wight, 1982), but only at large deformation levels (Noguchi and Kashiwazaki, 1992).

4. Development length of beam bar:

Bar slippage in the joint is likely to occur with the $20d_b$ length specified by ACI 352. Joint with development length of $28d_b$ exhibited little or no bond degradation (Leon, 1989).

5. Column axial load:

Beres et al. (1996) showed a positive effect of column axial loads on interior BC joints due to increased stiffness and capacity, as well as improved bond between column concrete and reinforcement, but others (Bonacci and Pantazopoulou, 1993; Fujii and Morita, 1991) stated that column axial load has no apparent effect on joint strength when axial load ratio is smaller than 0.5 (Kitayama et al., 1987).

Joint shear and bond-slip behavior are the two major contributors to the failure of non-ductile interior BC joints. Preventing bond and shear strength degradation have become two major tasks in newer design. In parallel, properly simulating the joint shear and bond-slip behavior has become

two major tasks in numerical analysis. The inconsistent opinions on the influence of concrete compressive strength and column axial load, which may come from different failure modes and design levels, are expected to be clarified through numerical methods.

2.3.2 Experimental Studies on Ductile Interior BC Joints

Since interior BC joints with newer designs will still exhibit diagonal shear cracking and bond deterioration, studies should aim to establish realistic limits for design parameters. Thus, it is imperative to develop robust analytical method that could validate observed damage patterns and behavior from laboratory tests.

Viwathanatepa et al. (1979) observed flexural deformation in the beam and bar slippage on an interior BC joint when loading cyclically. The first critical region which is adjacent to the column face contributes around 45% of the lateral displacement. It is recommended that bottom beam bars should be more than 50% the top beam bars to delay the excessive bond deterioration. The effectiveness of epoxy was proved in retrofitting the concrete cracks.

Leon (1989) performed four half-scale one-way interior BC joint tests to quantify the effect of nominal shear stress limit, nominal column to beam moment strength ratio, and the development length of reinforcement on the hysteretic and shear performance of BC joints. The influence that shear strain has on the deterioration of joint behavior was highlighted by the test results. With respect to development length, a length of 20 bar diameters was found to be sufficient to obtain initial yielding of the beam bars, but a length of 28 bar diameters is needed to insure the ultimate strength is reached and maintained for several cycles for the beam bars. This research also pointed out that modeling the joint as a rigid body is improper in analytical studies because even properly designed joints encounter sufficient deformation due to large shear and bond slip behavior (Leon,

1990). This series of tests are analytically evaluated in Chapter 3.

Kazuhiro et al. (1991) found that joint performance is not improved by increasing transverse reinforcement when its sectional ratio is already above 0.4%. Kamimura et al. (2000) noted that the main role of joint transverse reinforcement after beam flexural yielding is to confine the joint concrete. In the specific investigation, joint transverse reinforcement was shown to have no influence on strength and deformation of interior BC connections, and had a marginal contribution to improving the longitudinal reinforcement bond conditions.

Kitayama (1992) proposed a tri-linear backbone from experimental force-displacement curves for explaining RC joint shear behavior as shown in Figure 2-6. He concluded that the first stiffness decrease (point A) is caused by the initiation of diagonal cracking in the joint panel; The second distinct stiffness decline (point B) is caused by the yielding of the longitudinal beam reinforcing reinforcing bar when both yield of beam reinforcement and joint shear failure occurred, or the joint transverse reinforcement when only joint shear failure is recognized; The third stiffness change is by the initiation of concrete crushing within the joint panel (point C). Based on the above definition, Kim and LaFave (2007) constructed a database for one-way joint specimens subjected to cyclic loading with at least a minimum amount of transverse reinforcement in the joint. Concrete compression strength was found to be the governing parameter of the shear strength.

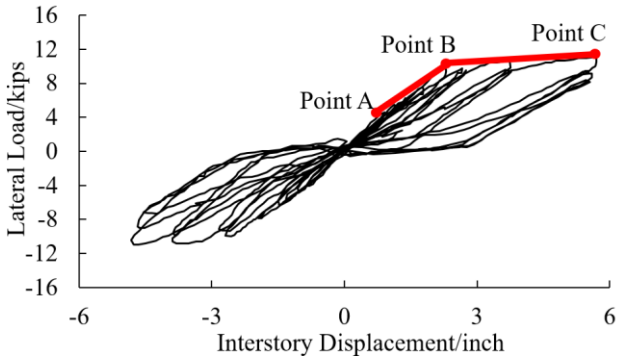

Figure 2-6 Distinct Stiffness Change Points (Leon, 1990)

Goto and Joh (2004) studied the influence of beam eccentricity on the shear failure mechanism by attaching a steel plate to the cover concrete of the beam to enforce shear failure of the joint. Joint shear strength was found to decrease with an increasing eccentric distance. Local concrete damage is found due to eccentric distribution on compressive and shear stress.

From the above references, there is a need to analytically verify the conclusions for properly confined interior BC connections from the experimental data. For example:

1. If increasing the transverse reinforcement ratio have influence on shear strength when its sectional ratio is above 0.4%;
2. If concrete compressive strength has the major influence on shear strength;
3. If there is an increased strength by using smaller transverse reinforcement at the same sectional ratio level;
4. If column axial load and longitudinal reinforcing bond have a minimal effect on joint shear strength.

2.3.3 Experimental Studies on Two-way Interior BC Joints

To date, extremely few experimental data are reported for RC two-way BC joints, with even less reported including slabs.

Leon (1985) tested fifteen two-way BCJ and concluded that beam geometry and floor slabs can have a significant influence on the behavior of BCJs. A monolithic slab provides additional negative moment capacity and confinement to the upper corner of the joint. Thus, it was bond deterioration rather than shear strength degradation that drove behavior in the latter part of loading. He determined that bond deterioration and yield penetration are important failure mechanisms which should be considered in design procedures.

Kurose et al. (1988) tested three BCJs with slabs under bi-directional loading, and stated that considerable pinching (a shape of joint hysteretic response that pinched in the middle due to the softening of the joint, for example, the curve shown in Figure 2-6) in story shear-drift angle relation observed in their tests was likely due to shear behavior in the joint, flexural behavior in the slab, beam and column cracking, and bond deterioration along beam bars. Bidirectional interaction was evident because loading in one direction brings damage and lowered the shear strength in the other direction. Moreover, the bottom longitudinal beam reinforcement lost bond capacity even though the column depth to bar diameter ratio was long (about 27 bar diameters).

Kitayama et al. (1988) tested two interior and one exterior beam-column-slab sub-assemblages under bi-directional cyclic loading. Due to the contribution from slab and also the two-way beams, the connections did not end up with joint shear failures despite a high shear stress level. The pinching effect in the global hysteretic response was due to a delay in crack closing because the authors regarded the bond condition as sufficient. The tensile force contributed by slab steel cannot be neglected, and also was found to exert torsional force on the edge beam.

Most of these observations need analytical verification to further explain the mechanism of the behavior. Several findings on joint shear strength also need to be proved including:

1. The way that beam width influence the joint shear strength;
2. If the amount of transverse reinforcement has little influence on two-way BC joints with slab;
3. If the development length of beam bar has no influence on shear strength of interior BC joint;
4. The reason that most interior-type joints with a beam reinforcement sectional ratio of 0.2 or more failed in shear prior to developing beam flexural yielding.

2.4 Numerical Investigation of Interior Beam Column Joints in RC Structures

Numerical simulation should be an efficient complementary tool to experimental research by capturing the interaction of large number of variables contributing to the behavior of an interior BC joint. It can also offer insights on the damage accumulation and failure mechanisms. Numerical models provide data and insights which are difficult or impossible to accomplish experimentally and play a significant role in understanding the joint behavior. Examples of where simulations are useful include finding the maximum bond slip location and value inside the joint, determining a continuous stress distribution along the reinforcement, indicating the first yield and rupture of reinforcement, and predicting the ultimate failure mechanism of the joint.

Many researchers have attempted to model the behavior of BC joints, and there are various numerical methods including simplified joint macro-models, nonlinear truss models, and finite element models. The accuracy of BC joint simulation mostly depends on the model's ability to capture joint shear deformation and bond-slip behavior.

2.4.1 Simplified Beam Model

Simplified beam models are efficient, especially for analyses of entire frames. The objective of beam models is to lump all the essential behavior of joints including beam/column flexure, joint shear and bond-slip behavior into a simple spring element.

The main approaches accounting for shear behavior for the simplified beam models include: 1) adding macro-level shear springs at beam ends to account for shear deformation of the joint, and/or 2) applying multi-dimensional constitutive concrete model which can capture the shear strain. The first approach is straight forward but highly empirical. The second approach is more

accurate compared with the first approach but still neglected the shear deformation of the panel (Feng and Xu, 2018), and need be combined with the joint macro model.

When accounting for bond-slip behavior, approaches include: 1) adding an empirical spring, which needs to calibrate parameters based on experiments; 2) adding an additional degree of freedom on the element to solve the slip-stress-strain field (Ayoub and Filippou 1999), which is elaborate and requires an iterative approach; and/or, 3) implicitly modify the strain-stress relation for reinforcement, which can only be applied within an assumed sufficient embedded length.

2.4.2 Simplified Joint Macro-models

Shear and bond-slip deflection, which are the major contributions of joint deformation, are the key factors that most simplified macro-models expect to simulate. Thus, the major task of these macro-models is to achieve realistic deformation and reaction force of the joint by properly defining characteristic curves for every component in the joint model. These components are trying to predict the deformation of the joints by semi-empirical equations. Some of these models, which are schematically illustrated in Figure 2-7, are described next.

Alath (1995) employed a single rotational spring (Figure 2-7(a)) at the intersection of the beam and column rigid end zones, with a tri-linear shear-strain relation to define the nonlinear behavior of the joint. The model was known as the “scissors model”. The pinching effect due to shear cracking and bond-slip behavior was further included by Pampanin et al. (2003) for this model. Models including strength degradation due to cyclic loading (Anderson et al., 2008) and shear resisting diagonal strut (Park and Mosalam, 2009) also have been developed based on the scissors model.

Biddah and Ghobarah (1999) applied two rotational springs at the beam-column intersection

(Figure 2-7(b)), one account for bond-slip effect and another for the shear deformation. Pinching due to concrete cracking and crushing near the bond was neglected in this multi-linear hysteretic model.

Youssef and Ghobarah (2001) represented the joint by four rigid members pinned at the corners (Figure 2-7(c)). Two diagonal springs were applied to account for the joint shear. Three concrete and three steel springs between each rigid element and beam/column members were utilized to account for the bond-slip behavior and concrete crushing.

Lowes and Altoontash (2003) defined a shear panel based on the modified compression field theory (MCFT). Three zero length springs between each panel edge and an interface element were applied to simulate the bond-slip behavior and beam-column interface shear (Figure 2-7(e)). Similarly, Altoontash and Deierlein (2003) simplified three zero length springs into one spring connecting the shear panel sides with the beam/column members, to account for member rotation during cyclic loadings (Figure 2-7(d)).

Based on the shear panel similar to those mentioned above, Shin and LaFave (2004) suggested one bond-slip spring on each side of the panel to account for bond-slip behavior, one plastic hinge rotational spring on each side to account for the inelastic deformation of beam, and one rotational spring at the corner of the panel to account for the shear deformation of the joint (Figure 2-7(e)).

Kim et al. (2017) extended a 2D RC BC joint model into a 3D macro-model, and validated the model with test results from beam-column-slab sub assemblages subjected to bi-lateral cyclic load. The hysteretic response captured considerable pinching effect compared with a rigid BC joint, but underestimated the joint strength approximately by 8% and the shear distortion by around 25%. Early degradation at larger lateral drift was observed in the analytical results compared with the test data. However, the slab is modeled by a T-shape beam section in this work, which cannot

simulate the bidirectional interaction. Moreover, the constraints added to the joint to simulate the extra stiffness from slab can only accurately capture the behavior with small deformations.

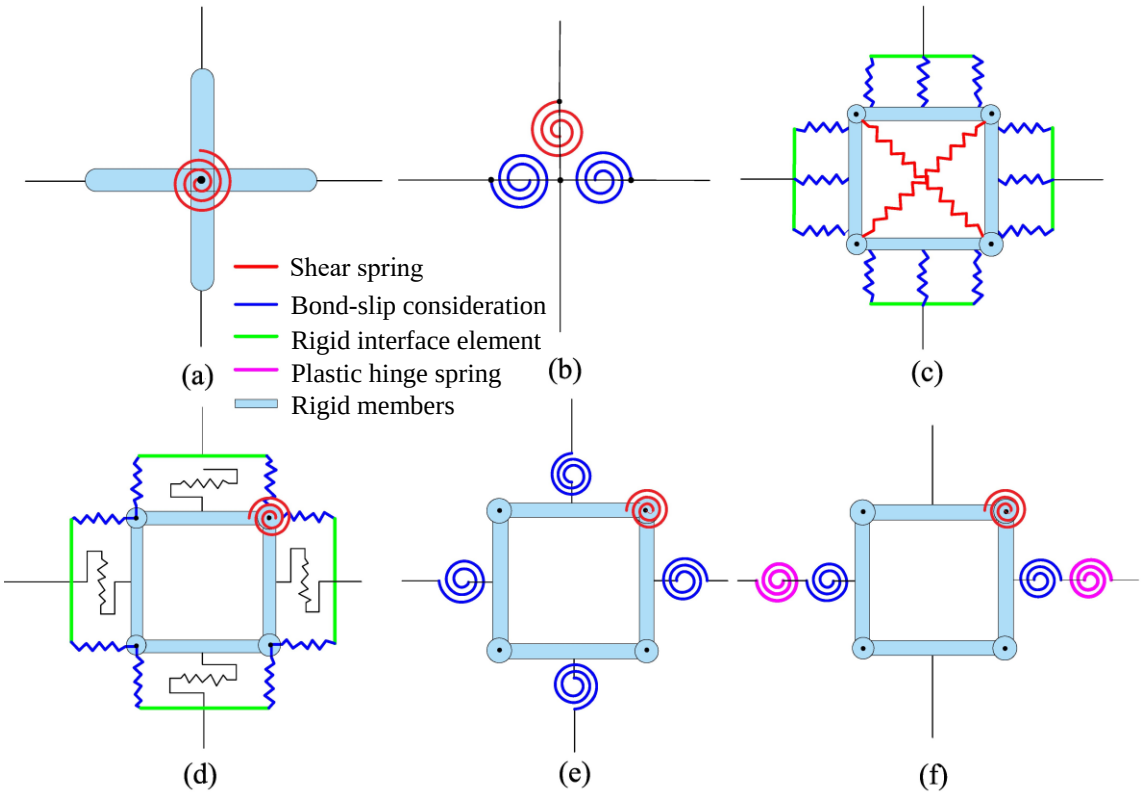

Figure 2-7 Existing macro-models for BC joints (a) Alath (1995); (b) Biddah and Ghobarah (1999); (c) Youssef and Ghobarah (2001); (d) Lowes and Altoontash (2003); (e) Altoontash and Deierlein (2003); (f) Shin and LaFave (2004).

One capability of these macro-models (Figure 2-7) is that they can be inserted into a frame analysis to capture the performance of the entire structure at a relative low computational cost. However, each spring needs significant calibration from existing experimental data, and there is no assurance of the accuracy for joints which have not been extensively tested. The physical meaning of few parameters in the model, which influence the hysteretic behavior and strength degradation subjected to cyclic loading, is ambiguous. Due to this inherent weakness, these models cannot be used to examine the damage or predict the true behavior of the joint. As a result, when

involved in a frame analysis, adopting the empirical response from experiments cannot provide realistic behavior of joints in the frame. In addition, multi-spring models have a high probability of inducing numerical divergence in the frame analysis. Beam column joints are frequently subjected to bidirectional lateral cyclic loading, and the above mentioned models are difficult to extend into 3D models. Thus, there is a need to establish a reliable analytical methodology, to provide calibration to the simplified joint model and release its dependence on experimental results.

The major advantage of empirical macro-models is their computational efficiency, which renders them attractive for simulations of multi-story buildings. However, the fact that these models require calibration with experimental test data implies that their predictive capabilities for configurations which have not been previously tested may be limited In addition, multi-spring models have a high probability of inducing numerical divergence in the frame analysis. Furthermore, the majority of these models can only be applied to one-way joints.

2.4.3 Nonlinear Truss Models

In nonlinear truss models, RC structures are represented by an assemblage of horizontal, vertical and diagonal nonlinear truss elements with properly defined constitutive law and material parameters. The horizontal and vertical truss elements are to represent the axial-flexural response of both concrete and reinforcement. The diagonal truss elements are to capture the inclined compressive stress field of concrete.

The origin of the truss methodology for reinforced concrete, initialized by Ritter and Mörsch in the early 1900s (Ritter 1899), was made up of a row of truss blocks alone the beam and inclined diagonal truss members inside each block. The diagonal truss elements are based on the assumption that cracks form in the same direction and thus create diagonal concrete struts in

compression.

The truss modeling approach was extended to a nonlinear analytical method for investigating the shear deformation of a 3-story framed-wall specimen under monotonic loading by representing each story with a single truss cell, together with two diagonal elements based on the crack pattern observed in the test (Figure 2-8) (Vallenas et al., 1979). Similarly, the hysteretic behavior of a flexural dominated shear wall under cyclic load was investigated (Hiraishi, 1984), with each story represented by a single truss cell. The strut mechanism based on a truss model was developed by Schlaich et al. (1987) for an exterior BC joint. A six-truss based model was presented by Hsu (1996) to allow for changes in the angle of inclination of the concrete struts. By placing multiple truss cells in each story, Mazars et al. (2002) examined the cyclic behavior of a shear wall.

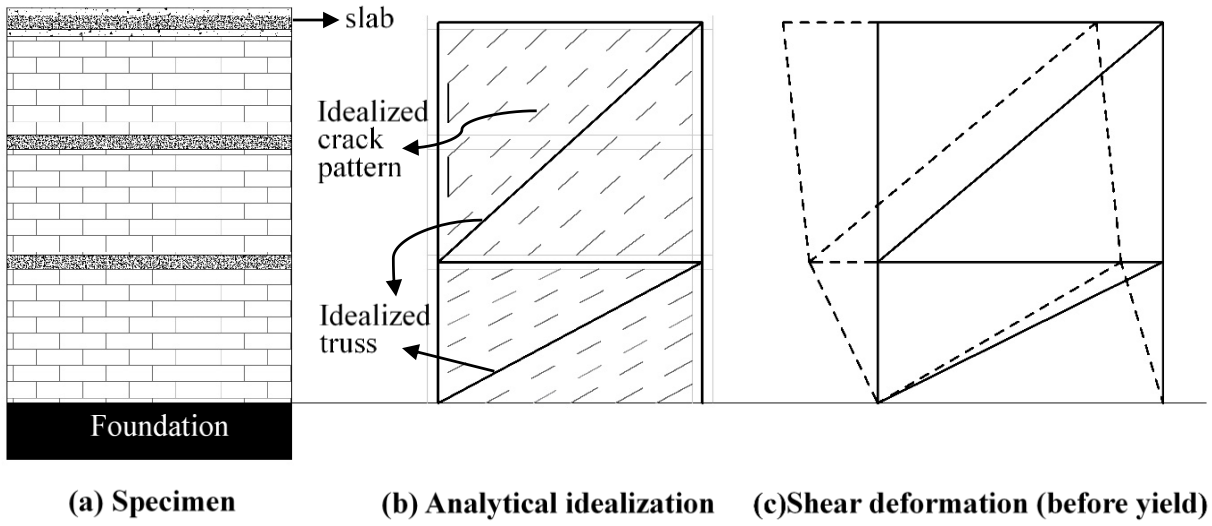

Figure 2-8 Idealization of the framed-wall specimen and shear deformation before reinforcing bar yield (Redrawn after Vallenas et al., 1979)

In the truss-based modeling approach from Park and Eom (2007), the material constitutive laws could capture confinement of concrete as well as buckling and rupture of reinforcing bar. The biaxial strain field on the concrete compressive behavior was based on the Modified Compression

Field Theory (MCFT) by Vecchio and Collins (1986).

Panagiotou et al. (2012) captured the hysteretic behavior and failure mode of RC shear walls using a nonlinear truss model. The geometry is based on simple repetition of the truss cells, thus could easily be applicable to various kinds of shear critical structures like shear walls, columns, beams and BC joints. The model has been extended by Lu and Panagiotouto (2014) to account for triaxial response of shear-wall structures, and thus is able to capture out-of-plane flexural behavior of walls under static and dynamic loadings.

A nonlinear truss model is quite efficient and at the same time is powerful enough to capture the shear-axial-flexure interactive response of RC structures. Reliable results have been obtained for RC structures such as a shear wall under seismic load subjected to cyclic loads (Mazars et al., 2002), nonplanar T-shaped wall (Panagiotou et al., 2012; Lu and Panagiotou, 2013), cantilever column and beam member (Miki and Niwa, 2004), shear dominated column (Moharrami et al. et al., 2015), twenty-story building subjected to earthquake load (Lu 2004).

Bowers (2014) extended the nonlinear truss analogy into non-ductile interior and exterior BC joints, and validated against three poorly-detailed RC BCJs. The analytical results were in satisfactory agreement with the experimental data including initial stiffness, strength and damage pattern (Figure 2-9) and satisfies both efficiency and capability of capturing shear and bond-slip behavior in the joint. The importance of including joint confinement and bond-slip behavior is validated. It was pointed out that there is a need to extend the model scheme to more ductile BCJs with modern design and validate against the strut and panel-truss force transferring mechanisms with a more refined bond-slip model, and also compare with more refined finite element results.

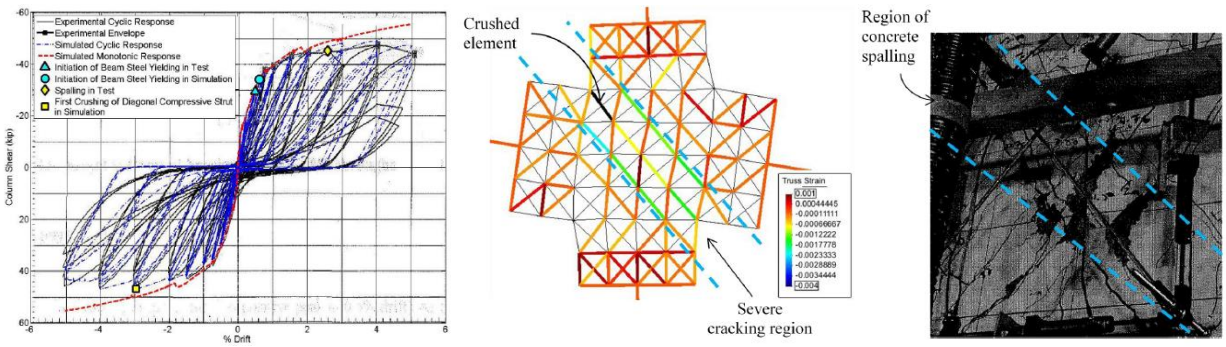

(a) Comparison of hysteretic response (b) Concrete crushing in analysis (c) Concrete crushing in test

Figure 2-9 Analytical results for interior BCJ by nonlinear truss model (Bowers 2014)

Based on the previous studies, there is a need to extend the nonlinear truss methodology to the interior BC joints to capture the variety of failure mechanisms. Further refinement referring to confinement of concrete and column axial level should be enhanced. Also, a more refined bond-slip model should be applied to study the local bond-slip behavior under cyclic loads.

2.4.4 Finite Element Models

The most refined analytical method for capturing the behavior of BC joints is based on nonlinear, continuum-based, finite element analysis (Cofer, 1999). The finite element method is a powerful tool which enjoys a variety of advantages such as a continuum representation of the of parameters of interest (such as stress, strain, damage etc.) throughout the whole model and the whole timeline, be able to launch collapse analyses which are inaccessible for experiments, applying various of loading combinations efficiently, economically and efficiently friendly, can satisfy any form of layout like including a slab etc. The inherent reason of these powerful capability is the reliability and accuracy of FE model in simulating the authentic behavior of real structures if being properly defined. This approach has become increasingly accessible due to the growing capacity of computers. As summarized in Section 2.3, properly capturing the bond-slip and shear

behavior are the two major tasks for analytical simulations on interior BCJs. At the same time, an accurate constitutive model for concrete is the fundamental requirement of capturing realistic behavior of BCJs.

2.4.4.1 Constitutive Model of Concrete

Based on the force transfer mechanisms and experimental observations summarized in previous sections, there are several important aspects that should be included in simulation to obtain realistic response of interior BCJs: 1) An accurate expression of concrete under triaxial compressive stress state is fundamental to simulate its increase in compressive strength, ductility and inelasticity, especially for concrete in the joint with high confining pressure contributed by transverse reinforcement and that in plastic hinge regions with significant compressive strains; 2) The irreversible accumulative inelasticity of concrete in compression is essential to account for compressive damage and concrete crushing, as well as the strength degradation due to concrete cracking; 3) Crack opening and subsequent closing under cyclic loading is crucial to be included, especially for the large diagonal crack in the joint and vertical crack at the beam-column interface. For instance, the previously opened crack at beam-column interface will be closed due to bond-slip behavior of beam longitudinal reinforcing bar under cyclic loading, to allow force transferring between compressive blocks and thus trigger the strut mechanism.

Typically, the most efficient way to simulate RC structures is to apply a uniaxial stress-strain law for concrete, and include the confinement effect by adjusting the parameters from the uniaxial material model. However, this simplification inherently lacks the capability of capturing multiaxial stress state of concrete in BCJs.

There have been various attempts to capture multiaxial stress states of concrete by defining

constitutive laws through continuum-based finite element analysis, while it is challenging to include all three aspects mentioned above:

1. When referring to the confinement effect, previously existing models 1) only make modification for minimum principal stress in compression (Selby and Vecchio 1997); 2) requires a large amount of history variables by utilizing the microplane model (Caner and Bažant 2012a) and considerably overestimated the damage and strength degradation (Eligehausen et al. 2006).

2. When considering compressive and tensile damage of concrete, previous models 1) don't include this effect (Selby and Vecchio 1997); 2) based on single scalar damage parameter and apply same strength degradation for tensile and compressive concrete (Murray 2007; Karagozian Valentini and Hofstetter and Case concrete model such as Malvar et al. (1997)); 3) Underestimate the stiffness and strength under cyclic loading (Valentini and Hofstetter 2013).

3. When regarding to crack opening and closing, previous models cannot lead to sufficient crack closure with unloading before compressive stress develop (Lee and Fenves 1998).

Many other similar models have been utilized for monotonic loading or cyclic loading at material level (Kang et al. 2000; Nguyen and Korsunsky 2008; etc.).

A recently proposed traxial constitutive model for concrete, has been validated to be able to capture all the aspects of behavior listed above by comparing single-element analytical stress-strain curve with experimental and empirical model (Moharrami and Koutromanos 2016). Further validations were conducted with experimental results for column, BCJ and wall under cyclic loading and earthquake loading (Moharrami and Koutromanos 2017). Its abilities in capturing triaxial compressive stress state of concrete under confinement, accumulative inelastic

compressive strain with concrete crushing, crack opening and closing are essential for simulating two-way BCJs subject to bidirectional cyclic loading. This concrete model will be introduced in more details and utilized in the FE scheme in Chapter 3.

2.4.4.2 Simulation of Bond-slip Behavior

Ngo and Scordelis (1967) where the first to account for the bond-slip behavior in finite element analysis. Various studies such as Beckingsale (1980) and Leon (1984) have verified the significant contribution from bond-slip behavior to lateral displacement of BCJs, especially when the joint is subjected to cyclic loads.

The main approaches that have been proposed for accounting for bond-slip effect include: 1) adjusting stress and stiffness of the reinforcement to implicitly simulate the decreased stress due to bond-slip behavior; 2) separate the joint and beam/column and build springs at the interface; 3) describe bond stress-slip relations explicitly and insert connecting elements between reinforcement and concrete.

Based on the first approach, Fleury et al. (1999) modified and implemented the bond-slip law by Eligehausen et al. (1983) into the constitutive law of the steel reinforcement. The bond-slip law is only invoked within the joint and extended into the beam for a short distance. The overestimation of bond strength as well as the insufficient ability for smeared crack model to capture joint shear distortion resulted in a lack of pinching effect. Also, this method is only suitable if the bond slip is caused by anchorage failure but not strain penetration, because the adjusted stress cannot capture the inelastic strains well.

By using the second approach, Sritharan et al. (2000) showed modelling improvement by applying nonlinear spring elements in modeling bond-slip behavior. Supaviriyakit et al. (2007)

applied a one-dimensional discrete interfacial joint element between the column and beam in the WCOMD software to model large vertical cracks and bar pull out observed in the test. It has to be pointed out that the force-displacement relation of those interface element relies on empirical formula, and needs calibration of parameters based on experiments.

The third approach, which is the most straight forward method, aims at capturing strain penetration in the longitudinal bar and the relative displacement between reinforcement and concrete. Simplified elastoplastic relation (Moharrami, 2016), monotonic backbone curves (Eligehausen et al., 2006; Noguchi 1981) or hysteretic relations (Deaton 2013) can be used to simulate the stress-slip degradation. However, these bond-slip models cannot capture the deterioration due to cyclic loading.

The attempts in analytically simulating the bond-slip behavior by the third approach mentioned above are explained with more details as follows.

A 2D analytical FE model was built by Noguchi (1981) to study the nonlinear behavior after the initiation of the inclined diagonal crack in the joint panel. The model pre-implanted shear interfaces based on the cracking observed in experiments and utilized a monotonic bond-slip model for the beam longitudinal bars. Strain penetration was observed when poor bond conditions existed.

A nonlinear 1D contact element was inserted between steel and concrete to perform parametric studies on joint transverse reinforcement by Pantazopoulou and Bonacci (1994). Modified Compression Field Theory (MCFT) was applied for concrete, and the bond-slip curves can only account for two bond conditions, namely satisfactory and unsatisfactory bond condition. Analysis showed the joint core concrete resistance decreased with more transverse steel.

The experiment of two-way BC joints with slab launched by Kitayama et al. (1988) was analyzed by Noguchi and Kashiwazaki (2004) to study the influence of bond-slip model. The

results of two bond-slip conditions were compared, namely a “normal bond condition” applying the bond-slip law by Morita (1975) and “perfect bond” condition. The model with perfect bond was found to have overestimated the strength, while the model with the “normal bond condition” failed to converge at large drift levels due to numerical problems, which is a common and important issue in the unsuccessful simulations of bond-slip behavior.

In the analysis of Eligehausen et al. (2006), the cyclic bond-slip effect was explicitly accounted for by a specific element. However, both the analysis and the bond-slip relation were monotonic, the backbone obtained undergoes faster degradation than what was observed in the experiment, and the results overestimated the ultimate strength by 20% when the joint encountered shear failure.

Noguchi et al. (2008) investigated the joint behavior in a frame as well as the influence of beam eccentricities on seismic performance of BC joints through a 3D nonlinear analysis. The bond-slip effect was accounted for through the introduction of spring elements, using the law by Morita (1975). Higher shear stress was observed in the analysis under bi-directional load compared with another 2D planar model using shell element. Pinching of hysteretic curve was properly obtained, while the initial stiffness was overestimated and the strength during post-peak cycles was underestimated. Yielding of the bottom reinforcement in the beam was found before that of the top reinforcement due to the existence of the slab.

Deaton (2013) employed a three-dimensional FE model to investigate the behavior of non-seismically detailed RC exterior BC joints under bidirectional cyclic loads. An interface element was applied to model bond-slip behavior in DIANA with hysteresis rules. However, the bond-slip law didn’t account for degradation due to cyclic loading as well as the transverse effect due to lateral confining pressure.

A 1D contact element was used by Bao et al. (2014) to simulate a BCJ under column-removed scenario which subjected to monotonic loading. The bilinear relation was applied to bond-slip model, which is not suitable to extend to cyclic cases. The same method was applied by Alaee et al. (2015) in simulating 3D interior and exterior BCJs under cyclic loading. Due to the simplification in bond-slip model and concrete cracking, the pinching effect was excessively underestimated.

2.4.4.3 Simulation of Shear Behavior

The primary methods to account for the shear behavior of joints in 3D finite element models includes: a) applying a reduction factor on the shear modulus of concrete; b) explicitly add a specific element to simulate the shear deformation; c) discrete-crack model by adding pre-specified diagonal shear crack and interface cohesive elements; d) smeared-crack model for continuous elements.

By the first method, Hegger et al. (2004) incorporated a shear retention factor to account for the reduction in shear modulus due to shear crack opening, and an effective compressive strength reduction factor α_c due to cracks parallel to the compressive strut in the joint. The bond-slip behavior was accounted for via local deformation adjacent to concrete. Tajima et al. (2004) performed both 2D and 3D analysis of the experiment lunched by Tajima et al. (2000). A link element accounting for the bond-slip behavior was explicitly simulated. The simulation was performed utilizing only a monotonic curve due to computational difficulties after including the bond-slip elements. Since the specimen encountered mainly shear failure, and the shear strength degradation was only simulated by the reduction of shear modulus, the 3D analysis overestimated the shear capacity of the joint. Also, the reduction of shear modulus by the factors heavily relied

on the existing experiments.

By the second approach, Elmorsi (1998) modeled the joint core by a single twelve-node element embedding a cubic displacement field to account for the shear deformation, which depends on empirical formulations and cannot be accurately applied on models until experimental counterparts are tested. Four ten-node transition elements surrounding the joint are applied to connect with the beam/column members. Bond-slip behavior was accounted for by the link elements between truss elements representing for the steel and nodes around both joint and transition elements representing for the concrete.

The third approach has been applied in shear dominated structures with quasi-brittle materials such as masonry wall, short concrete column (Koutromanos et al. 2011) and RC joints (Kashiwazaki and Noguchi, 2004; Zhang et al. 2002). Pre-specified diagonal shear cracks, together with a smeared crack concrete model and link elements accounting for the bond-slip behavior has been proved to be able to accurately represent the backbone curve of the hysteretic response from test results. Named as the Noguchi prototype (Deaton 2013), this series of models utilized an orthotropic hypo-elastic concrete model which incorporating the equivalent uniaxial compression curve concept by Darwin and Pecknold (1977), with the ascending portion defined by Saenz (1964) and a post peak softening portion by Park et al. (1982). The Willam (1975) yield surface under triaxial stress was applied by calibrating five corresponding parameters. The tension stiffening was defined according to Sato (1978) and the bond-slip model according to Morita (1975). A compressive strength reduction factor defined by Ihzuka (1992) was utilized for cracked concrete. Cyclic concrete behavior was governed by the hysteretic relation from Naganuma and Ohkubo (2000), and cyclic steel followed Menengotto (1973) model which do not account for cyclic deterioration. Even though the models above which accounting for bond, smear cracking, and

discrete diagonal cracks, most parts of the models contained various simplifications and could only get satisfactory results with monotonic loading. The strategy that utilizes accurate constitutive laws for all materials to account for all necessary behavior is quite powerful and meaningful when properly calibrated to capture the hysteretic response of the BC joint subjected to cyclic loadings.

The fourth approach, which includes fixed/rotating smeared-crack model, and models stand between both such as a disturbed Stress Field Model (DSFM) (Vecchio 2000), is used together with different concrete and steel models in analysis. Previous research (Lotfi and Shing, 1991; Bazant and Planas, 1997) has indicated that continuum-based, smeared-crack models suffer from the stress lock-in effect when dealing with strongly localized cracks. Nevertheless, the choices of concrete model, reinforcement and bond-slip model become more important in simulating the well confined BCJs with high triaxial compressive pressure subjected to cyclic loading. For example, the microplane model (Ožbolt et al., 2001) used by Eligehausen et al. (2008) for the concrete material is difficult to calibrate given the parameters involved, and changing the values of some parameters may lead to unpredictable results for the model. Also, some studies show that it failed to converge around half of the ultimate lateral drift (Sharma et al., 2011). Hawileh et al. (2010) developed a 3D FE model for precast BCJ in ANSYS. The model failed to capture the reinforcing bar rupture failure in the test due to several simplifications in the model. Such simplifications included turning off concrete crushing to avoid numerical difficulties and modeling the reinforcement using hexahedral solid elements that cannot account for rupture.

By combining a concrete model that can account for triaxial stress state under cyclic loading (Moharrami and Koutromanos, 2016) and a non-iterative reinforcement model which can account for buckling and rupture (Kim and Koutromanos, 2016), a model that can captured the concrete crush and bar buckling behavior properly and successfully validated the results of RC components

in static and dynamic tests was established.

Table 2-2 summarizes the aforementioned analytical studies with abbreviation descriptions listed afterwards. Given the aforementioned issue in simulating shear behavior, there is no satisfactory model that could accurately obtain large shear deformation and cracks for beam-column joints. The existing models are either too simplified and highly empirical, or contains complicated parameters and have difficulties in applying the cyclic loads.

2.5 Bond-slip Behavior of BCJs Subjected to Cyclic Loads

The prior research on complicated failure processes and existing models of bond performance based on pull-out tests subjected to cyclic loading has been summarized in state-of-the-art reports by *fib* (2000) and ACI408.2R-12 (2012).

There are two typical bond failure modes under cyclic loading: a) pull out failure due to shearing of concrete between ribs, and b) splitting of the concrete cover. Pullout occurs when sufficient concrete cover and transverse reinforcement prevent the growth of splitting cracks. Splitting occurs when insufficient confinement of concrete prevents the full pullout strength to be attained (ACI408.2R-12, 2002).

The cyclic load arising from seismic excitation is categorized as low-cycle high-amplitude fatigue, which means the structure is subjected to a low number of cycles at high stress or slip levels with relatively low strain rates (*fib*, 2000). Low strain rates refer to the fact that seismic loading results in strain rates substantially lower than that for blast, which is another common loading condition. The bond strength is significantly reduced under cyclic loading when compared with that in monotonic loading, and further deterioration was observed with increasing number of cycles in experimental studies by Eligehausen et al. (1983) and Viwathanatepa et al. (1979).

Table 2-2 Summary of Analytical Studies for Interior BC Joints

Author and year	Joint Type	Ties in joint	Loading Pattern	Failure Mode	Software	Concrete in Compression	Concrete in Tension	Concrete Element	Steel Model	Crack Model	Bond-slip Model
Noguchi 1981	1W	TR	UNI/MON/AX	JS/BS/BF	NA	Darwin	2L	2D	2L	DC	BL
Noguchi and Kashiwazaki 1982	1W	TR	UNI/MON/CYC/AX	JS/BS/BF	NA	Darwin	2L	2D	2L	DC	BL
Kwak and Filippou 1990	1W	TR	UNI/MON/CYC/AX	BS	Author	Darwin	Author	2D	2L/SH	SMR	3L
Conley 1993	1W	N	UNI/MON/AX	JS	Abaqus	Plasticity	TS	2D	embeded	SMR	perfect
Pantazopoulou and Bonacci 1994	1W	TR	UNI/MON/AX	JS/BS/BF	NA	MCFT	TS	2D	3L	SMR	3L
Elmorsi 1998	1W	N/TR	UNI/CYC	JS/BS/BF	PC-ANSR	NA	TS	2D	MEN-PIN	SMR	Eligehausen
Fleury et al. 1999	1W	TR	UNI/CYC/AX	JS/BS	Aster	Plasticity	NA	2D	SH	SMR	Fleury
Zhang et al. 2002	1W	TR	UNI/MON/AX	JS/BF	DIANA	Darwin/Kupfer	Sata-Shirai	2D	2L	SMR/DIS	Morita-Kaku
Li et al.2003	1W	N	UNI/CYC/AX	JS/BF	WCOMD	Plasticity	Hajime	2D	Kato	SMR/FI	Hajime
Hegger et al. 2004	1W	N/TR	UNI/MON	JS/BS	ATENA	Kupfer	NA	2D	EPP	SMR	NA
Goto and Joh 2004	1W	TR	UNI/MON/AX	JS	DIANA	MC90	Hordijk	2D	SH	SMR/FI/NO	MC90
Noguchi and Kashiwazaki 2004	2W	TR	UNI/CYC/AX	NA	Author	Darwin/Saenz	Sata-Shirai	3D	MEN-PIN	SMR/FI/RO	Morita-Kaku
Tajima et al.2004	1W	TR	UNI/MON	JS	DIANA	Drucker	Oh-oka	3D	2L	SMR/FI/NO	MC90/Kaku
Eligehausen et al.2006	1W	TR	UNI/CYC	JS/BF	MASA	Ožbolt	NA	2D	3L	Ožbolt	Eligehausen
Kim and Vecchio 2008	1W	N	UNI/CYC	BF	VecTor2	Distributed	2L	2D	Seckin	SMR/RO	Perfect
Li et al.2009	1W	N	UNI/CYC	JS/BF/BS	DIANA	Drucker	2L	3D	EPP	SMR/FI/NO	MC90
Noguchi et al. 2008	2W	TR	UNI/BI/CYC	JS/BF/BS	Author	Darwin	Naganuma	3D	MEN-PIN	SMR	Morita-Kaku
Sagbas et al. 2011	1W	TR	UNI/CYC	JS/BS/BF	VecTor2	DSFM	Bentz	2D	Seckin	SMR	Eligehausen
Deaton 2013	2W	TR	CYC	JS/BS	DIANA	MCFT	TS	3D	EPP	SMR/RO	MC90
Bao et al. 2014	1W	TR	MON	BF/BS	LS DYNA	CSCM	CSCM	3D	2L	CSCM	BL
Alaee et al. 2015	1W	TR	CYC	BF	DIANA	Drucker	MC90	3D	2L	SC	MC90

Category	Parameter Description
Joint Type	1W/2W:one-way/ two-way;
Ties in Joint	TR/N: with/without transverse steel in the joint;
Loading Pattern	UNI: one direction; BI: bi-directional; CYC: cyclic loads; MON: monotonic loads; AX: column axial load applied
Failure Mode	JS: joint shear; BS: bond-slip; BF: beam flexural
Concrete in Compression	Darwin: Darwin-Pecknold; MCFT: Modified Compression Field Theory; DSFM: Distributed Stress Field Model; Kupfer: biaxial failure criteria; MC90: CEB-FIP Model Code 1990 model; Drucker: Drucker-Prager yield surface; Ožbolt: Microplane model; CSCM: continuous surface cap model;
Concrete in Tension	2L: bilinear; TS: Tension Stiffening;
Concrete Element	2D: two dimensional; 3D: three dimensional;
Steel Model	2L: bilinear; 3L: trilinear; SH: Strain Hardening; EPP: Elastic Perfectly Plastic; MEN-PIN: Menegotto-Pinto;
Crack Model	SMR: Smeard Crack Model; DC: Discrete Crack Model; FI: Fixed Smeared Crack Model; RO: Rotating Smeared Crack Model; NO: Non-orthogonal Smeared Crack Model; SC: simplified stress cut off
Bond-slip Model	BL: one-dimensional Bond-link Element; 3L: trilinear; MC90: CEB-FIP Model Code 1990

The bond slip damage development under cyclic loads (Eligehausen et al., 1983) is illustrated in Figure 2-10. Before a shear crack develops in the concrete key (Figure 2-10(a)), the loading line OA is exactly the same as the monotonic curve. After unloading along path AF (Figure 2-10(b)), a gap with a width equal to the slip at point F remains open because only a small portion of the slip caused by elastic concrete deformation is recovered. When the frictional resistance is overcome (Point G), the bar slips in the opposite direction and begins to bear in the opposite lug. Due to the resistance from the concrete lug at point H, there is a sharp rise in stiffness (path HI). The closing of previous crack allows nearly no degradation on bond strength, which means path HI is highly close to the monotonic curve. When the loading is reversed, the path IKL is similar to path AFH earlier, and the bond strength starts to increase again at L when the lug starts to press against the broken piece of concrete. Lug and concrete are in fully contact at M, and the monotonic envelope is reached again after path HI.

The first cycle follows path OABC (Figure 2-10(d)) if the slip is reversed after shear crack initiates (Figure 2-10(c)) and the bond resistance is reduced when compared with monotonic curve (path CFGHI). When reversing the slip again (path IKLMN), the remaining parts of the concrete between the lugs is sheared off, resulting a lower strength than point I.

Figure 2-10(e) assumes a large slip during the first circle (path OABCD), wherein the concrete key is almost completely destroyed in the first excursion. When loading reversely (path DGHIJ, Figure 2-10(f)), the resistance at J is similar to the ultimate frictional resistance during monotonic loading because there is almost no concrete key left. After reloading along the path JKLMNP, even lower bond strength is reached because the concrete rugosity is smoothed in the first circle. From then on, bond is lost over a long length and the bars are free to slide (or slip) through large displacements.

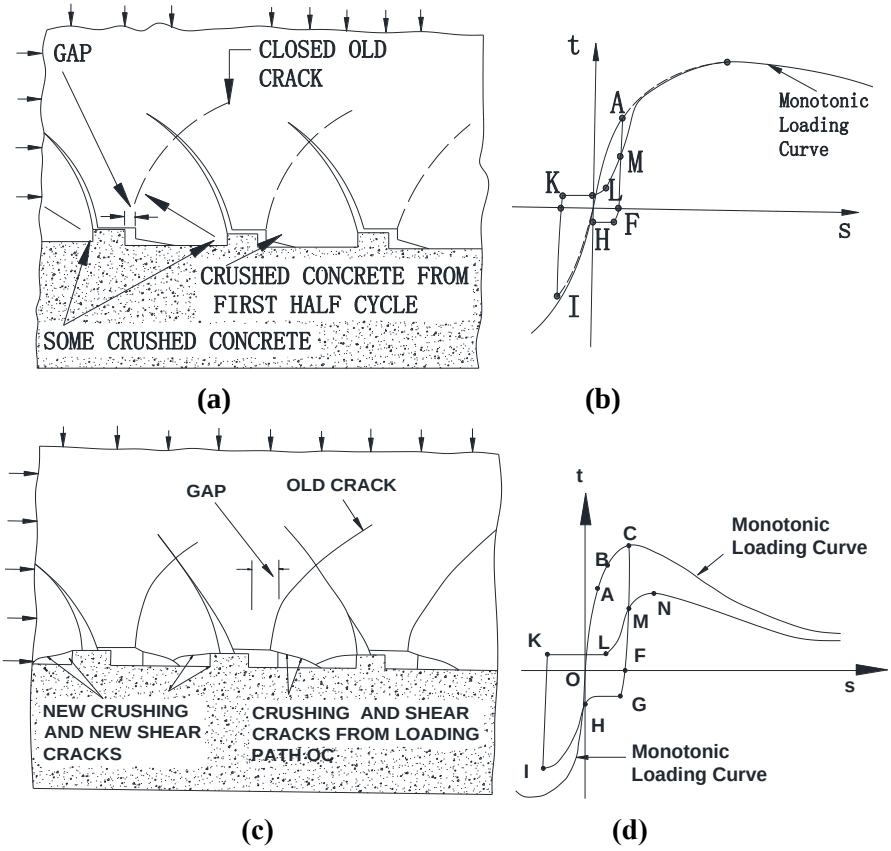

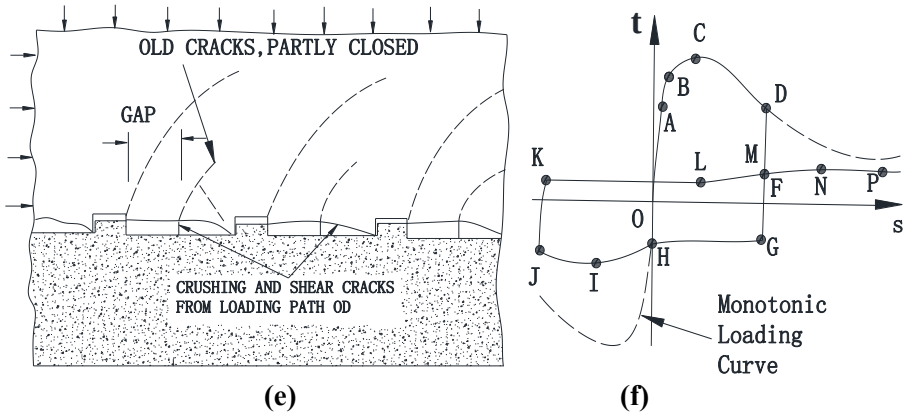

Figure 2-10 Bond Slip Damage Development under Cyclic Loads (Redrawn after Eligehausen et al., 1983)

Numerous factors are found to have effect on the deterioration of bond strength under cyclic loads (ACI408.2R-12, 2012) such as: concrete compressive strength, concrete cover, bar spacing, bar size, yield strength and transverse rib of bar, development length, the amount and distribution of transverse steel, strain/stress range of bond, type and rate of loading, construction quantity etc.

2.6 Modeling of Bond-Slip Behavior

There is no single unifying theory or model capable of including all relevant parameters summarized above due to their sophisticated interactions. Some hysteretic constitutive bond stress-strain relations have been developed to incorporate various aspects of these contributing factors, and have been involved in numerical simulations of BC joints. Bond-slip models have been classified into three categories: rib-scale, bar-scale and model-scale (Cox and Herrmann, 1998).

2.6.1 Rib-scale Models

Rib-scale models aim to develop the interaction between the concrete and the deformed bar by explicitly modeling the detailed geometry, including the ribs.

Continuous elements are applied to represent both the concrete and the deformed ribs of reinforcing bar to study the interaction between the two materials. Detailed definition of bar geometry and properly defined constitutive laws for concrete and steel are essential for these models. Other detailed local properties like contact conditions (Reinhardt et al., 1987), the steel-concrete transition zone (Okamura and Pimanmas, 2003), and the cement and aggregate phases inside concrete (Daoud et al., 2012) have been included in some of these research series to investigate the intrinsic characteristics of bond behavior.

It is obvious that rib-scale models are too computational expensive for analysis of RC sub-assemblages and structures. Also, the uncertainties related to friction, contact definition and the simplified concrete model may not yield precise results of concrete crack.

2.6.2 Bar-scale Models

In bar-scale models, a stress-relative displacement law is applied to a link element between concrete and reinforcement either with a continuous or discontinuous connection. This modeling approach is suitable for parametric studies of bond-slip effect inside structural members.

1. Continuous connection-smeared approach

   In the case of continuous connection, perfect bond is assumed between steel and concrete. The bond-slip behavior is stored either in the constitutive law of concrete which is modeled by two- or three-dimensional finite elements, or the reinforcement which is always modeled by truss or beam element.

   When storing the local bond stress-slip relation in a reinforcement constitutive model, a weighted residual method was proposed by Filippou et al. (1983) to approximate the displacement and stress field by shape functions; a flexibility-based finite element formulation

was proposed by Monti et al. (1997) to estimate the bond and bar stress field.

The strong influence of mesh size lay in this approach was minimized either by the so called crack band approach (Bažant and Oh, 1983), which assumes that the total energy dissipation of bond-slip behavior is localized into a shear band, or higher order methods (Bažant, 1991) which localized the damage into a volume of the material whose size is independent of mesh size (Mazars et al., 1990).

2. Discrete connection-bond interface approach

In this approach, the bond-slip behavior is explicitly accounted for by links between two materials. Local behavior of ribs such as crushing, shearing and radial cracking are lumped into the average stress-relative displacement relation between steel and concrete. The actions between two ribs are summarized as a tangential bond stress and a normal compressive stress. These shear and normal stresses are coupled due to the wedging effect of the ribs. Since the bond resistance (tangential component) depends on the normal component which reflects effects such as the confinement, the shear dilatation was extracted to account for the wedging action (Cox and Herrmann, 1998; Serpieri and Alfano, 2011; Murcia-Delso et al., 2013).

Early phenomenological models are limited to well-confined conditions with the pullout failure of the bar, which defined a monotonic nonlinear relation of bond stress and slip (Rehm, 1961; Eligehausen et al., 1983). Several methods were developed to account for the bond stress degradation due to cyclic slip, such as:

1) By damage parameter depends on the energy dissipation of bond-slip (Eligehausen et al., 1983), the maximum slip and the number of cycles (Lowes et al., 2004);

2) Scale the bearing and friction contribution to the total bond resistance independently based on the maximum slip and the number of cycles (Pochanart and Harmon, 1989);

3) By two damage parameters based on the slip history (Murcia-Delso et al., 2013).

Some of these models has been implemented into software, like OpenSees (Lowes et al., 2004); DIANA (Santos and Henriques, 2012), Abaqus and LS-DYNA (Murcia-Delso and Shing, 2014).

2.6.3 Member-scale Models

Member-scale models try to account for the relative movement between structural members by rotational springs or special element formulations, which is designed for the analysis of large structures, and highly depends on the calibration with existing experiments.

Monti and Spacone (2000) proposed a force-based fiber element to account for both bar strain and bond-slip. The beam section was assumed to be remain plane, and the model is suitable for various section as well as bidirectional loading. Lowes and Altoontash (2003) formulated a two-dimensional finite element model (Figure 2-2d) to account for bond-slip behavior by nonlinear springs. Similar strategies were used in representing the rotation at column foot (Zhao and Sritharan, 2007), or joint open due to slip and bar elongation due to strain penetration (Sritharan et al., 2000).

2.7 Summary

This chapter firstly reviewed the force transferring mechanisms of interior BCJs (Section 2.1) and compared briefly four design codes from different parts of the world with respect to the six aspects that significantly influence the performance of interior BC joints (Section 2.2). Relevant experimental investigations on non-ductile and ductile interior BC joints were then summarized (Section 2.3), emphasizing observations on bond-slip and shear behavior. The results of those research efforts indicate the necessity of accounting for both bond slip and shear cracking in

analytical simulations. The summary also indicated that there are limited experimental studies on two-way BC joints with slabs, which is the most realistic case.

Numerous analytical simulations were summarized in Section 2.4, with respect to simplified beam models, joint macro-models, nonlinear truss models and finite element models. Beam models and macro-model are efficient for analyses at the structural system level but rely on empirical relations in dealing with shear behavior in the joint, and cannot sufficiently capture the deterioration due to bond-slip behavior. The nonlinear truss model satisfies both efficiency and the ability of capturing shear and bond-slip behavior in the joint is properly defined. Thus, this methodology is chosen as the efficient choice of simulating the interior BCJ in Chapter 4.

The finite element analysis is the only option to study the joint behavior in detail, especially for those cases lacking sufficient experimental data such as 2-way joints with slabs. Despite that the ability of capturing extremely localized shear cracking is limited by continuum-based model, the right choice of concrete and reinforcement models still plays a significant role in a successful simulation. The majority of existing constitutive models are complicated to calibrate, particularly for the parameters in the concrete model, and it is hard to ascertain a priori if they can capture the triaxial stress state in the joint core and if the reinforcement models can capture rupture of the reinforcement when the concrete has relatively high compressive strength and leads to a high stress in steel. Since the joint is confined by four framing beams, a shear failure of the joint becomes a less dominant failure mode than the bond-slip behavior. In bidirectionally loaded columns, the anchorage demands for the corner bars could be sustainably higher than those in the beams (Leon and Jirsa, 1986), which also needs further verification in analysis.

Section 2.6 summarized different simulation methods for bond-slip models. Although the aforementioned studies have applied three-dimensional FE analysis for both one-way and two-

way interior BC joints, the bond-slip behavior was either not accurate enough when implanted into the concrete or steel constitutive law, failed to converge for large lateral displacement and/or could not account for cyclic deterioration.

Chapter 3 Finite Element Analysis of Interior Beam Column Joints

The literature review in Chapter 2 indicates that computational simulation is necessary to supplement experimental tests for obtaining an understanding of the behavior and damage patterns in beam-to-column (BC) joints, and for verifying the adequacy of modern seismic design provisions for such components. Continuum-based finite element models are the most reliable means for predicting the cyclic hysteretic behavior and damage accumulation, provided that the employed constitutive laws can account for all significant aspects of material behavior, e.g., concrete cracking and compressive crushing, reinforcing bar yielding, and bond-slip behavior.

This chapter describes a three-dimensional finite element modeling scheme for the analysis of beam-to-column joints based on the explicit finite element method, and its validation against experimental test data. The modeling scheme has been implemented into the commercial program LS-DYNA (LSTC 2007).The chapter begins with the description of the constitutive models used for the concrete, reinforcing bar, and bond-slip behavior, followed by validation using the results of experimental tests by Leon (1989) and Kurose et al. (1988). The validation analyses are accompanied by a sensitivity study, to investigate the impact of various model parameter values on the obtained analytical results.

3.1 Description of Modeling Scheme

3.1.1 Constitutive Model for Concrete

The constitutive model proposed by Moharrami and Koutromanos (2016) is used to describe the concrete material behavior. The model combines an elastoplastic law and a rotating smeared-

crack formulation, and can account for the cyclic crack opening and closing, the deterioration of concrete due to crush, the effect of confinement on the compressive strength and ductility of the material.

3.1.1.1 Uncracked Elastoplastic Law of Concrete

A modified yield criterion (MYS for short) was proposed (Moharrami and Koutromanos 2016) which the elastoplastic law relies on:

$$f\left(\{\hat{\sigma}\},\kappa\right)=\frac{1}{1-\alpha}\left[\alpha\cdot I_1+r\left(\theta,e\right)\sqrt{3J_2}\right]-c_c\left(\kappa\right)=0 \qquad (3\text{-}1)$$

where κ is a hardening parameter accounting for the cumulative effect from inelastic compressive deformation, c_c is a compressive strength parameter that shown to be equal to the uniaxial compressive strength of the material, I_1 and J_2 are the first invariant and the second deviatoric invariant of the stress tensor, α is a dimensionless material parameter, $r(\theta,e)$ is named as radial distance (Kang et al., 2000) to account for multiaxial response of concrete. The term $r(\theta,e)$ is set to 1 in the Drucker-Prager yield surface model, but can be less in the MYS approach, leading to smaller values of biaxial compressive stress in the deviatoric stress plane compared with Drucker-Prager surface (Figure 3-1(a)). The comparison of yield surfaces (Figure 3-1(b)) shows that the MYS generally has smaller values of $\sqrt{J_2}$ compared with Lubliner yield surface (Lubliner et al., 1989) as I_1 decreases (i.e., for larger confinement effect). The accuracy of the MYS model in predicting hysteretic response of RC structures was validated in several analytical simulations (Moharrami 2016), which also showed that the Lubliner yield surface overestimated the strength.

The compressive inelastic behavior is described by an isotropic hardening-softening law, giving the evolution of c_c with κ (Lee and Fenves 2001):

$$c_c(\kappa) = \frac{f_o}{a}[(1+a)\sqrt{\varphi(\kappa)} - \varphi(\kappa)] \geq f_{res} \qquad (3\text{-}2)$$

where $\varphi(\kappa) = 1 + a(2+a)\kappa$, a is a material constant can be calculated by the peak value of κ, and f_{res} is the residual strength of concrete.

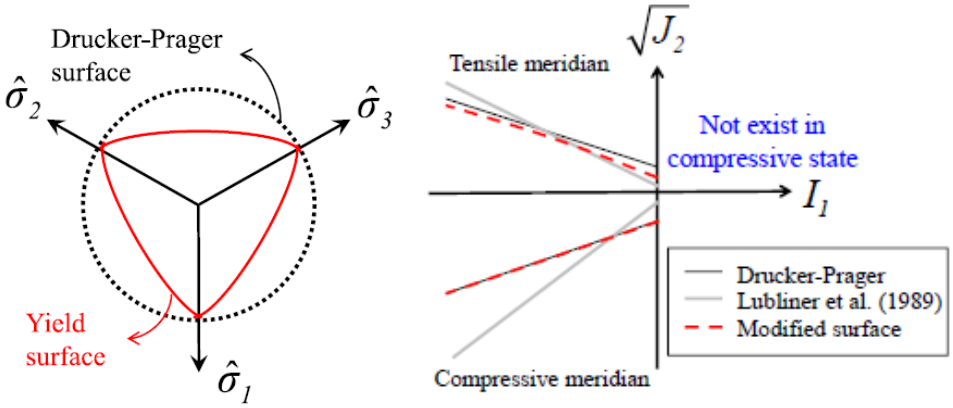

(a) Deviatoric plane **(b) Meridional plane**

Figure 3-1 Comparison of yield surfaces (Moharrami and Koutromanos, 2017; Moharrami 2016)

The maximum value of c_c is equal to the uniaxial compressive strength, f_c, of the material. Setting the peak value of parameter κ in the finite element analysis determines when the crushed concrete needs to be removed. By plotting the contour of κ, the compressive inelasticity parameter level and distribution of solid elements can be visualized from the analysis output.

The evolution of plastic strain is developed by a plastic potential function, g:

$$g = \alpha_p \cdot I_1 + \sqrt{2J_2} \qquad (3\text{-}3)$$

where α_p is the user-defined dilatancy factor for compressive inelastic states (Moharrami 2016) and suggests be taken as 0.15.

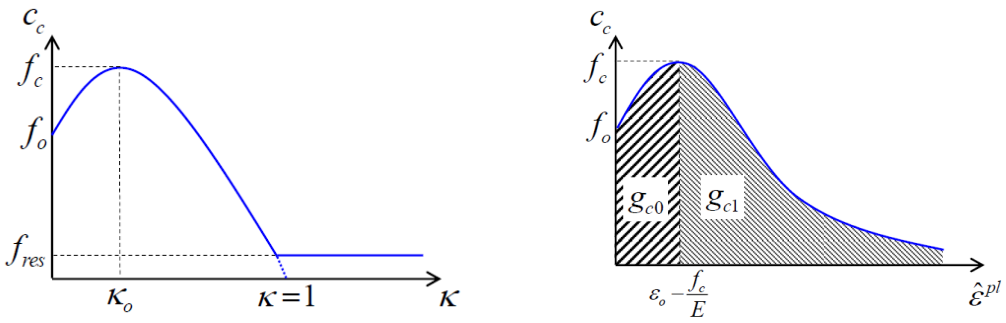

(a) Hardening-softening law **(b) Area under hardening and softening portions**

Figure 3-2 Hardening-softening law for elastoplastic model in compressive region (Moharrami and Koutromanos, 2016)

The confinement effect in the BCJ and plastic hinge region in the beam have a significant influence on the ductility of RC structures. In most circumstances, the confinement effect is based on using another set of material parameters for confined concrete which based on adjusting the values from uniaxial material models (Mander et al., 1998), and is not an accurate approach.

To address this shortcoming, Moharrami and Koutromanos (2016) defined the evolution of hardening parameter κ by the following rate function:

$$\dot{\kappa} = (1-r)\cdot\frac{c_c}{g_c}\cdot\frac{\partial g}{\partial \hat{\sigma}}\Big|_{\hat{\sigma}_{\min}}\cdot e^{d\cdot(1+X)\frac{p}{f_c}} \tag{3-4}$$

where g_c is a material parameter, $\partial g/\partial\hat{\sigma}|_{\hat{\sigma}min}$ is the component of the rate of plastic strain vector in the direction of the minimum principal stress, X is calculated as $I_1/\sqrt{3J_2}$ and d is a user-defined constant that expresses the effect of pressure p on the evolution of κ (Moharrami and Koutromanos 2016). The use of κ takes into account the confinement effect anywhere in the material automatically and multiaxially, which is much more accurate than amplifying the stress uniaxially within a specific region as is done in conventional approaches.

The exponential term in Equation (3-4), which is not included by Lee and Fenves (1998),

equals to 1 for uniaxial compression and decreases for multiaxial compression. This means that the hardening-softening evolution become slower in multiaxial compression, accounting for the increased ductility of confined concrete.

3.1.1.2 Crack Model

For the numerous constitutive models that have been proposed for concrete, their ability to properly track opening and closing of flexural and shear crack under cyclic loads is the ultimate test of their robustness. Since crack closure allows the subsequent development of significant compressive resistance, the strength of concrete under cyclic loading will not decrease in the same way as tensile strength. Previously proposed damage-plasticity models such as those proposed by Murray (Murray 2007) and Karagozian and Case (K & C) (Malvar et al. 1997) which simpliy apply the compressive strength reduction to tensile strength degradation will not be suitable for BCJ joints subjected to cyclic loading. Similarly, other damage-plasticity models, such as Lee and Fenves (1998) cannot capture crack closure properly.

In the concrete model utilized herein, the concrete stress is corrected in the principal stress field when one principal trial elastic stress surpasses the cracking stress by including the simultaneous production of a crack opening strain vector in the direction that the crack occurs. The cracking strength is equal to zero if the crack was closed and now reopens, and equals to c_t if a crack opens for the first time. Thus, the crack opens when tensile stress occurs and closes once compression develops, which reveals exactly what happens in reality. The crack correction is only made for tensile stresses, and the compressive strength is not reduced due to cracking. The principal stress of cracked concrete is a function of the principal strain in Equation 3-5 (Figure 3-3):

$$\hat{\sigma}_i = c_t \left[(1-M) e^{\left(-\lambda_t \frac{\hat{\varepsilon}_i - \hat{\varepsilon}_{ini}}{f_t} \right)} + M \right], \; i = 1,2,3 \tag{3-5}$$

where c_t is the tensile strength of material, f_t is the initial tensile strength, M is the percentage of residual tensile strength of tensile strength, $\hat{\varepsilon}_{ini}$ is the strain right before softening and λ_t is a parameter controlling the rate of tensile softening. The value of material tensile strength c_t is attained as:

$$\begin{cases} c_t = f_t, if \;\; \kappa \le \kappa_0 \\ c_t = \dfrac{c_c}{f_c} f_t, if \;\; \kappa > \kappa_0 \end{cases} \tag{3-6}$$

This implies that the tensile strength will encounters a similar reduction after the material has started compressive strength degradation.

The softening law illustrated in Figure 3-3 for the tensile field as well as the unloading-reloading behavior for the cracked material define the unloading and reloading curve in a fashion that always going through the origin, the negligible small error in irreversible strain brings huge improvement in convergence ability.

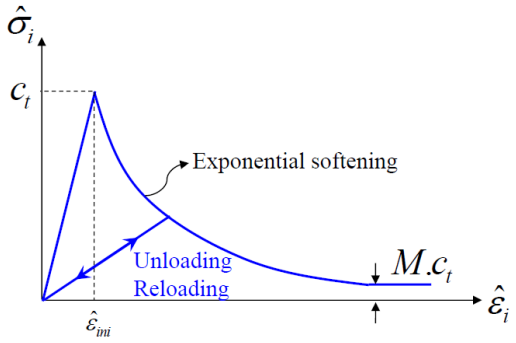

Figure 3-3 Material response for uniaxial tension (Moharrami and Koutromanos 2016)

To guarantee the compatibility of the cracked and uncracked material, the concrete model

proposed by Moharrami and Koutromanos (2016) formulates the cracked and uncracked concrete model separately, and then combines them together by enforcing the conditions that 1) the stress in each direction obtained from the crack model in Equation (3-5) should always be equal to the stress obtained from the elastoplastic constitutive model; and 2) the total strain vector equals to a summation of elastic strain $\hat{\varepsilon}^{el}$, plastic strain $\hat{\varepsilon}^{pl}$ and cracking strain $\hat{\varepsilon}^{cr}$:

$$\{\hat{\varepsilon}\}=\{\hat{\varepsilon}^{el}\}+\{\hat{\varepsilon}^{pl}\}+\{\hat{\varepsilon}^{cr}\} \tag{3-7}$$

3.1.1.3 Parameter Calculation

One advantage of the model is that all the parameters are calculated based on monotonic response. Besides the basic material parameters like compressive strength of concrete, there are only four parameters need to be decided: 1) the dimensionless confinement factor α which suggested as 0.375 for MYS; 2) the dimensionless ductility factor d which expresses the effect of confinement on material ductility; 3) the dilatancy factor α_p in Equation (3-3); 4) the tensile (mode-I) fracture energy G_t expressed as:

$$G_t = 2.5\alpha_0\left(\frac{f_c}{0.051}\right)^{0.46}\left(1+\frac{d_a}{11.27}\right)^{0.22}\left(\frac{w}{c}\right)^{-0.30} \tag{3-8}$$

where f_c is the compressive strength of concrete expressed in MPa, d_a is the maximum aggregate size in mm, w/c is the water/cement ratio, α_0=1 for rounded aggregate and α_0=1.44 for crushed or angular aggregates. Then, the fracture energy for compression G_c is obtained by multiplying G_t by 100, and the parameter g_c in Equation (3-4) can be obtained by stipulating the area under the hardening-softening curve in Figure 3-2(b) equals to G_c/h, where h is the mesh size of finite element model. The parameter g_c is related to the evolution of κ, and thus determines the yield criteria of the material. This energy criterion for crack propagation avoids the mesh sensitivity and

physically meaningless convergence compared with stress/strain criterion (Bažant 2002).

3.1.2 Constitutive Model for Reinforcing bar

The reinforcing bar material behavior is employing the constitutive model of Kim and Koutromanos (2016). The model is capable of capturing the cyclic hysteretic response of reinforcing bar, as shown in Figure 3-4.

The Kim and Koutromanos model is based on a model for the cyclic behavior of steel bars by Dodd and Restrepo-Posada (1995), with enhancements that include a non-iterative stress computation, and a capability to account for the inelastic local buckling and rupture due to low-cycle fatigue.

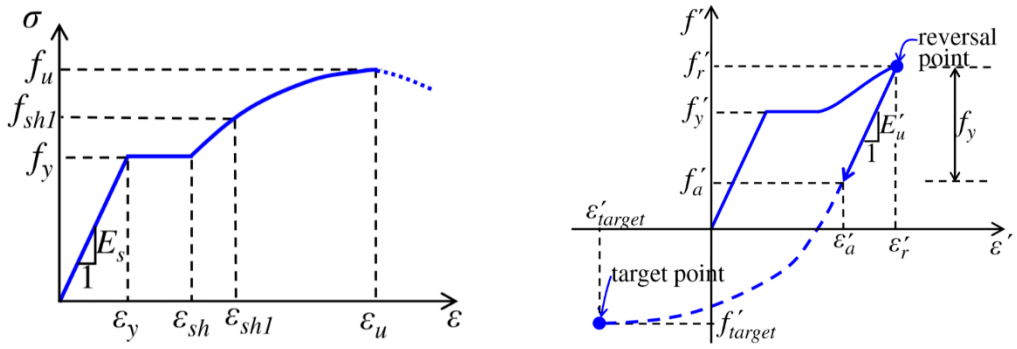

(a) Monotonic Tensile Response **(b) Cyclic Hysteretic Response**

Figure 3-4 Behavior of reinforcing bar model (Kim and Koutromanos, 2016)

The non-iterative characteristic is considerably advantageous to the converge of the whole model since the 3D model results in considerably extra degrees of freedom compared with 2D models and the discrete bond-slip model contributes additional convergence difficulties. The computational benefit accruing from the robustness and accuracy of each material model is the key factor towards the success of analytical simulations. Also, inelastic local buckling of the reinforcing bar is possible during and after the formation of a plastic hinge in BC connections.

3.1.3 Element Formulation

This section describes the element formulations employed in the simulations of BC joints in the following sections.

The concrete is modeled by hexahedral 3D solid elements. To reduce the computation cost of an analysis, the solid element uses uniform reduced integration (URI) and thus each element has a single quadrature point in the middle. The use of URI entails the presence of spurious zero-energy modes (hourglass modes) because URI-based elements cannot develop resistance to these type of deformation since it has no stiffness and no strain energy in these modes (Flanagan and Belytschko 1981).

There are twelve hourglass deformation modes that need to employ hourglass-control formulations to develop hourglass-resisting forces for an eight-node URI-based hexahedral element. A stiffness-based hourglass control is employed if nodal displacements are used to obtain the hourglass part of motion, and a viscous hourglass control is applied if nodal velocities are used. The stiffness-based hourglass control is used for elastic concrete elements in the loading region as well as cover concrete, with the value of 1 for a user defined hourglass coefficient for elastic part which gives best approximation of the flexural stiffness for elastic elements, and 0.05 for cover concrete based on the calculation from Flanagan and Belytschko (1981). Due to the reason that a redundant dynamic excitation from a combination of stiffness hourglass control and an explicit analysis may lead to oscillatory response when subjected to quasi-static cyclic loading. Thus the viscous-based hourglass with a value of 0.1 is used for confined concrete by the hourglass formulation developed by Belytschko and Bindeman (1993) to solve this issue.

The reinforcing bar bars are modeled by beam elements with the formulation of Hughes and Liu (2006), which is a continuum-based structural element capable of capturing large rotations and

deformations, thus inherently accounting for the effect of buckling. The sectional stress components (axial forces, shear forces, bending moments, and torsional moments) are calculated through integration of stresses over nine quadrature points over the cross section of the beam.

3.1.4 Bond-Slip Model

The cyclic-deteriorating bond-slip model proposed by Murcia-Delso and Shing (2014) is capable of capturing the bond deterioration caused by 1) cyclic bond-slip reversals in well-confined situation, 2) tensile yielding of the reinforcement, 3) the strain penetration of reinforcement, and 4) formation of splitting cracks between bar and concrete (

Figure 3-5).

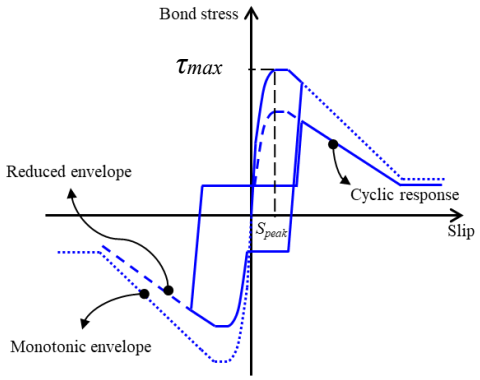

Figure 3-5 Cyclic bond stress-slip relation

In the monotonic stress-slip law proposed by Murcia-Delso and Shing (2014), the bond stress-slip relation is made up of a set of polynomial functions and the total bond resistance is made up of two components: bearing resistance and friction resistance. After reaching the peak bond stress, the friction bond resistance remains intact and the bearing resistance linearly decreases to zero when slip reaches the value of rib spacing. The function is given in terms of three governing parameters: the peak bond strength τ_{max}, the peak slip s_{peak} when τ_{max} is reached, and the clear

spacing between the ribs S_R. The peak bond stress τ_{max} and the slip at peak bond stress are defined as:

$$\tau_{\max} = 1.163 f_c'^{3/4} \quad \text{(in MPa)} \tag{3-9}$$

$$S_{peak} = 0.07 d_b \tag{3-10}$$

And S_R is calculated as follows:

$$\tau_b(S_2) = \begin{cases} 3.0 \dfrac{\tau_{\max}}{S_{peak}} S_2 & for 0 \le S_2 < 0.1 S_{peak} \\ \tau_{\max}\left[0.75 - 0.45\left(\dfrac{S_2 - S_{peak}}{0.9 S_{peak}}\right)\right] & for 0.1 S_{peak} \le S_2 < S_{peak} \\ 0.75\tau_{\max} & for S_{peak} \le S_2 < 1.1 S_{peak} \\ 0.75\tau_{\max}\left[1 - \dfrac{S_2 - 1.1 S_{peak}}{S_R - 1.1 S_{peak}}\right] & for 1.1 S_{peak} \le S_2 < 1.1 S_R \\ 0 & for S \ge S_R \end{cases} \tag{3-11}$$

where S_2 is the relative tangential displacement along the axis of bar.

For cyclic loading, the monotonic curve is reduced at each reversal using two damage parameters which distinguish the degradation of bearing and friction resistance separately. The total bond resistance is expressed as:

$$\tau_2 = \rho_n \left(\rho_{b,s} \cdot \rho_{b,c} \cdot \tau_b + \rho_{f,s} \cdot \rho_{f,c} \cdot \tau_f \right) \tag{3-12}$$

where the parameters are described as following:

1. ρ_n : a reduction factor accounting for splitting cracks in the concrete. It is a function of relative normal displacement, and is neglected in the following simulations;
2. $\rho_{b,s}$: a reduction factor accounting for the reduced bearing resistances due to the yield of reinforcement. It is a function of bar strain;

3. $\rho_{b,c}$: a reduction factor accounting for the cyclic bond deterioration on the bearing resistance. It is a function of peak slip and slip accumulation, and is based on the slip history.
4. $\rho_{f,s}$: a reduction factor accounting for the reduced friction resistance due to the yield of reinforcement. It is a function of bar strain;
5. $\rho_{f,c}$: a reduction factor accounting for the cyclic bond deterioration on the friction resistance. It is a function of peak slip and slip accumulation, and is based on the slip history.
6. τ_b : full bearing resistance of an elastic bar subjected to monotonic pull out;
7. τ_f : full friction resistance of an elastic bar subjected to monotonic pull out.

The advantages of this model are that 1) only three parameters need to be calibrated; 2) it can be applied to any bar size and concrete strength; and 3) no iteration is needed in calculating the bond stress. Thus, it is computationally efficient especially when used in large volume of simulations like the analyses described in this chapter, as the slip history is accounted for more precisely by tracing the peak slip value instead of counting for the number of cycles.

3.2 Validation of Modeling Scheme

The proposed modeling approach for is validated using the results of previously conducted experimental tests on one-way and two-way BC joint subassemblages. This section provides a description of the experimental tests, followed by the results of the validation analyses. The validation procedure is supplemented with a parametric study, to investigate the impact of the value of various modeling parameters on the obtained analytical results.

3.2.1 Description of Experimental Tests

The validation for one-way BC joints uses the results from three half-scale one-way

subassemblages tested by Leon (1989) (Figure 3-6 and Table 3-1).

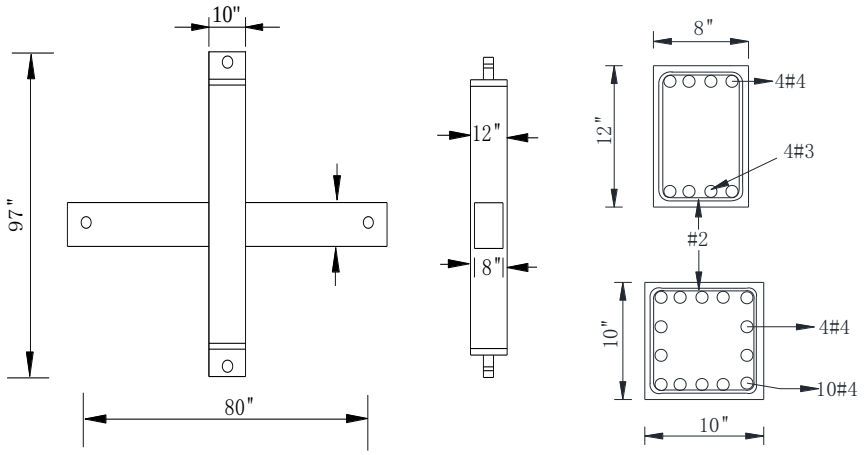

Figure 3-6 Details of SPECIMEN 2 tested by Leon (1989) (Unit: inch)

There were three specimens with similar characteristics except for the development length of the top beam bars in the column, which equals to the dimension of the column and varied from 20, to 24 and 28 bar diameters (Table 3-1 Specimen Details). The three specimens considered in this study were termed Specimens 2, 3 and 4.

Table 3-1 Specimen Details (Re-tabulated after Leon 1989)

Specimen	**Specimen 2**	**Specimen 3**	**Specimen 4**
Beam Size	$8\times12\,in$	$8\times12\,in$	$8\times12\,in$
Top beam reinf.	4 #4	4 #4	4 #4
Bottom beam reinf.	4 #3	4 #3	4 #3
Transverse reinf.[a]	#2 at 2 *in*	#2 at 2 *in*	#2 at 2 *in*
Beam length[b]	42 *in*	40 *in*	38 *in*
Column	$10\times10\,in$	$12\times10\,in$	$14\times10\,in$
Column reinforcement			
(face)	10 #4	10 #4	10 #4
(side)	4 #4	4 #4	4 #4
Joint transv. Reinf.	4 #2	4 #2	4 #2

[a]#2 deformed bar was obtained from PCA

[b] Distance from strut to column face

The specimens were subjected to a large number of cycles (Figure 3-7) applied slowly at the

bottom of the column. Loads, deflections, rotations, shear strain and local bond-slip value were measured. Test results showed that most of the horizontal shear forces in the joint were accomplished by a strut mechanism due to a lack of joint reinforcement; The beam bears in Specimen 2 was slipping more than that in Specimen 4, and the inelastic yielding of the beam bars was substantially greater for Specimen 4 than for Specimen 2.

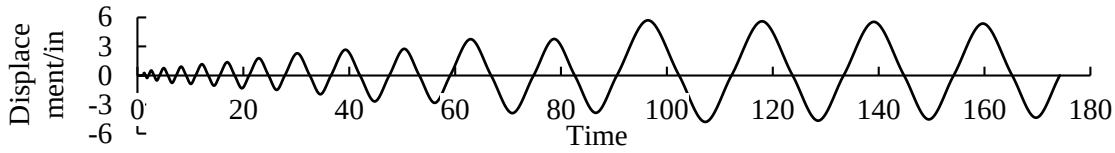

(a) Loading curve of Specimen 2

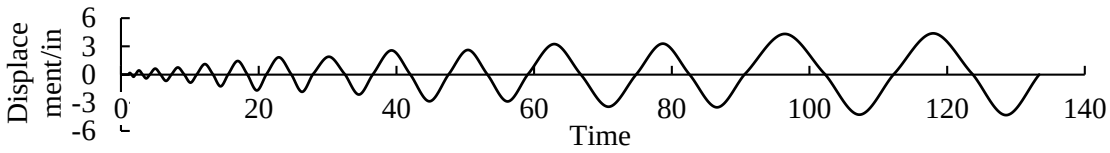

(b) Loading curve of Specimen 3

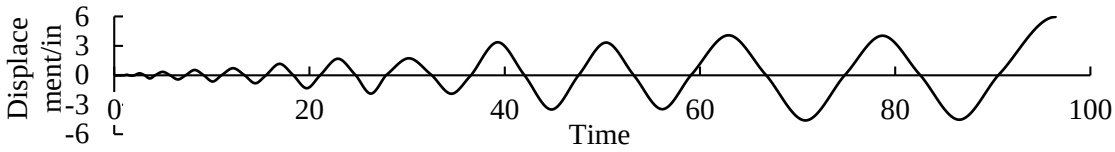

(c) Loading curve of Specimen 4

Figure 3-7 Loading curve of Specimens 2 to 4 tested by Leon (1989)

Half of a typical model is shown in Figure 3-8. It consists of 13392 (solid elements for confined and unconfined concrete in Specimen 2 (14928 for Specimen 3, 16464 for Specimen 4), 4124 beam elements for longitudinal and transverse reinforcement in Specimen 2 (4324 for Specimen 3, 4336 for Specimen 4). There are 18704, 18498 and 20235 nodes for Specimen 2 to Specimen 4, respectively. Elastic material applied same Young's modulus with concrete is used at the end of the beams and columns for the loading part to prevent severe local damage.

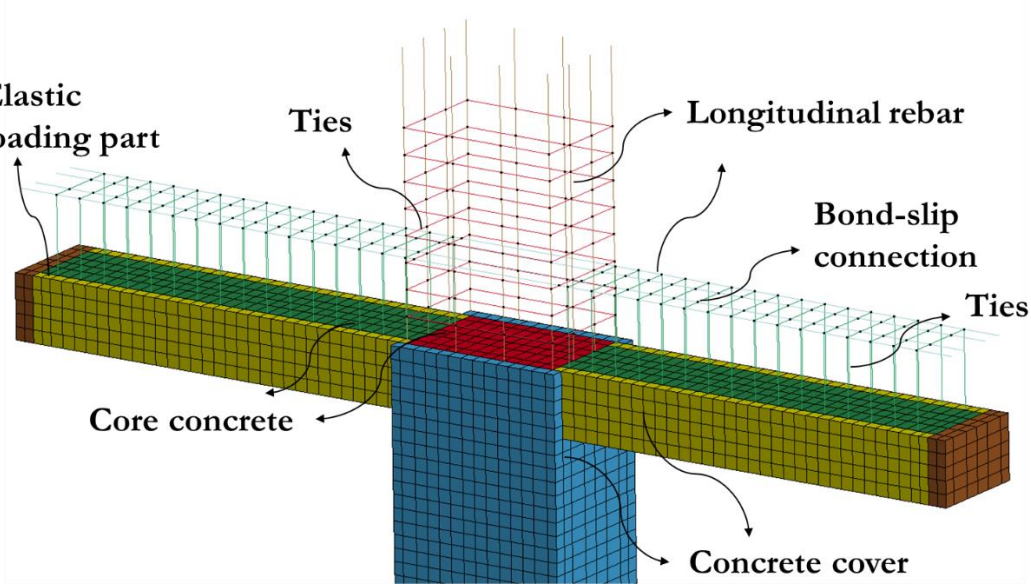

Figure 3-8 Finite Element Model

The parameters of the constitutive models for the concrete, reinforcing bar and bond-slip of bars are assigned identical values for the simulations of all three specimens.

In the simulation, exactly same parameters are used for all three specimens herein. The major material properties in the specimens are f'_c=5.5 ksi, and f_y=70 ksi, f_u=120 ksi, and τ_{max}=2 ksi according to Equation (3-9).

3.2.2 Analysis Results: Force-Displacement Response

The curves giving the applied force as a function of the horizontal displacement at the bottom of the column for the three specimens are compared with the corresponding experimental data in Figure 3-9, where the early loading cycles refers to the loading cycles with lateral displacement smaller than 3 in. to give a better illustration of comparisons on initial stiffness.

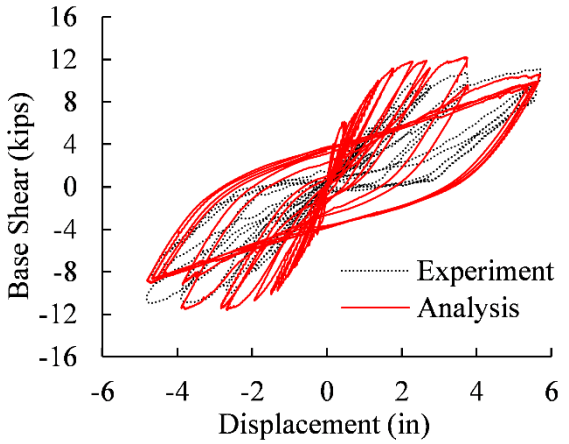

(a) Specimen 2

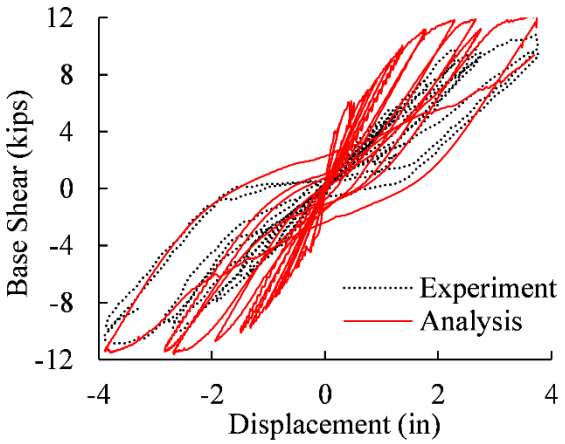

(b) Specimen 2 in early loading cycles

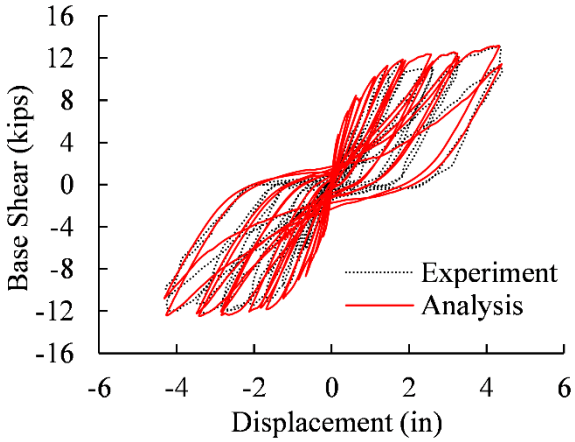

(c) Specimen 3

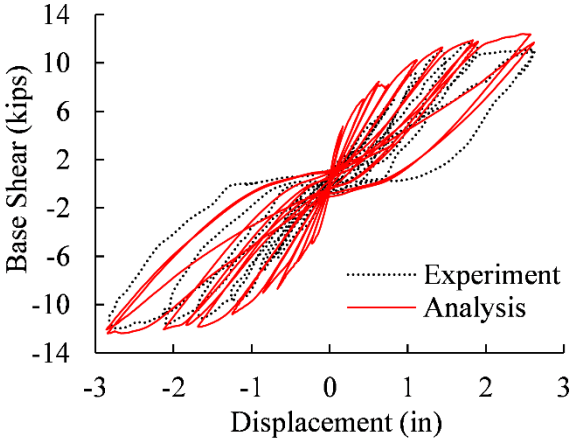

(d) Specimen 3 in early loading cycles

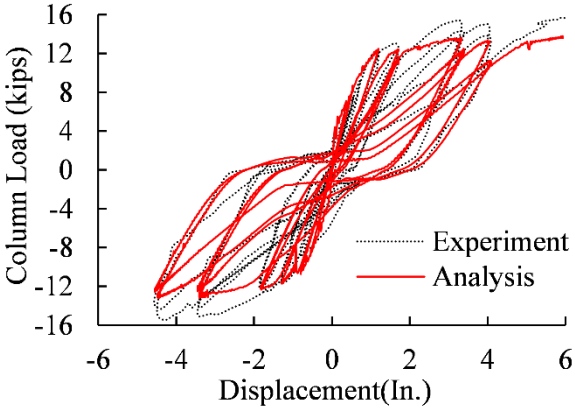

(e) Specimen 4

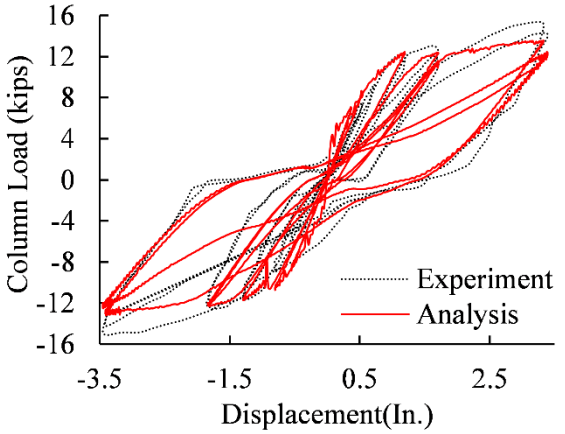

(f) Specimen 4 inearly loading cycles

Figure 3-9 Comparison of analytical and experimental results of column load versus story displacement of specimens tested by Leon (1989)

The results show best consistency for Specimen 3, which estimated the ultimate strength of the specimen in the test with an error of only 0.5% (13.10 kips analytically and 13.04 kips experimentally). The pinching effect due to shear deformation and bond-slip is also captured in the analysis. The strength of Specimen 4 is underestimated by 12% compared with the experimental data (13.14 analytically and 14.97 kips experimentally), while all other behavior, especially the pinching region, are accurately reproduced.

The least satisfactory agreement between analysis and experimental observations is obtained for specimen Specimen 2. This is due to the large diagonal shear crack formed in the joint region, which the model did not accurately capture and possibly by the occurrence of stress lock-in effects in the simulation (Rots and Blaauwendraad 1989), which is a well-known issue in continuum-based finite element analysis.

To explain the stress lock-in effect, two adjacent elements namely element 1 and 2 are illustrated in Figure 3-10. The stress lock-in effect occurs when element 2 is subjected to an inclined crack, as element 1 cannot truly separate from element 2 due to displacement compatibility. Thus, the stress in element 2 softens due to the reaction from element 1 while the stress in element 1 increases. If the stress in element 1 exceeds the tensile strength and the material starts softening, spurious cracking forms since it discourages localization; if the stress in element 1 is still increasing, the stress is locked-in due to spurious stiffening. The ability of the current model to capture large shear deformation needs to be improved by techniques like discrete-cohesive crack representation of highly localized fracture, such as cohesive interface elements at the location crack occurs (Lotfi and Shing 1994, Koutromanos and Shing 2012) or embedded crack formulations (Spencer and Shing 2002).

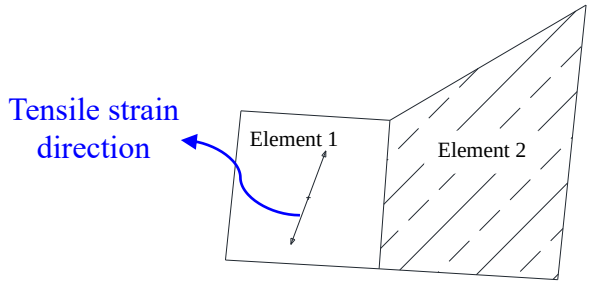

Figure 3-10 Strain of inclined crack in element 2 induces locked-in stress at element 1

3.2.3 Analysis Results: Damage Patterns

The visual damage to joint region at the occurrence of first yielding of the top bars is compared with test photos in Figure 3-11. The history of top beam bar stress is plotted, and the first yield time is selected as 19.4, 11.4 and 9.5 for Specimens 2, 3, and 4, respectively. This corresponded to the 9^{th}, 7^{th} and 5^{th} cycle at drift ratio of 2.6%, 1.9%, and 1.7% (lateral displacements of 2.52 in., 1.81 in. and 1.63 in.) for Specimens 2, 3, and 4, respectively.

3.2.3.1 Damage Pattern at First Yield of Reinforcing bar

In the test (Figure 3-11(a)), when Specimen 2 reached the first yield of longitudinal reinforcing bar in the beam, it had already encountered substantial shear crack in the joint area which indicates a contribution from the strut mechanism, and flexural crack in both beam and column was observed. Specimen 3 had substantially less cracking in the joint (Figure 3-11(b)), but more cracking in the beam and columns since the anchorage conditions were better and the shear stresses were lower (see Table 3-1). In the simulation, the cracking strain contour from Specimen 2 captured both diagonal shear damage in the joint, concentrated crack at beam ends, and flexural damage in the column. Less shear cracking and more flexural cracking in the beam was observed in Specimen 3. Specimen 4 evidenced the least cracking compared to previous two specimens

(Figure 3-11(c)). For this case, there was distributed flexural cracking in the beam, matching well the observed experimental behavior.

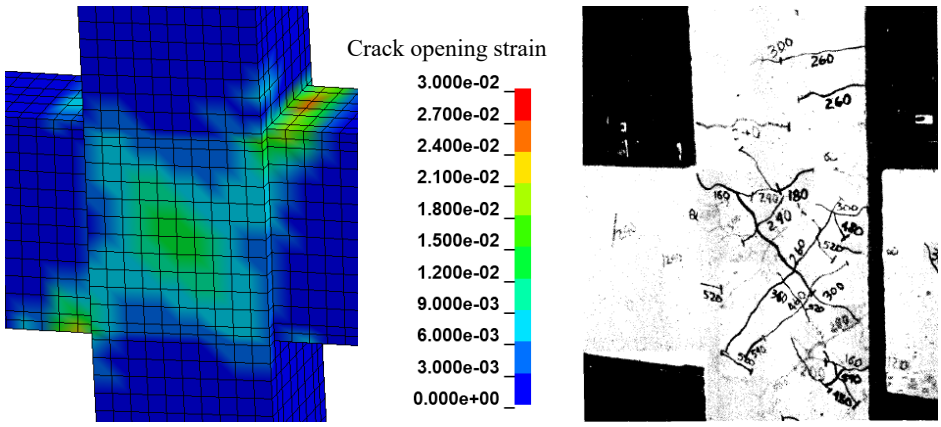

(a) Analytical and experimental crack pattern at yielding for Specimen 2

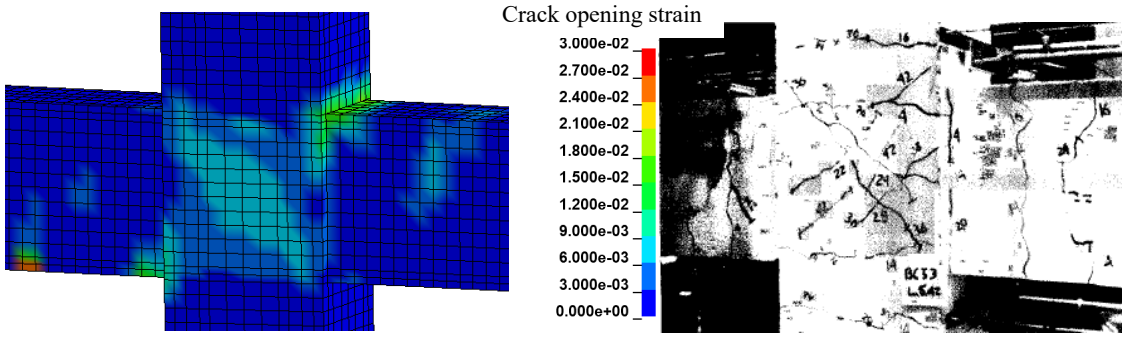

(b) Analytical and experimental crack pattern at yielding for Specimen 3

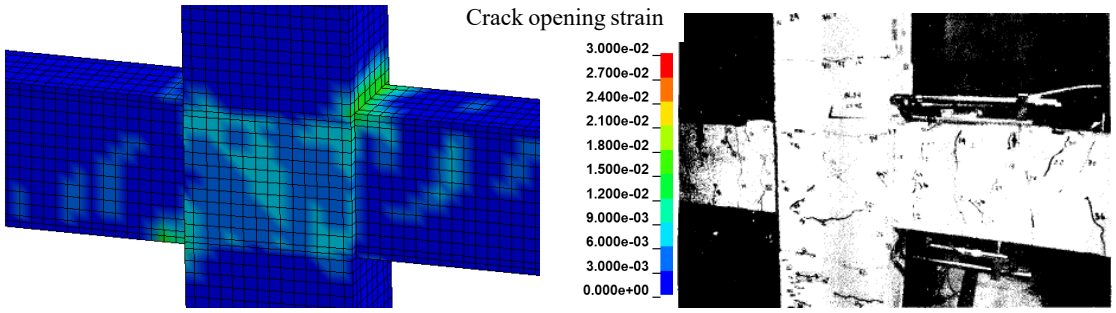

(c)Analytical and experimental crack pattern at yielding for Specimen 4

Figure 3-11 Cracking strain contour compared with crack pattern tested by Leon (1989)

The contour plots of the hardening parameter κ in Equation (3-4), captured both diagonal compressive inelasticity parameter in the joint and flexural damage in the column for Specimen 2

(Figure 3-12(a)). A smaller amount of diagonal compressive inelasticity parameter is observed at similar shear stress status in Specimen 3 (Figure 3-12(b)). Almost no joint damage is observed at the same range of contour distribution in Specimen 4, with considerably more damage at the corners (Figure 3-12(c)).

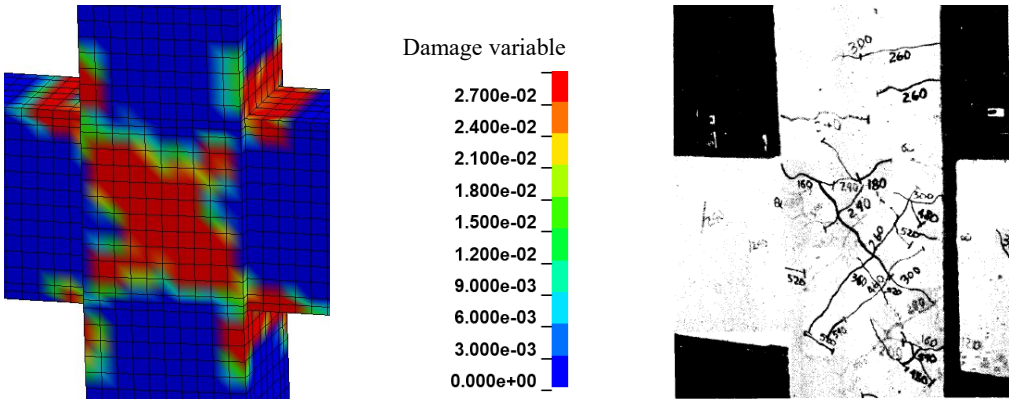

(a) Analytical and experimental damage pattern at yielding for Specimen 2

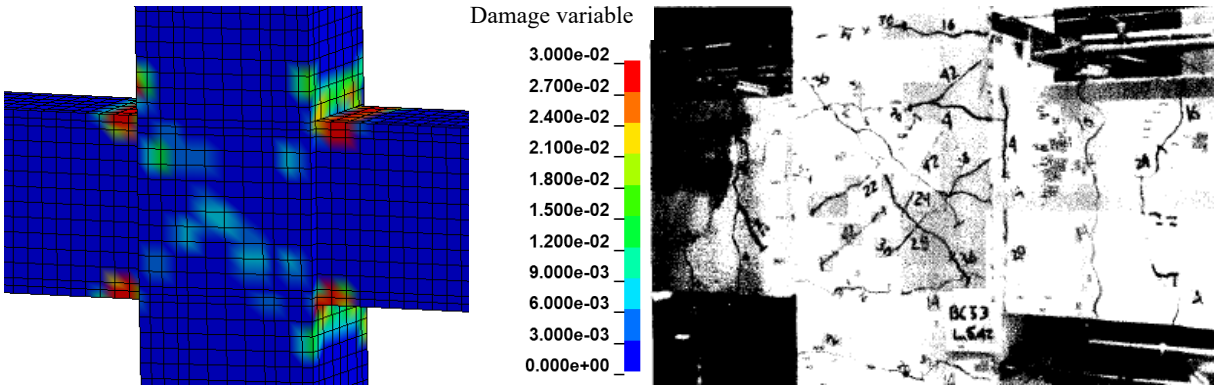

(b) Analytical and experimental damage pattern at yielding for Specimen 3

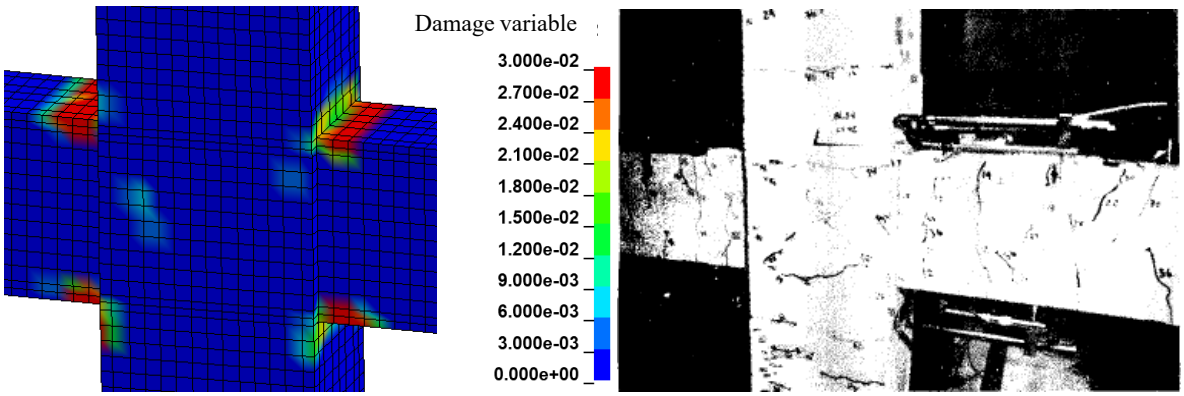

(c) Analytical and experimental damage pattern at yielding for Specimen 4

Figure 3-12 Compressive inelasticity parameter compared with crack pattern tested by Leon (1989)

3.2.3.2 Tri-linear Backbone

The tri-linear backbone from force-displacement curve proposed by Kitayama (1992) for explaining RC joint shear behavior is compared with the output from the simulation. The three points in the curve correspond to the initiation of diagonal cracking, yielding of the longitudinal beam or joint transverse reinforcement and initiation of concrete crushing are corresponded well as shown in Figure 3-13.

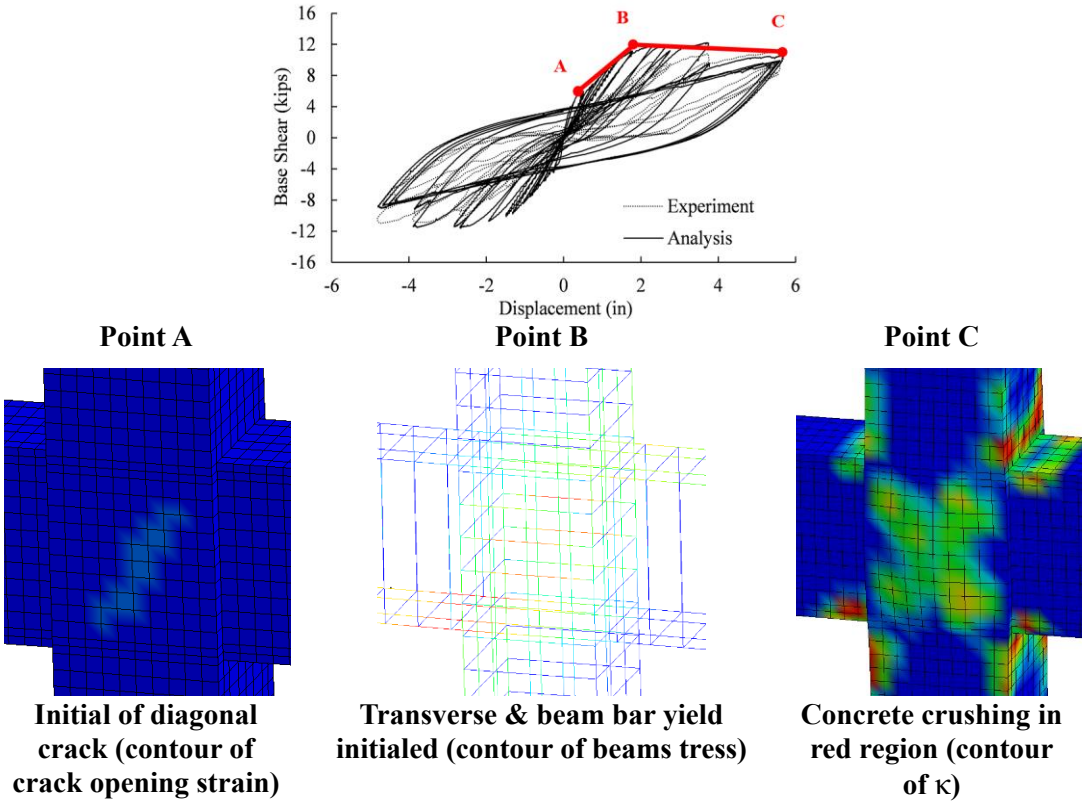

(a) Specimen 2

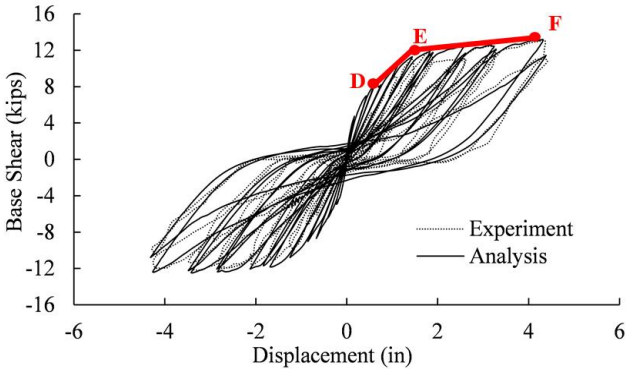

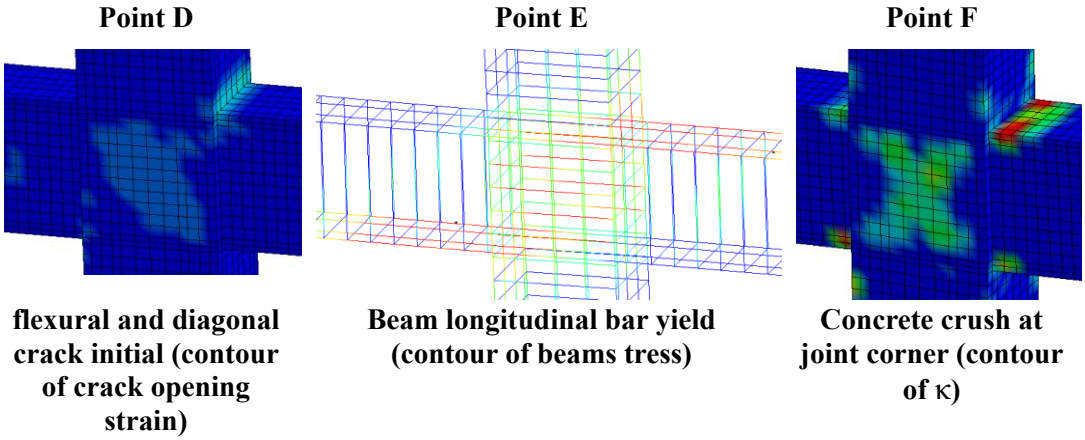

(b) Specimen 3

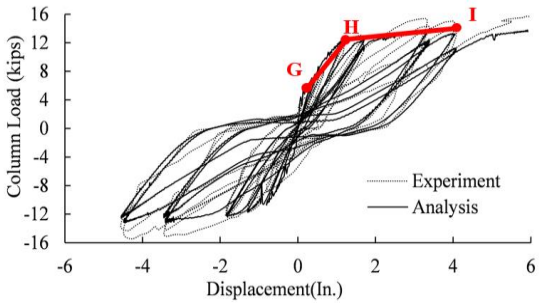

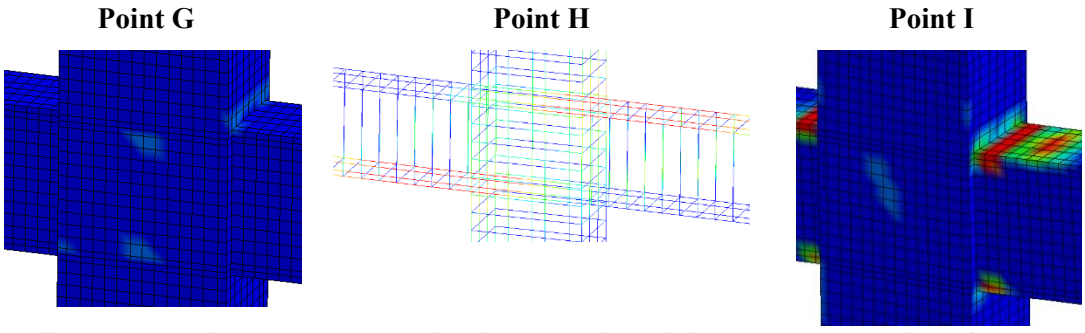

(c) Specimen 4

Figure 3-13 Key stages of damage accumulation for analysis of specimen Specimens 2 to 4 tested by Leon (1989)

It can be observed from the Figure 3-13 that, for the shear dominated connection (Specimen 2), initiation of diagonal cracking was observed in the first point, and yielding of the transverse reinforcement, rather than of longitudinal bar, was observed in the second point due to large shear

stresses in the joint. Concrete crushing at the joint corner and in the joint resulted in degraded strength for Specimen 2 at the third point.

For non-shear dominated joint Specimen 4, a diagonal crack is not obvious at the first point. Longitudinal bars rather than transverse bars in the joint yielded at the second point. The strength decline at the third point is due to the inelastic region (plastic hinge) in the beam.

The behavior of Specimen 3 falls between the other two specimens, such that both beam and transverse reinforcing bar yield was observed at the second point. Both diagonal shear damage and concrete crushing at the joint corners resulted in deterioration of the strength.

All the failure mechanisms observed in the analyses match what happened in the experiment, as well as the related theories, which further buttress the reliability of the proposed analysis.

3.2.3.3 Final Damage Pattern

As the third step, the final damage pattern is compared with what was observed during the experiment.

For Specimen 2, Figure 3-14 shows the compressive inelasticity parameter for the joint region. Since the range of the contour is 0 to 0.215, which is the parameter κ at peak displacement, the red color in the figure represents the concrete compressive stress has beyond the peak value and starts softening (also applies to Specimen 3 and 4 later). The figure illustrates the strut mechanism clearly as more damage is observed at joint corners, and reveals more damage in the confined concrete compared with concrete cover due to the insufficient capacity of the transverse reinforcement in the joint. This mirrors what happened in the test.

The stress and strain distributions in reinforcement at the drift ratio of 4.4%, 4.4%, 4.6% for Specimens 2, 3 and 4 are shown in Figure 3-15. The longitudinal beam bars, which yield at a stress

of 70ksi and a strain of 0.016 at the onset of hardening, show large stress and strain penetration into the joint. The column longitudinal bar encounters much smaller strain because there is smaller bar slippage in column bar. This mirrors what is discovered in the test and is also in agreement with the two force transfer mechanisms described in Section 2.1. The transverse reinforcement, which yield at a stress of 65 ksi and a strain of 0.006 at the onset of hardening, has extends its yielding from the joint into the column. The importance of transverse reinforcement in the joint and column is revealed herein as they are shown to be carrying large forces.

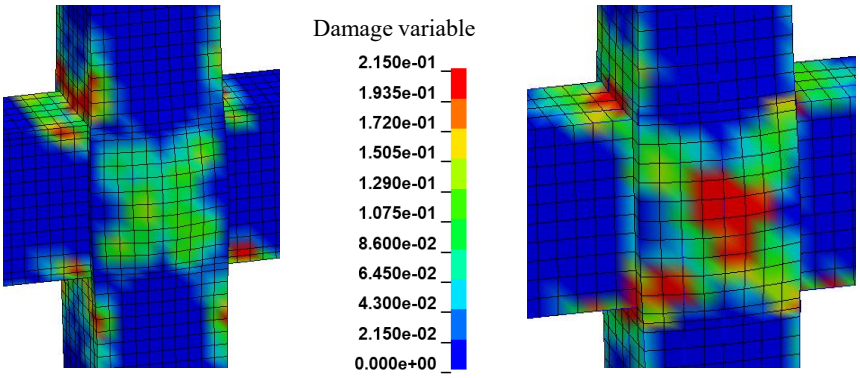

(a) Concrete cover **(b) Concrete beneath the cover**

Figure 3-14 Compressive inelasticity parameter contour with/without concrete cover for Specimen 2

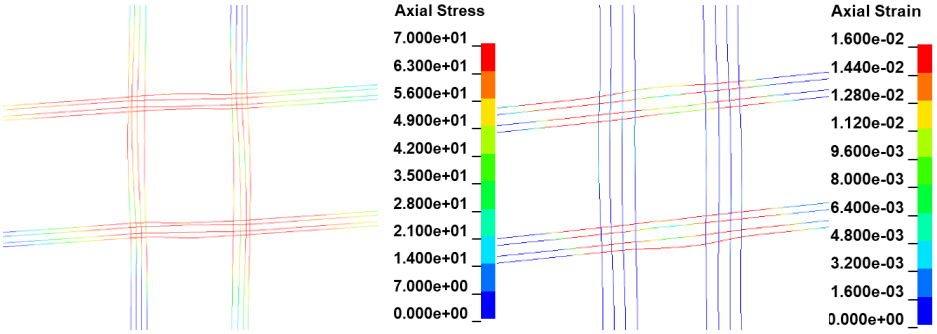

(a) Stress of longitudinal bar **(b) Strain of longitudinal bar**

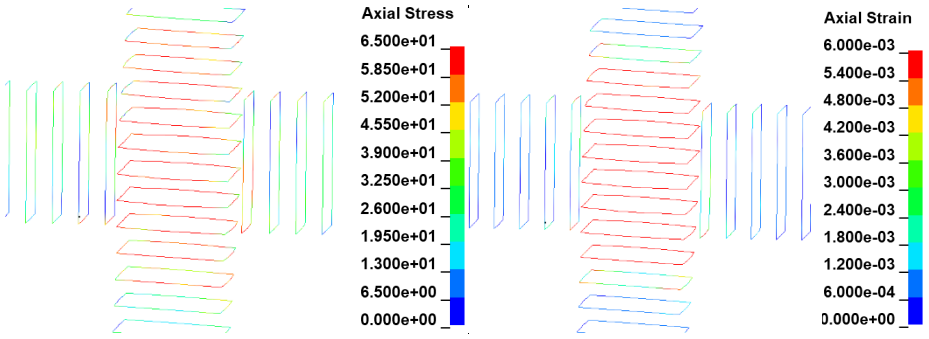

(c) Stress of transverse bar **(d) Strain of transverse bar**

Figure 3-15 Stress and strain in reinforcement for analysis of Specimen 2 tested by Leon (1989)

For a better comparison among all specimens, all contour ranges for the outputs are the same from Specimen 2 to 4 in Figure 3-16 through Figure 3-19; an exception is Figure 3-18 as will be noted later. For Specimen 3, Figure 3-16(b) depicts a confined concrete compressive inelasticity parameter region with less damage when compared with Specimen 2 (Figure 3-14(b)). The strut mechanism is still working efficiently.

A different damage pattern in the reinforcement is shown in Figure 3-17 for Specimen 3 when compared to Specimen 2 (Figure 3-15). The strain contours indicate lower strain penetration in the column bars, while the strain penetration in the beam longitudinal bar is limited to the area near the column bar, instead of through out the whole joint region as in Specimen 2. The stress in the transverse reinforcement extends further into the beam for Specimen 3 and the yield strain has been moved from the column to the joint region compared with those in Specimen 2. Both of these indicate that the transverse reinforcement is working as expected and that a mix of the strut and panel zone mechanisms are at work in Specimen 3.

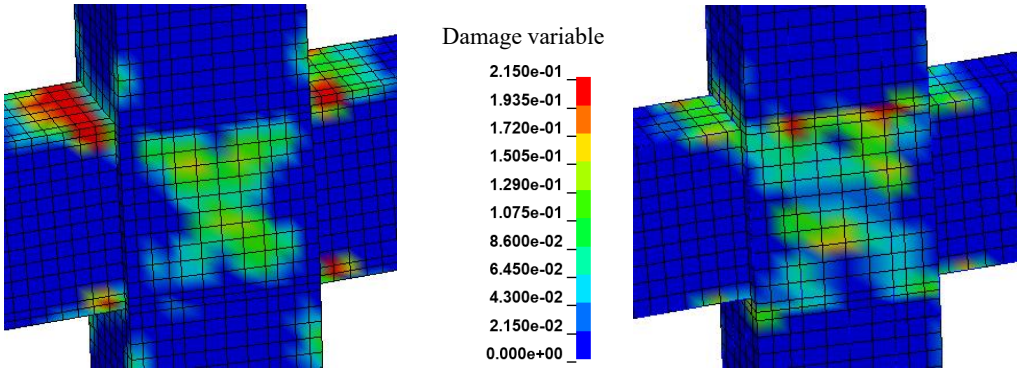

(a) Concrete cover **(b) Concrete beneath the cover**

Figure 3-16 Compressive inelasticity parameter with/without concrete cover for analysis of Specimen 3 tested by Leon (1989)

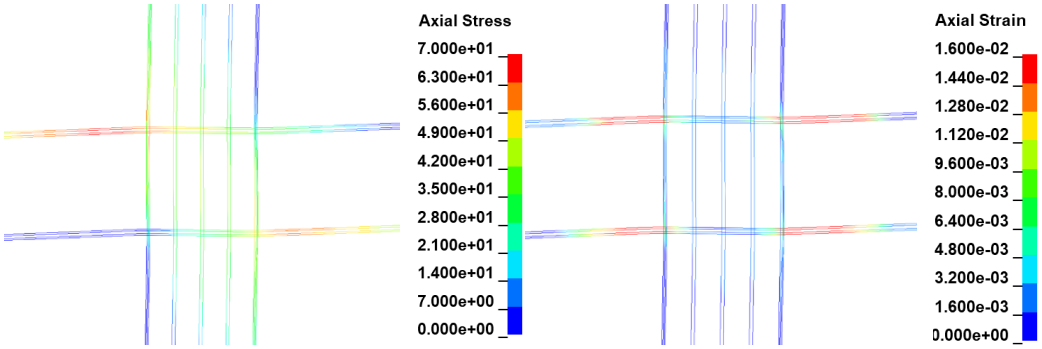

(a) Stress of longitudinal bar **(b) Strain of longitudinal bar**

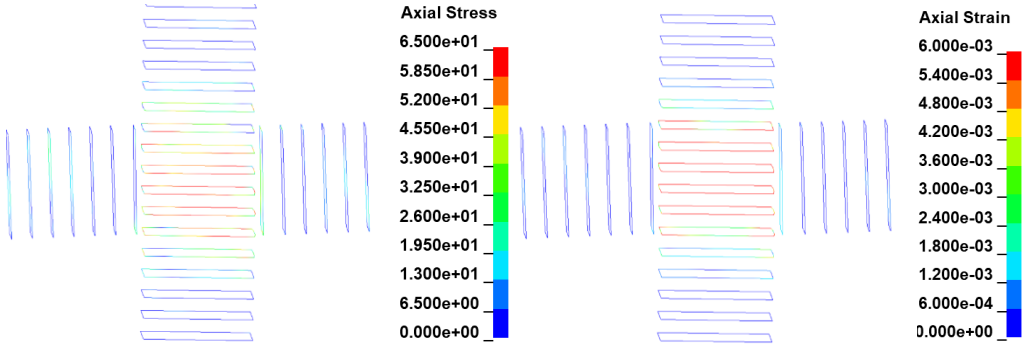

(c) Stress of transverse bar **(d) Strain of transverse bar**

Figure 3-17 Stress and strain in reinforcement for analysis of Specimen 3 tested by Leon (1989)

For Specimen 4, Figure 3-18 demonstrates even less concrete compressive inelasticity

parameter compared with Specimen 3 and Specimen 2 for both cover and confined concrete. Most of the damage is limited to the beam near the joint. It has to be pointed out that the range of contours for Figure 3-14(b) has been changed to 0~0.03 instead of 0~0.215 to visualize the distribution of smaller damages.

Further evidence of flexural behavior and the formation of a plastic hinge is shown in Figure 3-19 within the beam region. The yielding in the longitudinal beam reinforcement has extended to a greater distance away from the beam-column interface. Although the value of beam bar stress does not show appreciable difference, the locational of the yield stresses and strains into the beam region indicates that the failure mode has changed from a shear dominated one in the joint to a flexural damage dominated one in the beam. The yielded stress in the transverse reinforcement has been transferred further into the beam, with smaller values when compared with Specimen 3. Both the strain in the beam bars and the stress distribution in the transverse bars are evidence of plastic hinge formation.

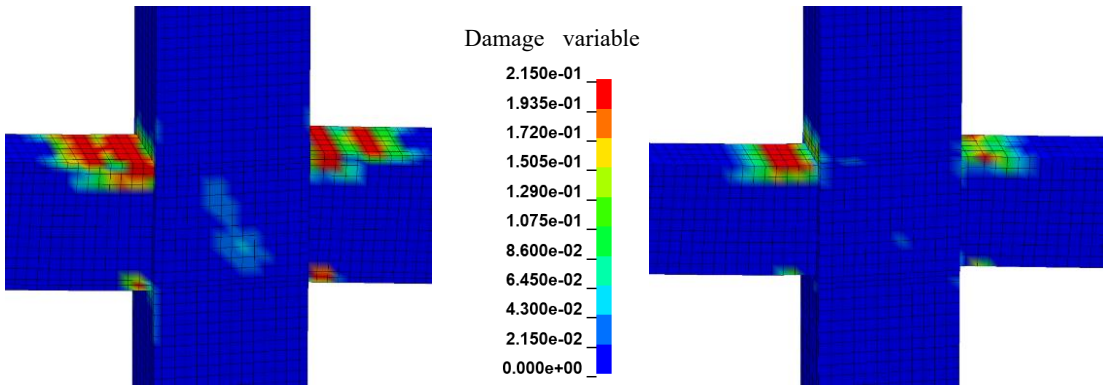

(a) Concrete cover **(b) Concrete beneath the cover**

Figure 3-18 Compressive inelasticity parameter contour with/without concrete cover for analysis of Specimen 4 tested by Leon (1989)

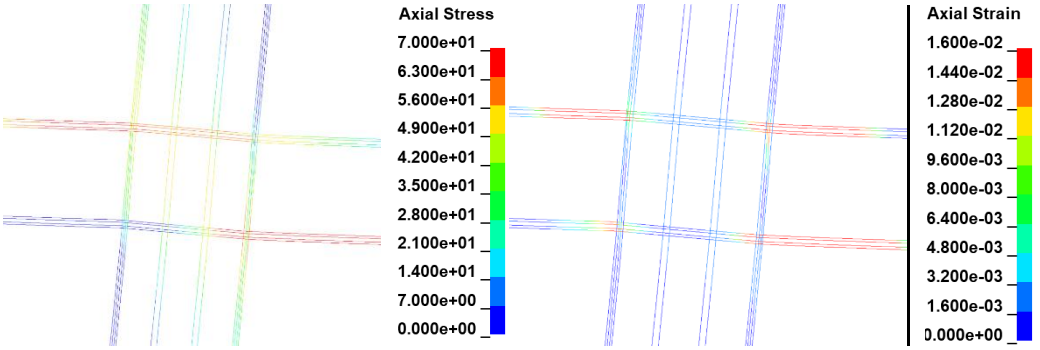

(a) Stress of longitudinal bar **(b) Strain of longitudinal bar**

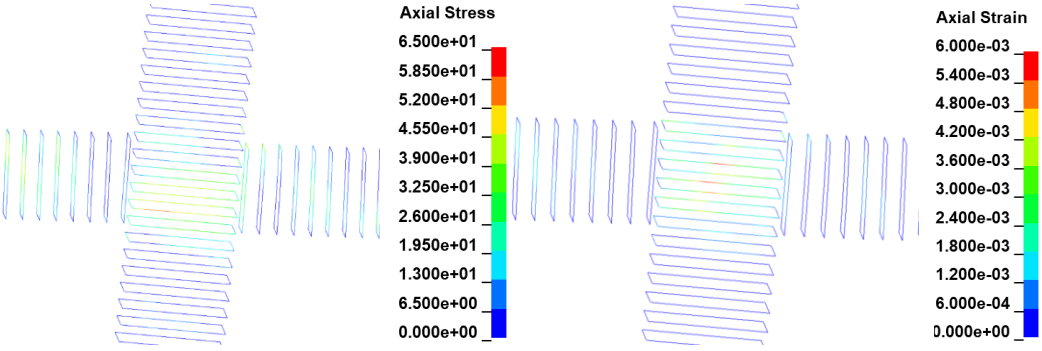

(c) Stress of transverse bar **(d) Strain of transverse bar**

Figure 3-19 Stress and strain in reinforcement for analysis of Specimen 4 tested by Leon (1989)

The force transferring mechanisms introduced in Section 2.1 are compared herein. The strut mechanism is validated by the Specimen 2 analysis. Figure 3-20(b) shows the strain in the loading direction in the A-A plane (Figure 3-20(a)) cut from the middle of the joint at the end of the loading curve, while Figure 3-20(c) shows the minimum principal stresses of Specimen 2. The figures show that large diagonal cracks across the joint interface have formed (Figure 3-20(b)), and yielding has penetrated through the whole joint (Figure 3-15(b)). The strut mechanism is formed then by the diagonal concrete band in compression (Figure 3-20(c)).

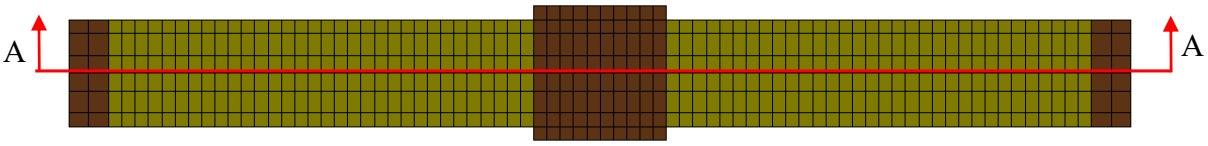

(a) Top view Specimen 2

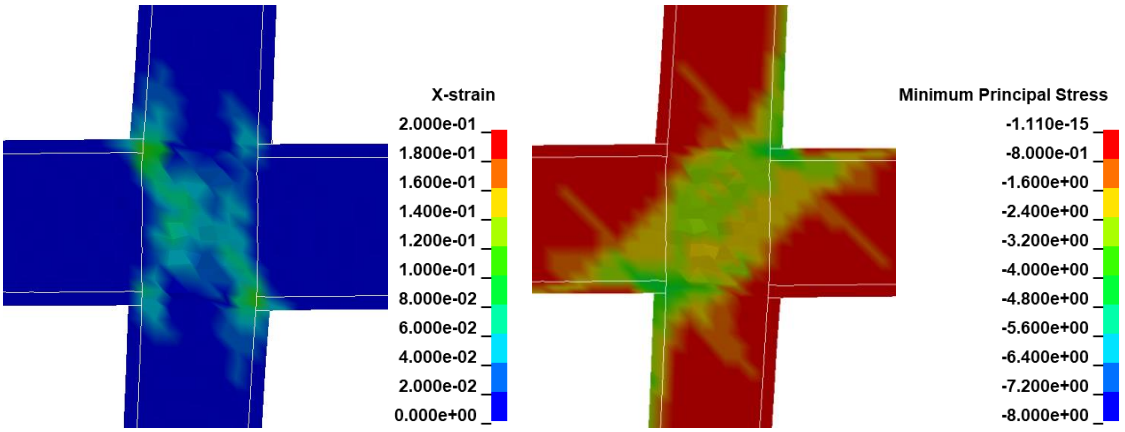

(b) Strain contour in A-A plane **(c) Minimum principal stress contour in A-A plane**

Figure 3-20 Force transfer mechanism for analysis of Specimen 2 tested by Leon (1989)

The panel truss mechanism is validated in Specimen 4. The x-strain in the A-A plane (Figure 3-21(a)), which is the strain in the horizontal direction of Specimen 4, is shown in Figure 3-21(b), when the lateral displacement is zero. Figure 3-21(c) illustrates the minimum principal stresses, Figure 3-21(b) reveals that large and unclosed flexural cracks have formed at the joint interfaces between the beams and columns with little yield penetration into the joint (Figure 3-19(b)). Panel trusses in compression take effect, with small distributed cracks form in the joint region (Figure 3-12(c)). A sufficient amount of transverse reinforcement in the joint area ensures the effectiveness of the panel truss mechanism by limited yield strain observed (Figure 3-19(d)).

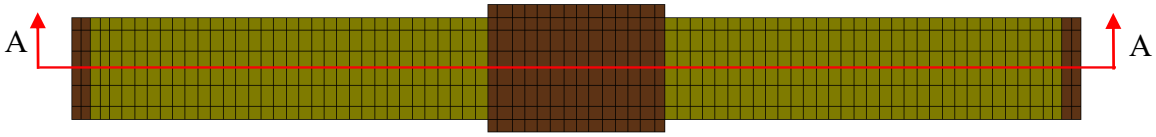

(a) Top view Specimen 4

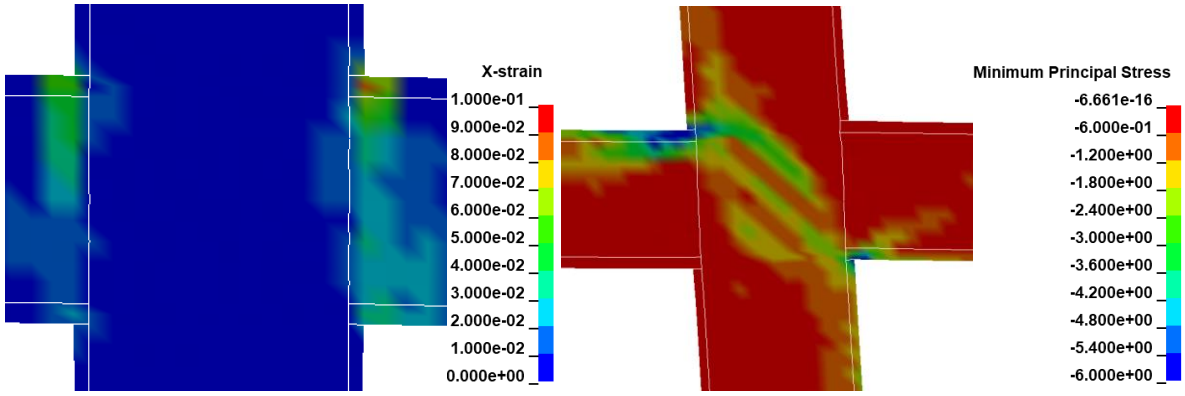

(b) X strain contour in A-A plane **(c) Minimum principal stress contour**

Figure 3-21 Damage and force transfer mechanism for analysis of Specimen 4 tested by Leon (1989)

3.2.4 Beam Reinforcement Stress

Local behavior is quantitatively compared with experimental records for beam stresses in Figure 3-22a to further approve the reliability of the analytical simulation herein.

First of all, the beam bar stress distribution is a time dependent field, especially when bond condition is taken into consideration. When bond condition is sufficient enough to transfer stress between reinforcement and concrete, the beam bar develops positive yield stress on one side of the column and compressive yield stress on the other side; after extensive stress and relative displacement grows for the bond, the stress distribution tend to present positive or negative on both sides of the column. Thus, parametric study is meaningful only when the two stress distribution is compared at the same time, which is exactly what Figure 3-22 to Figure 3-24 depict. For Specimens 2-4, the reinforcing bar stress distribution at the time of 17.2, 53.1 and 3.4 are plotted with the lateral displacement at 1.87 in., 3.92 in. and 1 in., respectively.

The peak bond strength τ_{max} which is defined in Equation (3-9, is found to have a significant influence on the beam bar stress distribution. A larger τ_{max} results in better bar stress transfer, and thus the stress on the other side of column can be in the opposite direction even after several cycles

of loading; while smaller τ_{max} brings worse bond strength and bar stress penetration may develop throughout the whole joint. For Specimens 2 to 4, the value of τ_{max} calculated in Equation (3-9 equals to 2.578 ksi. In parametric studies, τ_{max}=2 ksi and 0.7 ksi are compared for Specimen 2. The bar stress is in compression on the left side of column face for τ_{max}=2 ksi and, while a τ_{max}=0.7 ksi leads to tensile stress through the joint, as shown in Figure 3-22. Both Specimen 3 and Specimen 4 show a much better agreement in bar stress as shown in Figure 3-23(a) and Figure 3-24(a), respectively. Also, the trend is similar with the observation that the hysteretic curve of Specimen 3 reaches the best consistency from analysis to test.

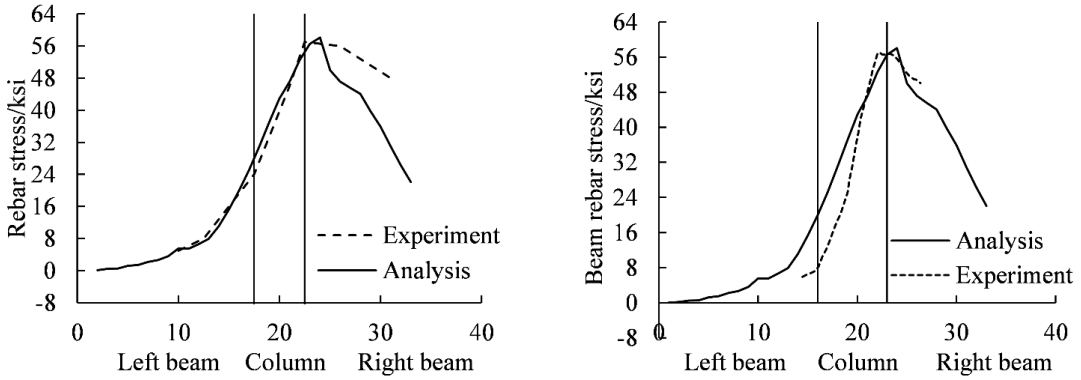

(a) τ_{max}=2 **(b) τ_{max}=0.7**

Figure 3-22 Top beam bar stress comparison for different values of peak bond stress in analytical models for Specimen 2 at 2.6% drift ratio tested by Leon (1989)

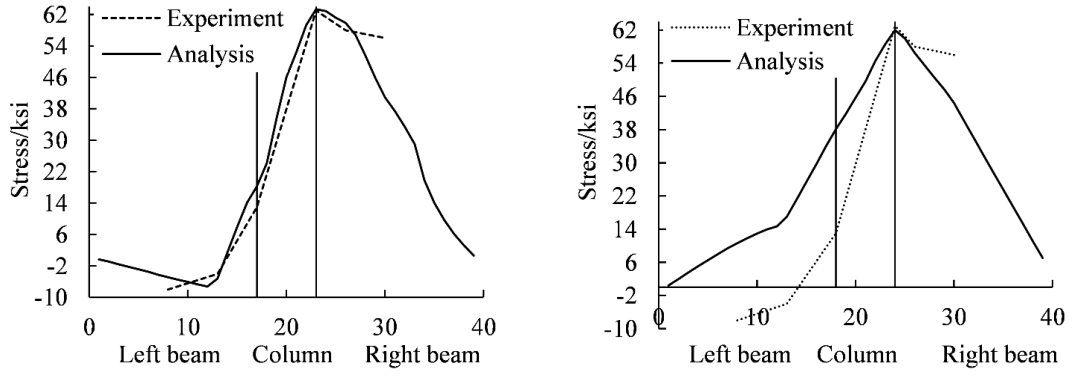

(a) τ_{max}=2 **(b) τ_{max}=0.5**

Figure 3-23 Top beam bar stress comparison for different values of peak bond stress in analytical models for Specimen 3 at 1.9% drift ratio tested by Leon (1989)

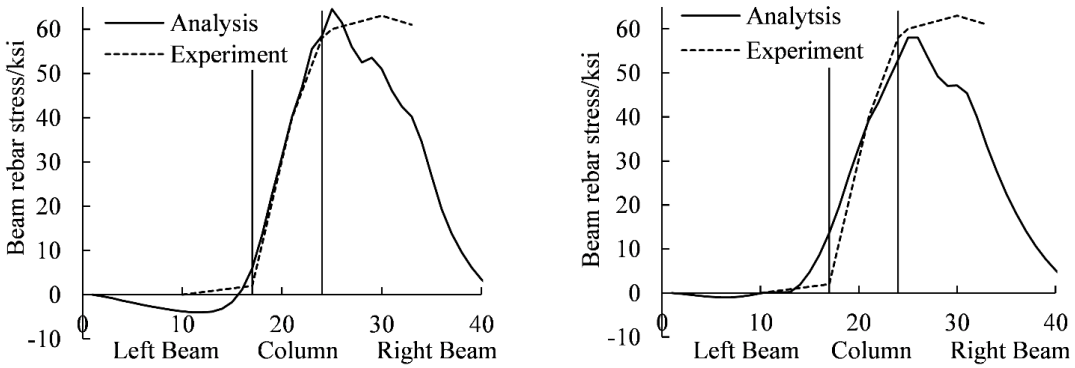

(a) τ_{max}=2 **(b) τ_{max}=1**

Figure 3-24 Top beam bar stress comparison for different values of peak bond stress in analytical models for Specimen 4 at 1.7% drift ratio tested by Leon (1989)

3.2.5 Moment v.s. Slip Relation

The bond-slip value was measured near joint corners in the experiment by an instrument as shown in Figure 3-25. The slip at a location next to the column face versus beam end moment relation from the simulation is compared with that from the test in Figure 3-26(a) and (b). Good agreements in strength, largest slip value and the overall shape are clear, thus further validating the ability of capturing local performance of the model. The slip value keep growing in one direction in both analysis and experiment, which is consistent with the conclusion from Peng et al. (2011) that irrecoverable extension of reinforcement brings elongation of plastic hinge in RC members.

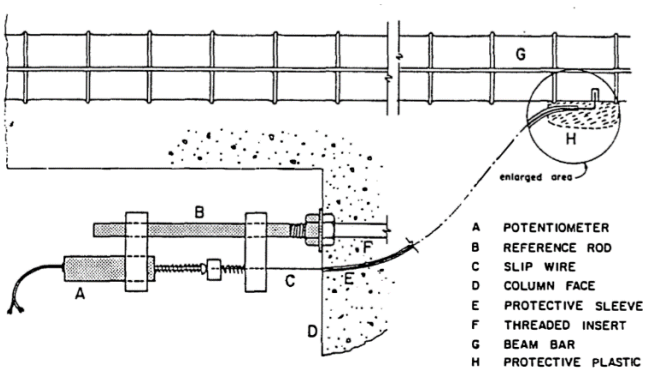

Figure 3-25 Slip-wire instrumentation (Leon 1985)

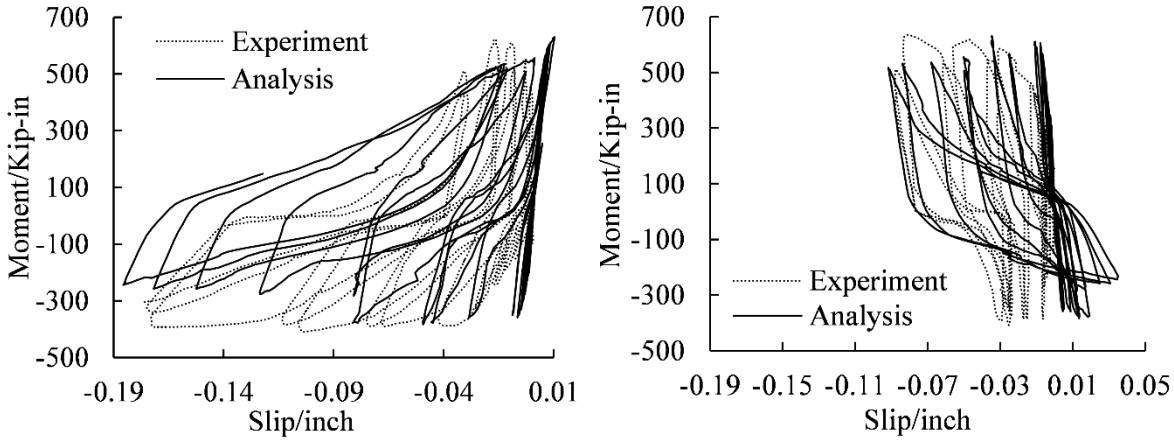

(a) Top beam bar **(b) Bottom beam bar**

Figure 3-26 Comparison of slip versus beam moment curve for beam reinforcing bar of Specimen 2 tested by Leon (1989)

3.2.6 Joint Shear Distortion versus Column Load

The shear angle of the panel was measured in the test by an instrument shown in Figure 3-27(a). The analytical results are collected at three nodes marked in the Figure 3-27(b) at the same locations in the test. The joint strain - column end loading force relations from experiment and analysis are compared in Figure 3-28. This comparison of Specimen 2 illustrated in Figure 3-28(a) represents a satisfactory agreement in the early stages but its ability to properly capture the shear cracking and associated shear strength deterioration is less clear from the later cycles. The comparison for Specimen 3 and Specimen 4, shown in Figure 3-28(b) and (c), respectively, is much better as Specimen 3 had much lower amounts of shear cracking in the joint. The almost elastic behavior of Specimen 4 is clear from Figure 3-28(c).

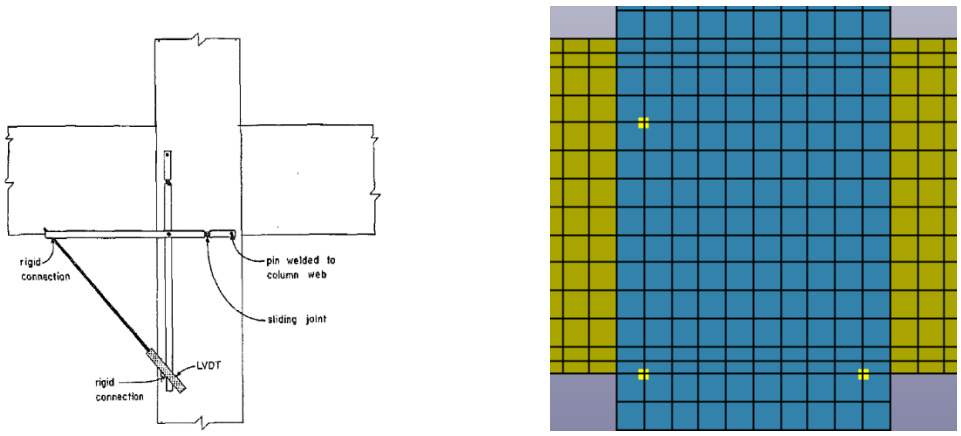

(a) Instrument in the experiment **(b) Nodes used to calculate strain in the analysis**

Figure 3-27 The way that shear angle of the panel is measured in experiment (Leon 1989) and analysis (Specimen 2)

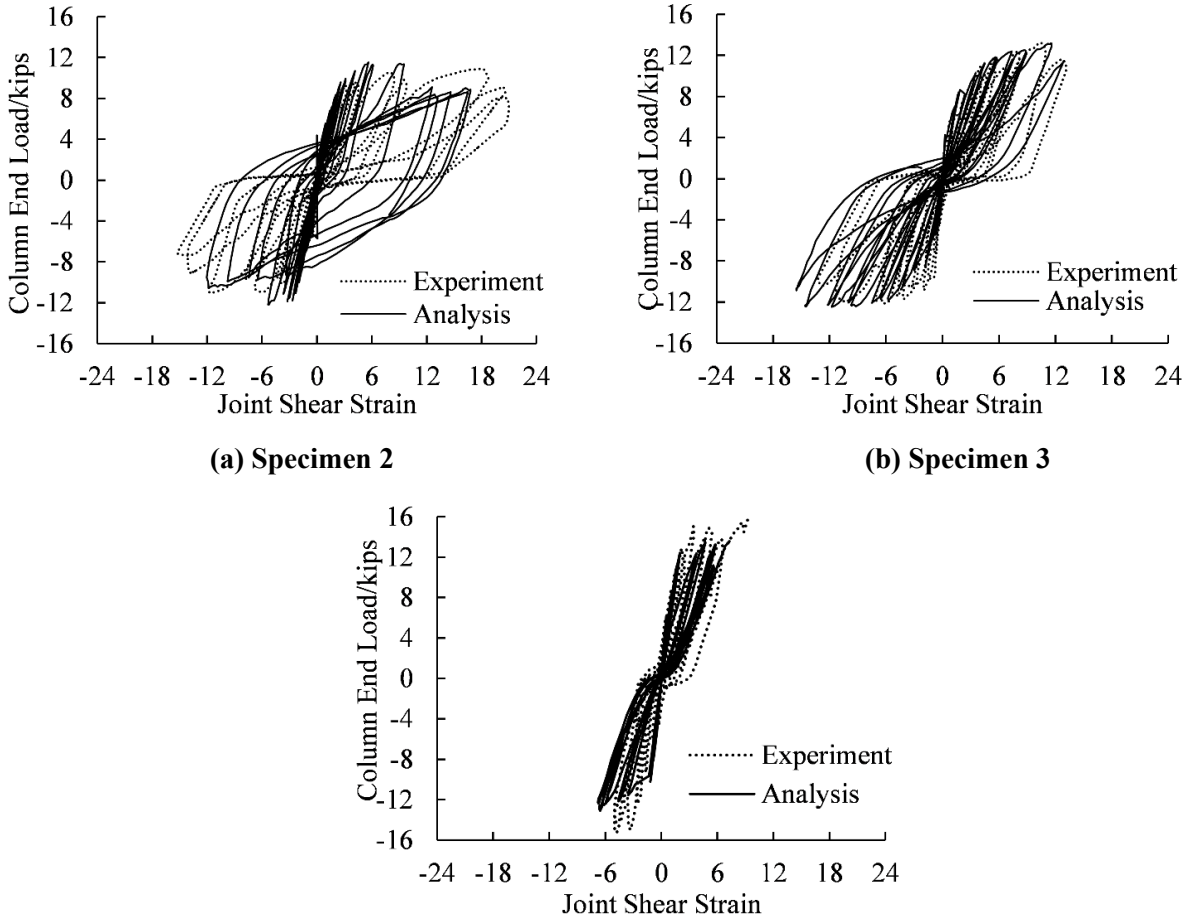

(a) Specimen 2 **(b) Specimen 3**

(c) Specimen 4

Figure 3-28 Joint shear versus shear angle of the joint panel for analysis of specimens tested by Leon (1989)

From Figure 3-28, the ability of capturing shear strain in the joint area is validated for the model. Even for Specimen 2 which failed due to large diagonal shear crack, the error for shear strain in the joint is still less than 20%.

3.4 Sensitivity Analysis

The validation analyses are supplemented by a brief parametric study, to investigate the sensitivity of the analytical results to the values of model parameters.

A list of some of the analyses carried out, along with the parametric variation is shown in Table 3-2.

Table 3-2 Parameters variation in analysis

Parameter	Values
f_c'/ksi	5.0, 5.5
f_y for bar/ksi	65, 70
Ductility factor d	5.0, 7.5
Peak bond strength τ_{max}/ksi	0.50~2.65
f_u for bar/ksi	100, 110, 120
f_t/ksi	0.05~0.60
G_c/kip·in^{-1}	0.05~0.11
f_{res}/ksi	0.01, 0.05

Since the same loading curve is used for all simulations, the peak strength at a lateral displacement of 4.32 inches will be compared from Table 3-3 to Table 3-10. In addition, the Total Area of Hysteretic Loops (TAHL) which reveals the energy dissipation ability is given as well as the value of an Influence Coefficient (IC) of the interested parameter on the strength calculated as:

$$IC=\frac{(result_1-result_2)/result_1}{(parameter_1-parameter_2)/parameter_1} \quad (3\text{-}13)$$

where “parameter” represents the interested parameter in sensitivity study, and “result” represents strength or TAHL of the two analyses. When there are more than two groups of results, the average value of IC is recorded in the tables. Absolute values are used in calculating the final average IC value.

The strength at the lateral displacement of 4.32 inches from the experiment is 13.03 kips, and the TAHL from the test is 160.31.

3.4.1 Physical Parameters

3.4.1.1 Yield Stress f_y of Longitudinal Reinforcement

The IC values from Table 3-3 reveals that higher yield strength improves the strength and also the energy dissipation ability of the joint, which can also be verified by theoretical methods.

Table 3-3 Effect of f_y

Model No.	f_y/ksi	Strength/kips	IC	TAHL	IC
78	70	13.15	0.74	160.36	0.20
87	65	12.50		158.04	
78	70	13.20	0.40	160.36	0.42
92	80	13.95		170.00	

3.4.1.2 Ultimate Stress f_u of Longitudinal Reinforcement

Higher ultimate strength of reinforcement does not significantly improve the joint strength since the longitudinal reinforcing bar already slipped before reaching the ultimate stress needed for rupture. Since a higher f_u provides less deformation at the same stress level, thus the TAHL is slightly smaller as demonstrated in Table 3-4.

Table 3-4 Effect of f_u

Model No.	f_c'/ksi	f_u/ksi	Strength/kips	IC	TAHL	IC
78	5.50	120	13.20	0.18	160.36	-0.33
79		100	12.81		169.07	
74	5.00	110	11.72	0.33	169.86	-0.73
75		100	11.64		181.18	

3.4.1.3 Concrete Compressive Strength f'_c

Based on the data, the concrete compressive strength significantly influences the ultimate strength and TAHL of Specimen 3. Higher compressive strength of concrete contributes to a higher strength directly and results in stiffer behavior and thus smaller area of the hysteretic loop as shown in Table 3-5.

Table 3-5 Effect of f'_c

Model No.	f'_c/ksi	Strength/kips	IC	TAHL	IC
74	5.00	11.72	0.34	169.86	0.07
91	8.00	14.08		176.67	

3.4.1.4 Tensile Strength of Concrete f_t

The tensile strength of concrete f_t has a positive impact on the ultimate strength of Specimen 3 as presented in Table 3-6. Higher f_t prevents large deformation of the joint, and thus result in a smaller TAHL value.

Table 3-6 Effect of f_t

Model No.	f_t/ksi	Strength/kips	IC	TAHL	IC
65	0.50	11.10	0.23	178.88	-0.11
66	0.40	10.60		182.68	

3.4.1.5 Peak Bond Strength τ_{max}

The effect of bond strength is complicated because the bond stress-strain relation is nonlinear, thus the performance of the joint heavily rely on if the bond deteriorates during the cycles. A τ_{max} smaller than certain value could result in dramatic strength decrease of the joint. Nevertheless, the peak bond strength has a decisive impact on the TAHL of Specimen 3 as presented in Table 3-7.

Table 3-7 Effect of τ_{max}

Model No.	τ_{max}/ksi	f'_c/ksi	f_y/ksi	Strength/kips	IC	TAHL	IC
26	2.19	4.00	66	12.84	-0.06	249.75	1.27
27	2.65			12.69		316.34	
28	2.40			11.96		274.03	
29	2.00	4.00	66	11.50	0.24	266.37	0.67
30	1.90			11.36		250.80	
71	1.50	5.00	70	12.66	-0.19	181.14	0.20
73	2.40			11.22		203.11	
76	2.00	5.50	65	12.37	0.10	168.38	0.44
77	2.40			12.62		183.17	
78	2.00	5.50	70	13.20	-0.11	160.36	0.63
81	2.58			12.77		189.64	

3.4.1.6 Compressive Residual Strength Factor of Concrete f_{res}

Compressive residual strength of concrete does not play an important role on Specimen 3, since Specimen 3 didn't encounter a huge shear failure and concrete crushing during the last several cycles does not compare with what is happening on Specimen 2. The difference of the absolute values is small for both strength and TAHL (Table 3-8).

Table 3-8 Effect of f_{res}

Model No.	Com. Residual	Strength/kips	IC	TAHL	IC
78	0.05	13.20	0.0028	160.36	0.01
88	0.01	13.17		159.08	

3.4.2 Model Parameters

3.4.2.1 Ductility Factor *d*

The ductility factor d demonstrates the increment on material ductility due to confinement effect on the nonlinear behavior of the specimen, and has found significantly influence the strength of the column under pressure (Moharrami and Koutromanos 2016). For a BCJ, it has influence on the concrete in the joint, as well as the plastic hinge region. The influence of *d* is displayed in Table 3-9.

Table 3-9 Effect of *d*

Model No.	*d*/ksi	Strength/kips	IC	TAHL	IC
62	5.00	10.61	-0.13	197.07	0.36
65	7.50	11.10		178.88	

3.4.2.2 Compressive Fracture Energy G_c

The compressive fracture energy for concrete can be calculated as the area under softening portion of stress-strain curve of concrete multiplied by the mesh size *h* of finite element model. Larger G_c gives a more ductile concrete under compression, and will help to improve the ultimate strength as well as the energy dissipation ability of the joint. Changing G_c does not brings a large difference on their absolute values though (Table 3-10), and the value of G_c actually should rely on the material properties of concrete such as the maximum aggregate size and water-cement ratio.

Table 3-10 Effect of G_c

Model No.	G_c/J	Strength/kips	IC	TAHL	IC
78	5.61e-2	13.20	0.0075	160.36	0.019
89	1.13e-1	13.30		163.53	

3.4.3 Summary of Sensitivity Study

The average IC values on strength and TAHL are summarized in Table 3-11 based on the calculations from Table 3-3 to Table 3-10.

Table 3-11 Average IC values

Parameter	Average IC on strength	Average IC on TAHL
f'_c/*ksi*	0.34	0.07
τ_{max}/*ksi*	0.15	0.66
f_y/*ksi*	0.40	0.42
f_{res}/*ksi*	0.0028	0.01
f_u/*ksi*	0.26	-0.53
G_c/*kip·in*$^{-1}$	0.0075	0.019
f_t/*ksi*	0.23	-0.11
d	-0.13	0.36

The observation from Figure 3-29 indicates that the main factor affecting the ultimate strength turned out to be the compressive strength of concrete and yield strength of longitudinal reinforcement. The energy dissipation ability is mainly influenced by the peak bond stress and yield/ultimate stress of longitudinal reinforcing bar.

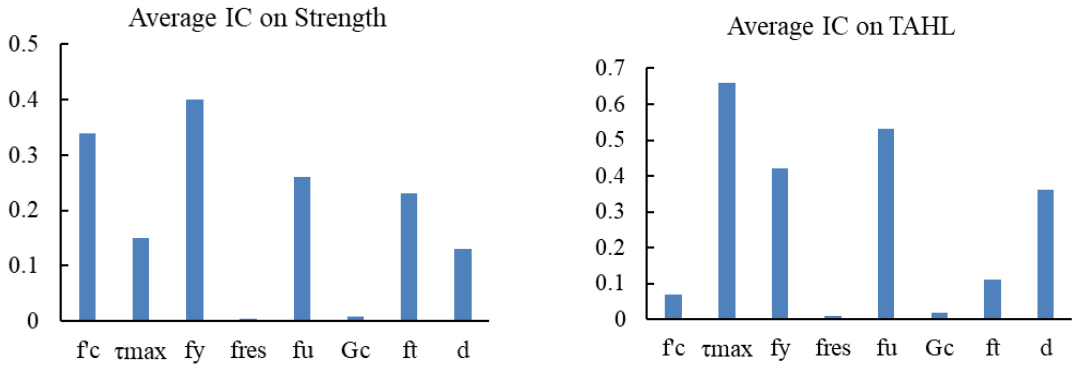

(a) **(b)**

Figure 3-29 Average IC on (a) strength and (b) TAHL

It can be concluded that, after the material properties are confirmed for concrete, the peak

bond stress is the parameter that has the largest impact on the performance of Specimen 3. Thus, further study is necessary to conclude how far the peak bond stress will impact on the performance of beam-column joint.

3.4.4 Influence of Bond-slip Effect

The criticality of including the bond-slip effect is depicted by comparing three specimens with and without bond-slip effect in Figure 3-30.

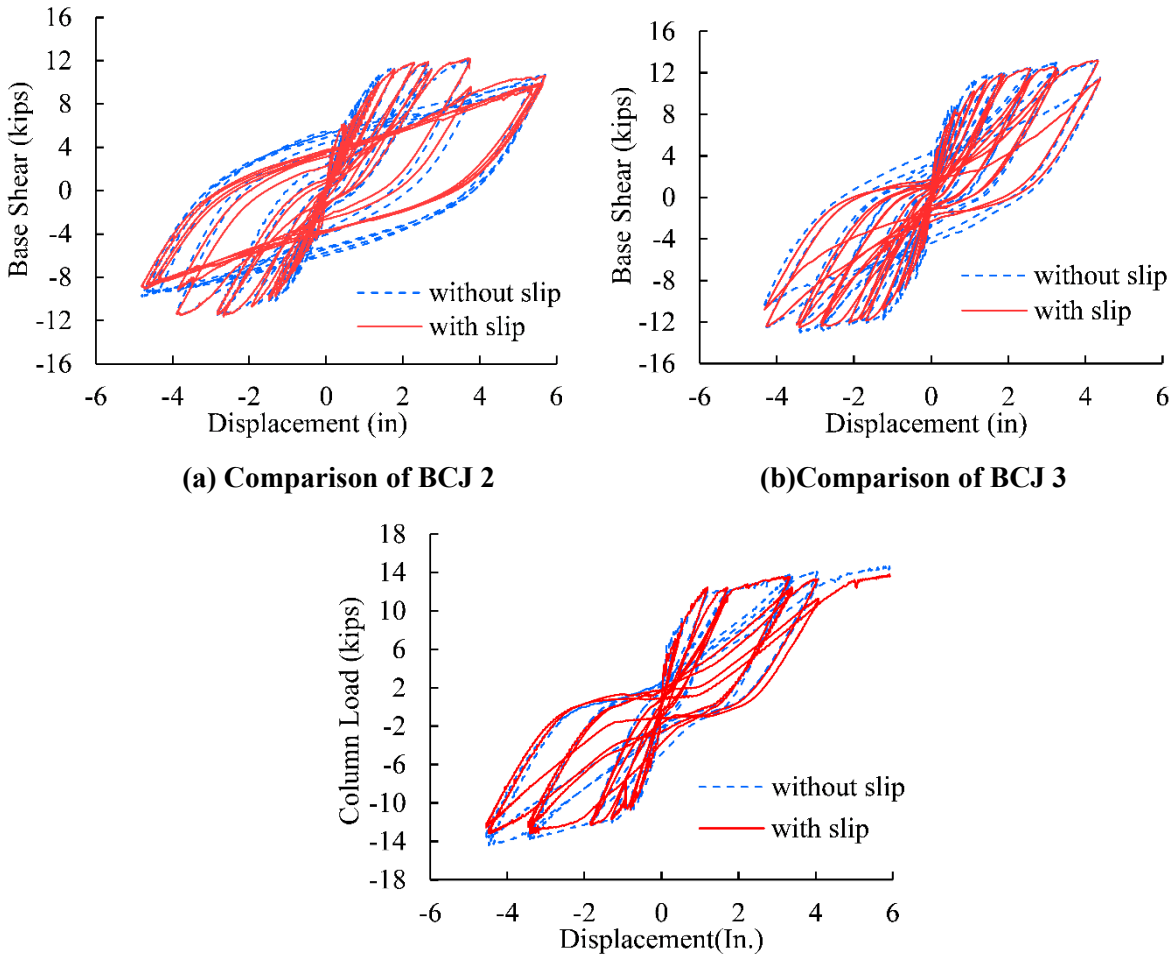

(a) Comparison of BCJ 2

(b)Comparison of BCJ 3

(c) Comparison of BCJ 4

Figure 3-30 Influence of bond-slip effect for analysis of specimen Specimen 2 to 4 tested by Leon (1989)

Major differences are found in the amount of pinching during the last loading circles, when the reinforcement is encountering slip and yielding, especially for BCJ 2 that has strain penetration all through the joint region. Specimen 4 encounters smallest influence of bond- slip model.

3.4.5 Influence of Mesh Size

Specimen 3 is re-analyzed with smaller element size in order to investigate the effect of the mesh size on the response. Specifically, the element sizes in two analyses are 1 inch and 0.5 inch, respectively. The analytically obtained response with the two different element sizes are compared with the experimentally recorded hysteretic response in Figure 3-31 (a) and (b). As can be observed from the figure, the initial stiffness and the strength of the BC joint is lowered by a smaller mesh size especially during the last several cycles. The pinching effect is less obvious due to the concrete crush in the joint. And the ultimate strength is lowered by smaller element size due to the compressive inelasticity parameter in the joint diagonal and at the joint corners. The cracking strain contour for two different element sizes is illustrated in Figure 3-32 when both analysis models are subjected to a lateral displacement of 0.75 inch with same contour color scale. The formation of an inclined crack is captured by both cases; this is also similar with what was observed in the experiment.

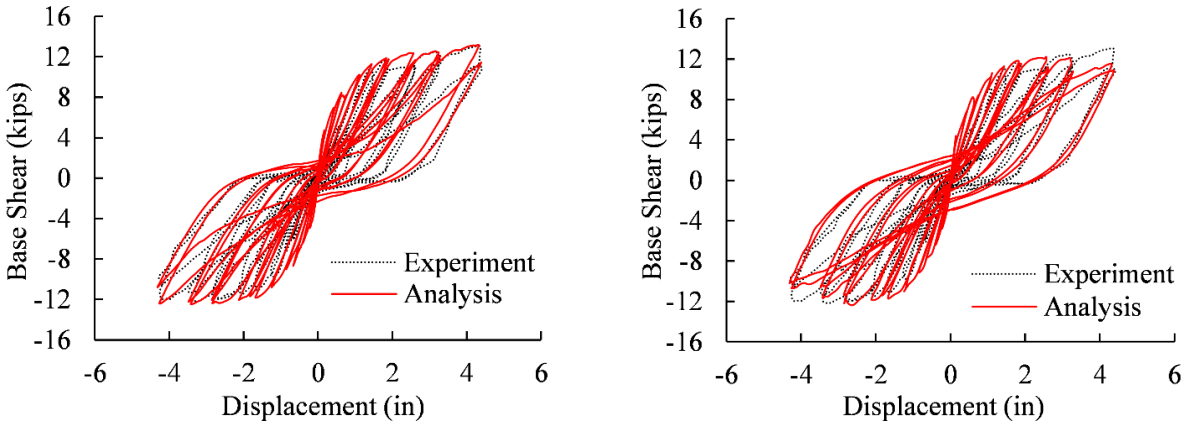

(a) Mesh size=1 inch **(b) Mesh size=0.5 inch**

Figure 3-31 Mesh size effects on overall hysteretic response of Specimen 3

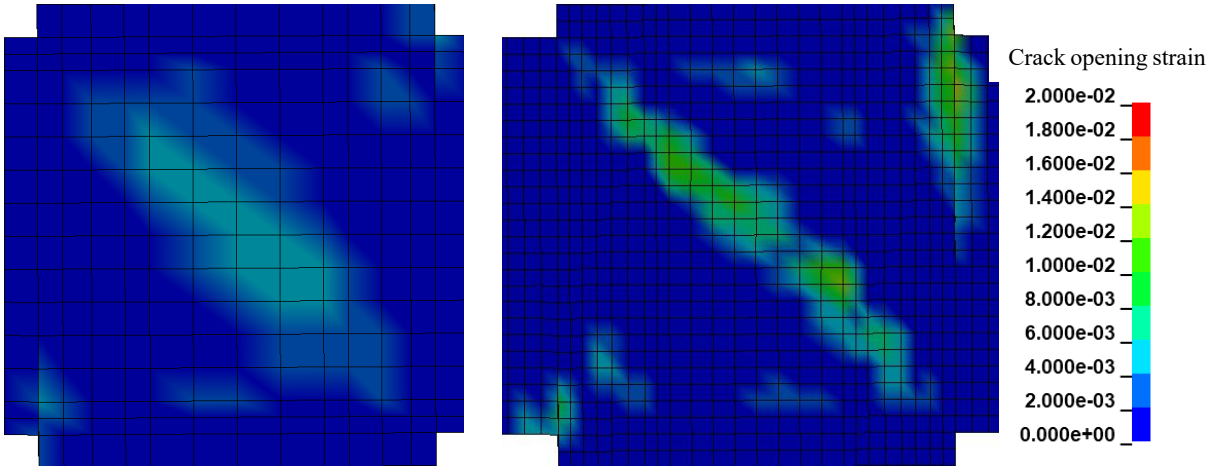

(a) Mesh size=1 inch **(b) Mesh size=0.5 inch**

Figure 3-32 Shear crack obtained with different element size

3.6 Validation of Two-way Interior Beam-Column Joint

As summarized in Section 2.3.3, a limited number of experimental studies in the literature have been focused on two-way interior beam-column joints, including the effect of the floor slabs subjected to bidirectional loading. In this section, the experiment performed by Kurose et al. (1988) is simulated by the analytical method aforementioned.

This section intends to compare the hysteretic response and the failure mode under bi-directional loading with the test results. Strain history of reinforcing bar, bond-slip behavior and other local response quantities will be examined.

3.6.1 Description of The Experimental Test

Three specimens were tested by Kurose et al. (1988) named J1, J2 and J3. Specimen J1 is an interior BC connection with one-way beam and slab, specimen J2 refers to an interior BC connection with two-way beam and slab, and specimen J3 is an exterior BC connection with two-

way beam and slab. The specimen J2 is selected based on the interest of the current research.

The geometry and detail of specimen J2 is shown in Figure 3-33; not shown are two layers of reinforcement in the slab consisting of #3 top reinforcing bar at 12 in. and bottom reinforcing bar at 24 in. on center.

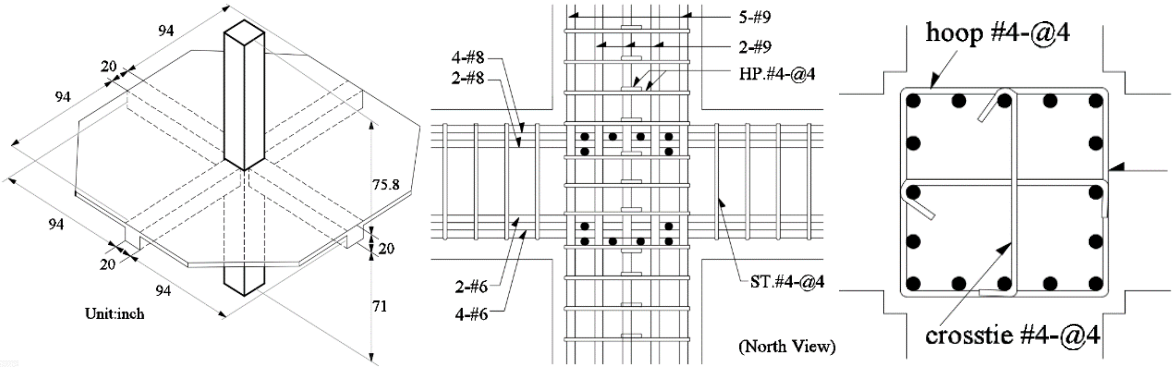

(a) Joint geometry **(b) Joint detail**

Figure 3-33 Geometry of specimen tested by (Redrawn after Kurose et al., 1988)

The bidirectional loading history for specimen J2 is shown in Figure 3-34. This is one of the most challenging type of loading curve for analytical simulation. Except for that it's bidirectional and cyclic, a large proportion of the loading is launched in one direction only and leave the beams in the other direction unloaded while still influenced by the beams being loaded. This requires the model to be able to accurately capture multiaxial stress state of the material. No axial load was applied on the column.

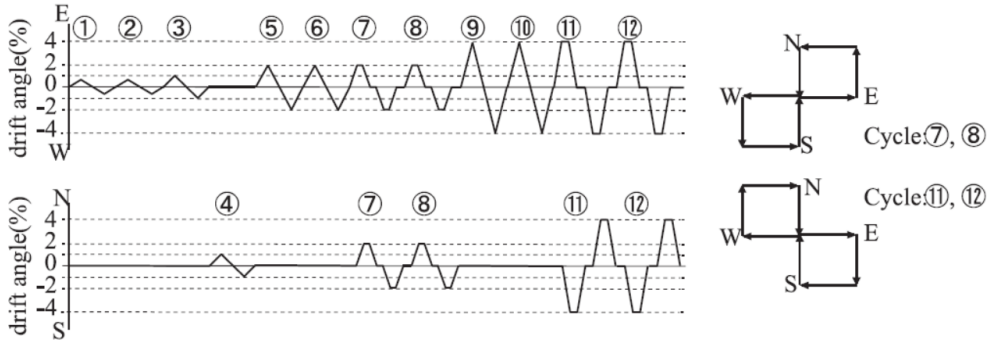

Figure 3-34 Loading curve in two directions of specimen J2 tested by Kurose et al. (1988)

The observations from the experiment include:

1. Considerable pinching was observed in story shear-drift angle relations, which was speculated as shear distress in the joint, flexural distress in the members, and bond deterioration along beam bars;
2. Bidirectional interaction was evident in which loading in one direction will significantly affect the strength in the other direction;
3. Yielding of lateral reinforcement in the joint was observed as well as shear distortion which further increased the lateral displacement.
4. The measured bidirectional strength exceeded the tested unidirectional strength, which reveals the necessity of using a concrete material which can account for triaxial stress state.
5. Top beam bar anchored with 20 d_b showed good bond behavior, while bottom beam bar with 27 d_b development length exhibited loss of bond stress.
6. The column encountered concrete crushing at 2% drift level under bidirectional loads and started to contributing the pinching on the hysteretic curve.

Comparing the above observations from the experiment with analytical output will further evaluate the reliability of the FE model used herein. The FE model of J2 is shown in Figure 3-35.

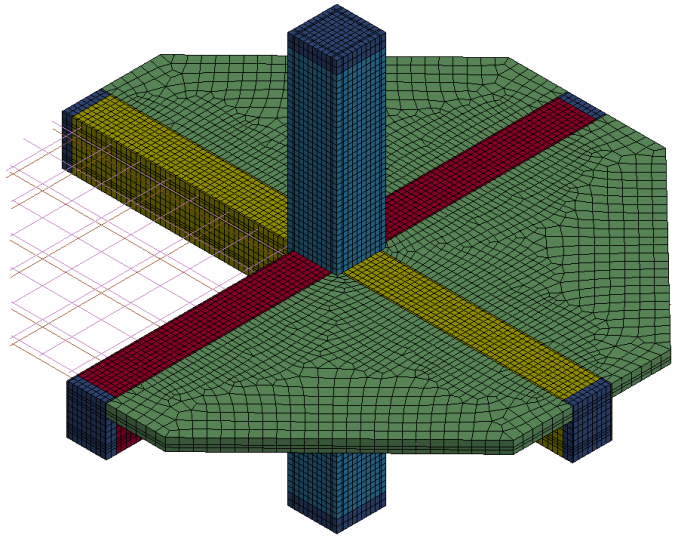

Figure 3-35 Finite element model of two-way interior BC joint

The model consists of 42336 solid elements for confined and unconfined concrete, 8896 beam elements for longitudinal, transverse and slab reinforcement, and 54823 nodes in total. One-fourth of the slab is hided to show the slab steel layers embedded in. All the material properties can be found in the report of Kurose et al. (1988).

3.6.2 Force-Displacement Response

The story shear versus the drift angle of the beam is compared with experimental data in both East-West (EW) and North-South (NS) directions in Figure 3-36.

The model generally provides accurate simulations of the initial stiffness and the degradation of strength. The plot shows a good consistency in the overall shape, which estimates the ultimate strength with an error of 7% in EW direction (71.46 kips experimentally and 66.43 kips analytically), and 3% in NS direction (57.54 kips experimentally and 59.77 kips analytically). Considerable pinching is observed in the plot, which is also identical with the experimental result. The reduction of strength in one direction due to the loading on the other direction is also observed in the plot, which clearly conveys the bidirectional interaction between beams in two directions.

The strength in NS direction at 0% drift ratio is overestimated because the slab steel is embedded in the slab for simplification without any bond-slip effect, thus overestimating the stiffness contribution from the slab and strengthening the collaboration of beams in two directions. Although the NS beams is not loaded during that time, it is influenced by the EW beams which are being loaded, resulting in a higher shear force as compared with the experimental result.

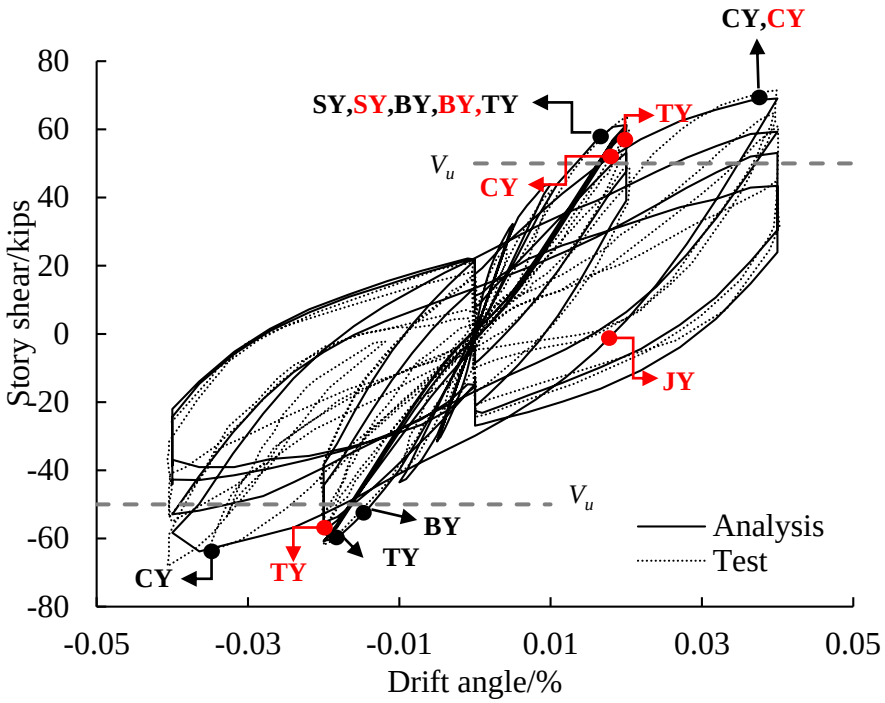

(a) E-W direction

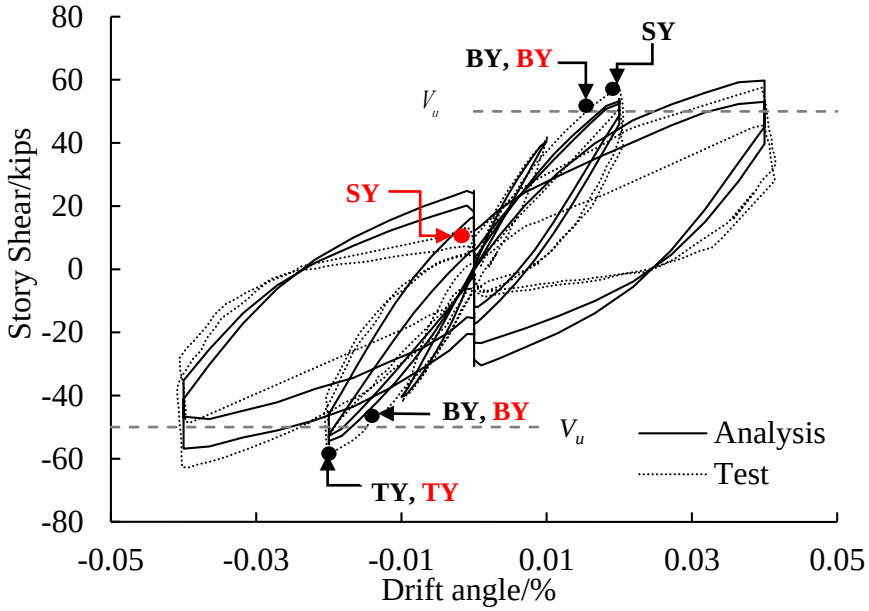

(b) N-S direction

BY: Bottom beam bar Yield; CY: Column longitudinal bar Yield; SY: Slab bar Yield; TY: Top beam bar Yield; JY: Joint transverse reinforcement Yield; V_u: Calculated ultimate load based on beam hinge mechanism

Figure 3-36 Analytical and experimental comparison of story shear versus drift angle of specimen J2 tested by Kurose et al. (1988)

One advantage of this model is that it can capture and compare all the detailed measurements from the experiment like the yield time of reinforcement in different locations as shown in Figure 3-36. The dots and labels in black represent the experiment results, and those in red represent the analytical results. If the analytical result coincides with the experimental result, it will be indicated by the label content in red right after the black one. In the EW direction, the model generally captures the right yield time of reinforcement in the column and bottom of beam. The top beam reinforcement yielding is delayed by one cycle due to the overestimated slab contribution but still happens during the 2% drift cycles, and the stress already reached 67.1 ksi (f_y= 67.2 ksi) for the target cycle. This difference does not result in a large influence on the overall analytical response. Due to the same reason, the slab steel yielding also occurs earlier in the NS direction.

3.6.3 Joint Shear Response

The drift angle and story shear orbits with respect to the 7^{th} , 8^{th}, 11^{th}, 12^{th} cycles (Figure 3-34) are shown in Figure 3-37, where the story refers to the entire height of the column. During these cycles, the drift angle in one direction keeps constant when the beams in the other direction are being loaded (Figure 3-37(a)). However, the interaction between beams in two directions is apparent indicated by the unique shape of the story shear orbit. Both orbits from the analysis match well with the experimental plot.

To study the relation of shear force and shear deformation of the joint, the joint shear distortion is calculated based on the displacement at beam ends and joint center as described in Figure 3-38(b). The displacements are measured by the instruments shown in Figure 3-38(a) in the experiment. Analytical results also rely on the same variables captured at the same location, and are compared in Figure 3-38(c) and (d).

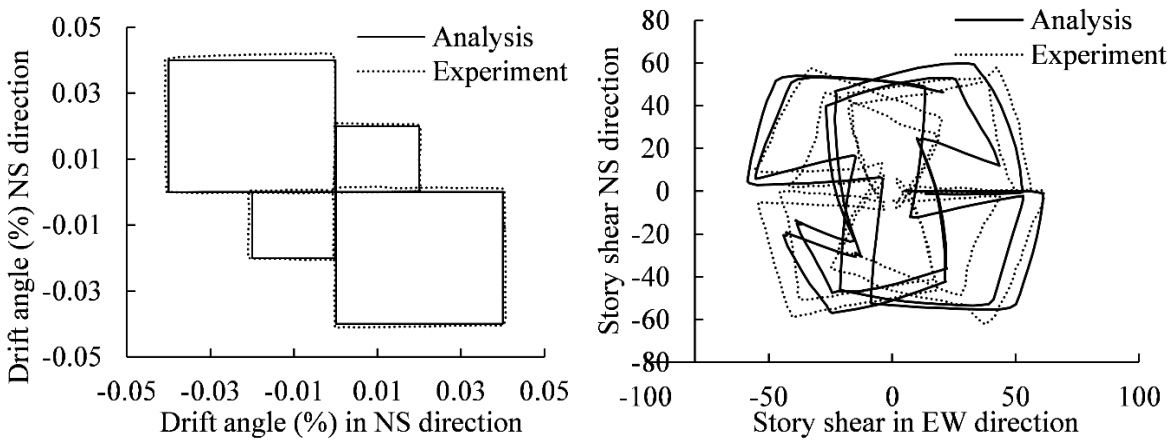

(a) Drift angle orbit **(b) Story shear orbit**

Figure 3-37 Comparison of drift angle and story shear orbits for J2

It is concluded from the report that apparent degradation of the joint is observed from the plots. The joint distortion keeps increasing especially in the EW direction even when the NS beams were loaded. The maximum joint shear exceeded the recommended design strength of $20\sqrt{f_c'}$ in both directions. The rapid increase of joint distortion up to 4% indicates that the specimen failed in joint shear.

The analytical results provide a satisfactory agreement in both the overall development and peak values of shear distortion. The compressive inelasticity parameter of the surfaces cut at the joint center is shown in Figure 3-39 in both directions. This figure verifies that severe damage forms in the joint area, with more damage observed in EW direction compared with NS direction. To demonstrate a better comparable contour, the range of the parameter κ is shown from 0 to 0.7. It has to be mentioned that the peak value of the parameter κ corresponding to the solid elements is 0.215, after which concrete starts softening.

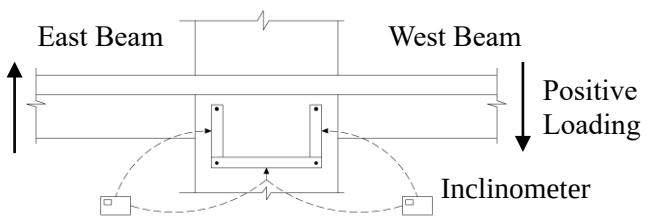

(a) The instrument used to measure inclination

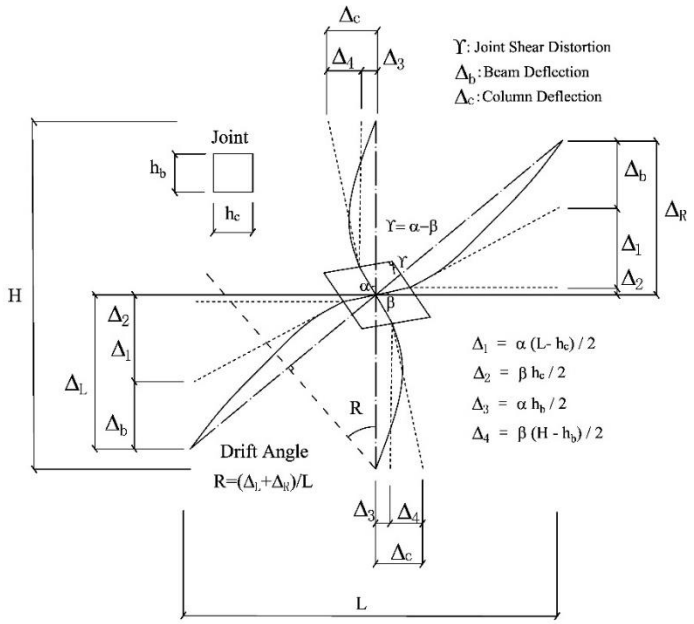

(b) Methodology for calculation of joint shear distortion (Redrawn Kurose et al., 1988)

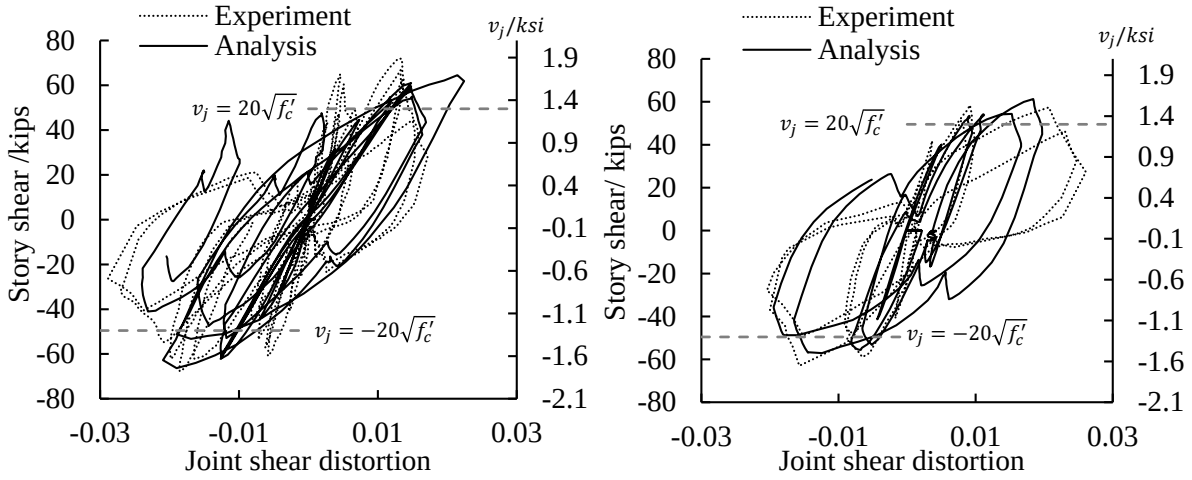

(c) EW direction **(d) NS direction**

Figure 3-38 Story shear-joint shear distortion of J2

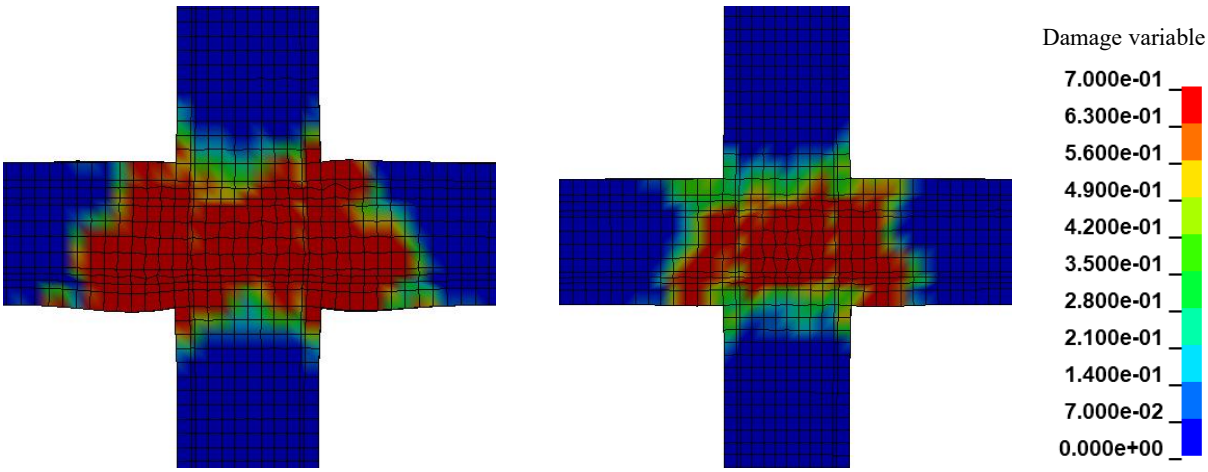

(a) EW direction **(b) NS direction**

Figure 3-39 Compressive inelasticity parameter from the cut in the joint center

3.6.4 Behavior at Final Loading Stage

3.6.4.1 Beam Bar Behavior

It was reported that the specimen developed beam flexural yielding during the 2% drift cycles and then failed in the joint shear at 4% drift cycles. The analytical and experimental comparison of strain-story shear relation of top beam reinforcing bar at location a and b (Figure 3-40(a)) is plotted in Figure 3-40 (b) and (c), where the vertical dashed line represents the yield strain of top beam bar, and the numbers in circles represent the specific loading cycle. The number with prime represents negative loading cycle. The analytical results show good agreement on both overall development and also the magnitude of the strain.

It has to be mentioned that during the negative loading (East beam loading downward) in cycle 9 in the experiment, the pin connection of the east ram fractured suddenly and the hydraulic pressure was released to zero as described in the report. The test was resumed after the pin was replaced. This scenario is not simulated in the analytical simulation, thus the experimental results show an unloading strain to nearly zero after the 9^{th} cycle, while this is not indicated in the

analytical result.

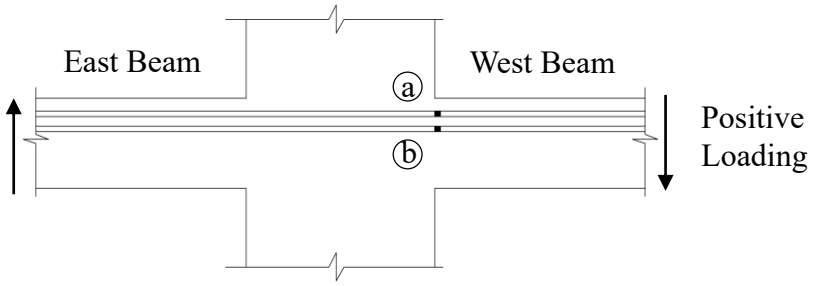

(a) Location of strain being compared

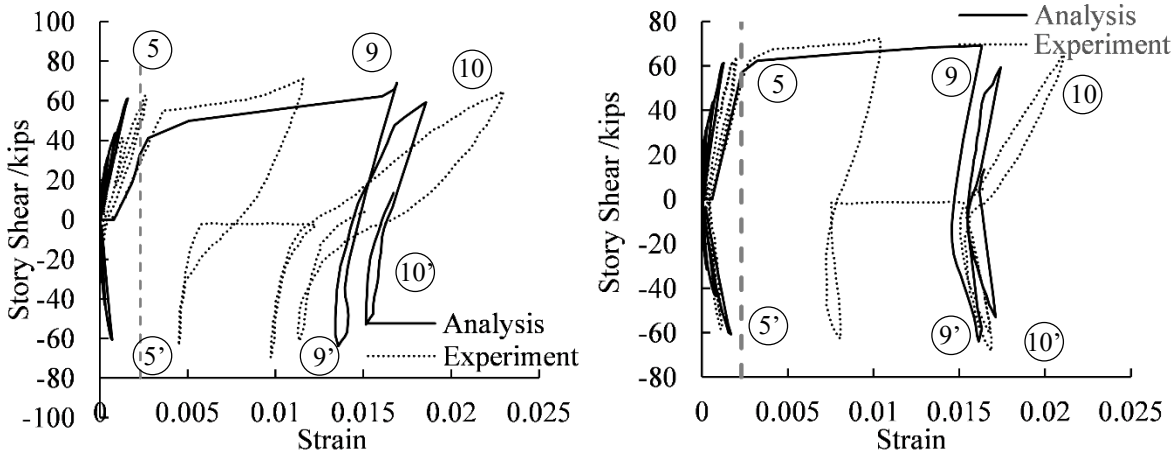

(b) Comparison of strain at location a **(c) Comparison of strain at location b**

Figure 3-40 Comparison of top beam bar strain

The comparison of strain-story shear relation of bottom beam reinforcing bar is plotted in Figure 3-41 (b) and (c), with the specific location indicated in Figure 3-41(a). Adequate agreement in the strain value and development is also obtained for the two layers of bottom beam reinforcing bar.

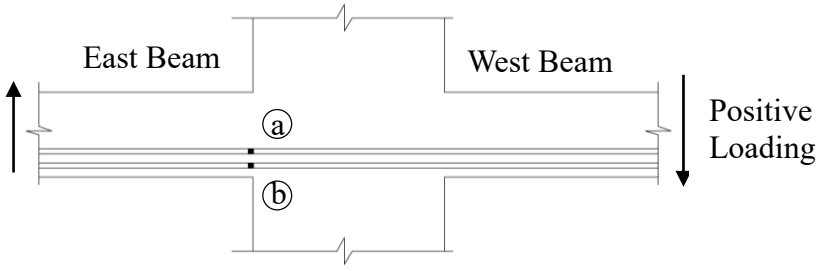

(a) Location of strain being compared

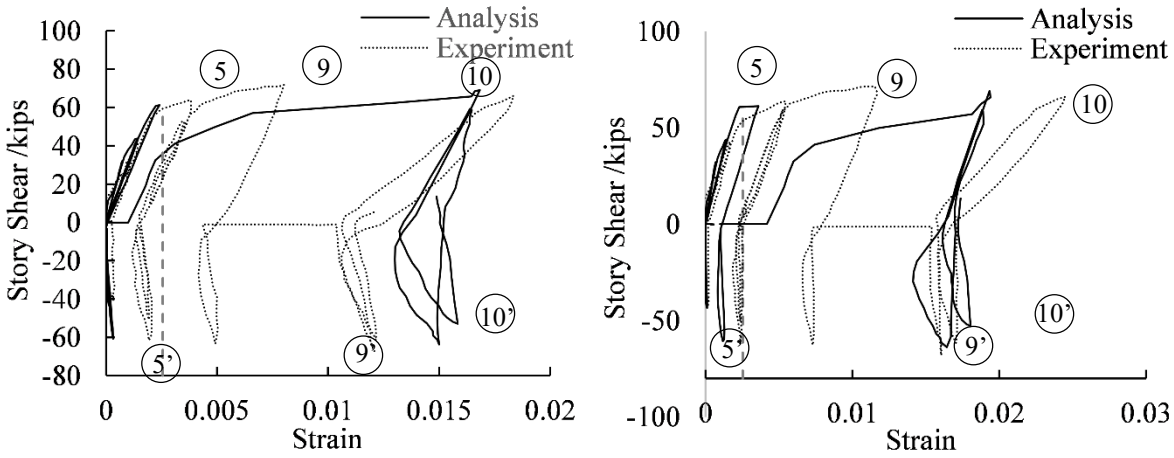

(b) Comparison of strain at location a **(c) Comparison of strain at location b**

Figure 3-41 Comparison of bottom beam bar strain

To verify if the specimen developed beam flexural yielding during the 2% drift cycles, the strain-drift angle relation of two beam elements from the upper and lower layer of top beam reinforcing bar are plotted in Figure 3-42. It can be observed that both elements yield at 2% drift angle.

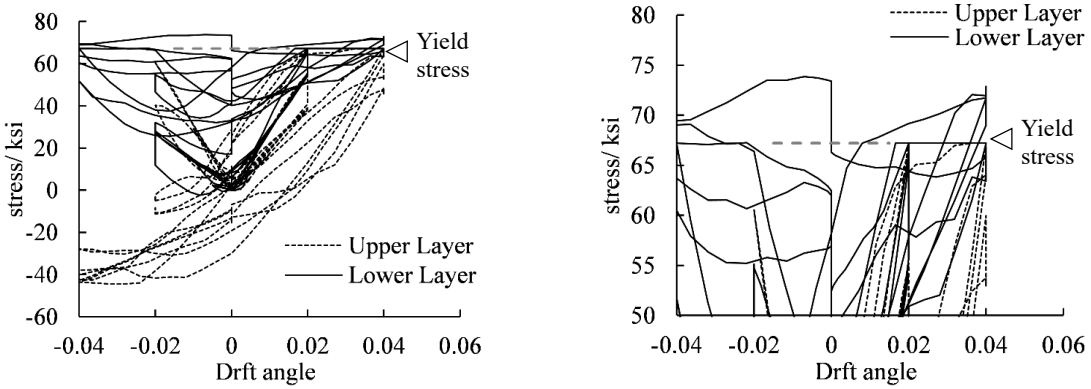

(a) The complete curve **(b) The amplified high tensile stress part**

Figure 3-42 Analytical stress-drift angle relation of beam bar element

3.6.4.2 Joint Transverse Reinforcement Behavior

The strains in the joint transverse reinforcement are compared from Figure 3-43(c) through (f). The strain output comes from 5 sets of transverse ties in the joint, among which three (Z2, Z3

and Z4) are located between the top and bottom beam bars, and the other two (Z1 and Z5) are above and below beam bars (Figure 3-43(a)). On every set of ties, strain from four locations labled X1 to X4 (Figure 3-43(b)) are compared from experiment and analysis; two are in the EW direction and the other two are in the NS direction. Results are compared from 7 different cycles at different drift ratios with lines indicated with different colors; dotted lines represent experimental results and continuous lines represent analytical results (Table 3-12).

Table 3-12 Color and drift ratios of lines in Figure 3-43

Line color	------	------	------	------	------	------	------
Drift ratio X(%)	+0.4	+1	0	+2	+2	+4	+4
Drift ratio Y(%)	0	0	+1	0	+2	0	-4
Loading cycle	1	3	4	7	7’	9	11

…….. Experimental results _____ Analytical results

The analytical results successfully capture the strain values within an acceptable range and evaluate the behavior of joint reinforcement, including:

1. All the analytical strain values fall in the same magnitude with experimental results.
2. The strain increases with the drift angle, especially for the three sets locate in the middle portion of the joint. The ties locate in the middle has higher strain than those on the top and bottom.
3. The strain in the EW direction (X1 and X2) increase when loading the beams in NS direction (cycle 7’), which validates that the ties are effective in confining the joint concrete.
4. The three sets of ties in the middle yield (at a strain of 0.00274) at all four locations, which is consistent with the experimental results and indicates significant shear distortion in the joint.
5. The analytical result complements the strain outputs which are missing in the experiment.

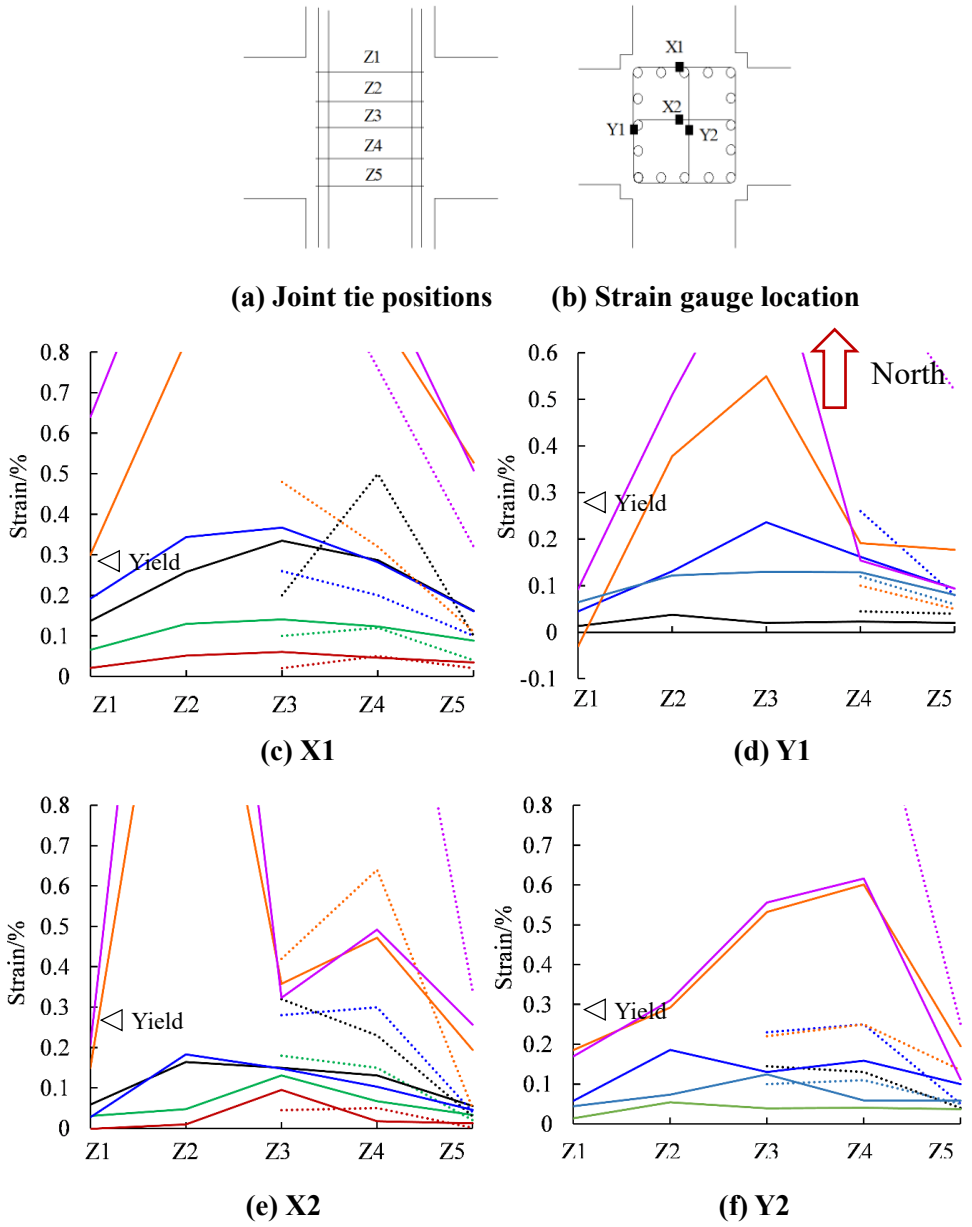

Figure 3-43 Strain comparison of joint tie in J2

3.6.4.3 Bond-slip Behavior

It is reported that the top longitudinal beam bars with a development length of 20 d_b showed good bond behavior under large deflection reversals, while bottom longitudinal beam bars with a development length of 27 d_b exhibited a loss of bond stress likely due to redistribution of compressive stresses from bars to concrete at the level of the bottom bars. The analytical bond slip

value at the locations indicated in Figure 3-44(a) is plotted versus drift angle. The locations on different sides of column face are selected to have slip value in the same direction. The result of relative bond slip value (Figure 3-44(b)) is consistent with the measurement from the experiment, where the bottom beam reinforcing bar encounters much larger bond-slip as compared with the top beam reinforcing bar. The reason is that the bottom beam bar yields earlier than top beam bar (Figure 3-44(c)). The accumulated tensile plastic strain disabled the ability to develop compressive strain in the reinforcing bar. Thus the bottom beam reinforcing bar only develops tensile stress during the last several cycles (Figure 3-44(c)). While the concrete adjacent is in compression, which results in a larger bond-slip behavior than top beam reinforcing bar.

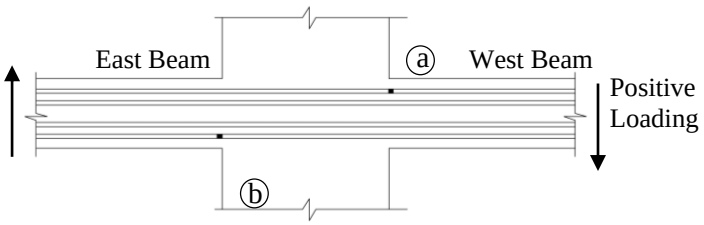

(a) Location of bond-slip value captured

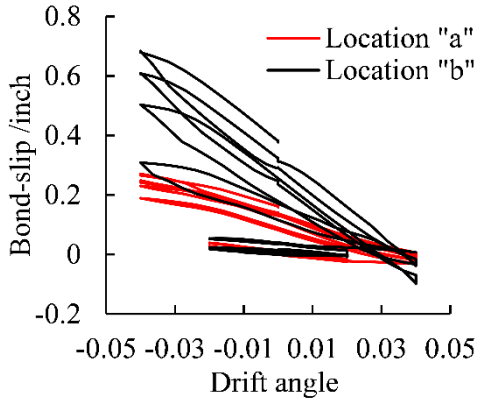

(b) Bond-slip comparison

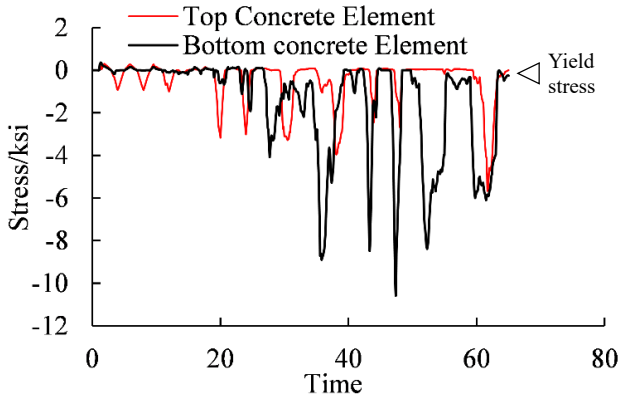

(c) Reinforcing bar stress history comparison

Figure 3-44 Bond-slip and reinforcing bar stress comparison at location a and b

3.6.4.4 Column Behavior

The story shear-strain relations at locations indicated in Figure 3-45(a) are compared in Figure

3-45(b) and (c). This analysis does not include the bond-slip effect of longitudinal reinforcing bar in the column, thus the chevron shape of the hysteresis curve from the experiment is not clear in the analytical result.

It is reported that the column developed concrete crushing at 2% drift levels under the bidirectional loading, which is less than the calculated capacity, and resulted in the pinching of the hysteric response. The compressive inelasticity parameter at 2% drift angle is illustrated in Figure 3-46 at a range from 0 to 0.215, which is the peak value of parameter κ and indicates the crushing and softening of concrete elements. It can be observed that the column crushed at corners both above the slab and below the beams, which also match with the experimental observation.

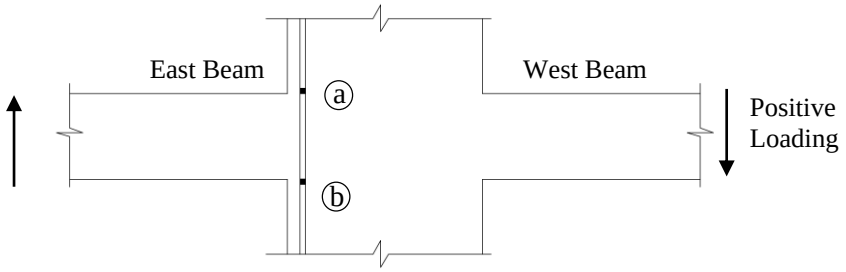

(a) Location of bond-slip value captured

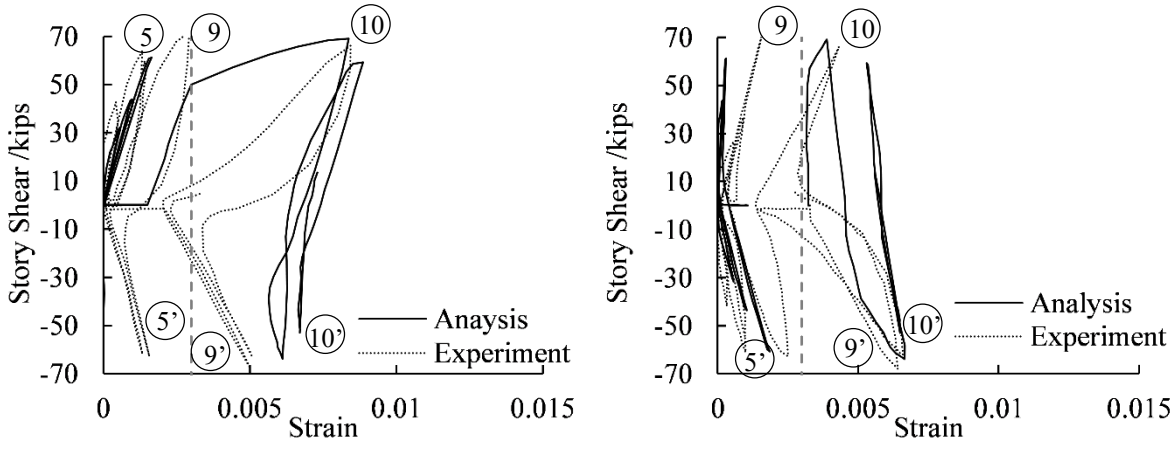

(b) Comparison of strain at location a **(c) Comparison of strain at location b**

Figure 3-45 Comparison of column bar strain at joint end

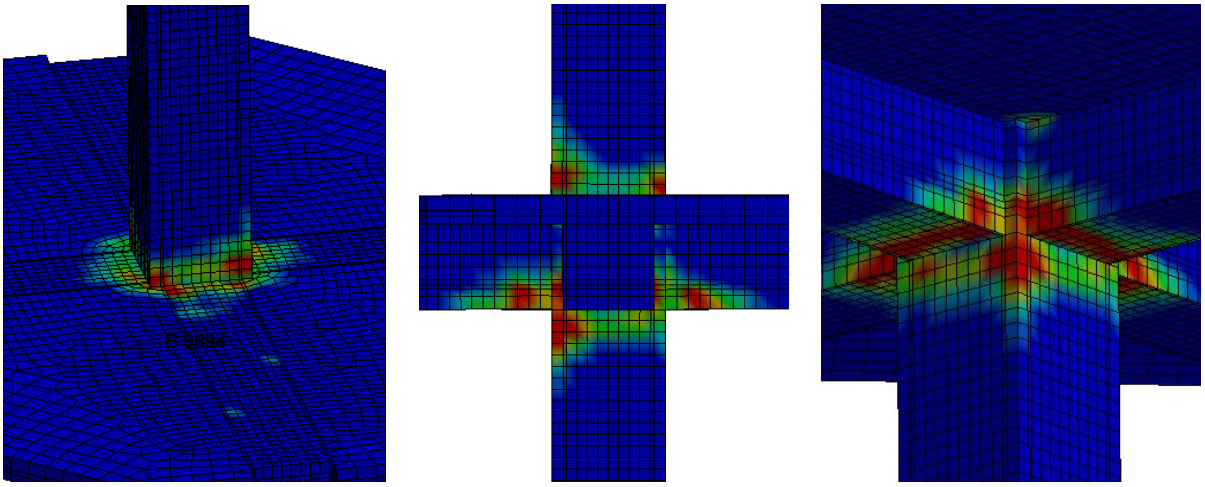

(a) View above the slab **(b) Side view** **(c) View below the slab**

Figure 3-46 Compressive inelasticity parameter at 2% drift angle

3.6.4.5 Slab Behavior

The story shear-strain relations at the locations indicated in Figure 3-47(a) are demonstrated in Figure 3-47(b) and (c). The upper slab steel encountered the most extreme force because it is close to the edge of concrete cover. Large deformation and stress concentration are indicated during the analysis but Figure 3-47(b) still presents good overall trends and acceptable values.

To improve the strain output of slab reinforcement, the bond-slip behavior can be included in specific regions, and also smaller sized beam element could be used to simulate the slab steel.

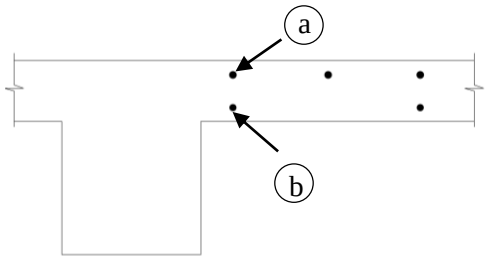

(a) Location of bond-slip value captured

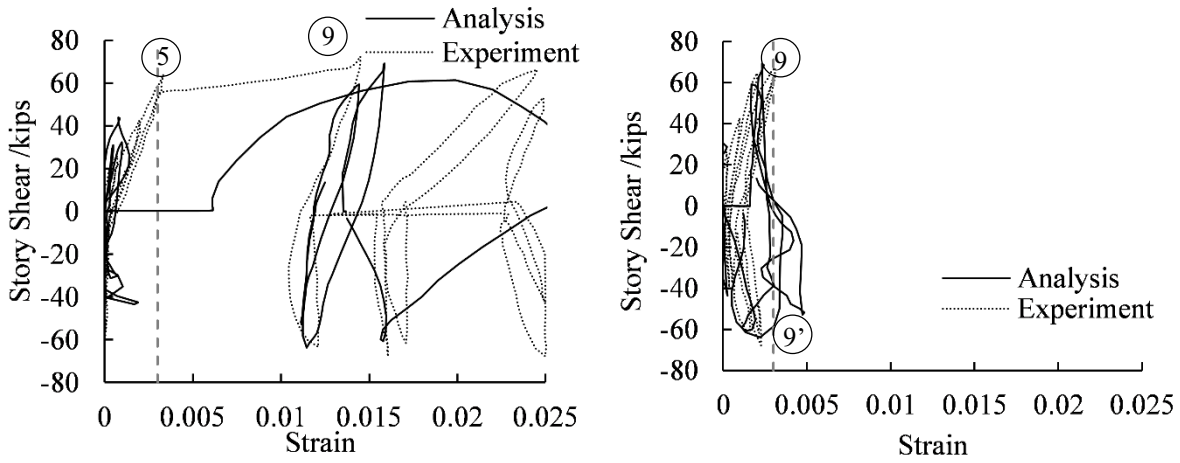

(b) Comparison of strain at location a **(c) Comparison of strain at location b**

Figure 3-47 Strain comparison of slab bars in EW direction

3.6.4.6 Crack pattern

The report depicted the crack pattern at different drift ratios, which is compared with the maximum principal strain contour in the analysis.

The 1% drift unidirectional loading gives an evenly distributed flexural crack starting from beam bottom (Figure 3-48(a)), and light crack through the column face in NS direction because more loading is applied in the EW direction. The joint does not show any visible damage. After 2% drift bidirectional loading, more flexural cracks are indicated along both beam and column face (Figure 3-48(b)). Concrete crushing is observed at the lower corners of the joint as well as the interface between slab and the upper column. After 4% drift bidirectional loading, with the joint severely damaged and extended into the beam region, the flexural crack on beam and column face is hard to visualize under the same color range of contour plot (Figure 3-48(c)).

Experimental Result **Analytical Result (range: 0~0.01)**

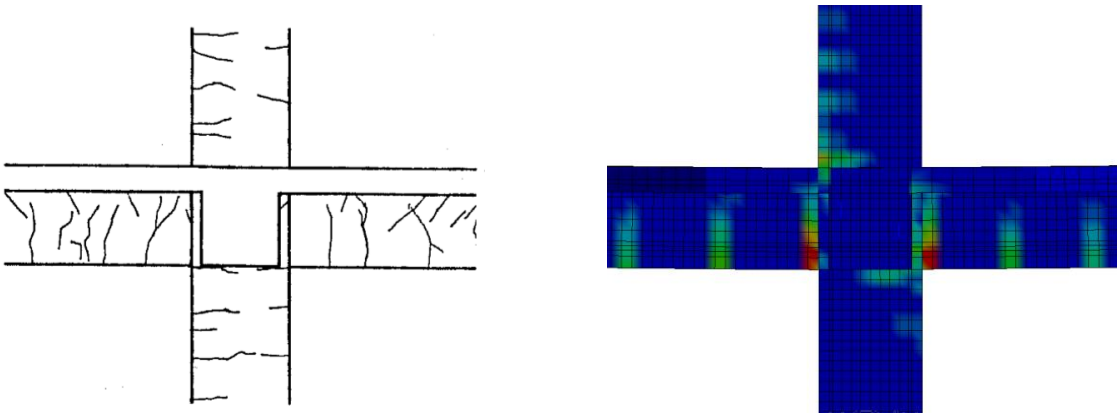

South View

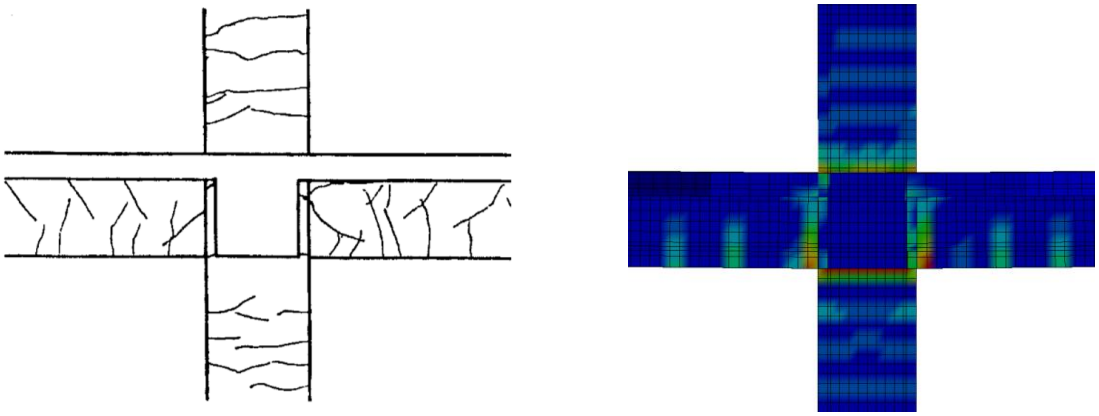

East View

(a) After 1% drift unidirectional loading (cycles 3&4)

Experimental Result **Analytical Result (range: 0~0.014)**

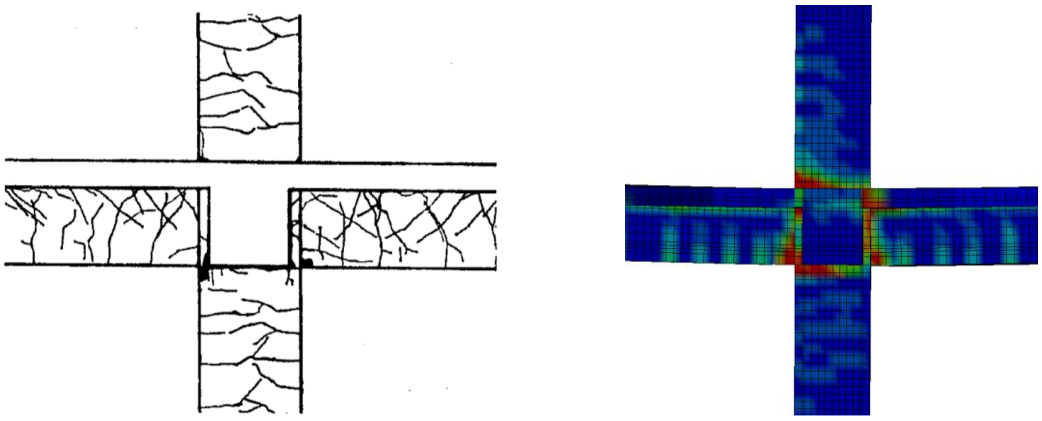

South View

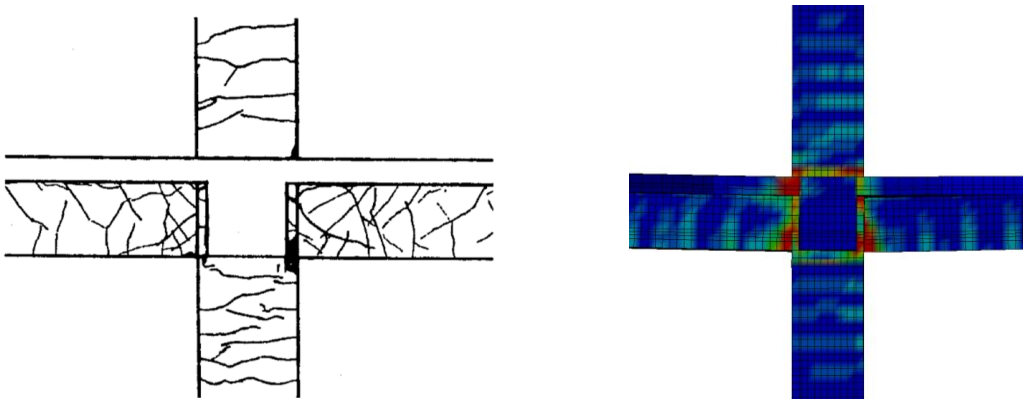

East View

(b) After 2% drift bidirectional loading (cycles 8)

Experimental Result **Analytical Result (range: 0~0.02)**

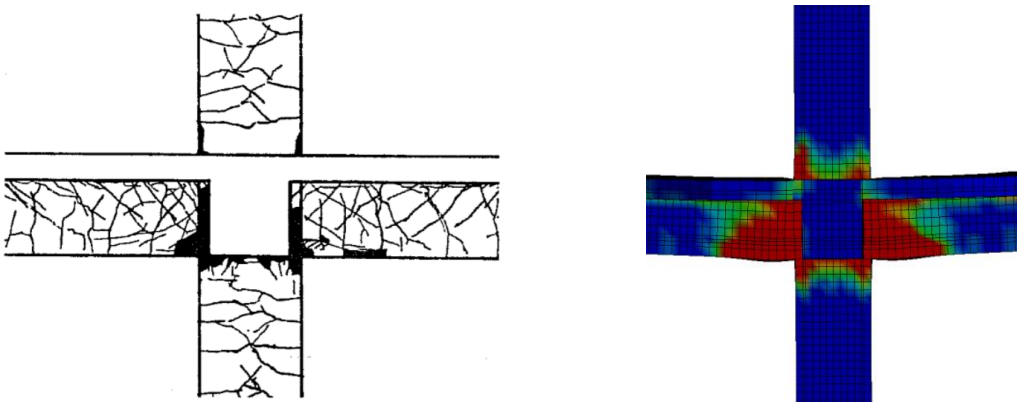

South View

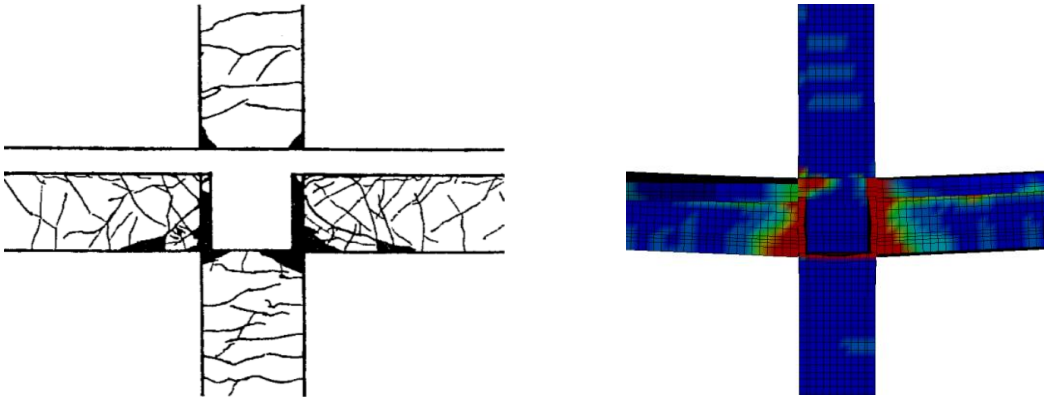

East View

(c) After 4% drift bidirectional loading (cycles 12)

Figure 3-48 Crack pattern of J2 at various loading stages (range 0~0.05%)

The top view of slab crack pattern is compared in Figure 3-49. The analysis captured both the crack concentration area at the beam-slab interface and also the radial crack pattern in the middle part of the slab. The analytical contour demonstrates a similar tendency in cracking development compared with the experiment. The major crack locations are also consistent with the experimental observation.

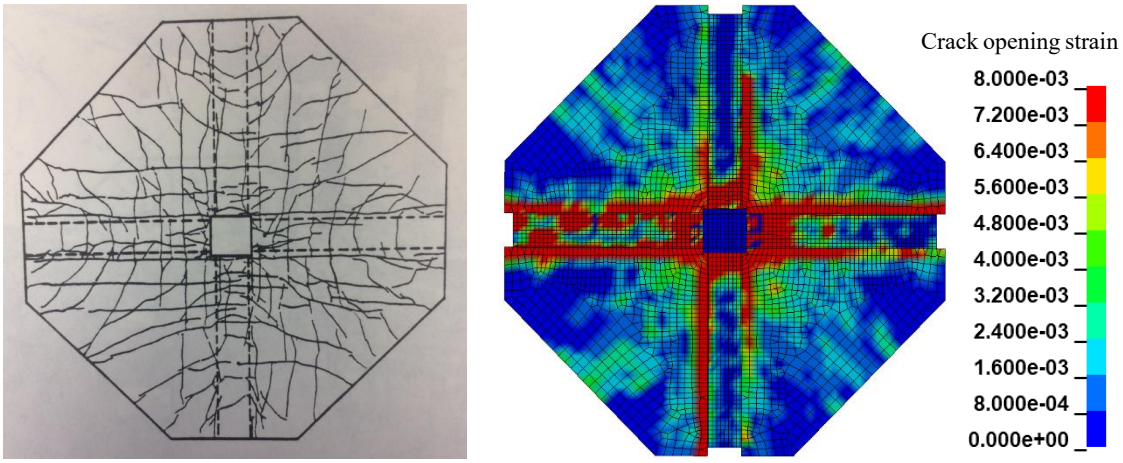

Figure 3-49 Comparison of slab crack pattern

3.6.5 The Influence of Bond-slip Effect

The criticality of including the bond-slip effect in the upper and lower beam longitudinal reinforcement in both directions is illustrated by comparing the overall hysteretic response in EW and NS direction with and without bond-slip behavior in Figure 3-50. All other parameters for the two analyses are the same.

Major differences are found in the pinching effect during the last loading cycles when the reinforcement is encountering slip and yielding, and also in the ultimate strength especially in NS direction. For both quantities, considering slip lowers the estimates. These conclusions are consistent with that for Specimen 2-4 in Section3.2.7.

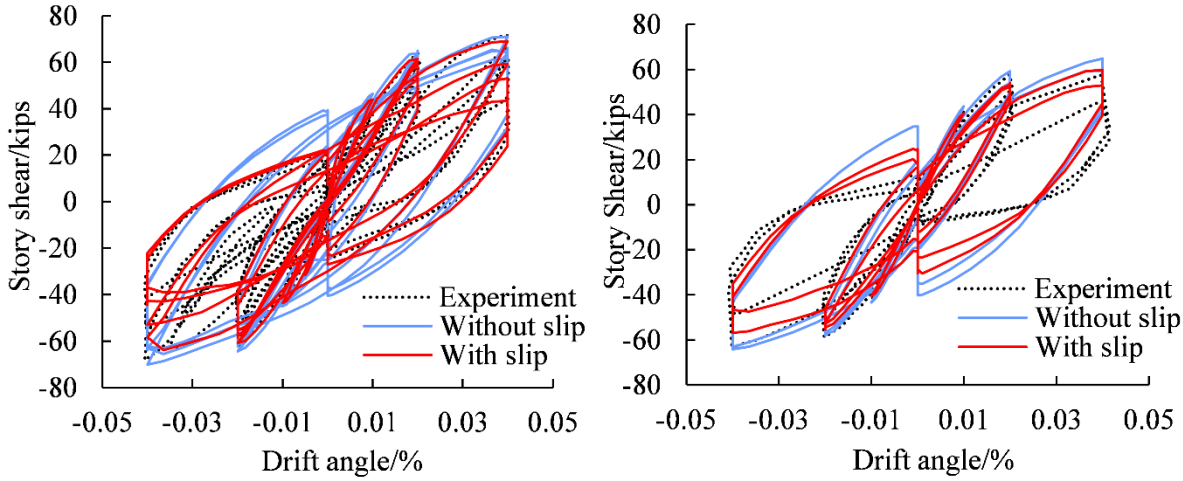

(a) EW direction **(b) NS direction**

Figure 3-50 Influence of bond-slip effect for analysis of specimen J2

The influence of including the bond-slip effect on the local performance is also looked into.

The story shear-local strain relations from Section 3.6.4.1 Beam Bar Behavior are compared with the case without bond-slip effect in the beam longitudinal reinforcement at the exactly same elements in the two analytical cases. The top beam bar strain is compared in Figure 3-51(a) and (b), at the same location in the curves in Figure 3-40.

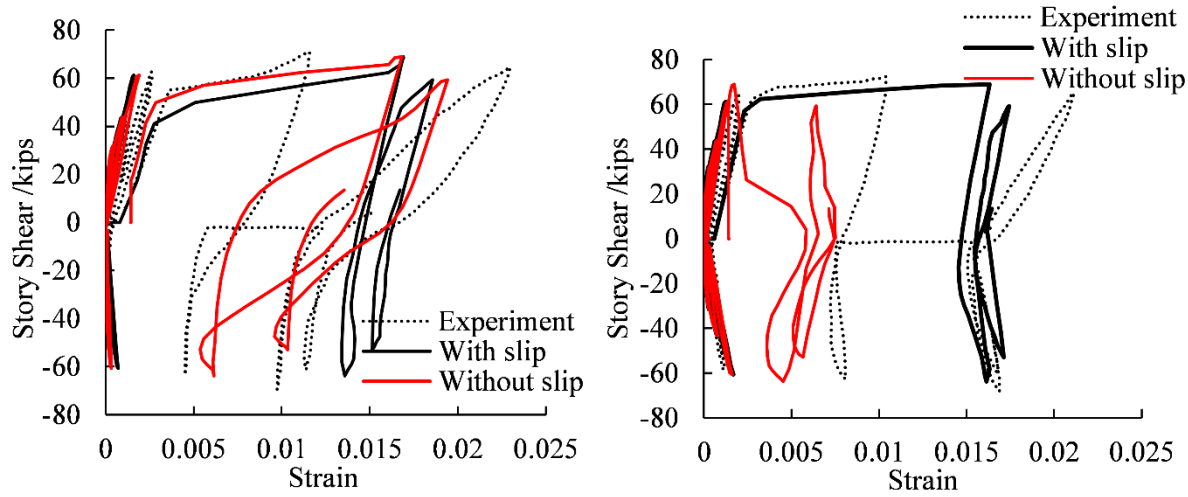

(a) Comparison for upper top beam bar **(b) Comparison for lower top beam bar**

Figure 3-51 Strain comparison for top beam bar with and without bond-slip effect

The strain relations for the upper top beam bar element in Figure 3-51(a) is surprisingly similar. One reason is that they are from loading cycle 10, which is before bidirectional loading at 4% and the bond-slip behavior is not that obvious. Another possibility is that this is a coincidence. The strain comparison for the lower top beam bar element in Figure 3-51(b) is reasonable that without bond-slip behavior and beam bar strength degradation, the lower level reinforcing bar has less opportunity in taking effect and thus has smaller strain value.

The comparison for bottom beam bar (Figure 3-52, same location with the curve in Figure 3-41) indicates an underestimation of upper bottom beam bar and overestimation of lower bottom beam bar strain, which is also reasonable given that the lower bottom beam bar is carrying more stress without bond-slip effect. It has to be mentioned that none of the curves without bond-slip effect reveals the saddle-shaped hysteretic curve, which indicates that adding the bond-slip effect is the key factor to obtain the correct hysteretic relation for reinforcement strain history.

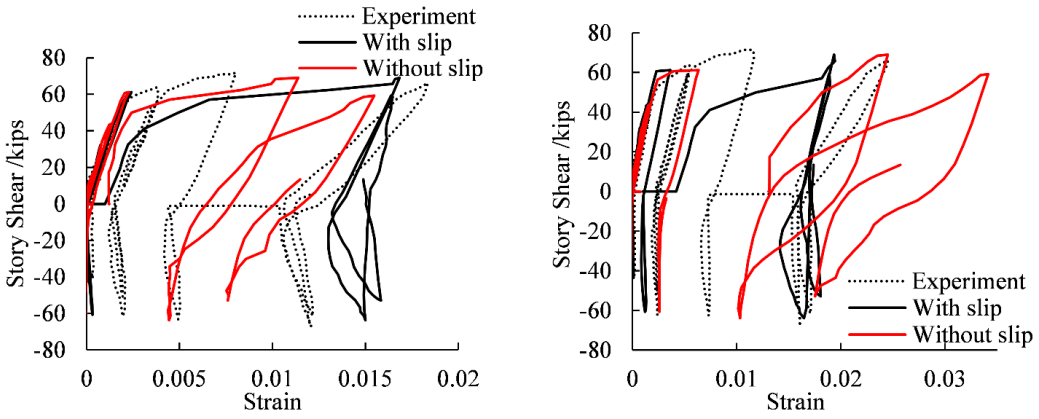

(a) Comparison for upper bottom beam bar **(b) Comparison for lower bottom beam bar**

Figure 3-52 Strain comparison for bottom beam bar with and without bond-slip effect

The hysteretic curve for column reinforcement strain in Figure 3-53 (same curve in Figure 3-45) shows an overestimation in both upper and bottom elements without considering the bond-slip effect for the beam reinforcing bar, due to the fact that all the reinforcement deformation is

considered as strain instead of strain plus bond-slip behavior in the beam. Thus, the column reinforcing bar needs to undergo larger strain as well under large drift ratio. Since no bond-slip effect in taken into consideration in the column, the strain hysteretic curve of column reinforcing bar does not display the saddle-shape, either.

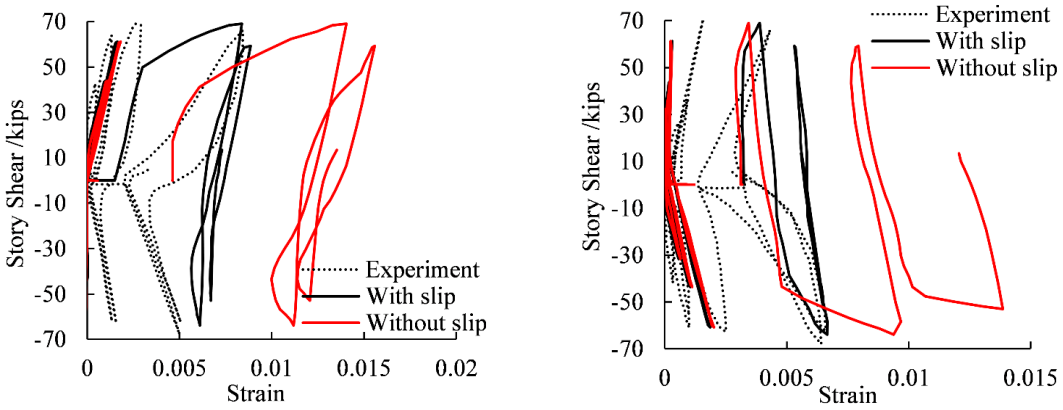

(a) Comparison for upper column bar element (b) Comparison for lower column bar element

Figure 3-53 Strain comparison for column bar with and without bond-slip effect

No bond-slip effect in the slab is taken into consideration in both cases, thus the underestimation in slab steel strain in Figure 3-54 (same in Figure 3-47) without bond-slip effect in the beam reinforcement is due to the fact that less local failure and deformation occurs in the beam and thus the slab is less likely to be affected. As a result, the slab steel performs better with less damage and remains integrally adhered to the rest of the specimen.

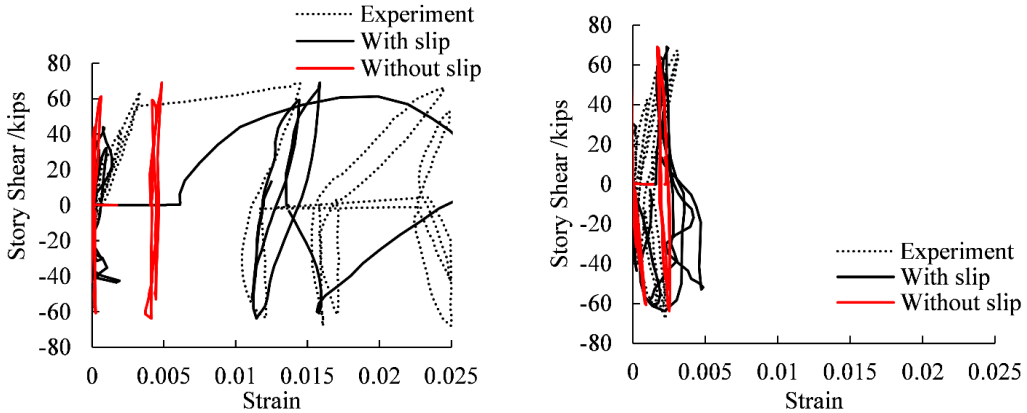

(a) Comparison for upper slab bar element (b) Comparison for lower slab bar element

Figure 3-54 Strain comparison for slab bar with and without bond-slip effect

The above comparison has limitations such as the strain relation does not extend into bidirectional loading cycles at a 4% drift ratio thus the bond-slip behavior is not obvious, also the strains are compared at limited number of locations. However, the results are still representative, and gives ideas on the effect to including beam reinforcing bar bond-slip effect on the reinforcement strain developments at different locations. Without considering the bond-slip effect, the global hysteretic curve lacks pinching effect in later cycles, and the local hysteretic curve cannot form the saddle-shaped curve. The column reinforcing bar strain is overestimated, and the slab steel strain is underestimated.

3.7 Conclusions

The reliability of the applied finite element model is evaluated in the previous sections by a serious of interior BCJs encountered different failure modes on a scale of both global and local response. Conclusions include:

1. The proposed model is able to capture the overall hysteretic behavior for both one-way and two-way beam-column joints under unidirectional and bidirectional cyclic loading (see Sections 3.2.2 and 3.6.2).
2. The applied model also successfully captures the joint shear response (Sections 3.2.6 and 3.6.3), including tracking the development of the joint shear distortion and also the development of joint shear damage.
3. The failure mode and damage pattern are evaluated with the experimental output of the two series of joints (Sections 3.2.3 and 3.6.4.). The type, time and location of the damage comparison matches well between the analytical and experimental results.

4. In addition to the satisfactory ability in simulating global performance of the joints, the applied model also reliably captures local performance on both overall shape and peak values. This includes the bond-slip measurements (Section 3.2.5) and strain history for all types of reinforcement (Section 3.6.4).

5. The importance of including the bond-slip behavior is evaluated in Sections 3.2.7 and 3.6.5. Since capturing the global performance is a precondition for obtaining reliable local performance, adding the bond-slip behavior is quite essential in both global and local scale.

6. Upon obtaining reliable analytical results, a parameter study will be launched in Chapter 5 to address conditions such as the effect of different beam longitudinal reinforcement configurations on joint behavior and the influence of slab in increasing the column-to-beam moment capacity ratio.

Chapter 4 Nonlinear Truss Methodology for Analysis of Interior BC Joints

Despite the accuracy of the 3D-finite element scheme discussed in the previous chapter, the vast majority of engineers may still prefer a simplified analytical method for the performance assessment of BCJs. The reason is that the finite element model is conceptually complicated and computationally demanding, especially for parametric performance assessment of prototype structural systems. To address the need for conceptually simplified and computationally efficient analysis approaches, this chapter formulates a nonlinear truss modeling scheme for simulation of BC joints.

The accuracy of nonlinear truss models has been demonstrated for shear-dominated components (Lu and Panagiotou 2014, Moharrami et al. 2015), and some simple interior and exterior BCJs (Bowers 2014). However, there is still a requirement to further develop the truss methodology for situations where shear behavior interacts strongly with flexure and bond behavior, such as in interior BC connections, to analytically evaluate both shear and bond-slip behavior for interior BC joints encountering concurrent failure modes.

This chapter introduces the nonlinear truss methodology established by Panagiotou et al. (2012) and Lu and Panagiotou (2013). Constitutive laws are introduced for concrete, reinforcement and bond-slip behavior and assessed. The ability of the nonlinear truss model for capturing strut and panel strut mechanism in interior BC joints is verified by the specimen tested by Leon (1989). Both global and local analytical outcomes are compared with experimental results and three-dimensional finite element analysis in Chapter 3.

4.1 Description of Nonlinear Truss Modeling Approach

The capability of an equivalent truss representation to capture the salient features of flexural resistance, shear resistance, and their interaction has been well established. The diagonal elements are utilized to capture the inclined compressive field due to the combination of axial force, shear force and bending moment (Vecchio and Collins, 1986). By relatively straightforward calibration of material properties and proper selection of element layout, truss modeling is a useful and accurate tool in analyzing RC members subject to bending and shear (Al-Nahlawi and Wight, 1992).

In this work, the incorporation of a bond-link element is capable of capturing the bond-slip behavior inside the BC joint. The modeling approach for BC joint idealizes concrete as an assemblage of truss cells, made up of horizontal, vertical and diagonal truss elements (Figure 4-1). The horizontal and vertical truss elements are primarily intended to capture the axial-flexural response, while the diagonal elements capture the inclined compressive field combining axial, shear and flexural responses. The steel reinforcement is also represented by truss elements for both longitudinal and transverse steel. Bond-slip behavior is simulated by zero length elements connecting the steel and concrete at coincident locations.

An interior BC joint idealized by the truss model methodology is shown in Figure 4-1. The joint is pinned at the top, has rollers on the two beam ends, and is loaded by a horizontal force at the bottom. Half of the length in beam and column as well as the joint part are represented by truss elements. The rest of the beam and column away from the joint is represented by a single nonlinear force-based beam element, which is connected to the truss elements by rigid beam elements with a node in the center with all degree of freedom restrained. The concrete material is modelled by nonlinear truss elements in Figure 4-1(a), with green dots representing zero-length bond-slip

springs. The reinforcement material illustrated by nonlinear truss elements in Figure 4-1(b) is connected with concrete truss elements in Figure 4-1(a) by those same green dots which represents zero-length bond-slip springs.

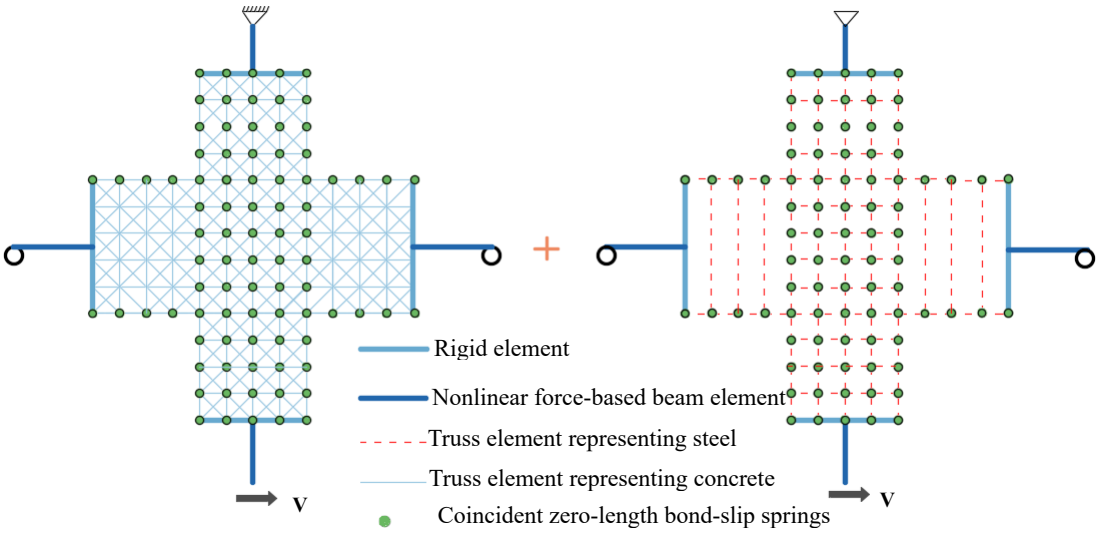

(a) Concrete material **(b) Steel material**

Figure 4-1 Layout of BC joint using nonlinear truss model strategy

4.2 Determination of Truss Geometry

The determination of the truss geometry described herein is based on the work by Panagiotou et al. (2012) and Lu and Panagiotou (2013), who developed and employed the truss methodology for analyzing RC walls.

4.2.1 Layout of Truss Elements

As the first step, the outline of the truss model (i.e. the longitudinal edge truss elements) needs to be established. It is the most convenient for modeling purposes if the centroid of the two longitudinal edge truss elements is placed at the center of outermost beam and column bars, thus establishing the overall geometry for the truss model.

The segment (i.e. the number of truss cells) along column depth and beam height needs to be determined as the next step based on column/beam dimensions and the angle of inclination of the diagonal elements. The number of truss cells that fits within these boundaries will be then determined by the inclination of diagonal element.

4.2.1.1 Inclination of Diagonal Elements

In reinforced concrete structures, it is assumed that the direction of the diagonal compressive field is parallel to the initial crack that occurs due to a combination of axial and shear force, which is the inclination of the diagonal elements of a truss element based on. In the analysis of shear-dominated RC wall, an angle equal to 45º has been found to provide accurate results (Panagiotou et al. 2012). Based on the strut mechanism for BC joints, the initial inclined shear crack angle is close to 45º. Thus 45º will be assumed as the ideal inclination of diagonal elements in simulating the interior BCJ. The idea is then to subdivide the model to obtain approximately square truss cells in the joint area. The number of longitudinal elements in the column and beam need to be determined based on a common factor of the beam height and column depth, so that the distance between two longitudinal truss elements in the column will be similar to that in the beam, thus the inclination of diagonal truss element would as close to 45° as possible. For the three specimens tested by Leon (1989) that will be simulated in later sections, the meshing in the joint area is decided to be 4 by 5, 5 by 5 and 6 by 5, so that the truss cell is close to a square.

4.2.1.2 Determination of Element Location

Based on the number of truss cells along the column depth, the location of the longitudinal element which are aligned with both the longitudinal column and beam bars can be determined.

From this layout, the number and location of the diagonal truss elements in the joint will be automatically settled. By extending the diagonal element centerline into the beam and column, the position of diagonal elements in the column and beam will then be determined. The location of the transverse elements is automatically settled at the intersection of vertical and diagonal elements. To simplify the calculation in sectional properties and also to maintain a consistent location for steel and concrete truss element so that the bond-slip springs can be properly inserted, the location of longitudinal truss element for concrete and bar should be identical with the reinforcement position.

4.2.2 Cross-sectional Area of Truss Elements

4.2.2.1 Longitudinal Elements

The tributary sectional depth for the longitudinal concrete elements in the column is determined by evenly dividing the area between two adjacent elements. The cross sectional area of each concrete truss element in the column is the product of the depth and the out-of-plane width (c_w). For the truss elements representing the longitudinal reinforcing bar, the cross-sectional area of the two outermost elements is equal to the total area of the reinforcing bar on the two edges of the column throughout the whole out-of-plane depth, and the rest of the reinforcing reinforcing bar area is equally distributed to the remaining longitudinal elements locate in the middle.

An example of determining the cross-sectional areas of the longitudinal concrete and reinforcing bar elements is presented in Figure 4-2. In this example, five vertical elements are placed along the column depth, h_c, and six rows of longitudinal truss elements are distributed along the beam height, h_b.

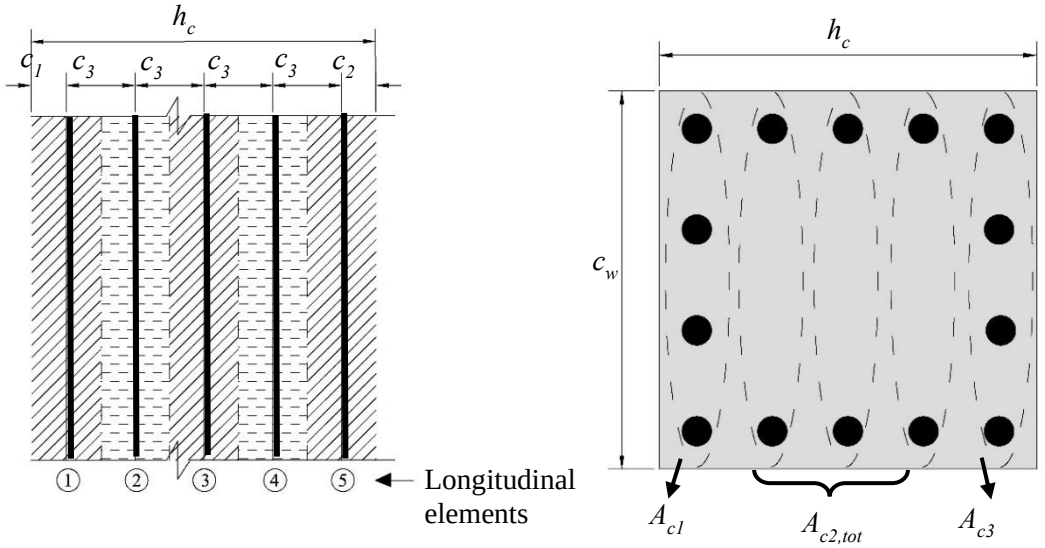

(a) Longitudinal truss element in the column **(b) Steel element sectional area in column**

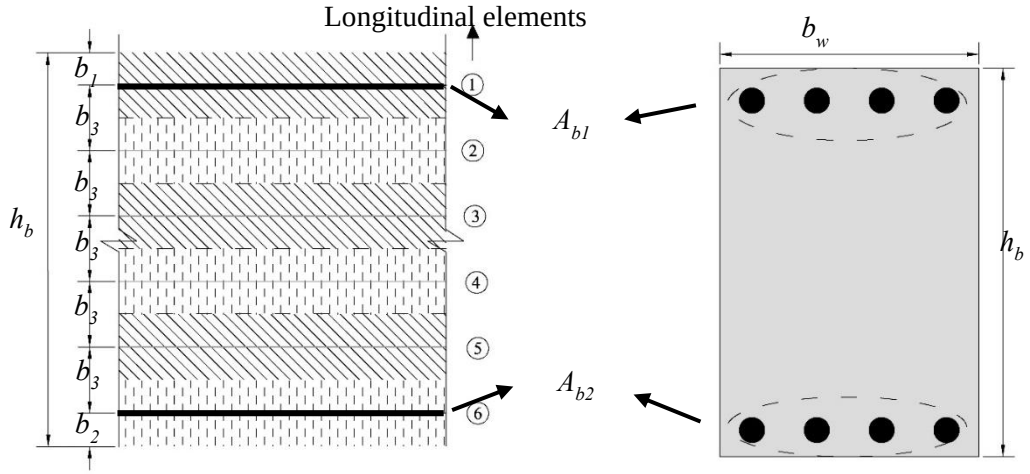

(c) Longitudinal truss element in the beam **(b) Steel element sectional area in beam**

Figure 4-2 Determination of cross sectional dimensions for truss elements in column of specimen BCJ2 tested by (Leon 1989)

The values of c_1 and c_2 for column, b_1 and b_2 for beam in Figure 4-2 are determined as the distance from concrete edge to the center of the bar on that side, and the spacing of longitudinal elements is equal to c_3 and b_3 for column and beam. The cross section of longitudinal steel truss element on the two sides equals to the total area of reinforcement at the same location. In Figure 4-2 for example, the steel section area for elements ① and ⑤ in column is A_{c1} and A_{c3}, respectively. The remaining steel area in the middle, $A_{c2,tot}$, is equally distributed to the longitudinal

elements in the middle from ② to ④. Similarly, the steel area of the longitudinal truss elements in the beam is A_{b1} and A_{b2} at the top and bottom, respectively, with four rows of concrete longitudinal truss elements evenly distributed in the middle. The corresponding concrete depth and steel element area of column and beam are summarized in Table 4-1 and Table 4-2.

Table 4-1 Calculation of sectional depth to longitudinal elements of column

Member	1	2	3	4	5
Concrete depth	c_1+0.5c_3	0.5c_3 +0.5c_3=c_3	0.5c_3 +0.5c_3=c_3	0.5c_3+0.5c_3=c_3	c_2+0.5b
Steel area	A_{c1}	$A_{c2,tot}$/3	$A_{c2,tot}$/3	$A_{c2,tot}$/3	A_{c3}

Table 4-2 Calculation of sectional depth to longitudinal elements of beam

Member	1	2	3	4	5	6
Concrete depth	b_1+0.5b_3	0.5b_3 +0.5b_3=b_3	0.5b_3 +0.5b_3=b_3	0.5b_3 +0.5b_3=b_3	0.5b_3 +0.5b_3=b_3	b_2+0.5b_3
Steel area	A_{b1}	0	0	0	0	A_{b2}

4.2.2.2 Transverse Elements

For concrete transverse truss element, the cross sectional area is achieved by dividing the distance between two consecutive elements equally, in a similar manner as was done for the longitudinal elements in Figure 4-2, and multiplying it by the width of beam. If the transverse reinforcement is evenly distributed over the beam and column, the cross sectional area for the truss element representing transvers reinforcement in the column and beam can be calculated by dividing the total area by the total number of transverse truss elements.

4.2.2.3 Diagonal Elements

The geometry of truss elements is finalized by resolving the sectional area of diagonal elements. The effective width of diagonal elements, b_{eff}, is determined as $\frac{a \times b}{\sqrt{a^2 + b^2}}$ (Figure 4-3).

Since the dimension of column depth and beam height varies, the inclination angle θ_d will not always be 45°. The inclination angle θ_d of diagonal element in truss model analysis of three specimens tested by Leon (1989) are 45.38°, 45.00° and 44.74° for Specimen 2, 3 and 4, respectively.

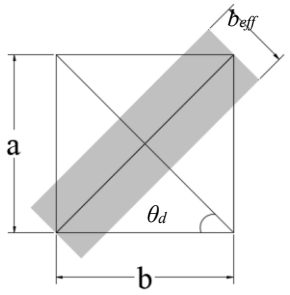

Figure 4-3 Concrete truss cell

4.3 Constitutive Laws

4.3.1 Constitutive Model for Concrete

The stress-strain law by Lu and Panagiotou (2013), schematically presented in Figure 4-4, is used to model the uniaxial behavior of confined and unconfined concrete in the truss models. In the compressive region, the stress strain relation is based on the Fujii concrete model (Hoshikuma et al., 1997) with an initial stiffness E_c=5000$\sqrt{f_c'}$ until the strain reaches ε_{co} and ε_{cc} for the unconfined and confined concrete, respectively (Figure 4-4). Then the unconfined concrete follows a linear softening path to an intermediate user defined stress-strain point (ε_{cint}, f_{cint}) along a line that intersects the strain-axis at the value ε_u, where ε_u is the strain value accounting for mesh-size effects based on the notion of concrete fracture energy in compression (Bazant and Planas 1998; Lu and Panagiotou 2013). Another constant line is followed after the point (ε_{res}, f_{res}), representing the residual strength value. The confined concrete on the other hand, reaches a larger peak stress value f_{cc} with a strain of ε_{cc} based on the equation from the Fujii concrete model (Hoshikuma et al.,

1997), which is followed by a linear softening path to an intermediate point ε_{cint} calculated as mentioned above for confined concrete but aiming for ε_{cu}. A secondary linear softening path is followed till a user-defined residual value of compressive stress is reached.

In the tensile region, which is the same for unconfined and confined concrete, the material is elastic until the tensile strength is reached. The post-crack response is governed by an exponential or a trilinear softening branch. For longitudinal and transverse concrete truss elements, the peak tensile strength f_t is defined with the same value as in Section 3.2. This law is capable of capturing stiffness degradation due to concrete cracking by either an exponential tension stiffening curve if the tension stiffening parameter (Stevens et al., 1991) is specified or a trilinear tension softening curve without the tension stiffening parameter. The trilinear tension softening curve starts from the point (ε_{cr}, f_t), to an intermediate point (ε_{tint}, f_{tint}) till the tensile residual point (ε_{tres}, f_{tres}).

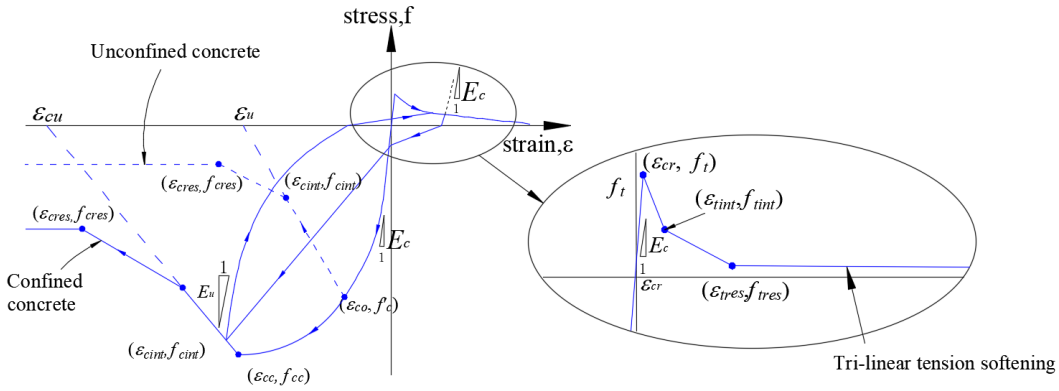

Figure 4-4 Constitutive model for concrete

For the diagonal truss elements, the strain-stress law accounts for the biaxial transverse strain effects on compression strength, as based on experimental observations by Vecchio and Collins (1986). As the transverse strain ε_n increases in the tensile direction, the compressive strength is decreased by a reduction factor β in the diagonal direction. The reduction factor β is defined by a tri-linear relation with the transverse strain ε_n as shown in Figure 4-5. As a result, every diagonal

element requires an additional fictitious "strain gage element" for measuring the transverse strain ε_n. For the sake of decreasing the number of nodes, the two nodes of the "strain gage element" are coincident with another two nodes in the same truss cell (Panagiotou et al. 2012). The ε_n is calculated as:

$$\varepsilon_n = \frac{1}{\sin\theta}(\varepsilon_{34} - \varepsilon_{12} \cdot \cos\theta) \tag{4-1}$$

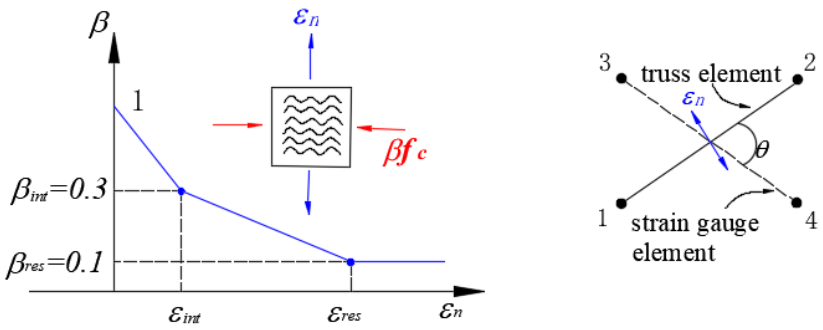

Figure 4-5 Relation of reduction factor β and transverse strain ε_n

To alleviate the overlapping area in calculating cross section of diagonal element, the tensile strength of diagonal element is set to zero. Satisfactory strength and pinching effect of the hysteretic response as well as failure behavior have been obtained in analysis of RC walls (Lu and Panagiotou 2013), columns (Moharrami et al., 2015) and BC joints (Bowers 2014) using this technique.

4.3.2 Constitutive Model for Reinforcement

The constitutive law for steel proposed by Dodd and Restrepo-Posada (1995) is used for reinforcement herein. It is an accurate model that requires a limited number of parameter to calibrate. The monotonic skeleton curve starts with a linear elastic part and followed by a yield

plateau, a strain hardening part and a post-peak softening curve (Figure 4-6(a)). The stress and strain at three points, based on engineering coordinates, are required as the inputs: ε_{sh} and f_y, which are strain and stress at the onset of strain hardening; ε_{sh1} and f_{sh1}, which belongs to strain and stress of an arbitrary user defined intermediate node; and ε_{su} and f_{su}, which represent the ultimate strain and strength with the zero-slope before the post-peak softening curve. The Bauschinger effect is captured by a nonlinear unloading path after a linear unloading part (Figure 4-6(b)).

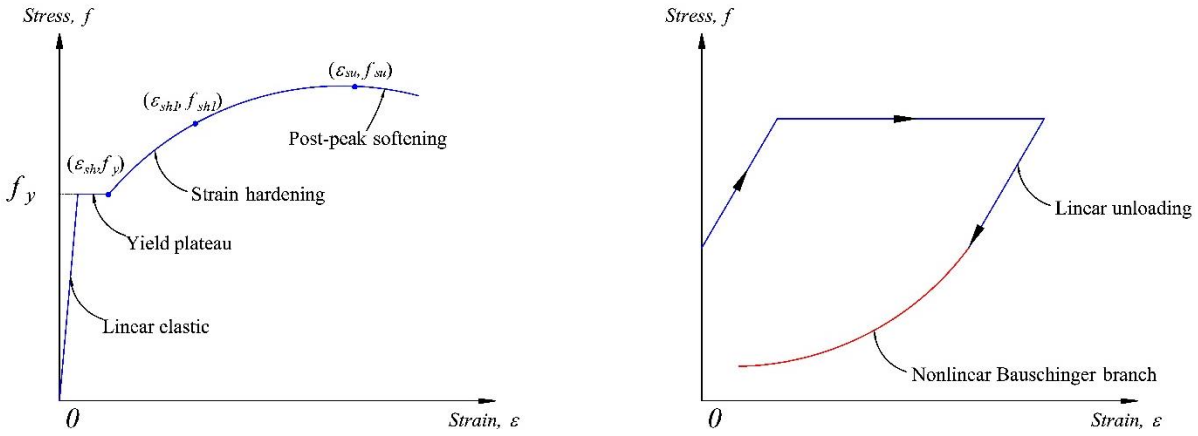

(a) Skeleton curve **(b) Hysteretic behavior**

Figure 4-6 Constitutive law for steel by Dodd and Restrepo-Posada (1995)

Unloading and reloading reversals are distinguished into four categories: major, minor, simple, and elastic (Figure 4-7(b),(c),(d)). A major reversal occurs when the reversal point occurs within the non-elastic range of the skeleton curve as shown in Figure 4-7(b). Major reversals consists of a linear unloading branch (blue line in Figure 4-7) and a nonlinear Bauschinger branch (red curve in Figure 4-7). Reversals with the yield plateau will rejoin the skeleton curve in the opposite direction with a shifted plastic strain based on results from the previous load cycle. Reversals within the strain-hardening region will target the ultimate stress-strain point in the opposite direction. Major reversals can also be triggered within the nonlinear Bauschinger branch of another

major reversal if the stress developed between two reversal points exceeds $2f_y$, otherwise, a minor reversal occurs (Figure 4-7(c)). A minor reversal is simply a linear region followed by a nonlinear Bauschinger branch that traces back to either the reversal point (Point A in Figure 4-7(c)) on the skeleton curve or to the major reversal without plastic strain development. A simple reversal happens during the Bauschinger branch of a reversal which is comprised of a linear branch and nonlinear Bauschinger curve. Similar to minor reversals, simple reversal contributes no plastic strain and always aim to rejoin the previous simple reversal (Point B in Figure 4-7(d)) or the major reversal (Point C in Figure 4-7(d)). Finally, a linear reversal occurs anywhere within the linear unloading branch (Figure 4-7(d)).

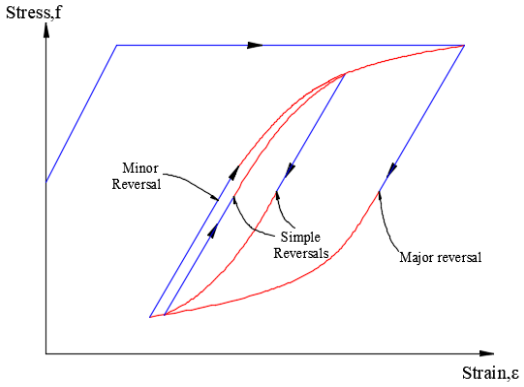

(a) Relations between reversals

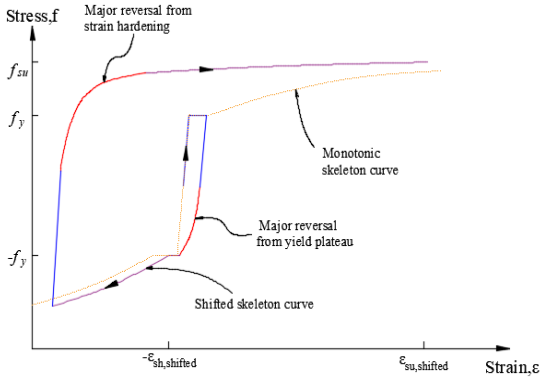

(b) Major reversal

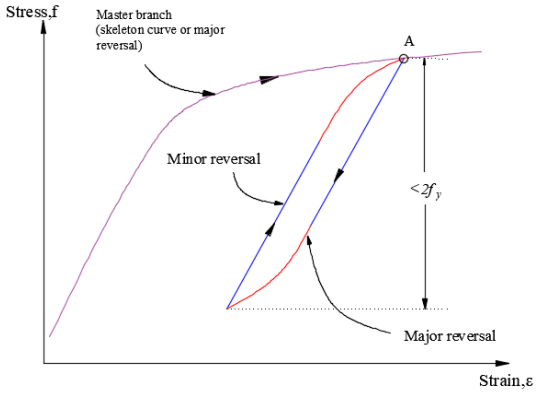

(c) Minor reversal

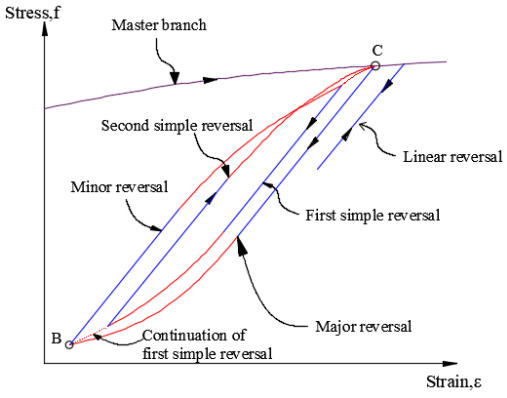

(d) Simple and linear reversal

Figure 4-7 Loading reversals

The nonlinear Bauschinger branch mentioned above is calculated by a family of nonlinear equations in the perfectly rigid-perfectly plastic coordinate with empirically determined exponent coefficients: P_{major} for major reversals and P_{minor} for minor and simple reversals. The coefficient P_{major} differs based on the amount of plastic strain, and P_{minor} is taken as 0.35 based calibration to test data (Bowers 2014). Both P_{major} and P_{minor} are user input parameters.

4.3.3 Bond-slip model

The bond stress-slip constitutive model applied was developed by Mitra and Lowes (2007). This monotonic bond stress-strain relation is compared with Viwathanatepa et al. (1979) in Figure 4-8(a) which consists of four linear branches: an elastic branch, a yield branch, a post-peak softening branch, and a constant residual branch. The hysteretic behavior exhibits degradation under cyclic loading in three ways: unloading stiffness k decreasing from k_1 to k_0 in Figure 4-8(b), reloading stiffness d_{max} decreasing from d_{max-1} to d_{max-3} in Figure 4-8(c), and strength degradation of f_{max} decreasing from f_{max-1} to f_{max-3} in Figure 4-8(d).

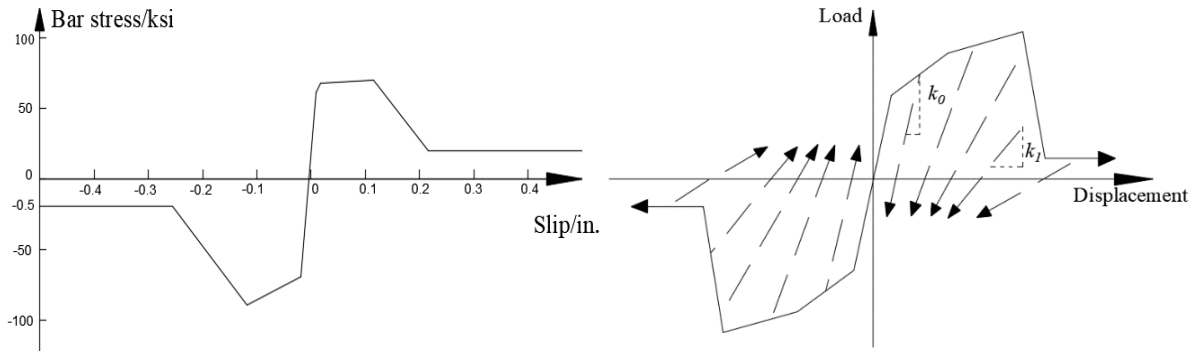

(a) Monotonic curve for the model **(b) Unloading stiffness degradation**

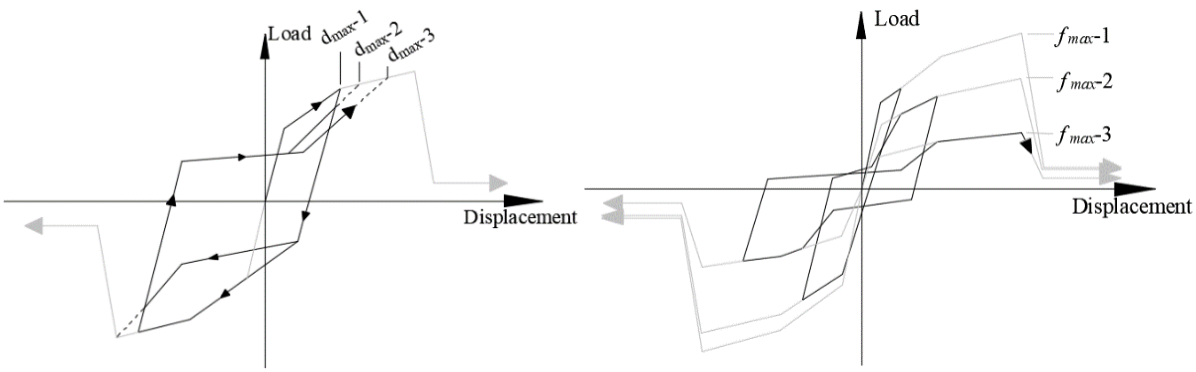

(c) Reloading stiffness degradation **(d) Strength degradation**

Figure 4-8 Monotonic and hysteretic behavior of bond stress-strain relation (Redrawn after Lowes et al. 2003)

This constitutive model, which exists in OpenSees as the uniaxial material named BARSLIP, allows the user to choose between weak and strong bond conditions, as well as damaged and undamaged material models. However, there is no detailed explanation in OpenSees of the definition and values of the damage coefficients; they appear to be empirically based.

4.4 Validation of Analysis Method

4.4.1 Force-Displacement Response

The loading force versus the horizontal relative displacement at the column bottom for three specimens mentioned in Section 3.2.1 tested by Leon (1989) are compared with experimental data in Figure 4-9.

Peak stress f_{cc} for confined concrete used for three specimen beams are 6.396ksi, 6.168ksi, 6.109ksi based on Richart et al. (1928), respectively.

The results show considerably agreement in all specimens, with an acceptable estimation in ultimate strength and a correct prediction of various degrees of pinching effect from Specimen 2

to Specimen 4. The pinching effect in the hysteric curve of Specimen 2 is distinctly depicted, which is not accurately captured by nonlinear finite element method in Chapter 3.

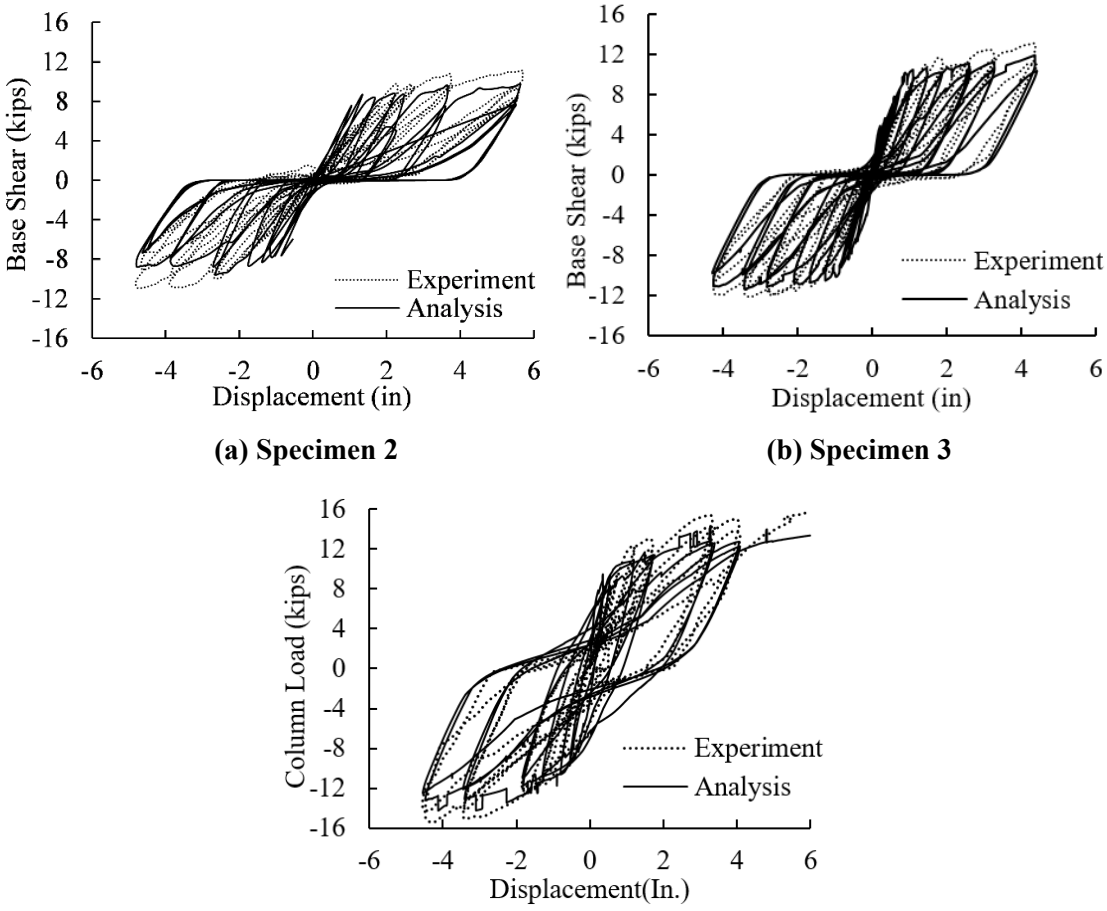

(a) Specimen 2

(b) Specimen 3

(c) Specimen 4

Figure 4-9 Analytical and experimental comparison of column load versus story displacement of Specimens 2 to 4 tested by Leon (1989)

4.4.2 Damage Patterns

The truss strain contours of concrete from the analysis are compared with crack pattern from the experiment. Specimen 2 exhibited a distinct diagonal shear cracking pattern in the test; this behavior is captured as a diagonal continuous red band in the truss strain contour plot (Figure 4-10a), and is also revealed by the significant pinching effect of the hysteretic curve (Figure 4-9(a)). The analytical result shows less damage in Specimen 3 (Figure 4-9(b)) since the strain values are

smaller compared with those with Specimen 2. For Specimen 3, the test indicated that more concrete in tention extended into the beam region as compared with Specimen 2; this is also illustrated in the analytical results (Figure 4-9(b)). Due to the larger shear strength provided by a larger column depth, Specimen 4 demonstrated more flexural cracks inside the beam and column as compared with Specimen 3. This result is also captured by the analytical output (Figure 4-10(c)).

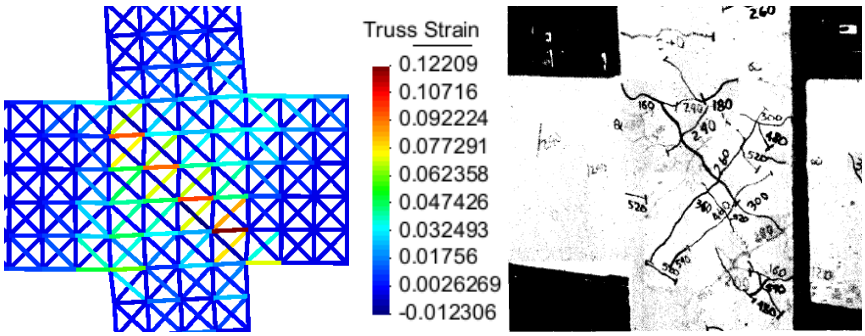

(a) Analytical and experimental damage pattern at yielding for Specimen 2

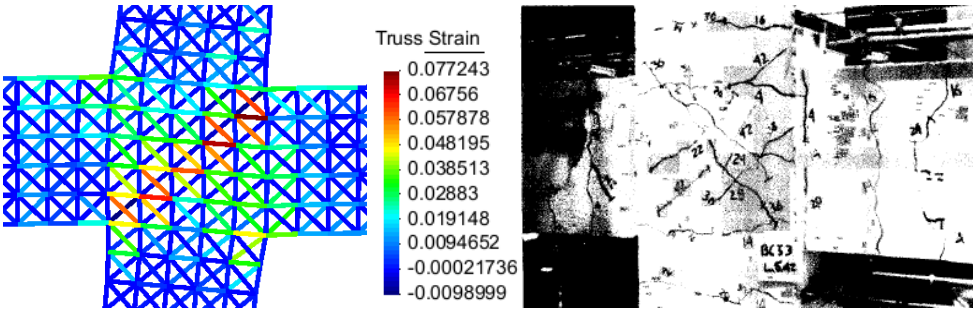

(b) Analytical and experimental damage pattern at yielding for Specimen 3

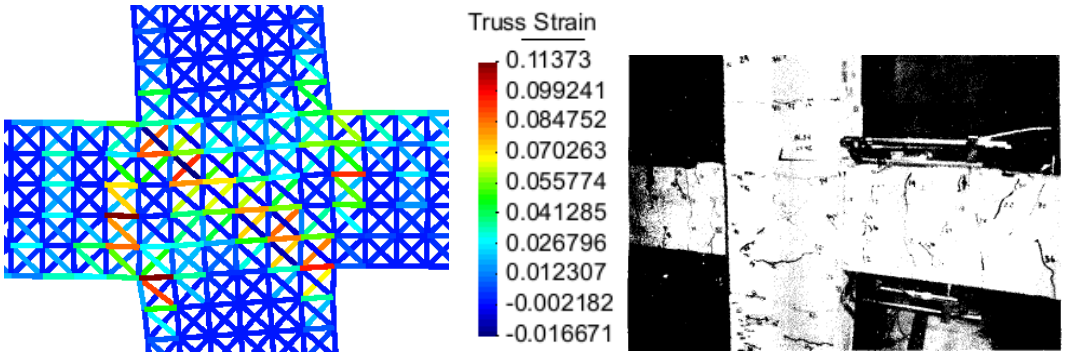

(c) Analytical and experimental damage pattern at yielding for Specimen 4

Figure 4-10 Truss strain contour of concrete compared with crack pattern tested by Leon (1989)

By plotting out the truss strain contours for the reinforcement, the various degree of strain penetration due to bond-slip behavior can be observed in Figure 4-11. Due to the underestimation of the bond-slip behavior degradation by the Mitra and Lowes (2007) model, the strain penetration behavior observed in the test is not accurately reproduced, and the computed slip values are much smaller than from the test data. The increment of strain in transverse reinforcement in the joint Specimen 2 due to shear cracking compared with other two joints, however, is well-captured.

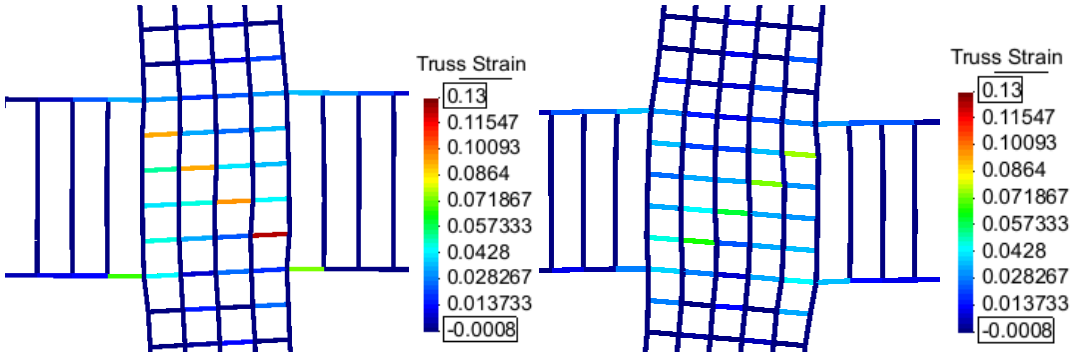

(a) Specimen 2

(b) Specimen 3

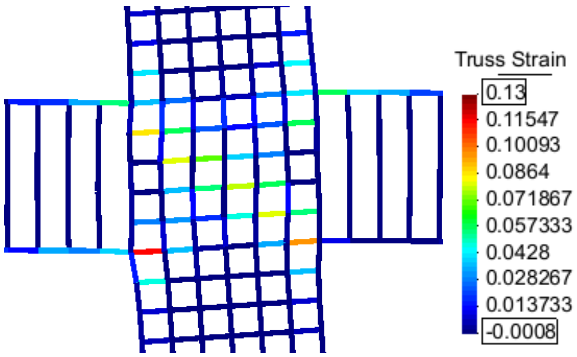

(c) Specimen 4

Figure 4-11 Strain contour of reinforcement analyzed by truss model tested by Leon (1989)

The final failure mechanisms in the Nonlinear Truss analysis are compared in Figure 4-12 with the basic shear carrying mechanisms described in Section 2.1 Force Transfer Mechanism and also the results from FE model in Section 3.2.3.3. The results validate the predominance of a strut

mechanism for Specimen 2. A large diagonal concrete strut forms in compression (Figure 4-12(a)), with x-shaped diagonal shear cracks formed in the joint region as illustrated by the truss strain contour in Figure 4-12(b). This was also captured by FE model as shown in Figure 3-20(b). The same conclusion can be reached when comparing the FE model result in Figure 3-15(c) with those in Figure 4-12(c). Due to bond-slip behavior, yield penetration behavior of longitudinal beam reinforcing bar goes through the whole joint (Figure 4-12(d)).

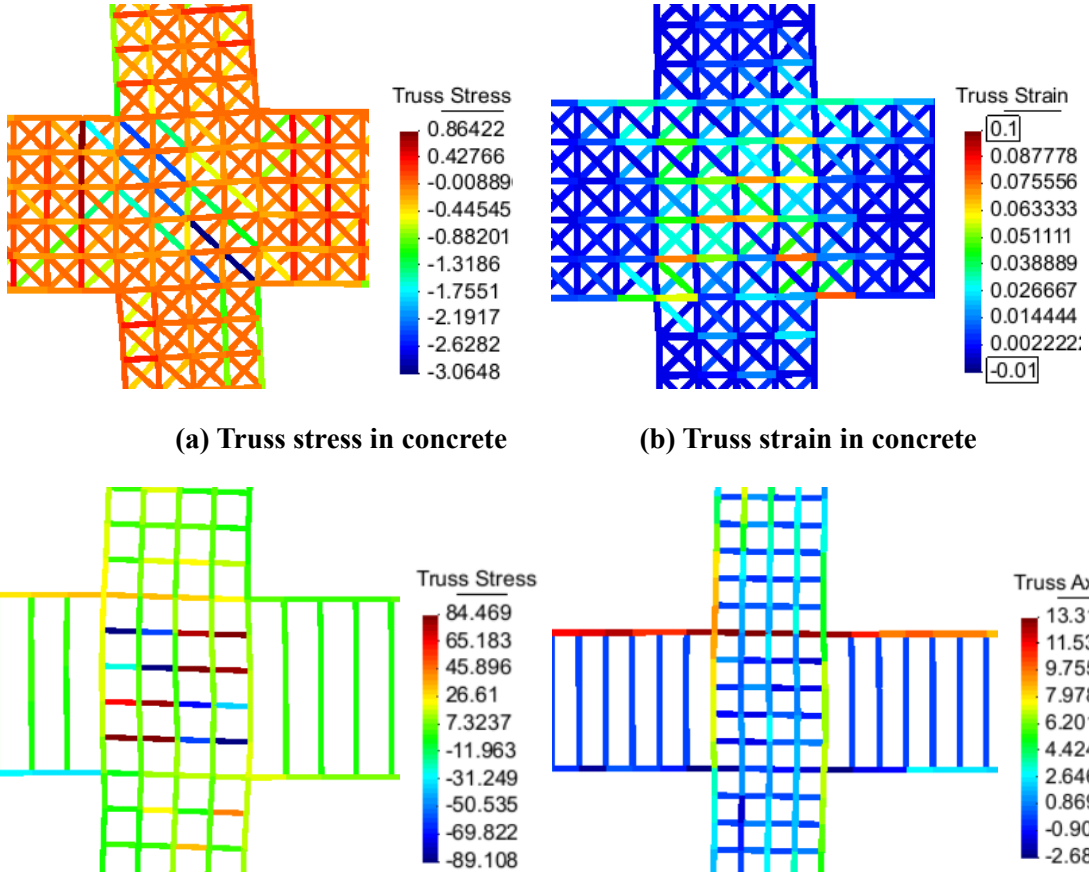

(a) Truss stress in concrete **(b) Truss strain in concrete**

(c) Truss stress in reinforcement **(d) Truss axial force in reinforcement**

Figure 4-12 Failure mechanism for analysis of Specimen 2 tested by Leon (1989)

The panel truss mechanism is validated again by the Nonlinear Truss methodology for Specimen 4. Same with the trend in Figure 3-21(a), large and unclosed cracks form at the interface

between the column and beam (Figure 4-13(a)), with limited yield penetration developing into the joint (Figure 4-13(c)). Similar to the FE result in Figure 3-21(c), several compressive panel trusses form in the joint (Figure 3-21(b)). This is activated by a relatively large amount of transvers reinforcement in the joint, which is reflected in a much smaller strains in the transverse reinforcement as compared with other two specimens (Figure 4-11(c)).

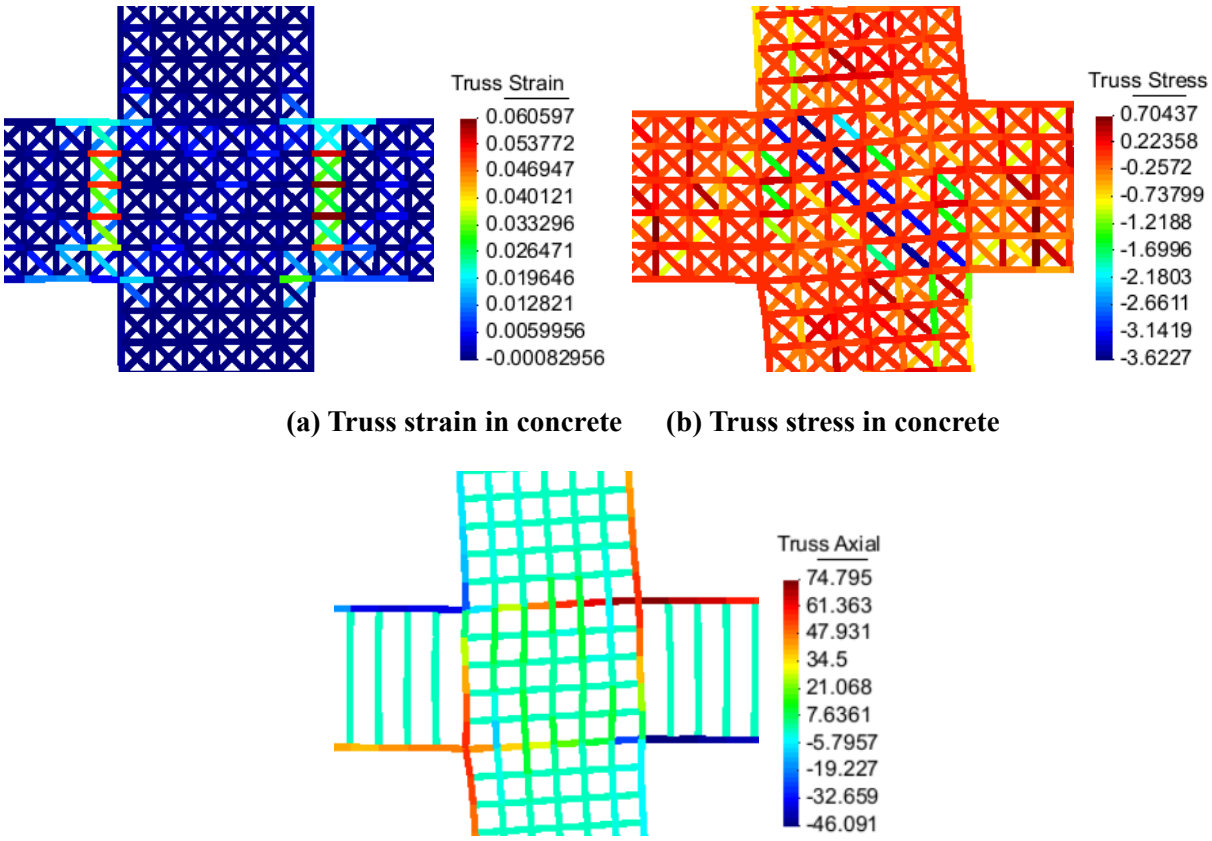

(a) Truss strain in concrete **(b) Truss stress in concrete**

(c) Truss axial force in reinforcement

Figure 4-13 Damage and load transfer mechanism for analysis of Specimen 4 tested by Leon (1989)

4.4.3 Moment v.s. Slip Relation

The slip response is highly dependent on the ability of the bond-slip model to reproduce the real behavior. The plot in Figure 4-14 reveals that even if the hysteretic response looks acceptable,

the local behavior of bond-slip is significantly underestimated compared with both the experimental data and the analytical results from the finite element model described in Section 3.2.5. Moreover, the strong bond condition without material damage (Figure 4-15(a)) is supposed to result in smaller slip values than the weak bond condition with material damage (Figure 4-15(b)). However, the results show the opposite trend.

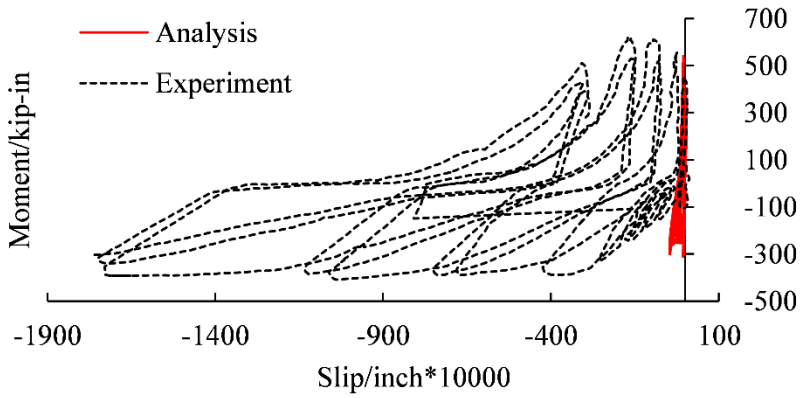

Figure 4-14 Slip versus beam moment curve for beam reinforcing bar of Specimen 2 tested by Leon (1989)

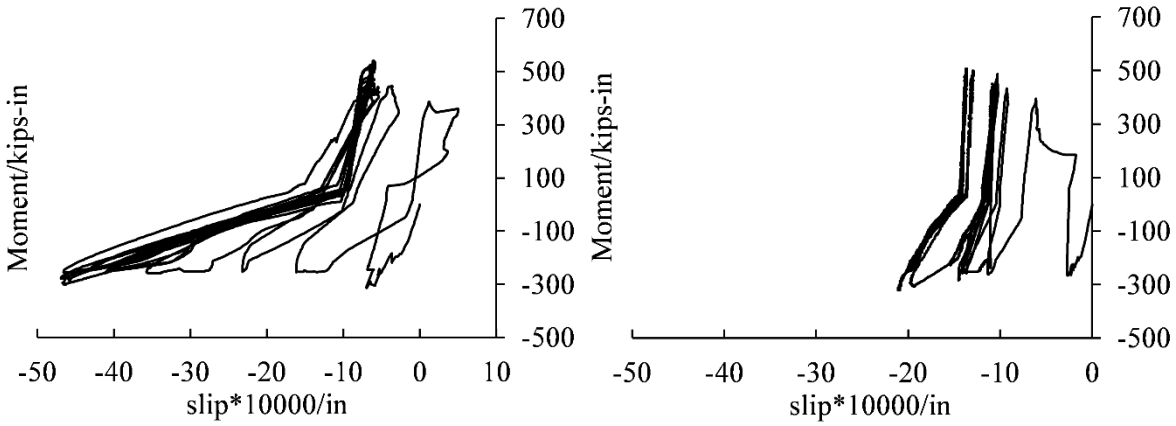

(a) Strong bond without material damage **(b) Weak bond with material damage**

Figure 4-15 Analytical results with different bond condition

A more reliable bond-slip model (for example, the Murcia-Delso and Shing (2014) model applied in Chapter 3) can be applied to get more realistic local bond-slip response.

4.4.4 Beam Reinforcement Stress

The analytical results of top beam bar stress distribution (Figure 4-16) of Specimen 2 tested by Leon (1989) strengthens the conclusion from the Section 4.4.3, that the bond-slip model overestimated the strength and underestimated the bond-slip behavior in the experiment. As a result, the strain penetration of top beam bar is not as evident as the results from finite element analysis in Section 3.2.4. For different bond condition in the current bond-slip model specifically, the difference from "strong bond without material damage" and the "weak bond with material damage" does not provide the expected behavior differences. Since the analytical results for "strong" and "weak" bond in Figure 4-16 are obtained at the same time from the loading time history, it can be concluded that the current bond-slip model has made the correct prediction that "strong bond" has slight better performance than the "weak" one.

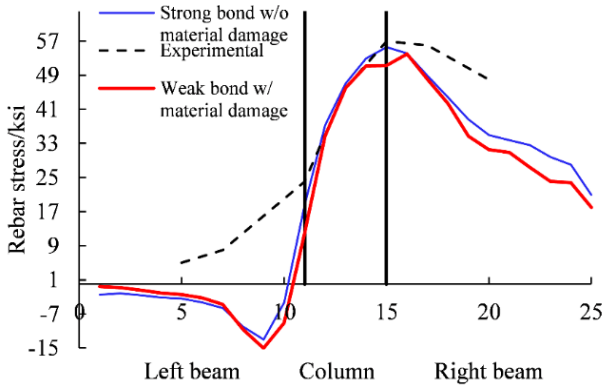

Figure 4-16 Top beam bar stress comparison for different bond condition in analytical models for analysis of Specimen 2 tested by Leon (1989)

4.4.5 Sensitivity Study

A sensitivity study has also been conducted on this two-way beam-column-slab joint under bidirectional cyclic loading, to evaluate the impact of several model parameters: the influence of including bond-slip behavior, the effect of parameters in the transverse tension law, compressive

residual stress, and concrete compressive strength.

4.4.5.1 The Influence of Including Bond-slip Behavior

The impact of different parameters from the bond-slip model, including strong/weak bond condition and if include the damage of material is compared with perfect bond as well as experimental data as shown in Figure 4-17. The perfect bond herein is simulated by elastic zero-length spring with a stiffness of 10^{15}.

Specimen 2 evidences the largest impact when different bond conditions are applied, which is reasonable as Specimen 2 was observed to have the largest bond-slip value during the test. However, the perfect bond condition, which is supposed to provide the largest strength, experienced degradation during last loops in all three simulations. The final strength provided by "strong bond with material damage" is larger than that from "strong bond without material damage for both Specimen 3 and 4, which is not reasonable. To sum up, the bond-slip model needs further study to ensure robustness.

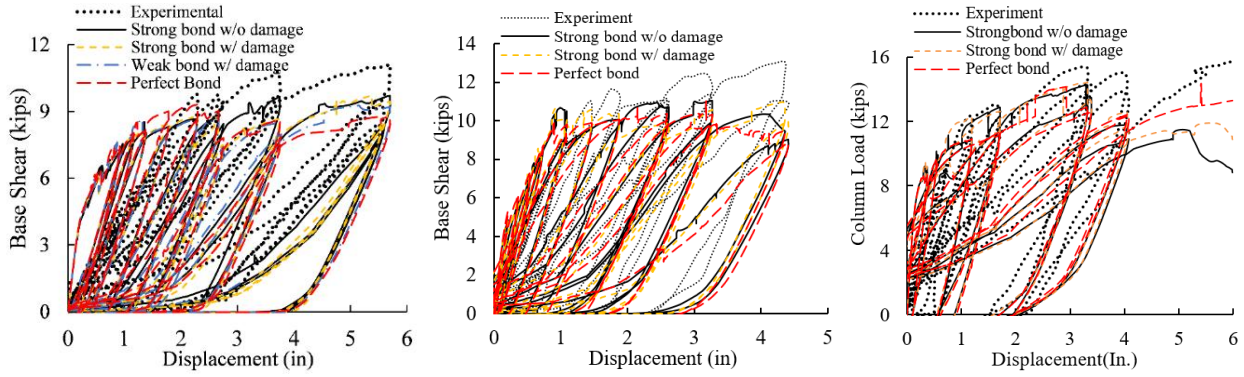

(a) Specimen 2 **(b) Specimen 3** **(c) Specimen 4**

Figure 4-17 Comparison of different bond-slip model parameters of specimens 2 to 4 tested by Leon (1989)

4.4.5.2 Parameters in the Transverse Tension Law

The compressive strength reduction factor β has a clear positive stimulate on the ultimate strength especially during the last several loops when concrete cracks and stress is continuously increasing (Figure 4-18). Among the three specimens, Specimen 2 experiences the largest influence from β because it encountered the most amount of cracks. A more accurate approach to the definition of β needs to be determined in future work.

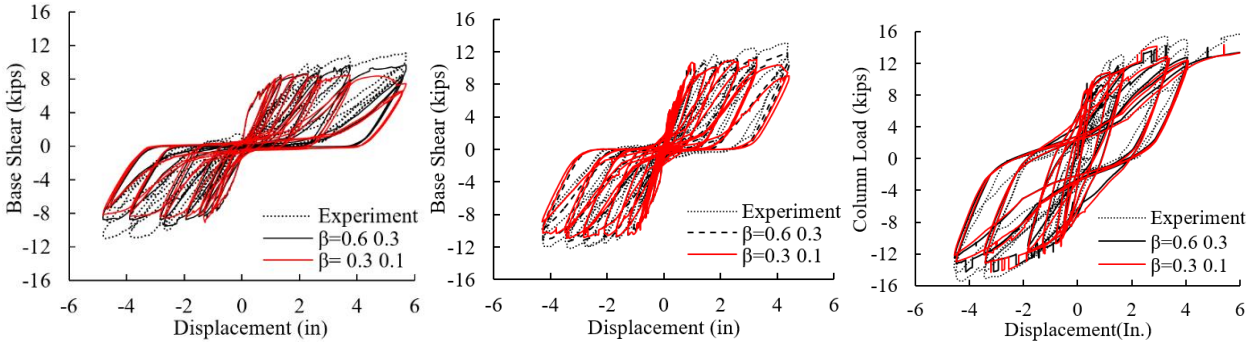

(a) Specimen 2 **(b) Specimen 3** **(c) Specimen 4**

Figure 4-18 Impact of compressive strength reduction factor β on specimens 2 to 4 tested by Leon (1989)

4.4.5.3 Compressive Residual Stress

The compressive residual stress has no impact on the overall hysteretic curve when increases from $0.1f'_c$ to $0.2f'_c$ for Specimen 2. The reason is that no concrete stress has reached the value of f_{res}.

4.4.5.4 Concrete Compressive Strength

In the finite element analysis, the concrete compressive strength is found to be the most critical parameter on the strength of the three specimens tested by Leon (1989). From the nonlinear truss studies, the results lead to a quite similar conclusion (Figure 4-19). When increasing f'_c from 5.0 ksi to 5.5 ksi for Specimen 3, the ultimate strength increased 5.5% and 5.4% for the FE model and nonlinear truss model, respectively.

For Specimen 2 and 3 with less damage in the joint, increasing f'_c does have positive increment in strength, especially from 5.5 ksi to 6.0 ksi and during the last several loading cycles. When increasing the f'_c from 5.5 ksi to 6 ksi, the strength increased 3.5% and 5.4% for Specimen 3 and 4. On the other hand, the concrete compressive strength f'_c has limited impact on Specimen 2. Because Specimen 2 encountered severe shear damage in the joint, increasing the concrete compressive strength is not sufficient to improve the strength.

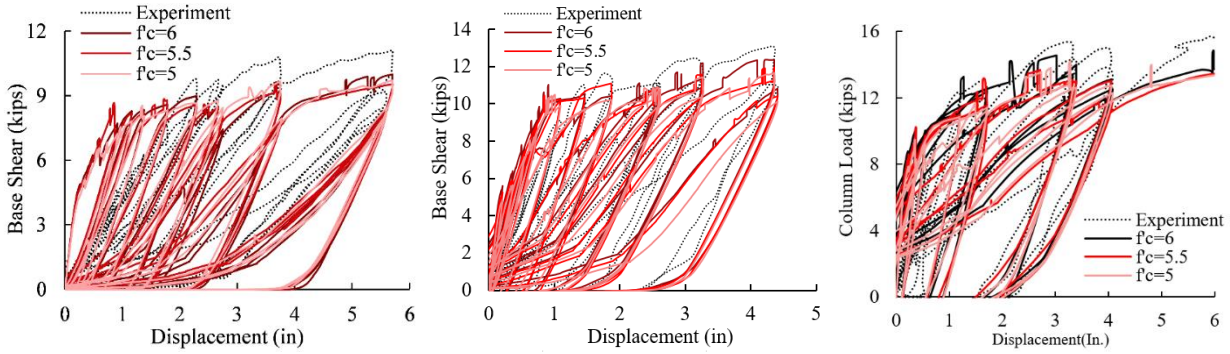

(a) Specimen 2 **(b) Specimen 3** **(c) Specimen 4**

Figure 4-19 Impact of concrete compressive strength f'_c on specimens 2 to 4 tested by Leon (1989)

4.5 Discussion

The ability in capturing shear-flexure interactive failure of planar interior BC joints has been proved to be an efficient supplement of finite element analysis with a simplified model setup and little computation cost.

The nonlinear truss methodology convincingly captures the overall pinching behavior in the hysteretic response, and has an inherent ability in capturing the shear behavior of the joint. It also gives correct damage pattern of concrete, reinforcement and the joint as a whole.

When considering the local performance, the ability of providing reasonable reinforcing bar stress distribution and bond-slip value highly depends on a reliable bond-slip model. A more

suitable bond-slip model is needed for the current model to present better results on local performance.

There are also some aspects need further study:

1. The ultimate strength was underestimated, especially with large lateral loads. More detailed explanation is needed. The peak compressive strength of the confined concrete has been found to significantly affect the obtained peak strength of the joint models. a more accurate peak stress of concrete with confinement is needed.
2. The fluctuations in the strength values observed in the hysteretic plots require further investigations in the future, to determine their cause and potential remedies.

Chapter 5 Parametric Analysis on Prototype Interior Beam-Column-Slab Connection Designed in Accordance with Modern Codes

As summarized in Chapter 2, it would be logical to believe that the level of shear stress in the joint should be below some maximum nominal design value. This value should be tied to minimum values of other quantities, including development of beam and column bars through the joint, minimum amounts of transverse joint reinforcement and ratio of column-to-beam moment capacity. The performance of beam-column joints designed for the limits currently proposed for these parameters by ACI352R-02 is poorly understood, as the limits were set based on a relatively small subset of experimental tests. No comprehensive analytical studies have been carried out to assess joint performance based on these criteria. Thus, there is a need to carry out a parametric study to better understand the failure mode of interior beam-column-slab joint designed to modern standards and rationalize the impact of various parameters on the design process. Without a reliable and efficient analytical methodology which can account for shear-flexural-bond interactive behavior of interior beam-column-slab joint, the only realistic way to carry out a parametric study is an experiment campaign. However, experimental studies are demanding in terms of costs, time and test conditions.

In this chapter, the finite element methodology described in Section 3.1, which was validated by a series of comparisons to tests of one-way interior BC joints (Section 3.2) and an interior bean-column-slab joints (Section 3.6) will be applied. A series of prototype Type 2 interior beam-column-slab connections designed based on ACI352R-02 is analytically simulated in this chapter as the first step towards a more complete evaluation of design recommendation and more comprehensive parametric studies.

5.1 Description of the Connection

5.1.1 General Summary of Design Parameters of Connections

Four groups with a total number of 24 Type 2 interior beam-column-slab connections are designed based on the design example in ACI352R-02. The detailed calculation of one example connection is shown in Appendix A, and the parameters of all the connections that are been simulated are shown in Appendix B.

Some of the most basic design parameters are shown in Table 5-1. The major difference between connection groups named P1 to P4 is the square column size, which increases from 20 in. to 32 in., together with an increasing beam width from 16 in. to 28 in. to meet the least beam width requirement from ACI352R-02. Every group consists of six connections, named from P*-1 to P*-6 (* represents the group number which varies from 1 to 4). Taking the group P1 for example, connection P1.1 is a benchmark design case which meets all the requirements from ACI352R-02; P1.2 has more beam longitudinal bars but with smaller reinforcing bar size as compared with P1.1; P1.3 has less beam longitudinal bars but with larger reinforcing bar size; P1.4 utilizes beam longitudinal reinforcement with yield stress of 70 ksi as compared with 60 ksi; P1.5 utilizes concrete with compressive stress at 8 ksi as compared with 10 ksi. For P1.2 to P1.5, all the other parameters remain the same with those from the connection P1.1.

The purpose in the design of P1.6 is to push the limits of the required shear demand for the joint, with lower concrete compressive stress at 6 ksi, a larger column longitudinal reinforcing bar size at No. 18, and also more beam longitudinal reinforcement.

Table 5-1 Important design parameters of specimens

	fy/ ksi	f'c /ksi	column size/in	column bar	beam size	Top beam bar	Bottom beam bar	layout of ties	Positive bending moment of beam/k-in	Negative bending moment of beam/k-in	Column shear /kips	Required shear Vu/kips	shear capacity Vn/kips	Po/kip	Mn of column/k-in	φ
P1.1	60	10	20	12No.9	16*24	10No.6	6No.6	4No.4@4	3989.1	8160.7	84.4	526.1	720.0	4018.0	10255.3	0.75
P1.2	60	10	20	12No.9	16*24	12No.5	7No.5	4No.4@4	3283.3	7219.5	72.9	451.3	720.0	4018.0	10255.3	0.75
P1.3	60	10	20	12No.9	16*24	5No.8	3No.8	4No.4@4	3583.9	7540.0	77.2	479.3	720.0	4018.0	10255.3	0.75
P1.4	70	10	20	12No.9	16*24	10No.6	6No.6	4No.4@4	4648.0	9399.1	97.5	614.7	720.0	4138.0	10326.0	0.74
P1.5	60	8	20	12No.9	16*24	10No.6	6No.6	4No.4@4	3981.5	8004.3	83.2	527.3	644.0	3358.4	9083.2	0.73
P1.6	60	6	20	12No.18	16*24	10No.8	6No.8	4No.4@4	7053.6	11585.7	129.4	901.1	557.7	4675.2	17073.7	0.65
P2.1	60	10	24	12No.9	20*24	10No.8	6No.8	4No.4@4	7118.8	13037.4	140.0	890.5	1056.0	5514.0	15685.6	0.80
P2.2	60	10	24	12No.9	20*24	16No.6	9No.6	4No.4@4	5960.8	11907.4	124.1	783.4	1056.0	5514.0	15685.6	0.80
P2.3	60	10	24	12No.9	20*24	7No.9	5No.9	4No.4@4	7503.7	11854.3	134.4	848.1	1056.0	5514.0	15685.6	0.80
P2.4	70	10	24	12No.9	20*24	10No.8	6No.8	4No.4@4	8286.3	14949.8	161.4	1040.9	1056.0	5634.0	15784.2	0.79
P2.5	60	8	24	12No.9	20*24	10No.8	6No.8	4No.4@4	7094.4	12702.4	137.5	893.0	944.5	4555.2	13709.0	0.78
P2.6	60	6	24	12No.18	20*24	12No.9	7No.9	4No.4@4	10301.9	16195.4	184.0	1323.5	818.0	5572.8	25284.4	0.65
P3.1	60	10	28	12No.9	24*24	12No.9	7No.9	4No.4@4	10444.2	18561.3	201.4	1306.1	1456.0	7282.0	22696.2	0.84
P3.2	60	10	28	12No.9	24*24	18No.7	12No.7	4No.4@4	10736.3	17057.9	193.0	1239.5	1456.0	7282.0	22696.2	0.84
P3.3	60	10	28	12No.9	24*24	9No.10	6No.10	4No.4@4	11348.7	17852.1	202.8	1308.5	1456.0	7282.0	22696.2	0.84
P3.4	70	10	28	12No.9	24*24	12No.9	7No.9	4No.4@4	12143.4	21194.8	231.5	1527.2	1456.0	7402.0	22838.2	0.83
P3.5	60	8	28	12No.9	24*24	12No.9	7No.9	4No.4@4	10390.8	17969.8	196.9	1310.6	1302.3	5969.6	19621.8	0.82
P3.6	60	6	28	12No.18	24*24	13No.10	8No.10	4No.4@4	14719.6	21006.2	248.1	1834.7	1127.8	6633.6	34194.2	0.68
P4.1	60	10	32	12No.9	28*24	13No.10	8No.10	4No.5@4	15019.2	24467.3	274.2	1808.5	1920.0	9322.0	31283.3	0.87
P4.2	60	10	32	12No.9	28*24	18No.9	12No.9	4No.5@4	17643.1	26201.2	304.5	2028.0	1920.0	9322.0	31283.3	0.87
P4.3	60	10	32	12No.9	28*24	14No.11	8No.11	4No.5@4	18322.7	30427.9	338.5	2318.0	1920.0	9322.0	31283.3	0.87
P4.4	70	10	32	12No.9	28*24	13No.10	8No.10	4No.5@4	17435.0	27832.6	314.4	2115.5	1920.0	9442.0	31543.4	0.86
P4.5	60	8	32	12No.9	28*24	13No.10	8No.10	4No.5@4	14906.8	23551.1	267.1	1815.7	1717.3	7601.6	26886.9	0.85
P4.6	60	6	32	12No.18	28*24	10No.14	6No.14	4No.5@4	19231.3	26731.5	319.2	2463.3	1487.2	7857.6	43878.3	0.72

The rest of design parameter are basically the same for all the connections; for example, the yield stress of transverse reinforcement is 60 ksi, the effective slab width is 76 in. with ten No.3 slab steel included in calculating the negative bending moment capacity of the beams, and the slab thickness is 6 in. The connection groups P2 to P4 are designed with the same trends as for P1.

5.1.2 Description of Analytical Model

The finite element model of one prototype connection is schematically shown in Figure 5-1. The model scheme described in Section 3.1 is again applied herein. It explicitly accounts for the bond-slip behavior of the top and bottom beam longitudinal reinforcement in all beams. There are two rigid plates on the top and bottom of the column, with boundary conditions applied in the middle of the plates. The connections are fixed at the column bottom in three translational directions, and restrained on the column top in two horizontal translational directions. The vertical force as large as 20% of the nominal axial capacity of the column section is applied on the top of the column. Vertical displacement loading curves are applied at the horizontal center line of four beam ends.

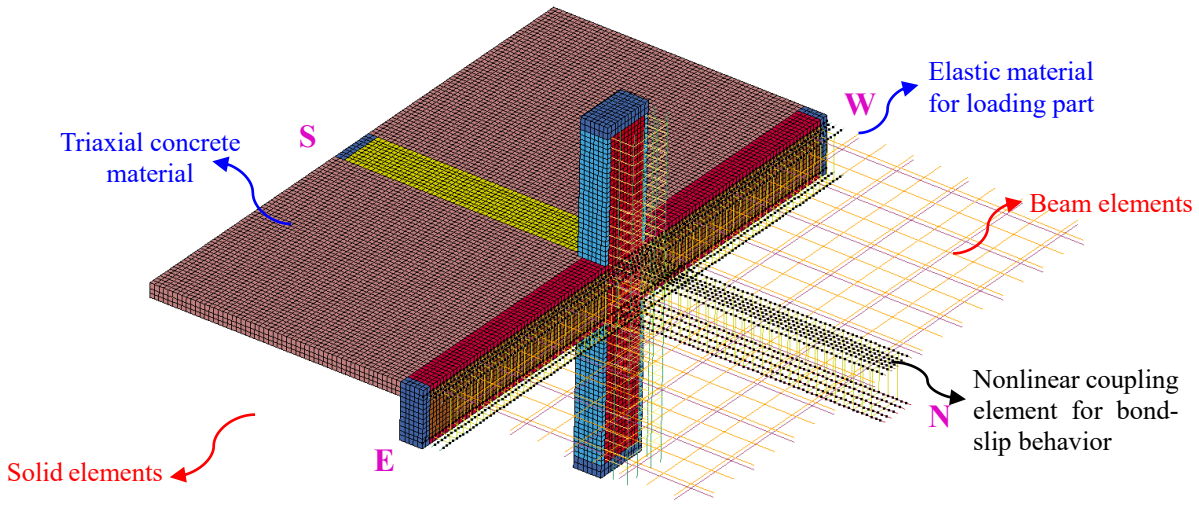

Figure 5-1 Finite element model of one prototype connection example

The connections will be subjected to unidirectional monotonic loading, bidirectional monotonic loading, unidirectional cyclic loading, and bidirectional cyclic loading as described in the following sections.

5.1.3 Three Key Factors in the Design Procedure

There are three key factors ensure the reliable performance of an interior BCJ in the design procedure, namely the ratio of development length of beam longitudinal reinforcement (which is regarded as the same value as the column width herein) over the beam bar diameter ("development length ratio" or "DR" for short), the ratio of total column flexural strength over total beam flexural strength ("moment ratio" or "MR" for short) and the ratio of required joint shear strength over the nominal joint shear strength ("shear ratio" or "SR" for short). Establishing the relation of these three factors provides an idea of their accepted boundaries and developing trends both within and beyond current design criteria.

To fulfill the parametric study and for a better comparison for all those four groups of connections, there is an effort to maintain the majority of the design parameters unchanged for the connections shown in Table 5-1. Thus some of the connections may not meet the requirements from ACI352R-02, especially for those named as P*.6. To illustrate the relation surface of the three key factors mentioned above, another set of connections that meet the design requirements are established, with major parameters tabulated in Table 5-2, and detailed parameters demonstrated in Appendix C.

Table 5-2 Design parameters for connections plotted in Figure 5-1

	MR	DR	SR	Col. Size /in	Beam Size	Top Beam Bar	Bottom Beam Bar	Layout of Ties	Positive Bending Moment of Beam /k-in	Negative Bending Moment of Beam /k-in	Col. Shear/ kips	Req'd Shear Vu/ kips	Shear Capacity Vn/kips	Col. Axial Force Po/kip	Pn Axial Load on Col. /kip	Mn of Col./k -in	φ
1	1.67	26.67	0.81	20	16*24	12No.6	6No.6	4No.4@4	3989	9350	93	584	720	4018	804	8906	0.81
2	1.89	32.00	0.71	20	16*24	15No.5	7No.5	4No.4@4	3283	8502	82	512	720	4018	804	8906	0.81
3	1.68	20.00	0.81	20	16*24	7No.8	3No.8	4No.4@4	3584	9682	92	583	720	4018	804	8906	0.81
4	1.82	20.00	0.74	20	16*24	6No.8	3No.8	4No.4@4	3584	8624	85	531	720	4018	804	8905	0.81
5	1.90	32.00	0.71	20	16*24	16No.5	6No.5	4No.4@4	2817	8921	82	512	720	4018	804	8906	0.81
6	1.85	26.67	0.73	20	16*24	12No.6	4No.6	4No.4@4	2666	9350	83	527	720	4018	804	8906	0.81
7	1.68	26.67	0.81	20	16*24	13No.6	5No.6	4No.4@4	3328	9933	92	584	720	4018	804	8906	0.81
8	1.95	26.67	0.69	20	16*24	11No.6	4No.6	4No.4@4	2666	8759	79	498	720	4018	804	8906	0.81
9	1.66	26.67	0.81	20	16*24	11No.6	7No.6	4No.4@4	4648	8759	93	583	720	4018	804	8906	0.81
10	1.69	22.86	0.80	20	16*24	9No.7	4No.7	4No.4@4	3629	9510	91	576	720	4018	804	8906	0.81
1	1.69	24.00	0.84	24	20*24	10No.8	6No.8	4No.4@4	7119	13037	140	891	1056	5514	1103	13626	0.84
2	1.91	32.00	0.74	24	20*24	16No.6	9No.6	4No.4@4	5961	11907	124	783	1056	5514	1103	13626	0.84
3	1.76	21.28	0.80	24	20*24	7No.9	5No.9	4No.4@4	7504	11854	134	848	1056	5514	1103	13626	0.84
4	1.95	27.43	0.73	24	20*24	13No.7	5No.7	4No.4@4	4528	12907	121	771	1056	5514	1103	13626	0.84
5	1.90	24.00	0.75	24	20*24	9No.8	5No.8	4No.4@4	5946	12000	125	787	1056	5514	1103	13626	0.84
6	1.98	32.00	0.71	24	20*24	16No.6	8No.6	4No.4@4	5305	11907	120	755	1056	5514	1103	13626	0.84
7	1.78	21.28	0.80	24	20*24	8No.9	4No.9	4No.4@4	6020	13167	133	849	1056	5514	1103	13626	0.84
8	1.94	27.43	0.73	24	20*24	12No.7	6No.7	4No.4@4	5425	12120	122	771	1056	5514	1103	13626	0.84
9	1.91	24.00	0.75	24	20*24	10No.8	4No.8	4No.4@4	4768	13037	124	788	1056	5514	1103	13626	0.84
10	1.78	21.28	0.80	24	20*24	8No.9	4No.9	4No.4@4	6020	13167	133	849	1056	5514	1103	13626	0.84

	MR	DR	SR	Col. Size/ in	Beam Size	Top Beam Bar	Bottom Beam Bar	Layout of Ties	Positive Bending Moment of Beam /k-in	Negative Bending Moment of Beam /k-in	Col. Shear / kips	Req'd Shear Vu/ kips	Shear Capacity Vn/kips	Col. Axial Force Po/kip	Pn Axial Load on Col. /kip	Mn of Col./k -in	φ
1	1.88	24.82	0.81	28	24*24	11No.9	6No.9	4No.4@4	8978	17311	183	1175	1456	7282	1456	19718	0.86
2	1.95	32.00	0.77	28	24*24	17No.7	10No.7	4No.4@4	8978	16291	175	1122	1456	7282	1456	19718	0.86
3	1.80	22.05	0.84	28	24*24	9No.10	5No.10	4No.4@4	9492	17852	190	1226	1456	7282	1456	19718	0.86
4	1.97	24.82	0.76	28	24*24	10No.9	6No.9	4No.4@4	8978	16034	174	1109	1456	7282	1456	19718	0.86
5	1.96	32.00	0.77	28	24*24	18No.7	9No.7	4No.4@4	8095	17058	175	1123	1456	7282	1456	19718	0.86
6	1.80	22.05	0.84	28	24*24	9No.10	5No.10	4No.4@4	9492	17852	190	1226	1456	7282	1456	19718	0.86
7	1.92	28.00	0.79	28	24*24	14No.8	7No.8	4No.4@4	8286	17387	178	1148	1456	7282	1456	19718	0.86
8	1.83	32.00	0.82	28	24*24	18No.7	11No.7	4No.4@4	9859	17058	187	1201	1456	7282	1456	19718	0.86
9	1.84	28.00	0.82	28	24*24	14No.8	8No.8	4No.4@4	9448	17387	186	1200	1456	7282	1456	19718	0.86
10	1.88	24.82	0.81	28	24*24	12No.9	6No.9	4No.4@4	8978	17311	183	1175	1456	7282	1456	19718	0.86
1	1.99	25.20	0.81	32	28*24	12No.10	6No.10	4No.5@4	11349	22948	238	1559	1920	9322	1864	27243	0.88
2	1.97	28.37	0.82	32	28*24	15No.9	8No.9	4No.5@4	11901	22657	240	1568	1920	9322	1864	27243	0.88
3	1.93	22.70	0.83	32	28*24	9No.11	6No.11	4No.5@4	13869	21477	245	1592	1920	9322	1864	27243	0.88
4	1.97	32.00	0.81	32	28*24	18No.8	11No.8	4No.5@4	12902	21700	240	1560	1920	9322	1864	27243	0.88
5	1.98	32.00	0.81	32	28*24	19No.8	10No.8	4No.5@4	11756	22669	239	1562	1920	9322	1864	27243	0.88
6	1.97	28.37	0.82	32	28*24	15No.9	8No.9	4No.5@4	11901	22657	240	1568	1920	9322	1864	27243	0.88
7	1.99	25.20	0.81	32	28*24	12No.10	6No.10	4No.5@4	11349	22948	238	1559	1920	9322	1864	27243	0.88
8	1.97	28.37	0.82	32	28*24	15No.9	8No.9	4No.5@4	11901	22657	240	1568	1920	9322	1864	27243	0.88
9	1.95	22.70	0.83	32	28*24	10No.11	5No.11	4No.5@4	11611	23383	243	1594	1920	9322	1864	27243	0.88
10	1.99	25.20	0.81	32	28*24	12No.10	6No.10	4No.5@4	11349	22948	238	1559	1920	9322	1864	27243	0.88

MR: the ratio of total column flexural strength over total beam flexural strength

DR: the ratio of development length of beam longitudinal reinforcement over the beam bar diameter

SR: the ratio of required joint shear strength over the nominal joint shear strength

Col.: Column

In order to extend the surface into a larger region, there would be at least one case with large shear ratio that may not meet the moment ratio requirement. There are 10 cases being designed and listed in Table 5-2 for every column size increasing from 20 in. to 32 in., and every case generates a node with three axes corresponding to the moment ratio, development length ratio and shear ratio of the connection, respectively. All the forty cases pass the requirements from ACI code, and share the same f'_c and f_y at 10 and 60 ksi, as well as 12 No.9 longitudinal bar in the column section.

The ten nodes for every column size form a polynomial surface in the pattern of x^2+y, where x represents shear ratio, and y represents development length ratio. The four surfaces corresponding to four column sizes are illustrated in Figure 5-2(a) to (d), and plotted in the same space in Figure 5-2(e) to demonstrate their relative position.

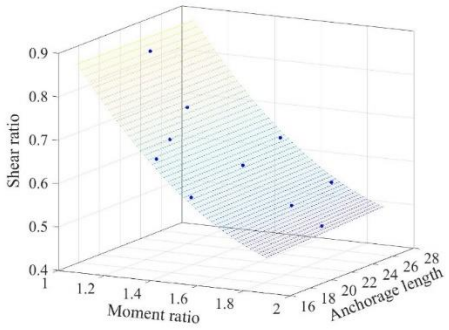

(a) Column size=20 in.

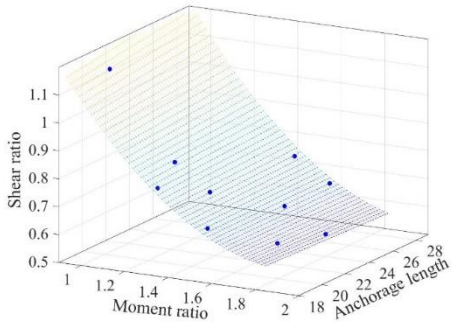

(b) Column size=24 in.

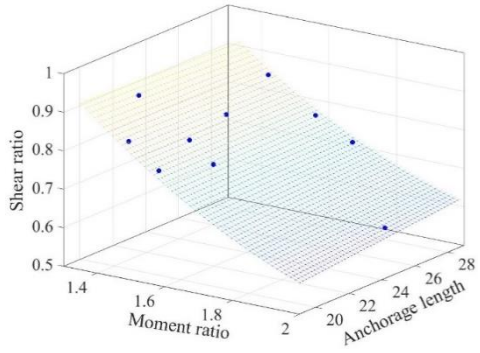

(c) Column size=28 in.

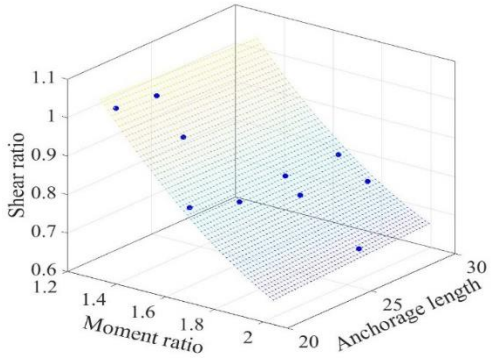

(d) Column size=32 in.

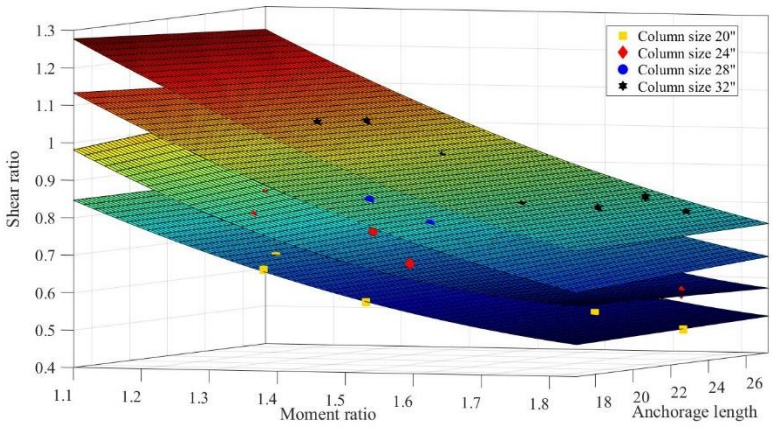

(e) Column size from 20 in. to 32 in.

Figure 5-2 Surface of three key design factors of the connections in Table 5.2

In Figure 5-2, the design becomes progressively less conservative as one moves from the bottom far right corner to the upper left near corner. The safe design zone, according to ACI352R-02 will be a cube delineated by a shear ratio of 1, a moment ratio of 1.2 and an development length of 20 bar diameters. The four surfaces in Figure 5-2 shows that the shear ratio encounters a nonliear increase when decreasing the moment ratio, which emphasises the importance to maintain the moment ratio within a larger domain. When putting four surfaces in the same space, they are almost parallel with each other. The surface with larger column sizes plot higher due to a larger shear ratio. It has to be mentioned that the cases for every group also share the same material properties except for the column size. The beam longitudinal reinforcement sizes and layouts are the only differences.

In theory, the performance of interior beam-column-connections can be predicted by comparing the value of three key factors with their recommended ranges in ACI352R-02. The predicted behavior are compared with analytical observations from cases which are subjected to unidirectional monotonic loadings in Table 5-3. The criteria of these empirical and analytical behavior is described and quantified as follows when beam ends are at 5% drift:

1. Bond-slip behavior (BS for short): The bond-slip will control behavior when DR is smaller than 20 as required by ACI; for analytical outputs, bond stress reaches the peak when the slip value exceeds $S_{peak} = 0.07d_b$ as described in Equation (3-10), the slip value of bottom beam longitudinal reinforcing bar in tension next to the column face is measured and marked with "BS" when beyond S_{peak};

2. Plastic strain accumulation in the beam region ("PA" for short): ACI 352 requires MR larger than 1.2 to ensure plastic hinge forms in the beams instead of column. In the analyses, the plastic strain accumulation of longitudinal reinforcing bar within a region away from column face is regarded as the indication of plastic hinge when subjected to unidirectional loading cases;

3. Shear damage in the joint ("SD" for short): the ACI 352 suggests an SR greater than 0.85. In the analyses, when the cumulative compressive inelasticity in the diagonal direction of the joint panel reaches its peak value together with cracking in perpendicular direction, and joint strength starts degrading.

It can be concluded from Table 5-3 that:

1. The two methods give consistent results on shear damage/behavior (SD). A shear ratio almost twice that suggested by ACI (the cases P*.6) will absolutely lead to shear failure in the joint. The cases with calculated SR range from 0.85 to 1.10 (one case with SR=1.21) that fall outside the limits recommended by ACI will not lead to severe shear failure when subjected to unidirectional monotonic loading according to the analytical results.

2. To focus on the influence of SR and DR, the values of MR are much larger than the suggested values of 1.2 in ACI to exclude its impact. The empirical and analytical results are consistent on MR, in that for the cases without joint shear damage, the plastic strain

accumulation only occurs in beam longitudinal reinforcing bar rather than those in the column. Smaller MR values result in larger peak plastic strain in the beam longitudinal reinforcing bar, which indicates that beam with larger moment capacity will carry larger force and thus brings larger strain in the reinforcing bar.

Table 5-3 Comparison of predicted and observed behavior (in.)

No.	Hand calculation based on ACI 352				Analytical results				
	MR	DR	SR	Prediction	Behavior	Slip	$0.07d_b$	slip/$0.07d_b$	peak plastic strain in beam
P1.1	2.11	26.67	0.73	PA	PA, BS	0.098	0.053	1.86	0.0470
P1.2	2.44	32.00	0.63	PA	PA, BS	0.065	0.044	1.49	0.0334
P1.3	2.30	20.00	0.67	PA	PA, BS	0.124	0.070	1.76	0.0271
P1.4	1.84	26.67	0.85	SD	PA, BS	0.071	0.053	1.35	0.0253
P1.5	1.89	26.67	0.82	PA	PA, BS	0.094	0.053	1.79	0.0195
P1.6	2.29	20.00	1.62	SD	SD, BS	0.312	0.070	4.46	0.0213
P2.1	1.95	24.00	0.84	PA	PA, BS	0.075	0.070	1.07	0.0500
P2.2	2.19	32.00	0.74	PA	PA, BS	0.084	0.053	1.60	0.0422
P2.3	2.03	21.28	0.80	PA	PA, BS	0.130	0.079	1.65	0.0373
P2.4	1.70	24.00	0.99	SD	PA, BS	0.076	0.070	1.09	0.0377
P2.5	1.73	24.00	0.95	SD	PA, BS	0.080	0.070	1.14	0.0326
P2.6	2.39	21.28	1.62	SD	SD, BS	0.252	0.079	3.19	0.0216
P3.1	1.96	24.82	0.90	SD	PA, BS	0.086	0.079	1.09	0.0339
P3.2	2.04	32.00	0.85	SD	PA, BS	0.067	0.061	1.09	0.0413
P3.3	1.94	22.05	0.90	SD	PA, BS	0.099	0.089	1.12	0.0481
P3.4	1.71	24.82	1.05	SD	PA, BS	0.080	0.079	1.01	0.0378
P3.5	1.73	24.82	1.01	SD	PA, BS	0.084	0.079	1.06	0.0321
P3.6	2.39	22.05	1.63	SD	SD, BS	0.153	0.089	1.72	0.0184
P4.1	1.98	25.20	0.94	SD	PA	0.081	0.089	0.91	0.0398
P4.2	1.78	28.37	1.06	SD	PA, BS	0.100	0.079	1.27	0.0398
P4.3	1.60	22.70	1.21	SD	PA	0.095	0.099	0.96	0.0314
P4.4	1.74	25.20	1.10	SD	PA	0.084	0.089	0.94	0.0409
P4.5	1.75	25.20	1.06	SD	PA, BS	0.091	0.089	1.02	0.0306
P4.6	2.39	18.90	1.66	SD, BS	SD	0.020	0.119	0.17	0.0099

BS: bond-slip behavior; PA: plastic strain accumulation in the beam region; SD: shear damage/behavior in the joint;

3. The value of bond-slip is not simply linear with DR. It is influenced by SR and column size, as follows:

1) When the joint encounters shear failure, the slip value increases dramatically (for example P2.3 and P2.6) and the impact from large SR decreases when the column size become larger and the beam becomes shallower correspondingly (for example, compare P2.3/P2.6 with P3.3/P3.6);

2) When the joints are exempt from shear failure and have similar values of SR/MR, higher DR gives smaller bond-slip values (for example, P1.2 and P1.3, P3.2 and P3.3).

5.2 Unidirectional Behavior

5.2.1 Beam Flexural Capacity

In order to further evaluate the reliability of the FE model, and also provide reference to the accuracy of the design procedure, the flexural capacity of the beam subjected to positive and negative moment are compared for connection P2.1. The connection P2.1 (Table 5-3) has a common column size (24 in.), a moderate moment ratio (1.95), an intermediate development length (24.00 bar diameters with #8 bars) and a moderate shear ratio (0.84). It meets all ACI352R-02 requirements and is expected to form plastic hinges in the beams with little strength degradation. The comparison between the result from this finite element model, a nonlinear beam model with fiber section in OpenSees (material properties shown in Table 5-4), and simple theoretical hand calculations per ACI352R-02 in shown is Figure 5-3.

Table 5-4 Material properties used in Nonlinear Beam analysis

	f'_c	ε_0	f_{res}	ε_{res}	f_t
Unconfined concrete	10	0.003	0.5	0.006	1
Confined concrete	13	0.007	2	0.015	1.3
	f_y	E	ε_{sh}	f_u	ε_u
reinforcement	60	29000	0.01	90	0.15

The comparison of the corresponding moment vs. drift ratios for a typical beam is shown in Figure 5-3, with parts (b) and (d) corresponding to the initial portions of curves in Figure 5-3(a) and (c). The comparisons in Figure 5-3(b) and (d) demonstrate a satisfactory consistency on the initial stiffness between the FE model and nonlinear beam model.

For the positive moment (Figure 5-3(a) and (b)), which has bottom beam bar in tension and top slab in compression, the curves from nonlinear beam analysis encounter a strength drop around 1.5% drift ratio due to the softening in concrete strength. The strength drops around the value calculated in ACI352R-02, which assumes all tensile reinforcing bar reaches yield stress at the bottom. The strength recovers quickly after a slight drop because compressive concrete blocks is not crushed yet. The curve from FE analysis is mostly continuously increasing (Figure 5-3 (a)).

For the negative moment, beam strength deteriorates dramatically in the FE model around 5% drift ratio due to large deformation of the unsupported compressive reinforcement after the surrounding concrete elements are crushed and removed (Figure 5-3(c)). This phenomenon is not accounted for in nonlinear beam analysis and also in the theoretical calculation, which thus overestimated the strength.

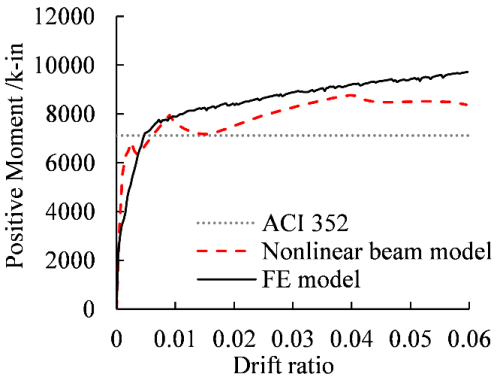

(a) Positive moment

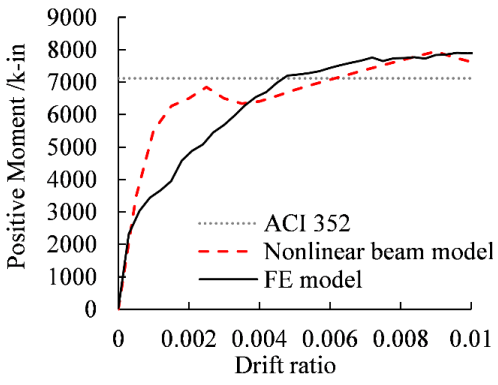

(b) Positive moment at early stage

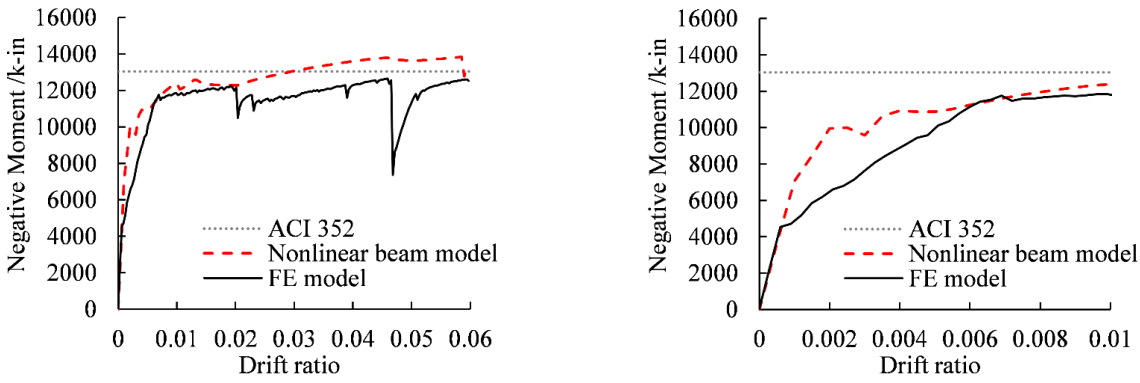

(c) Negative moment **(d) Negative moment at early stage**

Figure 5-3 Comparison of flexural moment of connection P2.1 (column size 24 in.)

5.2.2 Behavior under Unidirectional Monotonic Loading

The discussion for this section will be centered initially on a comparison of Specimens P.1.1, P1.6, P4.1 and P4.6. P1.1 (Table 5-3) has a narrow column size (20 in.), an adequate moment ratio (2.11), a slightly high development length (26.67 bar diameters with #6 bars) and a moderate shear ratio (0.73). This specimen satisfies all ACI352R-02 requirements, and one would expect this specimen to clearly form plastic hinges in the beams and undergo relatively little degradation. P1.6 (Table 5-3) has the same narrow column (20 in.), a high moment ratio (2.29), a low development length (20.00 bar diameters with #8 bars) and a very high shear ratio (1.62). This specimen doesn't satisfy ACI352R-02 conditions, and one would expect this specimen to encounter a shear failure in the joint and huge strength degradation. P4.1 (Table 5-3) has a wide column (32 in.), a moderate moment ratio (1.98), a moderate development length (25.20 bar diameters with #10 bars) and a slightly high shear ratio (0.94). This specimen satisfies all ACI352R-02 conditions except for a slightly higher shear ratio, and one would expect this specimen to clearly form plastic hinges in the beams and fail by crushing of the beam compressive blocks and shear deformation of the joint. P4.6 (Table 5-3) has the same wide column (32 in.), a high moment ratio (2.39), a low development

length (18.90 bar diameters with #14 bars) and an unacceptably high shear ratio (1.66). This specimen doesn't satisfy ACI352R-02 conditions, and one would expect this specimen to experiences shear failure in the joint and huge strength degradation.

The normalized moment-drift ratio relation of the mentioned connections are plotted in Figure 5-4. The normalized moment from analysis is calculated by dividing the summation of moment at beam ends with the corresponding theoretical value in ACI352. The connections with regular shear ratio (P1.1 and P1.4) present a ductile behavior, with little degradation due to crushing of the compressive concrete on the edge of beam. On the other hand, the normalized moment of connections designed with high shear ratio (P1.6 and P4.6) seldom reach the normalized value of one, and experience huge strength degradation.

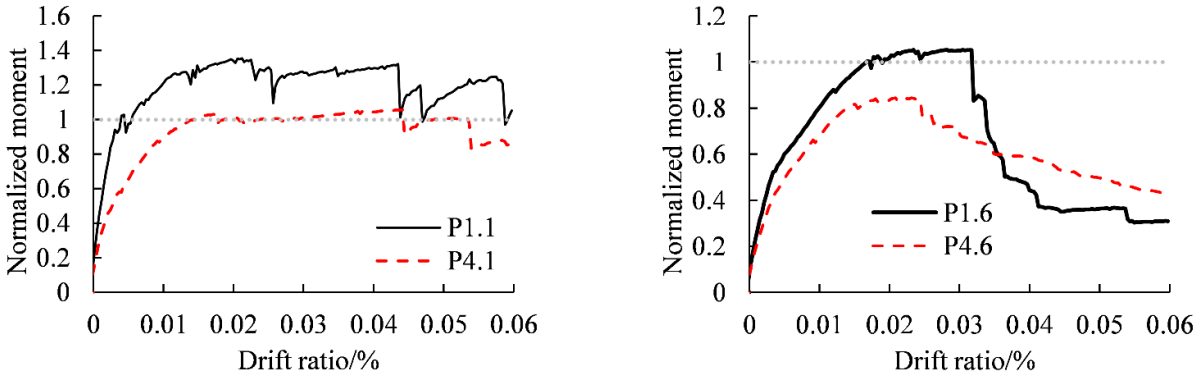

(a) Regular shear ratio **(b) High shear ratio**

Figure 5-4 Normalized moment-drift ratio relation of different shear ratios

The contour plot of the parameter κ, which represents the inelastic accumulative compressive strain of concrete is plotted in Figure 5-5 to demonstrate the compressive inelasticity parameter of concrete. As expected, there is almost no damage in the column (Figure 5-5(a)(b)). The beam shows damage due to crushing of the compressive concrete and the yielding of tensile reinforcing bar. With column size increases from 24 inch to 32 inch and also the beam width increases from

16 to 28 inch, the beam subjected to positive moment (moving upwards) encounters more concrete crushing on the top (Figure 5-5 (a)-(b)), because higher compressive stress is needed to balance the high tensile force in the reinforcement on the bottom. The beam subjected to negative moment loading (moving downwards) experiences less concrete crushing on the bottom (Figure 5-5 (c)-(d)) due to larger area of concrete in compression.

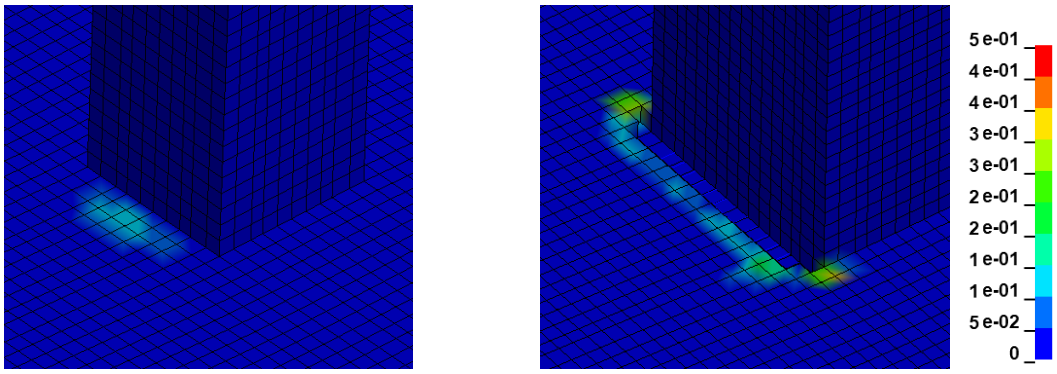

(a) Slab damage of P1.1 **(b) Slab damage of P4.1**

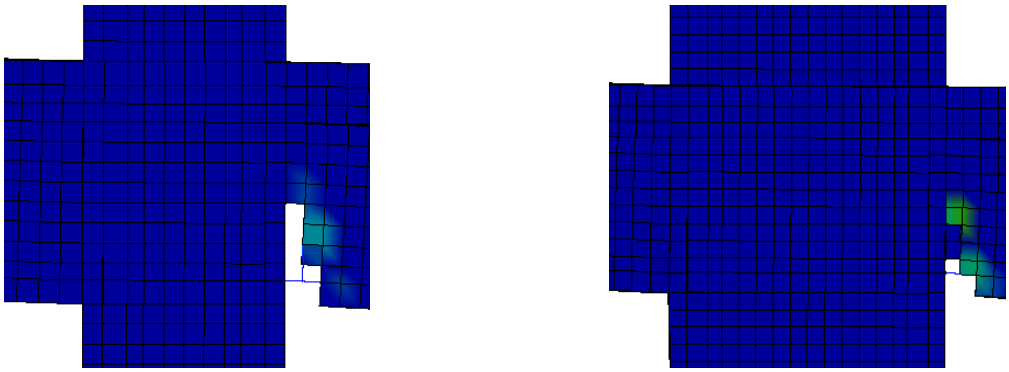

(c) Beam damage of P1.1 **(d) Beam damage of P4.1**

Figure 5-5 Compressive inelasticity parameter of concrete at 6% drift ratio

For a connection designed outside the ACI352R-02 parameters, i.e., with a shear ratio of 1.62, the integrity of the joint is no longer guaranteed. The minimum principal stress contour for the concrete is plotted in Figure 5-7 to illustrate the force transferring mechanism in the joint, which demonstrate an impressive amount of degradation as the strut mechanism is no longer efficient in transferring forces due to the damage. The maximum principal strain contour for the concrete is

plotted in Figure 5-9 to provide an insight on the cracking pattern of concrete. The beam loading downward loses more concrete due to crushing on the bottom (Figure 5-8), and the beam loading upward develops more concentrated cracks on the bottom (Figure 5-9). The slip value measured at the bottom reinforcing bar also indicates larger slips after reaching a 3% drift ratio in the connection with high shear ratio (Figure 5-10).

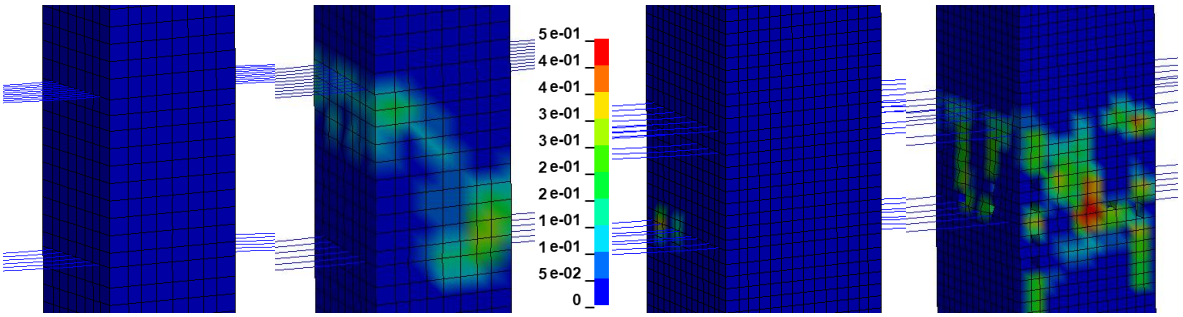

(a) P1.1 **(b) P1.6** **(c) P4.1** **(d) P4.6**

Figure 5-6 Compressive inelasticity parameter of concrete in the joint at 6% drift ratio

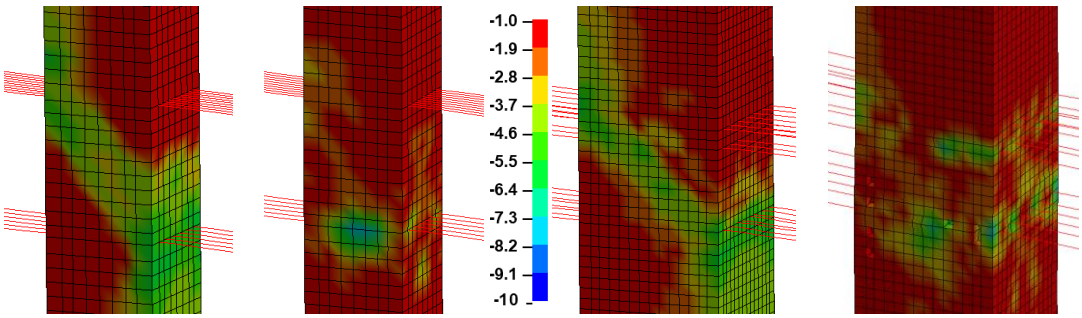

(a) P1.1 **(b) P1.6** **(c) P4.1** **(d) P4.6**

Figure 5-7 Minimum principal stress contour at 6% drift ratio

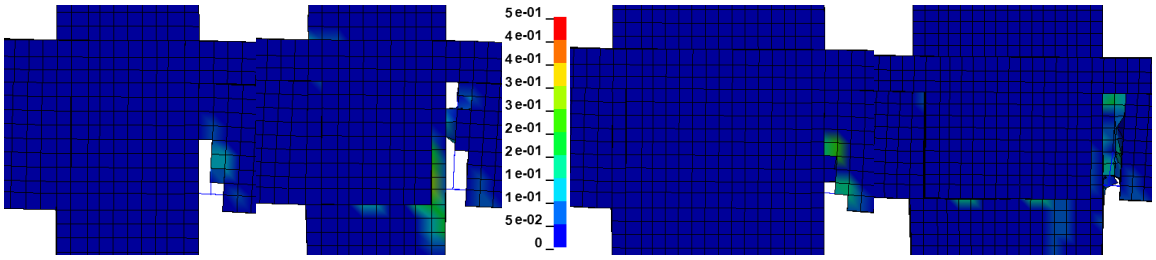

(a) P1.1 **(b) P1.6** **(c) P4.1** **(d) P4.6**

Figure 5-8 Compressive inelasticity parameter of beam at 6% drift ratio

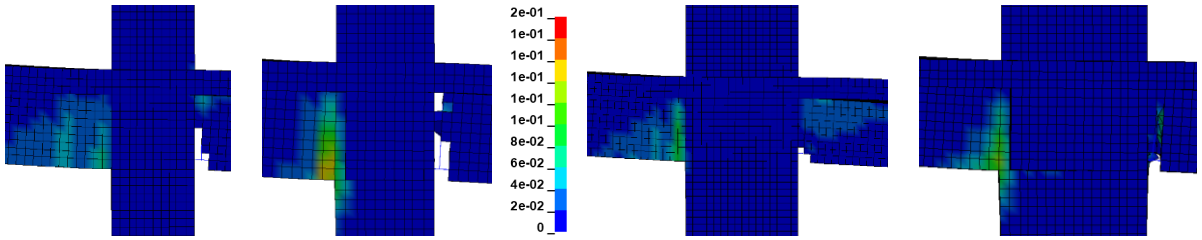

(a) P1.1 **(b) P1.6** **(c) P4.1** **(d) P4.6**

Figure 5-9 Maximum principal strain contour at 6% drift ratio

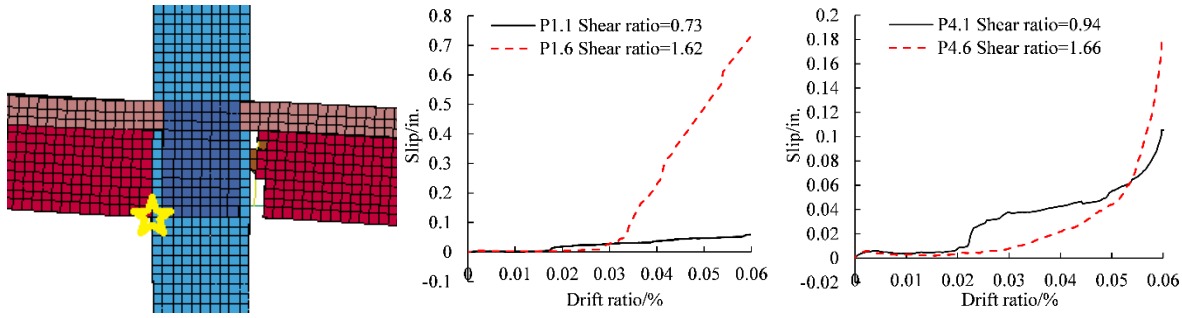

(a) Location of slip measurement **(b) P1 (column size=24")** **(c) P4 (column size=32")**

Figure 5-10 Comparison of bond slip values with shear ratio of 0.73 and 1.62

5.2.3 Behavior under Unidirectional Cyclic Loading

The connections are analyzed by a unidirectional cyclic loading curve as shown in Figure 5-11 which is made up of two cycles at 0.1%, 0.25%, 0.5%, 0.75%, 1%, 2%, 3%, 4%, 5% drift ratio, respectively.

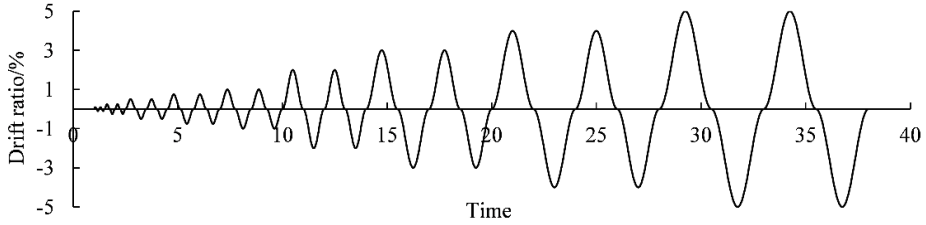

Figure 5-11 Cyclic loading curve

The total moment is calculated by multiplying the moment of east beam by -1 and adding the

moment of the west beam. The total moment-drift ratio relation shown in Figure 5-12(a)-(b) for connection P1.1 presents a good agreement between the unidirectional monotonic and cyclic analysis insofar as the initial stiffness, the gradual strength increase and stiffness decrease for the cycles before 3% drift ratio, and a strength degradation during the final cycles. Similar results are obtained for connection P4.1.

When comparing the time at which first yield occurs for the two connections, connection P4.1, with larger column size and thus relatively shallower beam due to the increased beam width, encounters earlier concrete crushing at the beam bottom, earlier yielding of top beam reinforcing bars, smaller stress in joint transverse reinforcing bar, and similar yielding time for reinforcement in the slab and top of the beam. Neither of these two connections reach stresses corresponding to yielding of column longitudinal reinforcement.

The contour plots shown in Figure 5-13 to Figure 5-15 demonstrate consistency in joint damage, force transfer mechanisms, crack pattern development and slip level of the series of joints with moderate ACI 352-02 design criteria as the column size increases from 20 inch to 32 inch (P1.1 to P4.1, respectively).

As far as the cyclic loading curve in Figure 5-11 is concerned, connections that meet the design requirements maintain both satisfactory integrity and an efficient force transfer mechanism in the joint, as well as the an evenly distributed crack pattern in the beams. The slip measurement from monotonic cyclic analysis develops more in one direction due to the beam growth, and follows the trend shown in the monotonic analysis.

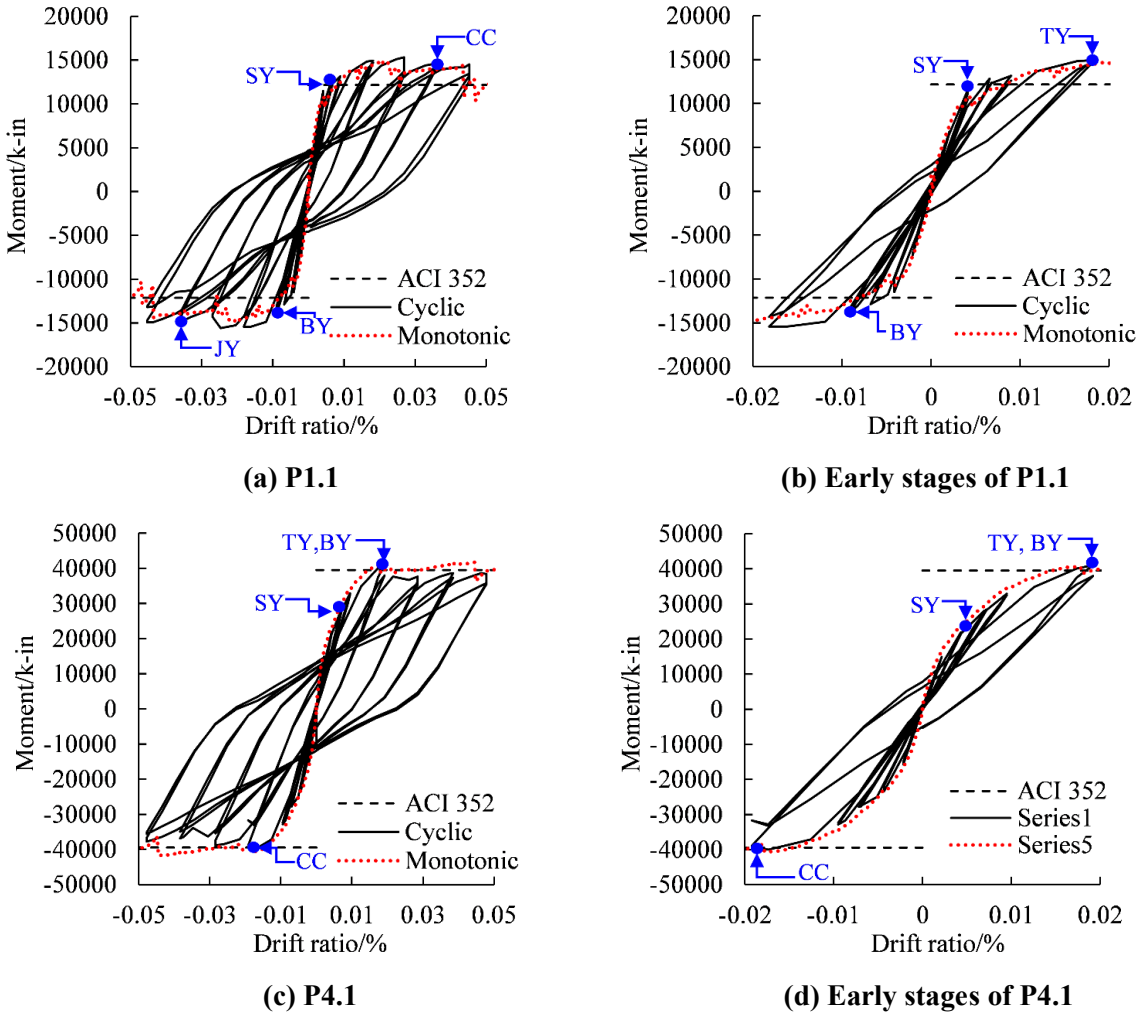

(a) P1.1 (b) Early stages of P1.1

(c) P4.1 (d) Early stages of P4.1

TY: Top beam bar Yield BY: Bottom beam bar Yield
SY: Slab bar Yield CC: Concrete crushing
JY: Joint transverse reinforcement Yield

Figure 5-12 Comparison of unidirectional monotonic and cyclic result for P1.1 and P4.1

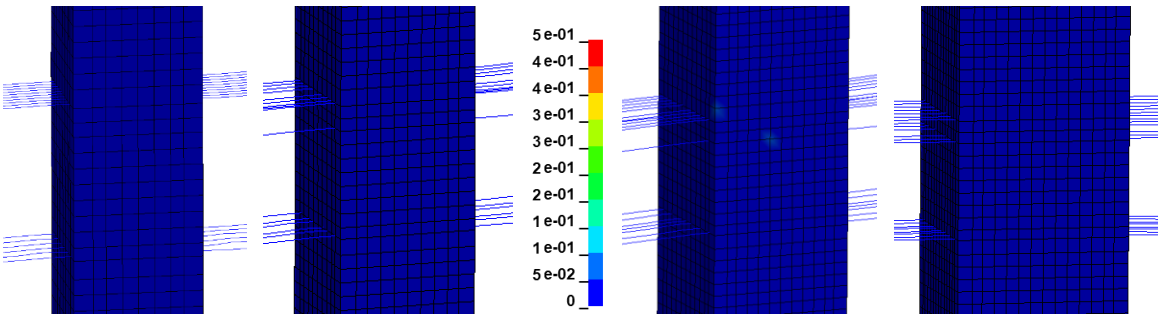

(a) P1.1 (b) P2.1 (c) P3.1 (d) P4.1

Figure 5-13 Compressive inelasticity parameter of the joint at 5% drift ratio during the last

cycle

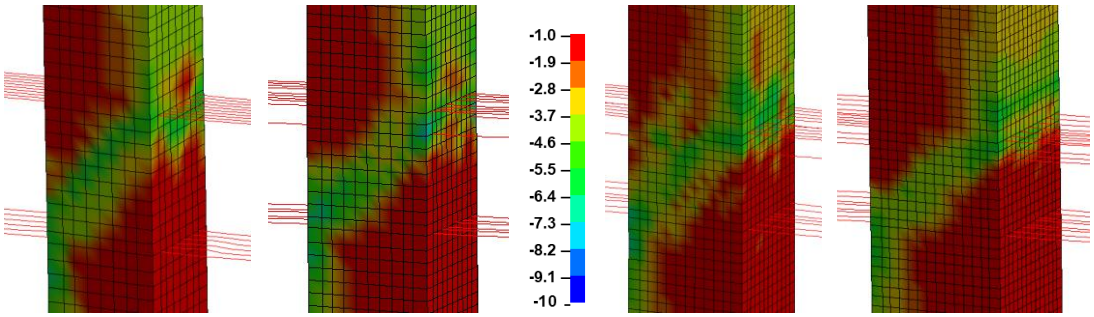

(a) P1.1 (b) P2.1 (c) P3.1 (d) P4.1

Figure 5-14 Minimum principal stress contour at 5% drift ratio during the last cycle

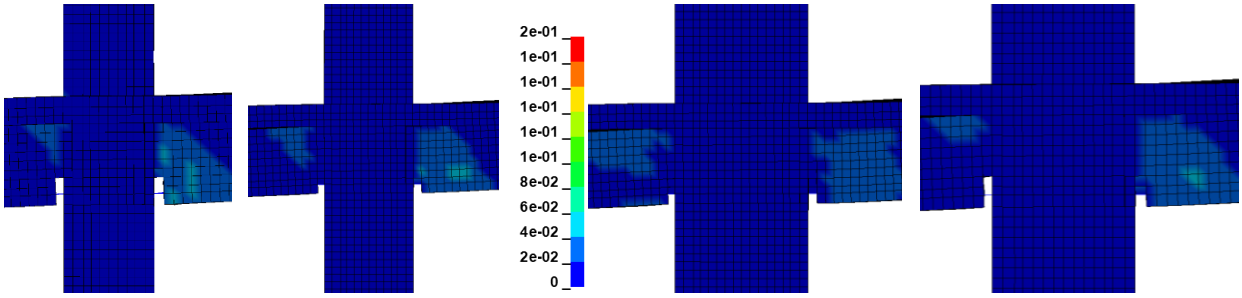

(a) P1.1 (b) P2.1 (c) P3.1 (d) P4.1

Figure 5-15 Maximum principal strain contour at 5% drift ratio during the last cycle

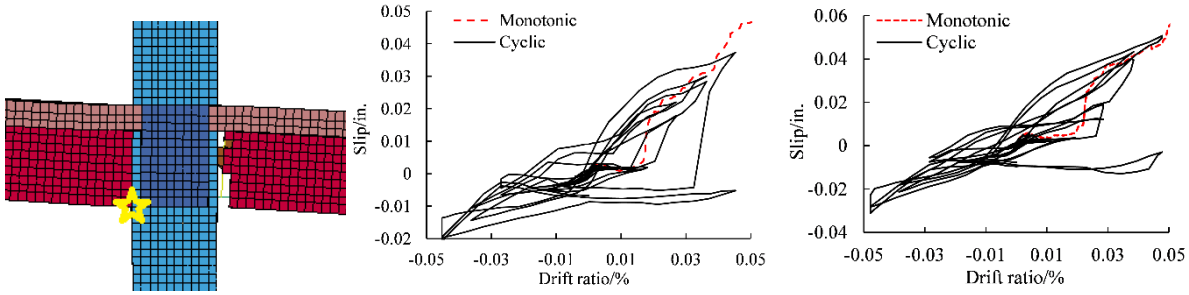

(a) Location of slip measurement (b) P1.1 (c) P4.1

Figure 5-16 Comparison of slip development

It is also worth comparing again to see the impact of shear ratio on the cyclic performance. Connections P2.3 and P2.6 are compared herein. P2.3 (Table 5-3) has a moderate column size (24

in.), a moderate moment ratio (1.76), a low development length (21.28 bar diameters with #9 bars) and an acceptable shear ratio (0.80); P2.6 (Table 5-3) has the same column size (24 in.), an acceptable slightly higher moment ratio (2.22), the same development length (21.28 bar diameters with #9 bars) and a high shear ratio (1.62). Connection P2.3 meets all requirements from ACI 352 and is expected to form plastic hinges in the beam without great strength degradation; P2.6 has an unacceptable high shear ratio and would come across shear damage in the joint.

The contour plots in Figure 5-17 indicate substantial damage on the joint that as a consequence of the high shear ratio (Figure 5-17 (b)). The efficient force transfer mechanism (Figure 5-17(c)) is weakened and the joint starts unloading (Figure 5-17 (d)). The distributed crack pattern (Figure 5-17(e)) is replaced by large cracks at beam-column interface (Figure 5-17(f)). The massive joint deterioration is also evident from the moment-drift ratio relation in Figure 5-18.

The slip development is worth looking into to develop a better understanding of the influence of joint and beam damage on the bond-slip behavior. The slip value computed falls in a similar magnitude range at location *b* (upper longitudinal beam reinforcing bar (Figure 5-19(b)), but differs substantially at location *a* (lower longitudinal reinforcing bar (Figure 5-19 (c-d)) due to damage in the joint and beams. This gives a hint on the locality of bond-slip behavior and the influence from damage.

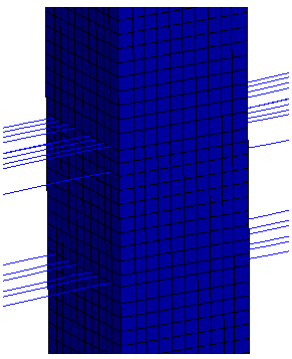

(a) Joint damage of P2.3

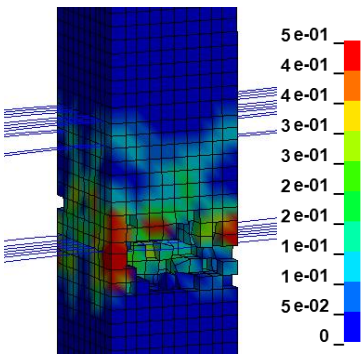

(b) Joint damage of P2.6

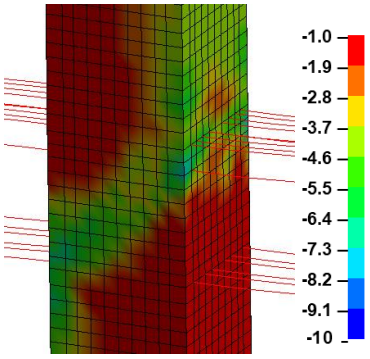

(c) Min. principal stress of P2.3

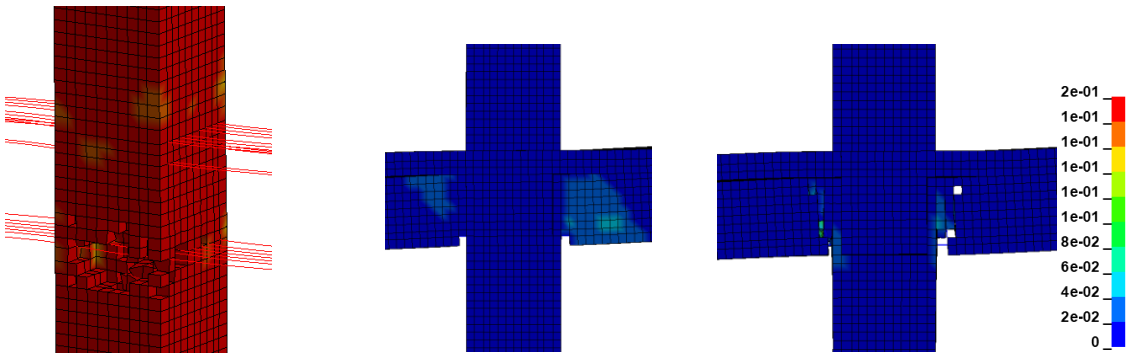

(d) Min. principal stress of P2.6 (e) Max. principal stress of P2.3 (f) Max. principal stress of P2.6

Figure 5-17 Comparison of damage pattern between archetypes P2.3 and P2.6

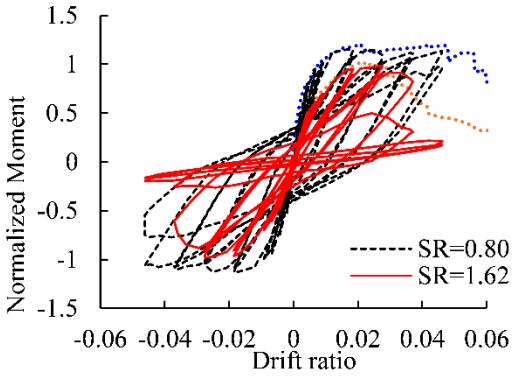

Figure 5-18 Comparison of moment-drift ratio relation between P2.3 and P2.6

To have a better understanding on how individual measurements of bond-slip behavior differ from an average value along a given length, the average value is compared with individual measurements from seven locations as indicated in Figure 5-20(a). Locations 1 and 6, at beam-column interfaces, have the largest slip value especially during later stages. This implies that the slip value is influenced by the localized damage, and measurements at these locations can be regarded as the worst situation. Slip measurements from other locations fall between the two extreme cases at the interface, and are quite close to the average value.

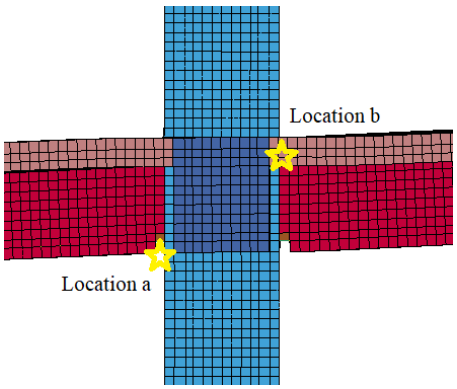

(a) Location of slip measurement

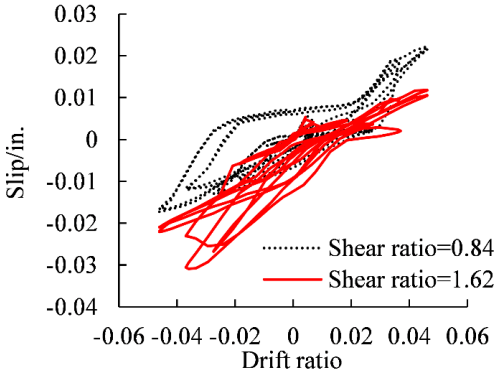

(b) Comparison at location b

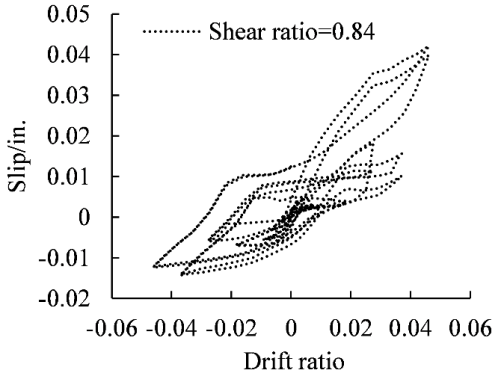

(c) Result of P2.1 at location a

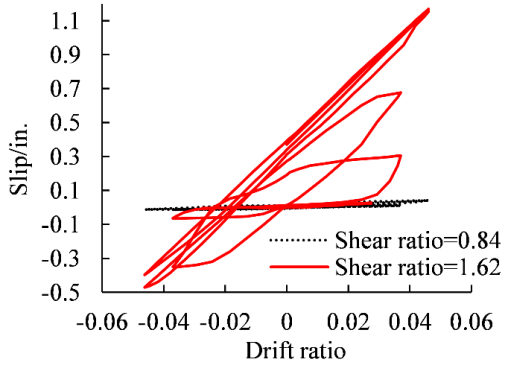

(d) Comparison at location a

Figure 5-19 Comparison of bond-slip measurement

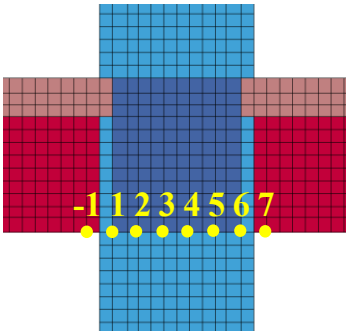

(a) Location of slip measurement

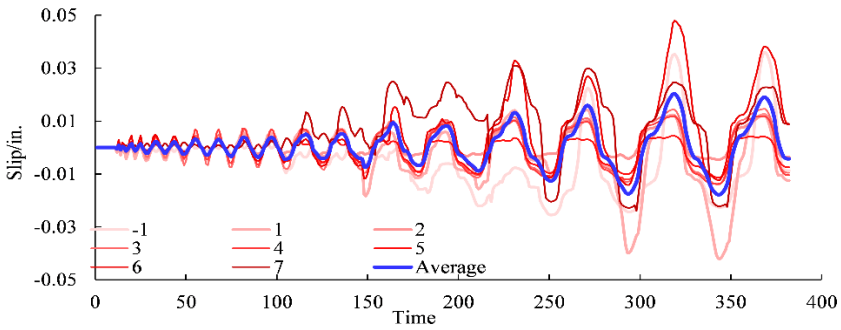

(b) Average and individual slip measurement

Figure 5-20 Average and individual slip measurement distribution

To determine the effect from repeating cycles on joint performance, connection P2.6 is analyzed subjected to a unidirectional cyclic loading which is repeated at a 2% and 3% drift ratio

for four times, respectively. The drift ratio 3% is a moderate drift level at which the beam longitudinal reinforcement has already yielded and its plastic strain value is around 0.04. The compressive concrete cover of beam has already crushed, while the concrete in the joint has not been severely damaged (Figure 5-21(e)). The influence on the overall peak strength is that it drops by 5% during the previous 2% drift ratio cycles, while climbs to similar strength in the first 3% drift ratio cycle compared with the benchmark case in black line (Figure 5-21(a)-(b)). Then the peak strength decreases by 13% during the 3% drift ratio cycles. The local bond-slip behavior does not increase a lot during the 2% drift ratio cycles, while grows gradually during the 3% drift ratio cycles together with the yield penetration of beam reinforcement and the shear damage in the joint (Figure 5-21(e)). The force transferring mechanism is slightly influenced as can be identified that the band become narrower.

The whole procedure gives a good hint on how the global BCJ behave under cyclic loading together with the development of local performance such as the increase of bond-slip value, the damage accumulation in the joint and the changing of force transferring mechanism.

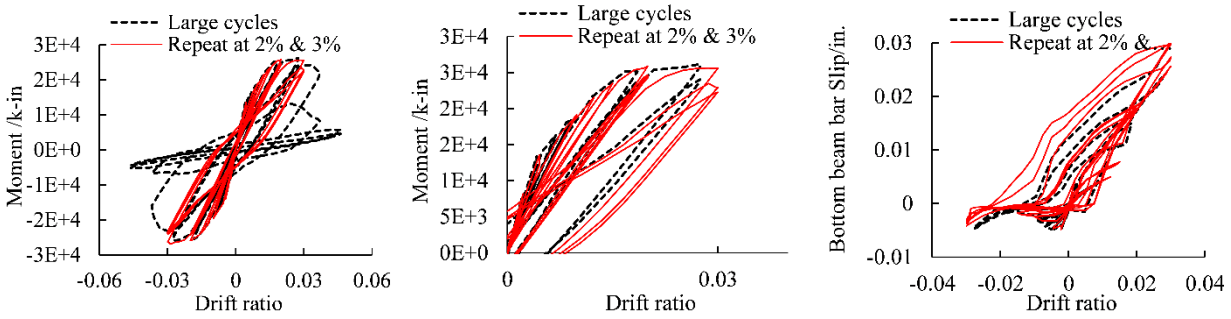

(a) Influence on strength **(b) Detailed influence on strength** **(c) Influence on bond-slip behavior**

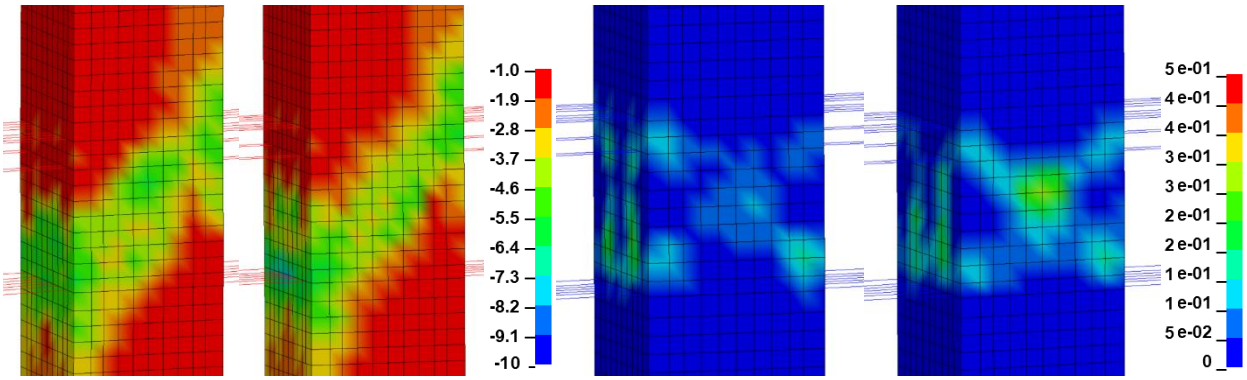

(d) Min. principal stress contour w/ & w/o repeat (e) Compressive inelasticity parameter w/ & w/o repeat

Figure 5-21 Influence on repeated loading cycles

5.2.4 Shear Stress in the Joint

The ratio of the required shear stress over $\sqrt{f_c'}$ gives a insight on the magnitude of shear force that the joint encounters. The shear force from FE analysis and ACI calculation is compared in the first part of Table 5-5 by calculating the FE shear as the total moment divided by the height of the joint, which equals to the height of the beam.

The ratio is calculated by dividing the shear force from unidirectional monotonic analysis by that from ACI352R-02 calculation; no resistance factors are used. The smaller the ratio is, the less accurate the ACI calculation becomes. The shear stress in the second part of the table is then calculated by dividing the shear force obtained with the gross sectional area of the column. Finally, the ratio against $\sqrt{f_c'}$ is attained by dividing the shear stress over the value of $\sqrt{f_c'}$.

The ratio of analytical results over theoretical results from ACI code in the third column of Table 5-5 indicates that the design code is not conservative for these specific cases. The results also indicate that the connections with large shear ratios are not safe; a similar conclusion occurs with larger size columns and relatively shallower beams.

Table 5-5 Comparison of joint shear force subjected to unidirectional monotonic loading

	$\frac{M_p+M_n}{d}$ /kips			$\frac{M_p+M_n}{d*A_g}$ /ksi		$\sqrt{f_c'}$ /ksi	$\frac{M_p+M_n}{d*A_g*\sqrt{f_c'}}$	
	Unidirectional	ACI352	Ratio	Unidirectional	ACI352		Unidirectional	ACI352
P1.1	685	506	1.35	1.71	1.27	0.10	17.14	12.66
P1.6	818	777	1.05	2.04	1.94	0.08	26.56	25.22
P2.1	1148	840	1.37	1.99	1.46	0.10	19.94	14.58
P2.6	1128	1104	1.02	1.96	1.92	0.08	25.44	24.89
P3.1	1322	1208	1.09	1.69	1.54	0.10	16.86	15.42
P3.6	1388	1488	0.93	1.77	1.90	0.08	22.99	24.66
P4.1	1739	1645	1.06	1.70	1.61	0.10	16.98	16.07
P4.6	1617	1915	0.84	1.58	1.87	0.08	20.51	24.29

5.3 Bidirectional Behavior

To simplify the design procedure, the two-way interior beam-column connection follows the unidirectional criteria in both directions based on ACI352R-02. It is interesting to investigate if the bidirectional behavior of the joint is as expected based on the current design requirements.

5.3.1 Behavior under Bidirectional Monotonic Loading

The same four connections in Section 5.2.2 are compared in this section again to show changes in damage pattern when subjected to bidirectional monotonic loading simultaneously in two directions. The plots in Figure 5-22 demonstrate declines in peak strength for all four connections. Joints with smaller column size encounter larger strength declines during later stages. For the connection with higher shear ratio, the bidirectional case represents a higher ductility during later stages, especially for smaller column sized connection because reinforcing bars from both directions begin to develop force.

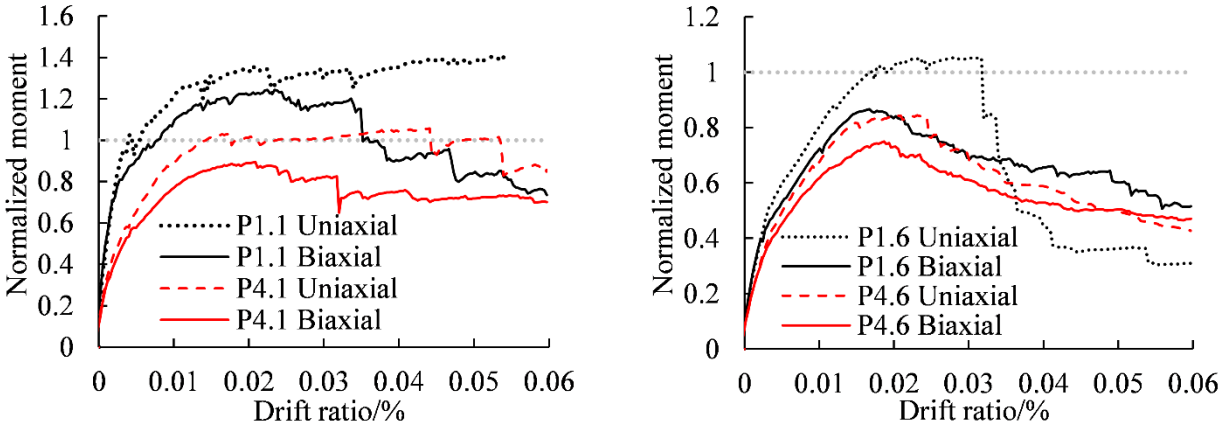

(a) Regular shear ratio **(b) High shear ratio**

Figure 5-22 Comparison of normalized moment for unidirectional and bidirectional monotonic analysis

By comparing the contour plots from Figure 5-23 to Figure 5-26 (bidirectional monotonic loading) with those from Figure 5-6 to Figure 5-9 (unidirectional monotonic loading), one can deduct the impact of bidirectional loading.

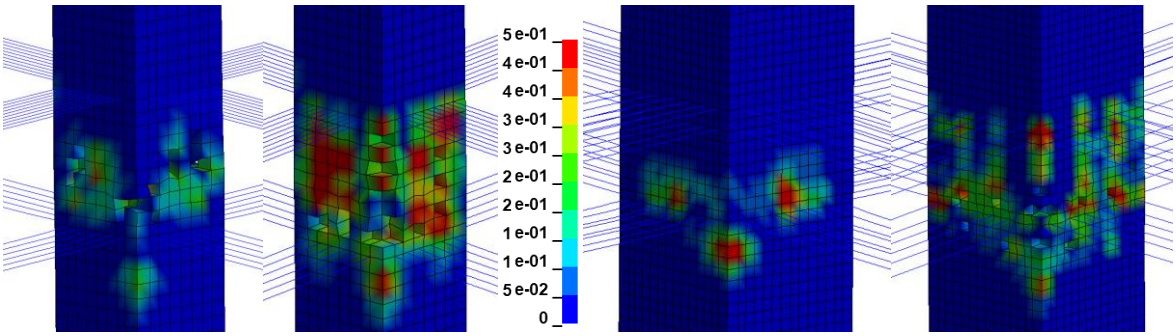

(a) P1.1 **(b) P1.6** **(c) P4.1** **(d) P4.6**

Figure 5-23 Compressive inelasticity parameter of concrete in the joint at 6% drift ratio

For the connection with normal shear ratio (P1.1 and P4.1), the confined joint starts to have element removal along the diagonal column corner (Figure 5-23(a)) and beams are crushed on the bottom in both directions (Figure 5-25). This results in a large stress concentration in the lower

corner of the column (Figure 5-25(a)).

There is more damage for connections with higher shear ratio. In this specific case, the joint almost loses all the elements along the edge (Figure 5-23(b)), and the corner cover of the joint spalls (Figure 5-25(b)). The stress contour in Figure 5-24(b) shows lower values compared with that in Figure 5-24(a) because the connection has started a post-peak unloading process. The maximum principal strain contour in Figure 5-26 indicates deeper cracks that spread into a larger region when compared with that from monotonic loading. For an easier comparison, all the contour plots apply the same color range that was used in Section 5.2.2.

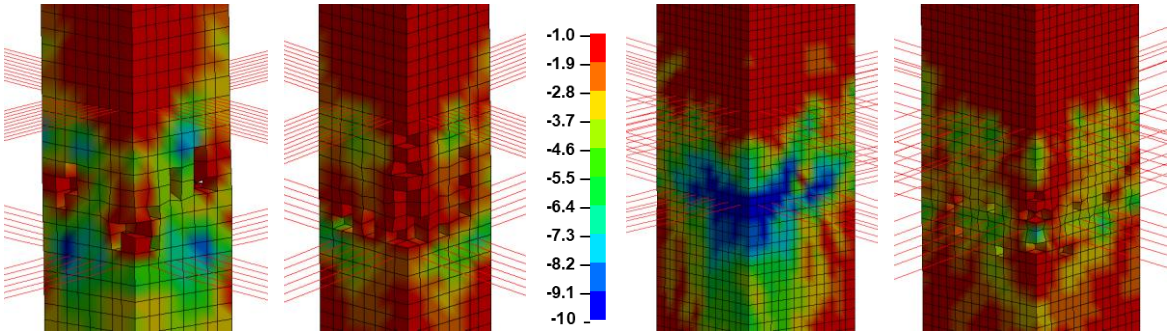

(a) P1.1 **(b) P1.6** **(c) P4.1** **(d) P4.6**

Figure 5-24 Minimum principal stress contour at 6% drift ratio

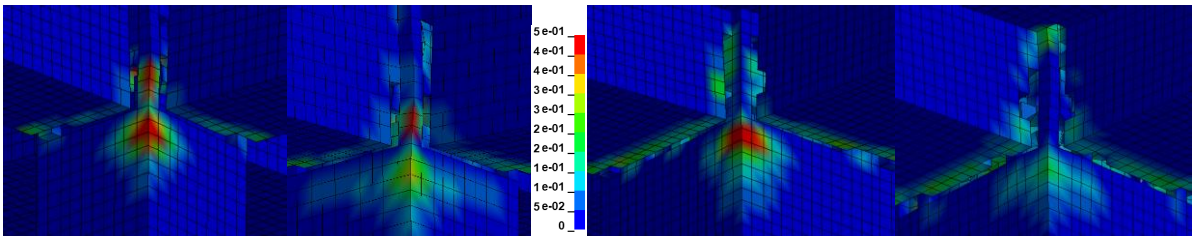

(a) P1.1 **(b) P1.6** **(c) P4.1** **(d) P4.6**

Figure 5-25 Compressive inelasticity parameter of beam at 6% drift ratio

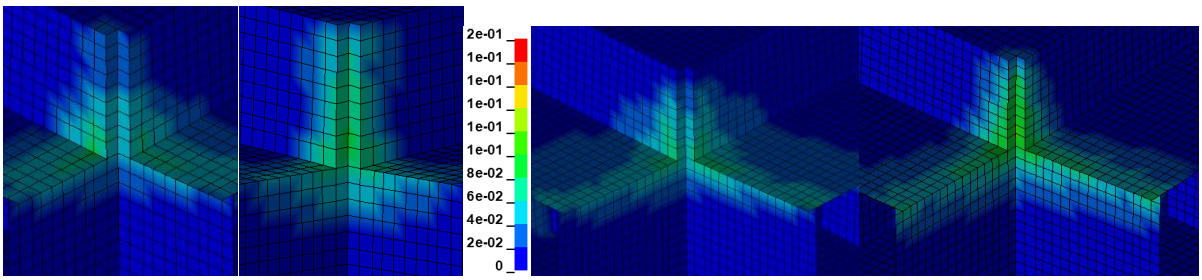

(a) P1.1 **(b) P1.6** **(c) P4.1** **(d) P4.6**

Figure 5-26 Maximum principal strain contour at 6% drift ratio

5.3.2 Behavior under Bidirectional Cyclic Loading

The same cyclic loading curve shown Figure 5-11 is applied at all four beam ends simultaneously for the bidirectional cyclic analysis.

The total moment in East-West direction is calculated by multiplying the moment of East beam by -1 and adding the moment of West beam; a similar procedure is used in the North-South direction. The moment-drift ratio relation shown in Figure 5-12(a)-(b) for connection P1.1 presents satisfactory agreement for monotonic and cyclic analysis loaded unidirectional insofar as the initial stiffness values, the gradual strength increase before reaching the 2% drift ratio, and a strength degradation after that. The bidirectional cyclic analysis result, however, experiences an extensive decline in strength and stiffness starting at the 2% drift ratio (Figure 5-27(a)-(b)). The peak strength from bidirectional cyclic analysis in one direction (13667 k-in) is 12.1% lower than that from unidirectional cyclic analysis (15319 k-in) and 20.4% lower than that from unidirectional monotonic analysis (16453 k-in). Since the curve in South-North direction is very close to that in East-West direction, the curve in one direction only is illustrated in Figure 5-27(a) and also for similar future figures unless otherwise noted. The connection P4.1 experienced similar degradation but relatively later than P1.1. It also shows less degradation in peak strength; the peak strength from bidirectional cyclic analysis in one direction (37784 k-in) is 8.5% lower than that from

unidirectional cyclic analysis (41000 k-in) and 10.5% lower than that from unidirectional monotonic analysis (41737 k-in).

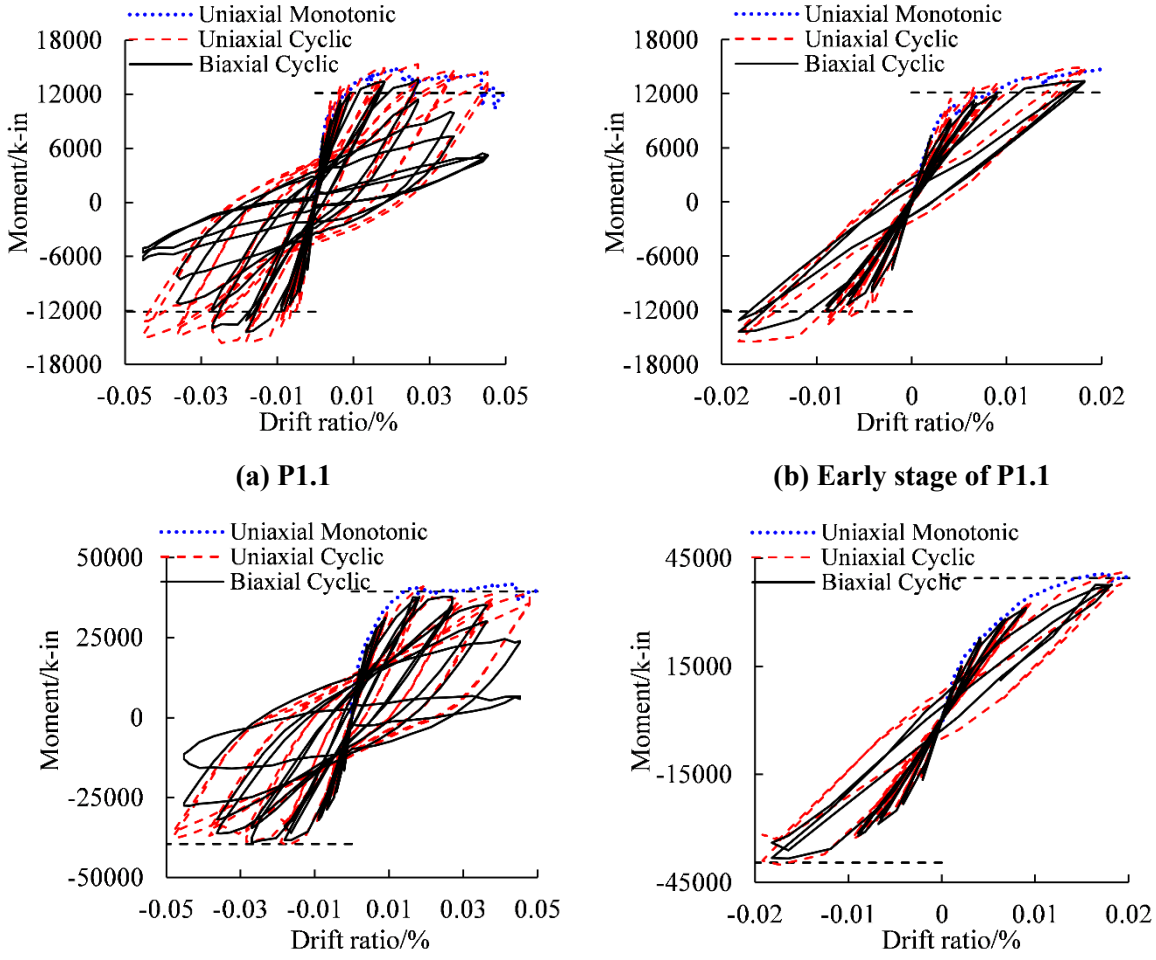

(a) P1.1 **(b) Early stage of P1.1**

(c) P4.1 **(d) Early stage of P4.1**

Figure 5-27 Comparison of unidirectional monotonic and cyclic result for P1.1 and P4.1

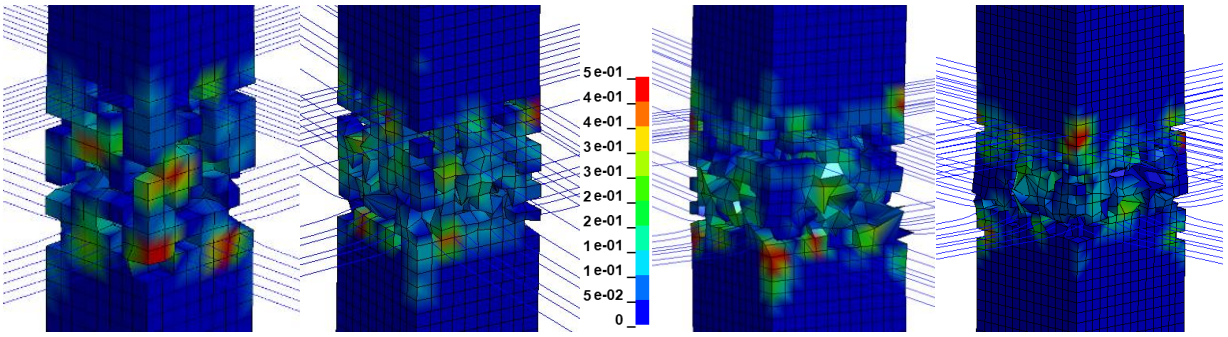

(a) P1.1 **(b) P2.1** **(c) P3.1** **(d) P4.1**

Figure 5-28 Compressive inelasticity parameter of the joint at 5% drift ratio during the last

cycle

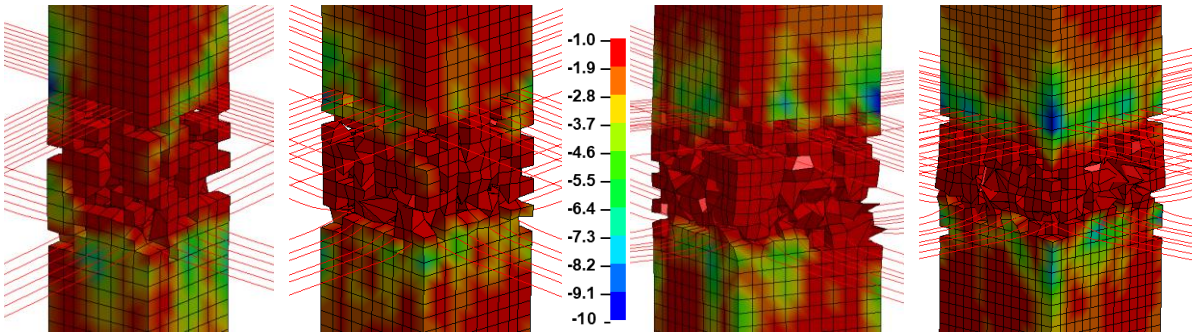

(a) P1.1 (b) P2.1 (c) P3.1 (d) P4.1

Figure 5-29 Minimum principal stress contour at 5% drift ratio during the last cycle

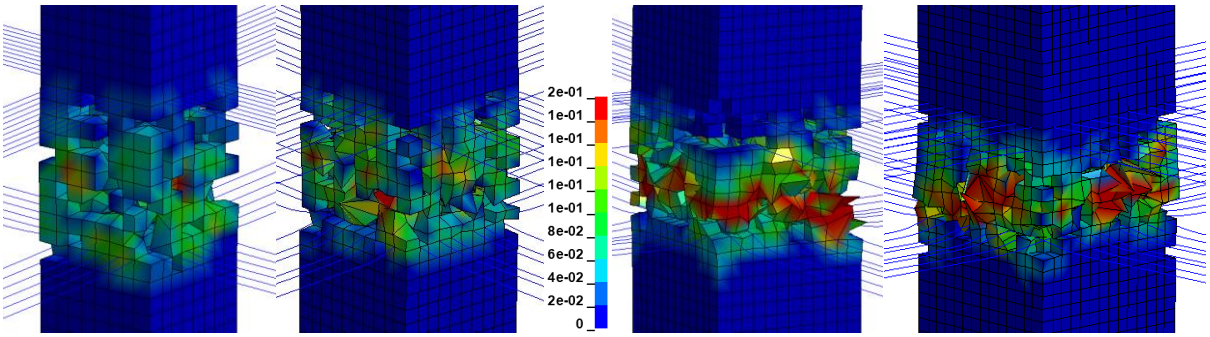

(a) P1.1 (b) P2.1 (c) P3.1 (d) P4.1

Figure 5-30 Maximum principal strain contour at 5% drift ratio during the last cycle

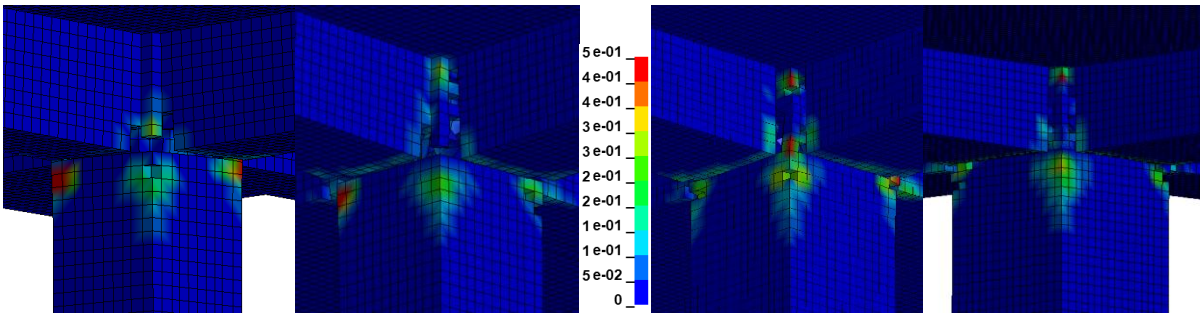

(a) P1.1 (b) P2.1 (c) P3.1 (d) P4.1

Figure 5-31 Compressive inelasticity parameter of the connection at 5% drift ratio during the last cycle

The bond-slip development in Figure 5-32(a-b) demonstrates a much larger value from

bidirectional cyclic analysis than that from unidirectional cyclic analysis. Both bond-slip histories are obtained at the location next to the column face, which is influenced by the damage of beam and joint. Thus the bond-slip value from the later cycles increase in one direction due to the inelastic growth of beam, and becomes unstable in P4.1 due to the severe damage of concrete.

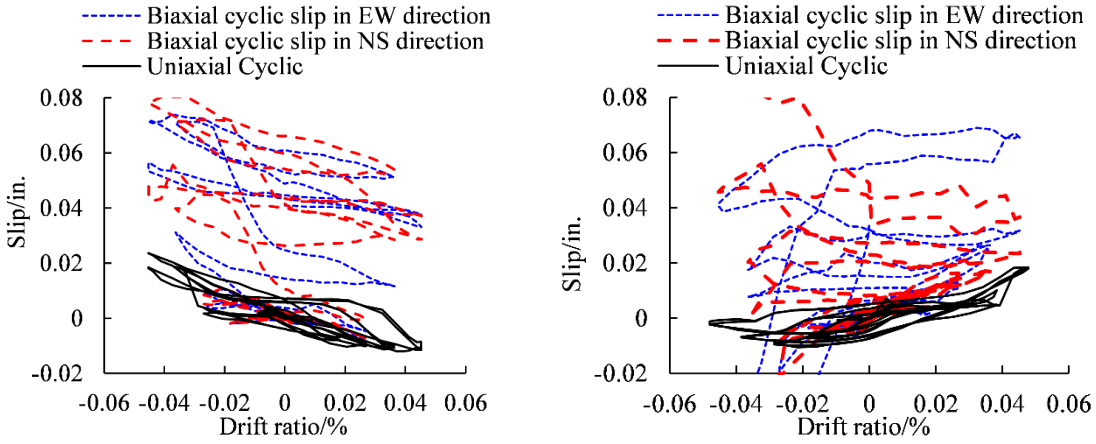

(a) P1.1 **(b) P4.1**

Figure 5-32 Comparison of slip value

It is also worth comparing again to see the impact of shear ratio on the bidirectional cyclic performance. Connections P2.1 and P2.6 with column size of 24 inch are investigated again and compared with unidirectional cyclic performance in Section 5.2.3. However, this time, there is no distinct difference between two connections because they both encounters massive damage inside the joint (Figure 5-33(a-b)). The stress in the confined concrete in the joint goes down to nearly zero (Figure 5-33(c-d)). Both concrete cover and confined concrete at the end of the beams in the two directions are crushed (Figure 5-33(e-f)).

The moment-drift ratio relation in Figure 5-34(a) for two connections follows the same degradation pattern, and result in similar final strength, which is the residual strength of concrete. The comparison of slip measurement exhibits similar magnitude of slip value until the connection

with high shear ratio comes across a surge in slip during the last two cycles.

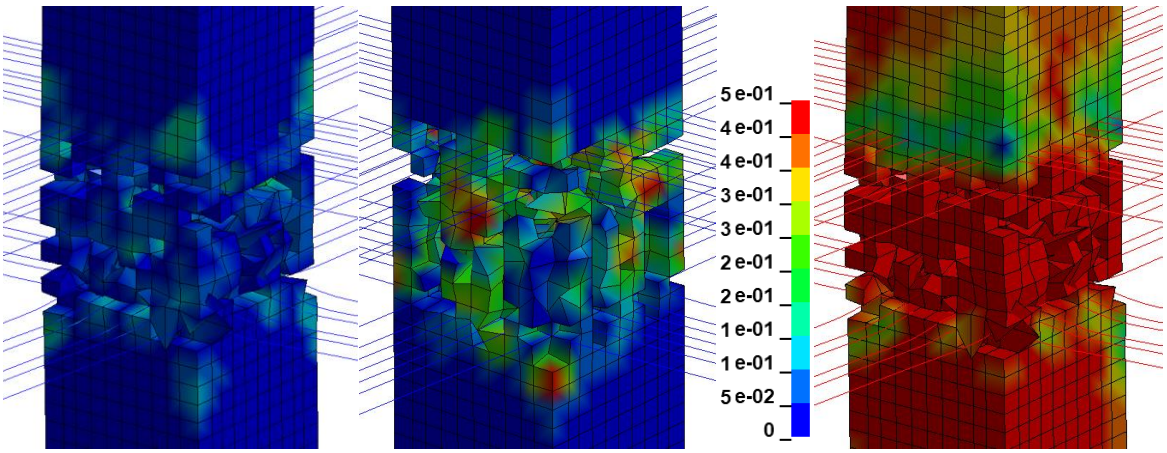

(a) Joint damage of P2.1 **(b) Joint damage of P2.6** **(c) Min. principal stress of P2.1**

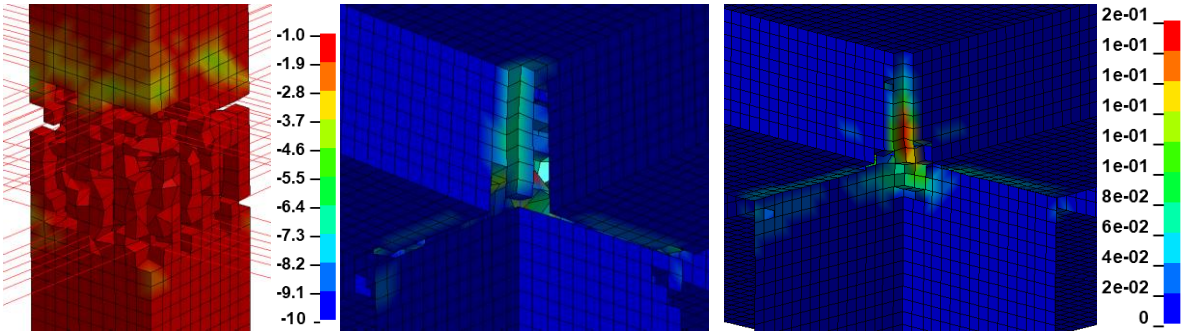

(d) Min principal stress of P2.6 **(e) Max principal stress of P2.1** **(f) Max principal stress of P2.6**

Figure 5-33 Compressive inelasticity parameter at 5% drift ratio during the last cycle

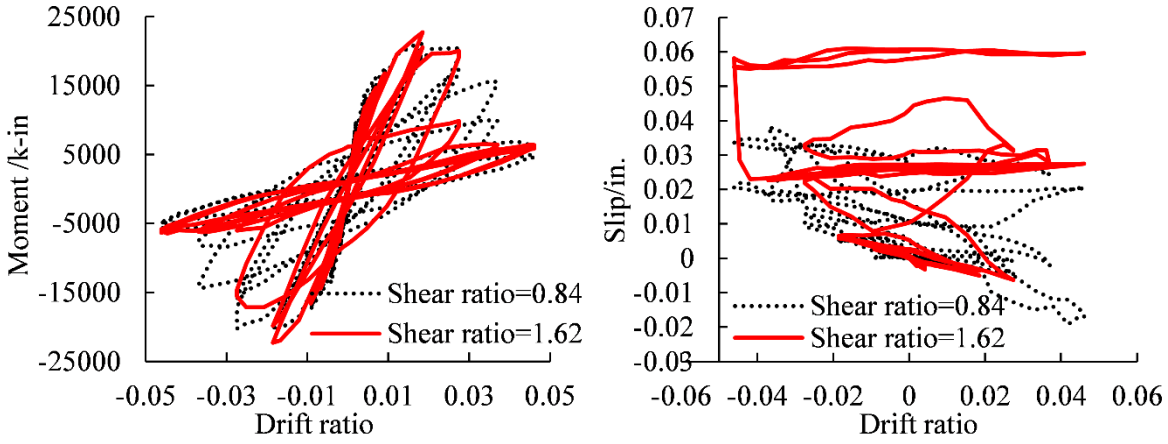

(a) Moment development **(b) Slip measurement**

Figure 5-34 Comparison of P2.1 and P2.6

In summary, the reliability of interior beam-column-connection under bidirectional cyclic loading is no longer guaranteed even when meeting the design criteria from ACI352R-02. This conclusion applies to all the four column sizes analyzed above, increases from 20 inch to 32 inch.

5.3.3 Shear Stress in the Joint

The ratio of shear stress calculated by the loading force at beams ends over the value of $\sqrt{f_c'}$ is summarized for bidirectional monotonic loading, and compared with those from unidirectional loading in Table 5-6. For the bidirectional case, the ratio of analytical results over theoretical results from ACI code in the third column of Table 5-6 decreased by 10%~26% compared with that from unidirectional analysis in Table 5-5. For the connection with the largest column size, the strength from FE model is smaller than that from ACI 352 even with regular design criteria.

Table 5-6 Comparison of joint shear force subjected to bidirectional monotonic loading

	$\frac{M_p+M_n}{d}$ /kips				$\frac{M_p+M_n}{d*A_g}$ /ksi		$\sqrt{f_c'}$ /ksi	$\frac{M_p+M_n}{d*A_g*\sqrt{f_c'}}$	
	Bidirectional	ACI352	ratio	Compare with unidirectional	Bidirectional	ACI352		Unidirectional	ACI352
P1.1	624	506	1.23	-9.9%	1.56	1.27	0.10	15.59	12.66
P1.6	670	777	0.86	-22.2%	1.67	1.94	0.08	21.74	25.22
P2.1	913	840	1.09	-25.8%	1.59	1.46	0.10	15.85	14.58
P2.6	962	1104	0.87	-17.4%	1.67	1.92	0.08	21.68	24.89
P3.1	1225	1209	1.01	-7.8%	1.56	1.54	0.10	15.63	15.42
P3.6	1212	1489	0.81	-14.5%	1.55	1.90	0.08	20.08	24.66
P4.1	1526	1645	0.93	-13.9%	1.49	1.61	0.10	14.90	16.07
P4.6	1448	1915	0.76	-11.7%	1.41	1.87	0.08	18.37	24.29

5.3.4 Bidirectional Behavior of Column Section

The joint damage pattern from the bidirectional analysis in Figure 5-23 indicates that bidirectional loading results in the spalling of corner cover of the joint, and this may in turn accelerate the deterioration of joint strength. It is interesting to see how much influence losing

column cover has on the strength. The connection P1.3 is examined on the shear-drift ratio relation in three cases by a nonlinear beam fiber model: unidirectional monotonic loading with whole section, bidirectional monotonic loading with whole section, bidirectional monotonic loading without column corners in the diagonal direction from the very beginning (Figure 5-35 (b)). Then the results in one direction (need to multiply by √2 to obtain the total biaxial force) are compared with that from FE model (Figure 5-35 (a)). The connection P1.3 (Table 5-3) has a narrow column (20 in.), a slightly high moment ratio (2.30), a low development length (20.00 bar diameters with #8 bars) and a low shear ratio (0.67). This specimen satisfies all ACI352R-02 conditions, and one would expect this specimen to clearly form plastic hinges in the beams and undergo relatively little degradation.

The plot shows a consistency in bidirectional results from nonlinear beam model and FE model (Figure 5-35). Losing the cover accelerates the strength degradation. Results from nonlinear beam shows a slight recovery after the initial strength drop since it's a single element with fixed end. While FE model presents a stair-like drop. The peak strength decreased by 6% from unidirectional (140.83 kips) to bidirectional (94.12*√2=133.09 kips) analysis. It has to be mentioned that the curve from FE model is the reaction force from the top pf the column, and is amplified in abscissa to provide a reference on the peak and ultimate strength the column obtained.

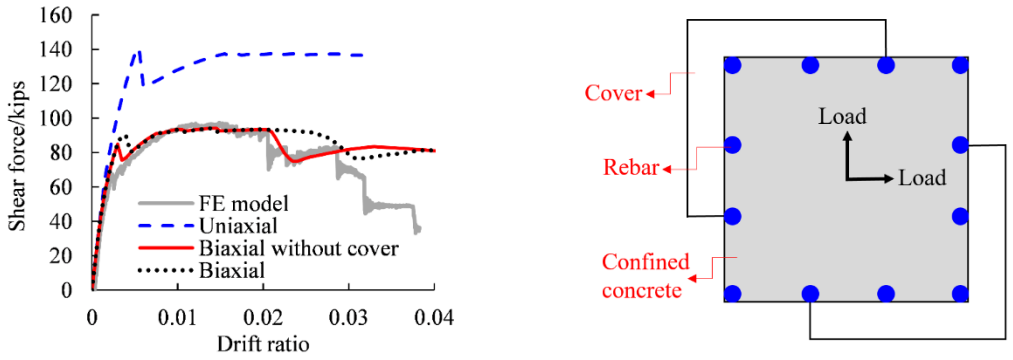

(a) Comparison of shear force **(b) Column section without cover**

Figure 5-35 Influence on losing column cover

5.4 Parametric studies

5.4.1 Physical Parameters

5.4.1.1 Material Property

The four benchmark connections which meets all the requirements from ACI352R-02 and have column size diverse from 20 to 32 inch (P1.1 through P4.1) are analyzed with different material properties, i.e. with concrete compressive stress at 8 ksi (compared with 10 ksi) and yield stress of reinforcing bar at 70 ksi (compared with 60 ksi). The peak strengths of the new connections subjected to unidirectional and bidirectional monotonic loading are summarized in Table 5-7. The moment-drift ratio relations are plotted in Figure 5-36. The peak strength from bidirectional analysis represents for the summation of moment for two beam ends in one direction.

Table 5-7 Peak strengths of connections subjected to unidirectional and bidirectional loading

column size	Unidirectional					Bidirectional				
	benchmark	f_y=70		f'_c=8		benchmark	f_y=70		f'_c=8	
		peak	%	peak	%		peak	%	peak	%
20	16453	17621	7.1%	16540	0.5%	14970	15740	5.1%	14689	-1.9%
24	24003	25559	6.5%	23602	-1.7%	21914	23450	7.0%	21449	-2.1%
28	31719	34354	8.3%	31616	-0.3%	29411	31187	6.0%	28416	-3.4%
32	41737	44665	7.0%	40001	-4.2%	36629	39662	8.3%	36186	-1.2%

The results from bidirectional analysis share the same trend with that from unidirectional analysis. If looking at the peak strength merely (the 28” column size connection for example), promoting the yield strength of reinforcement by 16.7% could bring an 8.3% increment on strength, while reducing the compressive strength of concrete only result in a 0.3% drop in peak strength.

The moment-drift ratio relations provide more apparent discrepancies on the strength development. The red curves come across sudden decreases due to concrete crushing, which indicates that a higher compressive strength of concrete could help with preventing crushing and

improve the ductility of the connection. A lower concrete compressive strength leads to earlier strength deterioration due to concrete crush as indicated by the red lines below.

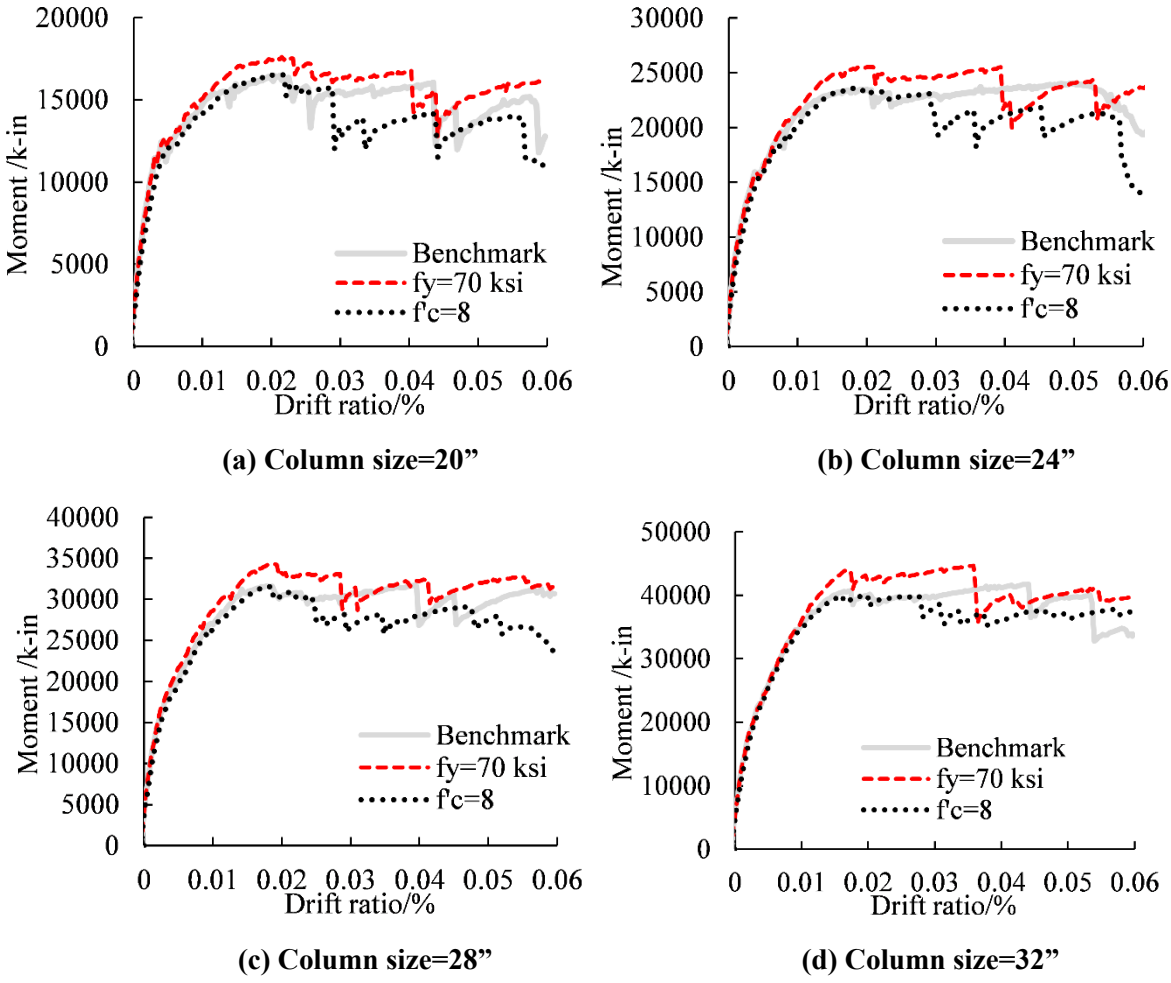

(a) Column size=20” **(b) Column size=24”**

(c) Column size=28” **(d) Column size=32”**

Figure 5-36 Moment-drift ratio relations for connections subjected to unidirectional monotonic loading

5.4.1.2 Influence of Development Ratio

The two connections P2.2 and P 2.3 are investigated in this section. P2.2 (Table 5-3) has a moderate column size (24 in.), a high moment ratio (2.19), high development length (32.00 bar diameters with #6 bars) and an intermediate shear ratio (0.74); P2.3 (Table 5-3) has the same column size (24 in.), an acceptable slightly lower moment ratio (2.03), low development length

(21.28 bar diameters with #9 bars) and a similar shear ratio (0.80). These two connections satisfy all ACI352R-02 conditions, and are expected to clearly form plastic hinges in the beams and undergo relatively little degradation. This expectation is validated by the normalized moment-drift ratio relations under unidirectional monotonic loading plotted in Figure 5-37(a)-(b). It can be observed from Figure 5-37 that, a small DR may result in a sudden huge slip (Figure 5-37(c)) which leads to an immediate strength degradation (Figure 5-37(b)) even though the connection meets all other design requirements. The huge bond-slip behavior happens within half cycle and is hard to predict since there is no apparent large strength degradation among previous cycles. This behavior, draws attention to the importance of sufficient development length of beam reinforcement through the joint.

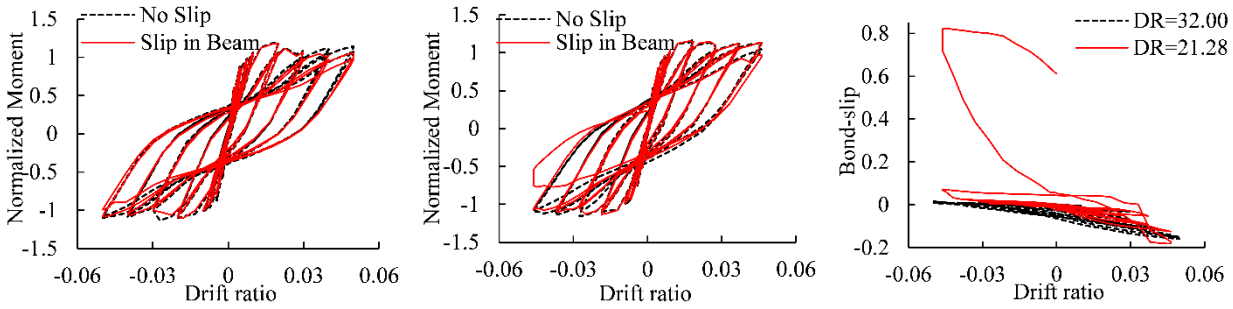

(a) P2.2 with DR=32.00 **(b) P2.3 with DR=21.28** **(c) Bond-slip development**

Figure 5-37 Influence of Development length ratio

5.4.1.3 Axial Force of Column

There is no solid agreement on the impact of column axial force on the behavior of interior BC joints (Bonacci and Pantazopoulou 1993; Kitayama et al. 1991). In this section, various levels of column axial stress are placed on the column top to investigate their influence on the prototype connection. The connection P2.1 which meets all ACI352R-02 requirements is used herein subjected to unidirectional monotonic loading. This connection has a common column size (24

in.), an adequate moment ratio (1.95), an intermediate development length (24.00 bar diameters with #8 bars) and a moderate shear ratio (0.84).

The nominal axial strength of the column section P_0 is calculated as: $0.85*f'_c*(A_g-A_s)+f_y*A_s=0.85*10*(24*24-12*1)+60*12*1=5514$ kips. The maximum allowable design strength $P_{umax}=\varphi P_n=0.65*0.8*P_0=2867.3$ kips, where $\varphi=0.65$ (ACI 318-14 Table 21.2.2).

Table 5-8 summarizes the comparison of analytical results based on FE analysis and theoretical results based on ACI code for column P2.1. The first column labelled "No." refers to seven cases with different axial forces, corresponding to their analytical results illustrated in Figure 5-38(b); the second column labelled "Axial Force" is the total axial force applied on the top of the column for each case; the third and fourth column gives the ratio of axial force over P_0 and P_{umax} to give a better understanding on how large the axial force is compared with values suggested by ACI code; the fifth column is the theoretical M_n value of column P2.1 from the P-M interaction diagram in Figure 5-38(a); the sixth column is φ calculated based on Table 21.2.2 in ACI 318-14 and the seventh column gives the value of φM_n ; the eighth column labelled "Analytical Peak M_n from Column End" represents the analytical horizontal response at column top multiplied by the height from column top to the surface of slab, which is the moment subjected to the column right above the joint; the ninth column labelled "Analytical-Theoretical ratio" gives the ratio of eighth column over φM_n, which provides information on the comparison of analytical and theoretical results. On this final column, anything above one means that the analytical result exceeded the nominal ACI capacity. The comparison of analytical and theoretical results for the beams in connection P2.1 is tabulated in Table 5-9, where the third column gives theoretical flexural capacity of beam, which is calculated by the summation of positive and negative moment divided by two; the "Analytical Peak M_n from Beam End" from the fourth column is obtained by dividing

the summation of moment at two beam ends from the analyses by two; and the fifth column gives the ratio of fourth column over third column.

Table 5-8 Comparison of analytical and theoretical results for column P2.1

No.	Axial Force	Ratio over P_0	Ratio over P_{umax}	Theoretical M_n for column from P-M diagram	φ	φM_n	Analytical Peak M_n from Column End	Analytical-Theoretical ratio for M_n of column
1	0.0	0.00	0.00	7446.4	0.90	6701.7	8565.9	1.28
2	1102.7	0.20	0.38	15685.6	0.80	12547.5	10578.0	0.84
3	1433.7	0.26	0.50	16965.3	0.70	11893.0	10365.1	0.87
4	2007.1	0.36	0.70	17710.2	0.65	11511.6	10808.7	0.94
5	2867.3	0.52	1.00	17046.1	0.65	11079.9	10928.9	0.99
6	3010.7	0.55	1.05	16771.2	0.65	10901.2	10974.1	1.01
7	3154.0	0.57	1.10	16437.1	0.65	10684.1	10314.3	0.97

Table 5-9 Comparison of analytical and theoretical results for beam P2.1

No.	Axial Force	Theoretical M_n from ACI code	Analytical Peak M_n from Beam End	Analytical-Theoretical ratio for beam
1	0.0	10078.1	9790.8	0.97
2	1102.7	10078.1	12008.9	1.19
3	1433.7	10078.1	11769.6	1.17
4	2007.1	10078.1	12305.8	1.22
5	2867.3	10078.1	12447.8	1.24
6	3010.7	10078.1	12432.2	1.23
7	3154.0	10078.1	11716.4	1.16

The comparisons in Table 5-8 and Table 5-9 give an idea on how beam and column behave in a joint compared with their theoretical capacity. It has to be pointed out that the theoretical result comes from pure bending of the column sections, while the analytical results are obtained from the moment applied on the column section which belongs to a joint. A column from a joint is subjected to flexural-shear-bond interacted forces, and thus its comparison with pure flexural theoretical results provide comparisons to behavior under more complicated and realistic situations.

From cases 2 to 6 in Table 5-8 and Table 5-9 analytical outputs for column are about 0.93 times the theoretical calculations while the column did not fail. The beam on the other hand, has around 1.21 times the analytical over theoretical results, indicating that for this specific connection, the strength degradation is triggered by the failure of beam (the sudden strength drops in Figure 5-38(b) are due to concrete crushing at beam ends), and the beam in the analysis have enough capacity compared with that from ACI code.

In case 1, the nominal flexural moment of column can reach 1.28 times larger than that of theoretical results under a zero axial force situation, indicating the ACI code is conservative under low axial forces. A large amount of longitudinal reinforcing bar in the column is yielding due to huge flexural deformation compared with that in case 2 (Figure 5-39(a)-(b)). The beam loading upwards cannot develop its full force and thus results in a lower strength in the column, beam and joint, which is also consistent with the trend in the theoretical results. In case 7, the connection failed due to concrete crushing at the column bottom (Figure 5-39(c)). The theoretical result underestimates 3% the strength compared with analytical result. But considering the axial force reaches as large as 1.1 P_{umax}, the ACI code is still conservative in this situation.

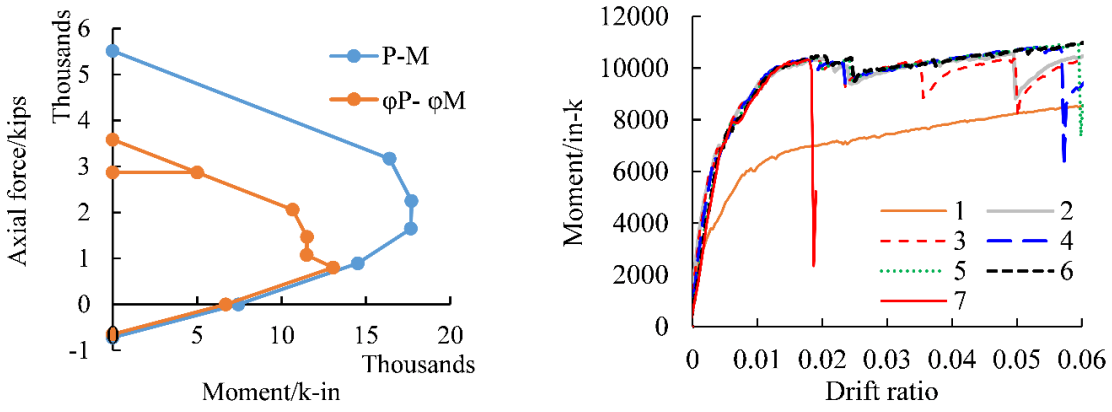

(a) P-M interaction diagram of column P2.1 **(b) Moments of column v.s. drift ratio**

Figure 5-38 Theoretical and analytical results for cases with different axial loads

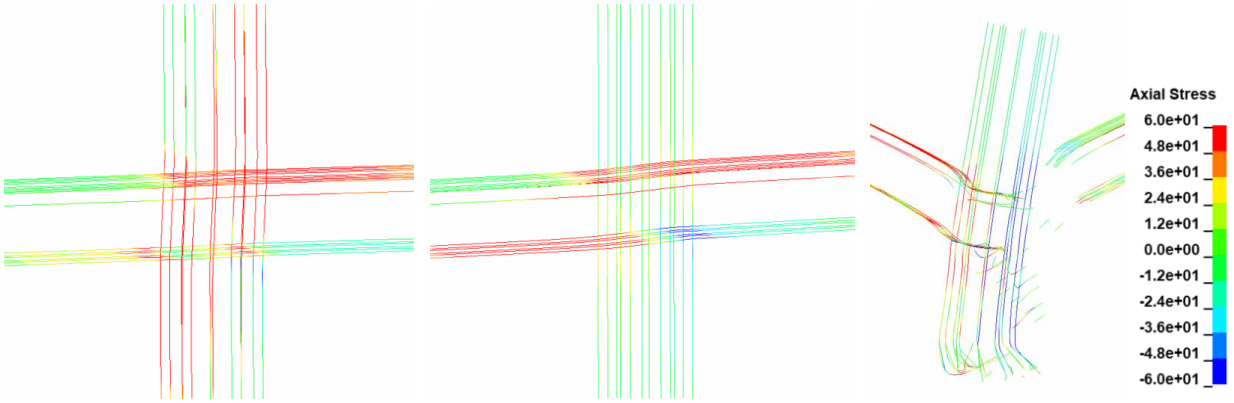

(a) Case 1 at 6% drift ratio **(b) Case 2 at 6% drift ratio** **(c) Crushed column bottom of Case 7 at 2% drift ratio**

Figure 5-39 Stress contour in reinforcing bar

Note that the column for P2.1, as shown in Figure 5-38(a) shows a very large decrease in flexural strength from the balance point to the pure flexural case (by more than a factor of two); this is due primarily to the use of high strength concrete.

In summary, this specific connection fails due to excessive flexural deformation in the column when axial force on the column top is smaller than 0.38 P_{umax}, and the ACI code is conservative enough when considering the flexural strength of column (28% larger); the connection fails due to large flexural behavior in the beam when the axial force falls between 0.38 P_{umax} and 1.05P_{umax}. The ACI code gives a 21% more conservative value on the flexural strength of beam; the connection fails due to irreversible compressive deformation at the column foot when axial force equals to 1.10P_{umax}, and the ACI code underestimate 3% the flexural strength of column based on the analytical result.

5.4.2 Model Parameters

As with any analytical model, there are a number of parameters that are selectable by the user and which may influence the results. In this section, the effect of varying several of those

parameters is investigated. These parametric studies were carried out to validate the choices used in the analyses described in this chapter.

5.4.2.1 Ductility Factor *d*

Increasing the ductility factor *d* will enhance the ductility of the material due to the confinement effect (Moharrami 2016). The impact of the ductility factor has been investigated in Section 3.4.2.1 on interior BCJs, and now will be further studied on the prototype connection by looking at connection P2.6 which failed in excessive shear behavior in the joint. Two cases are compared, with the value of parameter *d* set to f'_c and $0.5f'_c$ for the confined concrete in the column.

The difference in the moment-drift ratio curves in Figure 5-40 indicates that increasing *d* of confined concrete in the column can increase slightly post-peak strength in both positive and negative moment. The compressive inelasticity parameter contour of connection P2.6 with different values of *d* under unidirectional and bidirectional loading in Figure 5-41 further explains that larger *d* improves the ductility of the column and contributes to less damage in the joint, especially for the unidirectional loading cases.

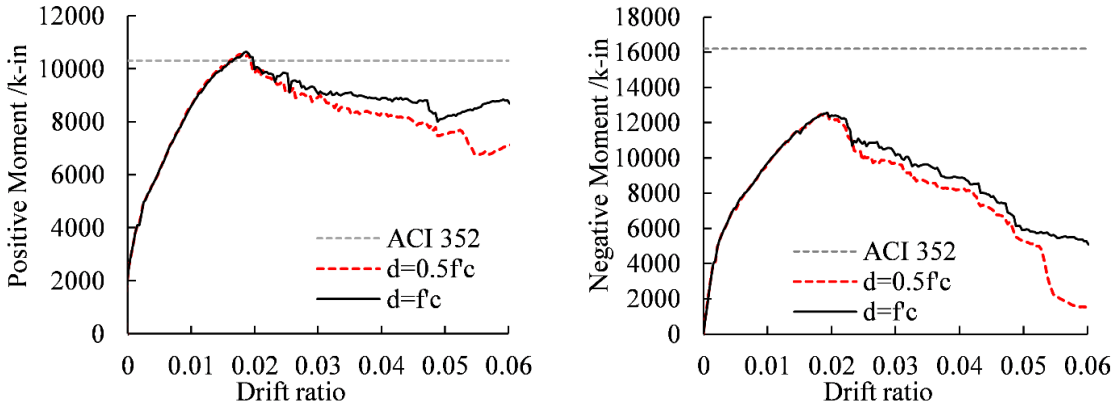

(a) Positive moment **(b) Negative moment**

Figure 5-40 Influence of *d* on moment

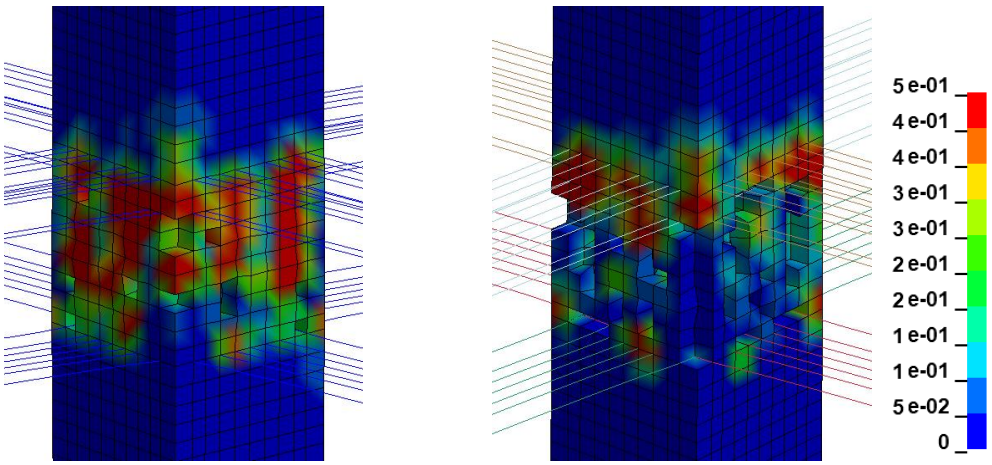

(a) *d*= f'c (P2.6 Unidirectional load) **(b) *d*=0.5 f'c (P2.6 Unidirectional load)**

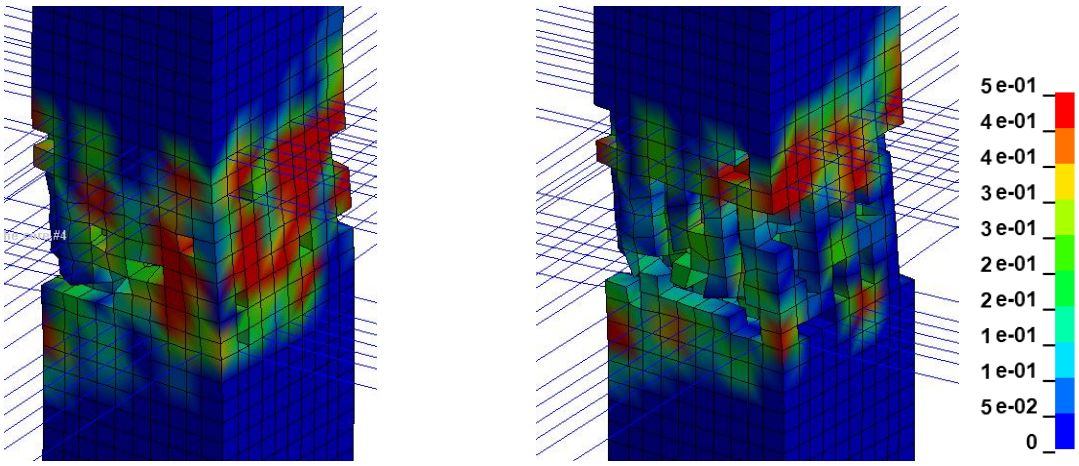

(c) *d*= *f'c* (P2.6 Bidirectional load) **(d) *d*=0.5 *f'c* (P2.6 Bidirectional load)**

Figure 5-41 Damage contours for confined concrete in the joint with different values of *d*

5.4.2.2 Peak Value of Hardening Variable K

The peak value of hardening variable K is a user input variable indicated as the peak value of abscissa of Figure 3-2(a). When the inelastic cumulative deformation of the compressive concrete κ reaches the value of K, the concrete element will be removed. The connection P2.1 is analyzed here with different values of K subjected to various loading scenarios to investigate the influence of this parameter.

The connection P2.1 meets all ACI352R-02 requirements and has a common column size (24

in.), an adequate moment ratio (1.95), an intermediate development length (24.00 bar diameters with #8 bars) and a moderate shear ratio (0.84), which is expected to form plastic hinge in the beam and encounters little strength degradation.

The normalized moment-drift ratio relations are plotted in Figure 5-42 for connection P2.1 with different values of K for the column under various loading scenarios, where the normalized moment is calculated by adding analytical moment outputs from two beam ends and divided by the theoretical value calculated based on ACI 352. Thus values larger than 1.0 is not recommended by ACI 352. The contour plot of parameter κ for confined column is illustrated in Figure 5-43.

Since the value of K only influences when to delete the element after it reaches residual compressive stress (Figure 3-2(a)), the cases with K=1 and K=10 for the column under unidirectional monotonic loading shows no difference on global response (Figure 5-42(a)) or damage state of column (Figure 5-43(a)-(b)) because the elements in the confined column have not reached residual compressive stress yet. The connection with K=10 encounters more damage after 5.3% drift ratio when subjected to bidirectional monotonic loading, thus the global response experiences a drop at 5.3% drift ratio and then recovers almost to the same level compared with that of K=1 (Figure 5-42(b)). The removed elements and difference in damage pattern are clearly illustrated in Figure 5-43(c)-(d). When loaded with bidirectional cyclic loading simultaneously at four beam ends, the global curve with K=10 remains the same with the curve for K=1 before the first cycle at 4% drift ratio, and encounters more severe degradation afterwards. The difference on strength is mainly due to the residual compressive strength of elements being deleted. The performance of bidirectional cyclic loading does not improve significantly with larger values of K.

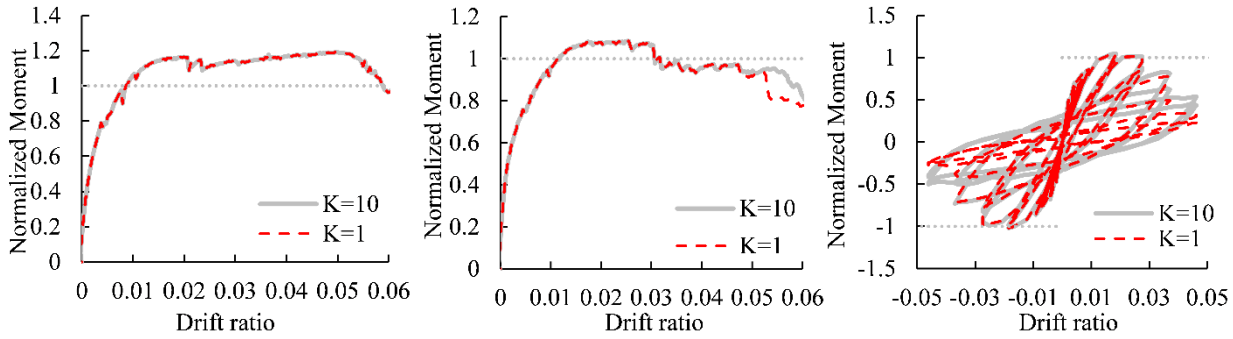

(a) Unidirectional monotonic **(b) Bidirectional monotonic** **(c) Bidirectional cyclic**

Figure 5-42 Comparison of different K value on P2.1 with different loading types

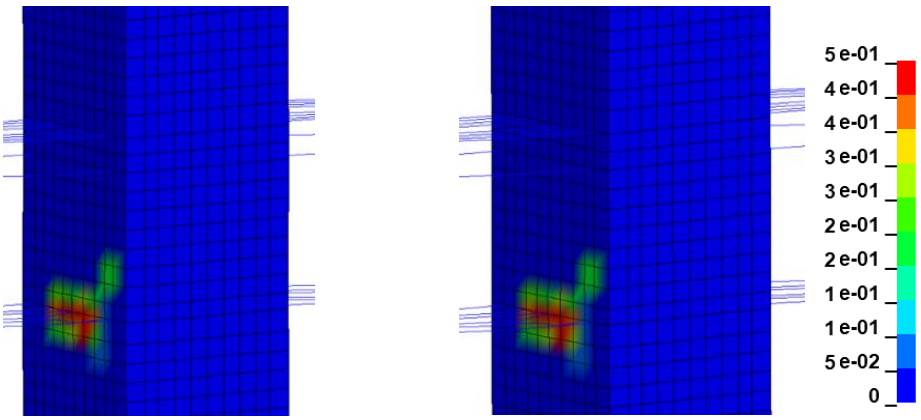

(a) K=1 Unidirectional Mono. at 5% drift ratio **(b) K=10 Unidirectional Mono. at 5% drift ratio**

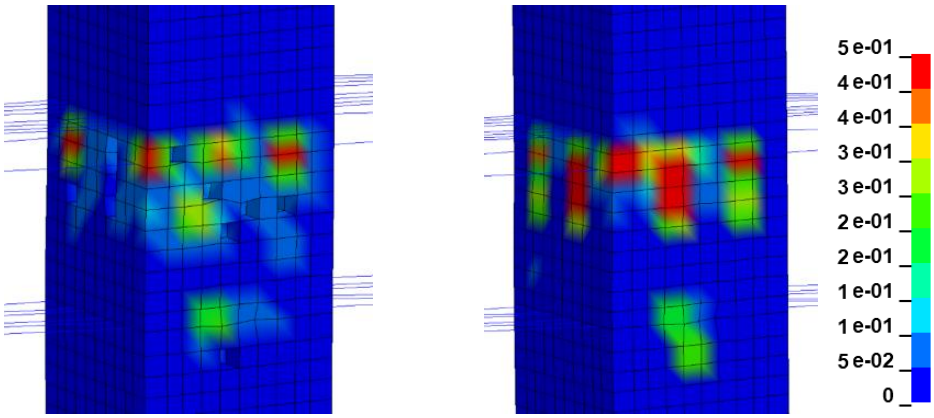

(c) K=1 Bidirectional Mono. at 5% drift ratio **(d) K=10 Bidirectional Mono. at 5% drift ratio**

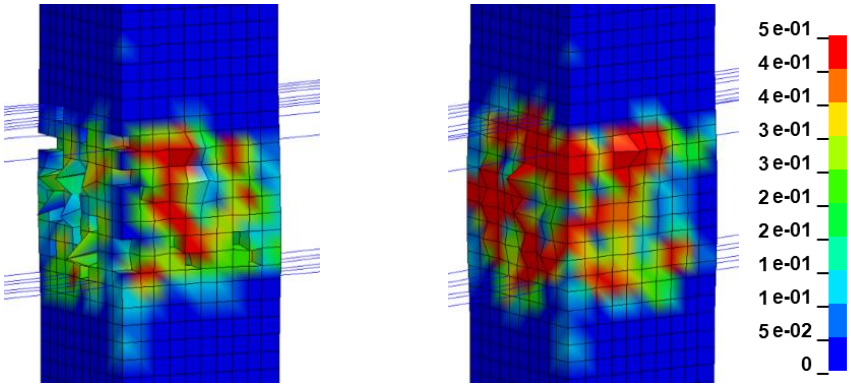

(e) K=1 Bidirectional Cyclic at 4% drift ratio **(f) K=10 Bidirectional Cyclic at 4% drift ratio**

Figure 5-43 Comparison of compressive inelasticity parameter with different K values and loading types

5.4.2.3 Mesh Size

A parametric study on mesh size is launched again on the connection P2.1 subjected to unidirectional monotonic loading to assess the sensitivity of results to mesh size and type. The three refined cases and the original mesh pattern are shown in Figure 5-44. The comparison of positive and negative moment in Figure 5-45 is based on a local refinement, i.e., refined concrete cover on the bottom of the beam and refined slab concrete.

It is clear from the comparison curves in Figure 5-45, especially the negative moment curves, that the more refined mesh tends to reach higher strength and larger ductility later. However, the error between each case is negligible for the most of the load history.

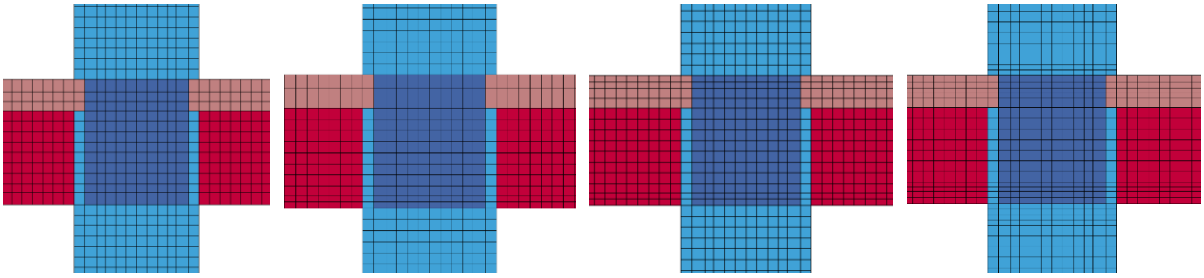

(a) Before refine **(b) Refined bottom** **(c) Refined bottom and slab** **(d) Most refined**

Figure 5-44 Refinement patterns

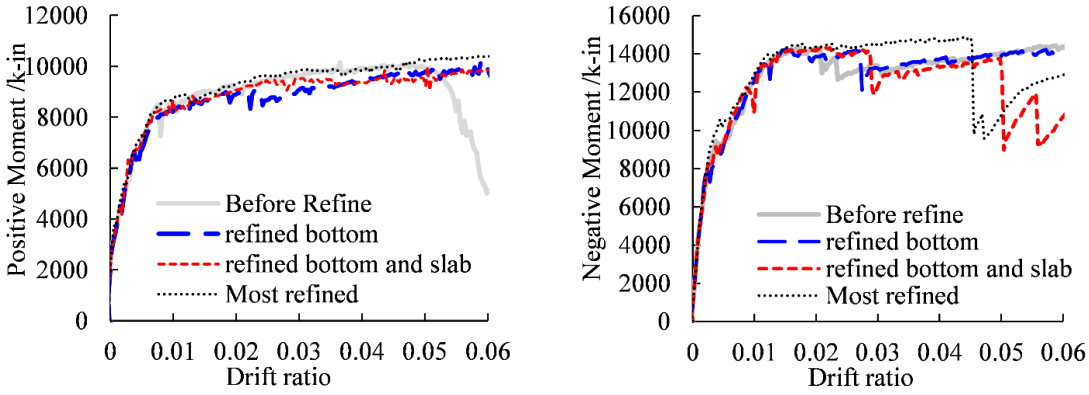

(a) Positive moment **(b) Negative moment**

Figure 5-45 Comparison with different element size

5.5 Influence of Bond-slip Effect

It is recommended by ACI352R-02 that a 28-bar-diameter length be used to maintain bond integrity under cyclic deformations; ideally, this implies that the joint will exhibit little or no bond degradation under cyclic loads. The reliability of the development length in this case will be examined subjected to a low-frequency large-displacement cyclic load.

Connections P2.1 and P2.6 with anchorage ratios equal to 24.00 and 21.28 respectively are analyzed in three situations: with no bond-slip effect, only with bond-slip effect in beam longitudinal reinforcing bars, with bond-slip effect in both beam and column longitudinal reinforcing bars. Connections are loaded with bidirectional cyclic loading, and the results are illustrated in Figure 5-46. The influence of bond-slip effect is not as dramatic as the one-way joint in Section 3.2.7 and two-way joints in Section 3.6.5; the reasons is that both P2.1 and P2.6 lose strength so quickly due to concrete crushing that no significant bond-slip behavior is triggered. The damage contours in Figure 5-47 for different connections provide evidence on how joint damage has an impact on the effect of bond-slip behavior.

The beam stress history of the element next to beam-column interface from connections P2.6

and J2 (Kurose et al., 1988) are compared in Figure 5-48. This figure shows that the element from J2 yields much more than that from P2.6. The two horizontal lines represents their yield stress, respectively. One interesting finding from Figure 5-46 is that adding bond-slip effect in column brings larger impact than adding that in beams. This is worth looking into for future research.

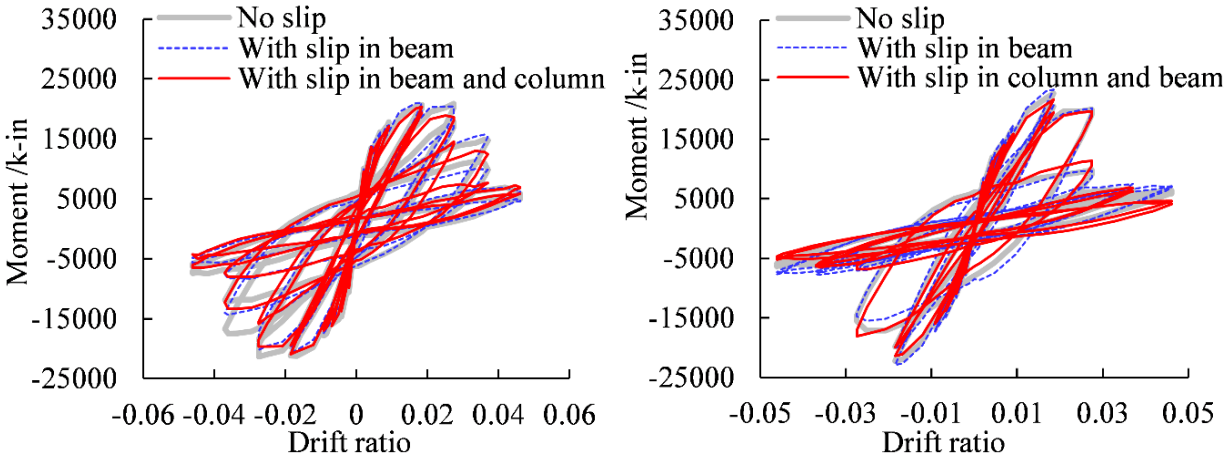

(a) Anchorage ratio=24.00 **(b) Anchorage ratio=21.28**

Figure 5-46 Influence of including bond-slip behavior

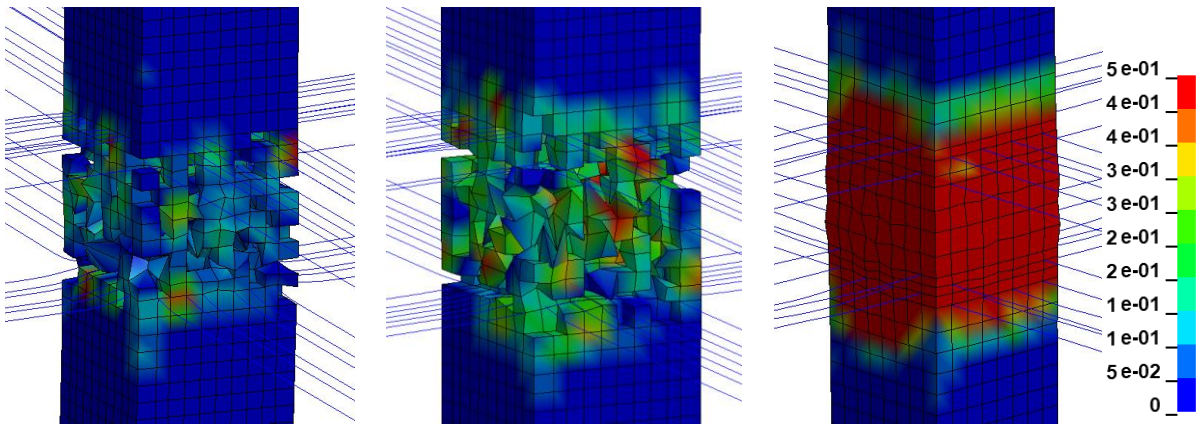

(a) P2.1 **(b) P2.6** **(c) Connection from Kurose 1988**

Figure 5-47 Compressive inelasticity parameter of different joints

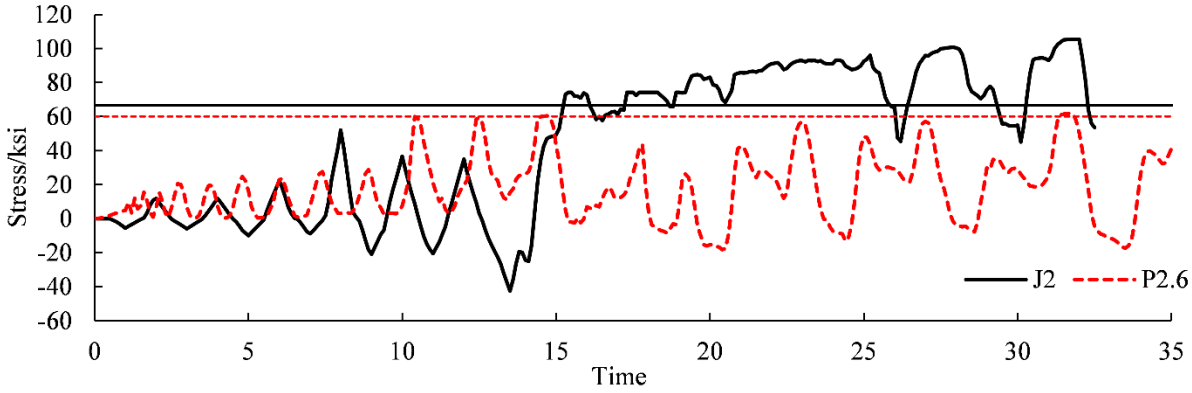

Figure 5-48 Stress history of beam element where significant bond-slip effect occurs

5.6 Relation between Local and Global Performance

Finding the relation between local and global performance provides a way for calibrating responses on both scales and explain the behavior that can only be verified by combining results on both scales. Two pairs of connections are chosen to study the relations between local and global responses: one pair with distinct DR values to investigate the relationship between bond-slip behavior and global shear force; another pair with dissimilar SR values to explore the relation between joint shear distortion and global shear force.

5.6.1 Bond-slip Behavior and Joint Shear Force

The connections P1.3 and P3.2 are compared in Figure 5-49(a) due to their distinguished development ratio (DR for short) and similar moment/shear ratio. P1.3 (Table 5-3) has a narrow column size (20 in.), a high moment ratio (2.30), a low development length (20.00 bar diameters with #8 bars) and a moderate shear ratio (0.67). P3.2 (Table 5-3) has a wider column (28 in.), a similar moment ratio (2.04), an adequate development length (32.00 bar diameters with #7 bars) and a moderate shear ratio (0.85). Both specimens satisfy all ACI352R-02 conditions, and one

would expect these specimens to clearly form plastic hinges in the beams and undergo relatively little degradation.

The curves indicate that a low anchorage ratio results in large bond-slip values (grey and black curves in Figure 5-49(a)) and a more dramatic strength drop from unidirectional to bidirectional loading (grey and black curves in Figure 5-49(b)) even for a connection that meets all ACI352R-02 conditions. Poor bond-slip performance leads to strength loss for P1.3 in the bidirectional analysis (black curves in Figure 5-49(b)).

For the connection with low DR value (P1.3 with DR=20.00), the global curve cannot provide enough information on the reason for strength degradation, especially for the bidirectional case. The local performance curve (Figure 5-49(c)), with the large increase in slip, provides the additional needed evidence. This is an example that how local bond-slip response plays a significant role in explaining the global performance when the bond-slip effect is extensive. For the connection with high DR value (P2.3 with DR=32.00), the bidirectional loading does not accelerate the bond-slip behavior. Other local responses are needed to explain the lowered strength compared with unidirectional loading case, i.e., the concrete crushing in compressive regions of the beam and the stress history of the beam reinforcing bar.

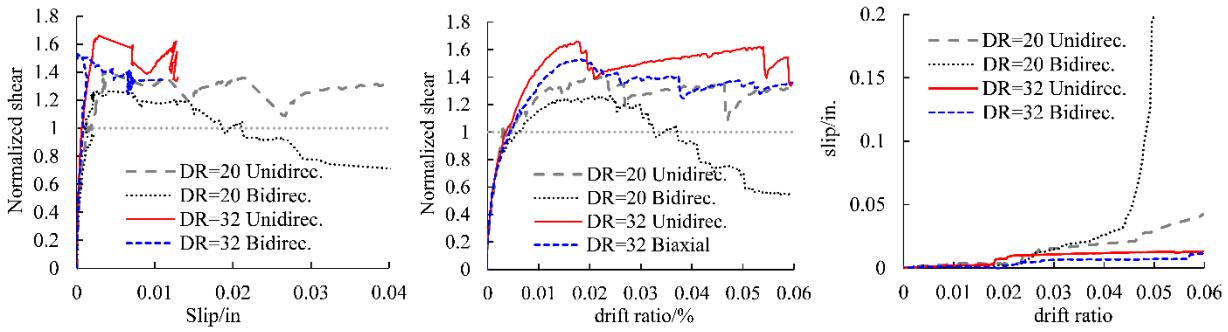

(a) Local performance **(b) Global performance** **(c) Bond-slip development**

Figure 5-49 Influence of development length ratio on local bond-slip and global response

5.6.2 Shear Behavior and Joint Shear Force

Connections P1.2 and P1.6 are compared in Figure 5-50 due to their different DR and SR. Connection P1.2 (Table 5-3) has a narrow column size (20 in.), a high moment ratio (2.44), a long development length (32.00 bar diameters with #5 bars) and a moderate shear ratio (0.63). This specimen satisfies all ACI352R-02 conditions, and one would expect this specimen to clearly form plastic hinges in the beams and undergo relatively little degradation. P1.6 (Table 5-3) has the same column size (20 in.), a similar moment ratio (2.29), a low development length (20.00 bar diameters with #8 bars) and an unacceptable shear ratio (1.62). This specimen has two times the shear ratio that has been suggested by ACI352R-02 which foresees this specimen to encounter joint shear failure.

The joint shear strain is measured in the same way as introduced in Section 3.2.6. The plots in Figure 5-50 demonstrates another example that how global response is validated and explained by local response. Connections P1.2 encounters slightly lower joint shear distortion and bond-slip behavior from unidirectional to bidirectional loading, while the strength is smaller for the latter case (Figure 5-50(a)(c)(d)) because: 1) the joint shear distortion is measured along the beam centerline, and is smaller than the actual diagonal value when subjected to bidirectional loading; 2) the column encounters more damage under bidirectional loading and failes to further maintain the strength.

The situation is more complicated for connection P1.6. The global response indicates severe strength degradation for both unidirectional and bidirectional cases, with the latter one both reaching a smaller peak value and decreasing more slowly in the post-peak region. The bidirectional case comes across considerably larger joint shear strain (Figure 5-50(a)(b)) and significantly lower bond-slip behavior compared with unidirectional case (Figure 5-50(a)(d)). The

local responses indicate that for this specific connection with both disadvantageous DR and SR values, the major reason for strength degradation is the much larger joint shear distortion under bidirectional loading and extensive bond-slip behavior under unidirectional loading. One interesting finding from the global response (Figure 5-50(a)) is that the red dashed line for unidirectional case is more ductile than the solid curve for bidirectional analysis. This implies that joint shear behavior may bring lower peak strength compared with massive bond-slip behavior while the slip may lead to a sudden strength lose and a more brittle system.

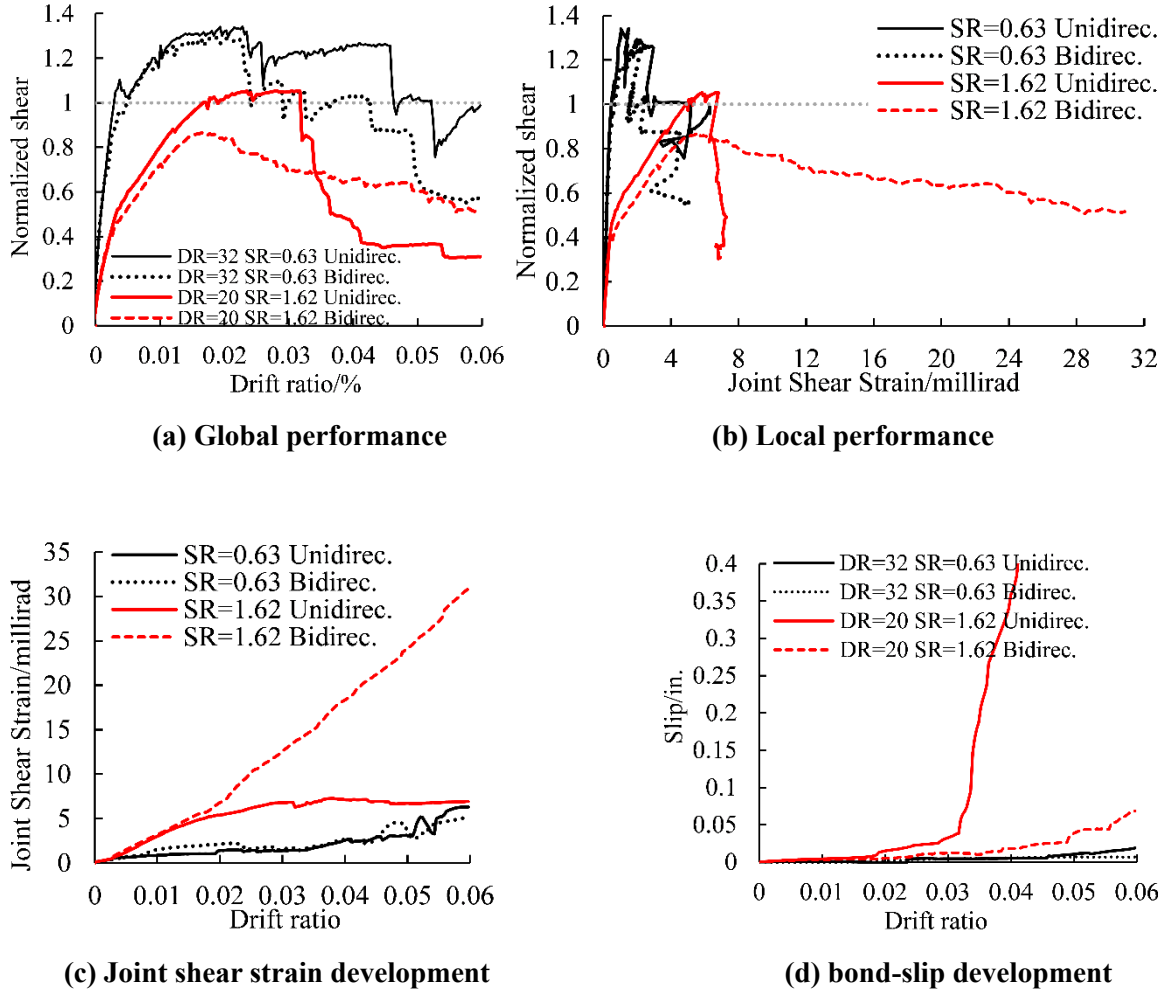

(a) Global performance **(b) Local performance**

(c) Joint shear strain development **(d) bond-slip development**

Figure 5-50 Influence of shear ratio on joint shear strain and global response

5.7 Reinforcing Bar Stress Distribution around Plastic Hinge

The stresses in reinforcing bars in a typical experiment are measured at a few discrete locations with strain gages, while the real distribution is a continuous stress field. It is interesting to evaluate from the analytical result how the average stress compares with the localized stress values.

The connection P2.2 is explored again with unidirectional cyclic loading. The connection P2.2 (Table 5-3) has a common column size (24 in.), a moderate high moment ratio (2.19), a high development length (32.00 bar diameters with #6 bars) and a relatively low shear ratio (0.74). This specimen satisfies all ACI352R-02 conditions. With high MR/DR and low SR, one would expect this specimen to clearly form plastic hinges in the beam regions.

The cumulative plastic strain along the longitudinal beam reinforcement is plotted to identify the location of plastic hinge. The numbering of elements along the top beam longitudinal bar is shown in Figure 5-51(a), which spreads symmetrically about the centerline of the column with positive numbers in one side starts and negative numbers on the other side. The location of the two column faces coincides with numbers -6 and 6, respectively. The plastic strain distribution from element number -18 to 18 at different drift levels is plotted in Figure 5-51(b), which shows gradual increment of plastic strain accumulation with increasing cycles and specifies the location of plastic hinge region about 22 in. away from the column face.

The plotting of strain and stress distribution along the longitudinal beam bar gives more clues on the development of plastic hinge region. With more inelastic strain accumulated around element number 11 in the longitudinal reinforcement, the reinforcing bar around that region has already yielded in compression (dashed lines in Figure 5-52(a) and (b)). When loaded reversely, the strain in that region is much lower than adjacent elements. Thus, a strain gage larger than a certain size

may not be accurate enough to capture the extensive strain difference along the reinforcing bar. It has to be mentioned more smooth strain/stress distributions can be obtained a with more refined mesh.

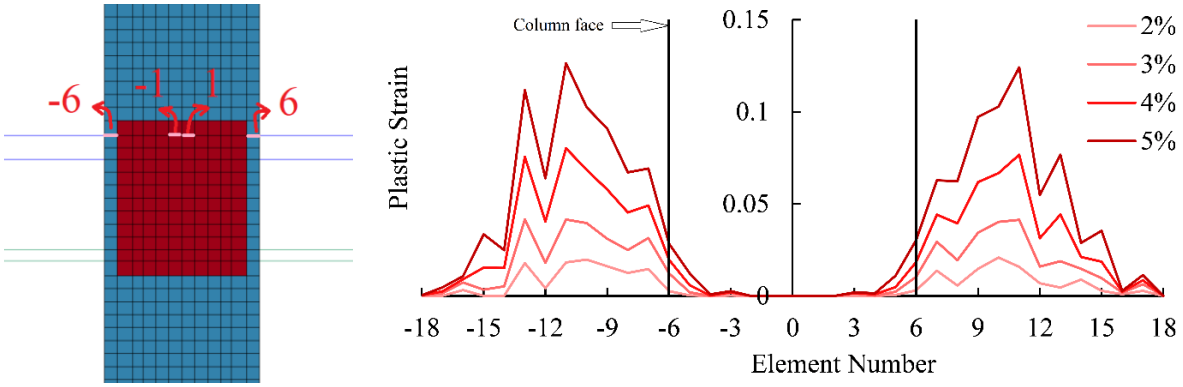

(a) Element layout **(b) Plastic strain distribution at different drift ratios**

Figure 5-51 Plastic strain distribution of bottom beam bar of P2.2 at different drift ratios

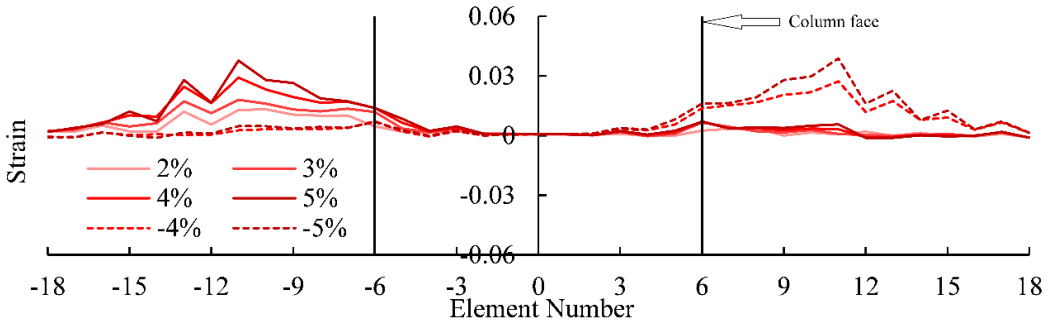

(a) Strain

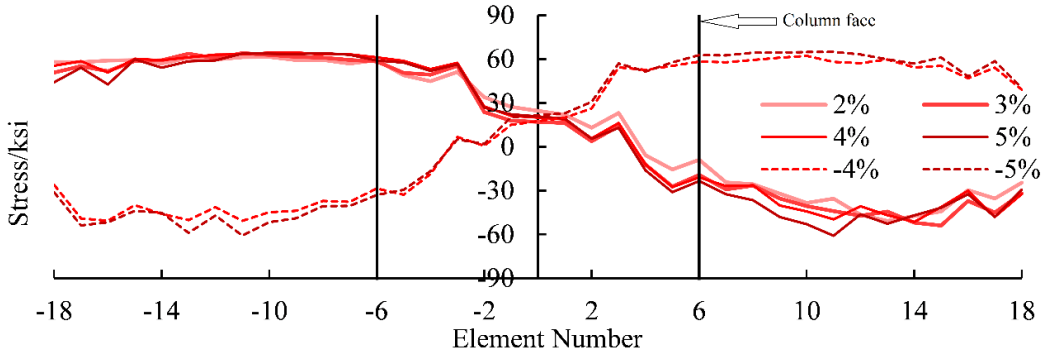

(b) Stress

Figure 5-52 Strain/stress distribution of bottom beam bar of P2.2 at different drift ratios

5.8 Conclusions

This chapter described numerous parametric studies to quantify the behavior of joints designed under current guidelines. These studies indicate that:

1. When subjected to unidirectional monotonic loading, connections that meet all the requirements of ACI352R-02 achieve satisfactory performance, with little or no serious joint damage, low values of slip, and efficient force transfer in the joint.

2. Connections designed with a shear ratio well in excess of that permitted by ACI 352 encounter severe damage in the joint, and thus cannot transfer forces efficiently, and also result in unneglectable bond-slip behavior as well as strength drop. This occurs even when the development length and moment ratios meet the requirements in ACI code.

3. When joints are subjected to unidirectional cyclic loading, the observations are similar to those from unidirectional monotonic loading, although some cases show somewhat more deterioration.

4. When subjected to simultaneous bidirectional monotonic loading, even the connections meeting the requirements from ACI352R-02 will evidence appreciable joint damage. The force transfer mechanism is no longer as efficient due to the loss of concrete at the column corners. The shear force predicted by ACI352R-02 is 10%~26% smaller compared with that from unidirectional monotonic cases. The situations for the connections with high shear ratio are even worse.

5. When subjected to simultaneous bidirectional cyclic loading, all the connections experience severe damage in the joint as well as the beam ends, which result in very significant strength degradation. The influence of bond-slip behavior and high shear ratio is no longer dominant.

6. The ACI352R-02 requirements are less accurate when applied to larger column sizes and shallower beams, even though the shear stress is not significantly higher compared with cases corresponding to smaller sized columns.

Chapter 6 Summary, Conclusions, and Recommendations for Future Research

6.1 Summary

The work presented herein aimed to provide a reliable analytical method to study the behavior of interior beam-column joints by formulating two types of analysis schemes, one based on three-dimensional continuum finite element models and the other on two-dimensional truss models. The analysis of beam-column-slab connections by the finite element method relied on accurate constitutive laws for describing the concrete, reinforcing bar and bond-slip response of the individual bars. Validation analyses have indicated the capability of the method to capture the global hysteretic response and damage patterns of RC joints, as well as local aspects of behavior such as the stress distribution of the beam longitudinal bars and local bond-slip response of the reinforcement. The nonlinear truss methodology is suitable for system-level simulations thanks to its computational efficiency. Truss models are capable of capturing shear failure in the joint panel region.

A parametric study was developed based on a prototype design of a two-way interior beam-column-slab connection from ACI 352 by finite element analysis. Results enables an understanding of the behavior of the connection and the influences of various design parameters.

6.2 Main Observations and Conclusions

The realization of detailed finite element analysis of BC joints is accomplished by (a) incorporating accurate material constitutive models for concrete, reinforcement and bond-slip behavior into the LS DYNA code, and (b) implementing a computationally efficient and robust

stress-strain update law for each material and bond-slip behavior. To capture the nonlinear behavior for concrete, including concrete crushing and cracking, the constitutive model for concrete must account for the multiaxial stress state, especially for the highly stressed concrete in the joint. To capture the nonlinear behavior in the plastic hinge region due to flexural behavior, including bar rupture and buckling, the constitutive law for reinforcement requires the ability of capturing nonlinear strain development with a stress-strain update law that converges rapidly and reliably. To capture the local bond-slip behavior in the BC joint, the bond-slip relation should be able to carefully track the loading and unloading sequences. Otherwise, even if one bond-slip law can result in acceptable global hysteretic response, the local slip will not correspond to that from the experimental data.

The methodologies developed in this study are capable of capturing the local bond-slip values and beam reinforcement stress distribution under cyclic loads accurately. I believe this is the first time that this has been achieved and it constitutes the main original contribution of this work. The finite element analyses in Chapter 3 describes the modeling of the local bond-slip response in the beam bars and compares their response with the experimental data. More local results from the analysis such as strain development of reinforcing bars at various locations are compared with experimental data in Chapter 3 for the first time.

The main conclusions from the present study are the following:

1. The finite element methodology has been evaluated through comparisons with a series of one-way interior BC joints under cyclic loading. In particular, the good matching between experiments and simulations encountered for both global hysteretic relations and local bond stress distribution after severe cycling indicate the reliability of the applied finite element

methodology and the importance of a robust bond-slip model in capturing local bond-slip behavior.

2. Further validation of the 3D finite element methodology was accomplished through comparisons a two-way beam-column-slab interior joint subjected to bidirectional cyclic loading tested by Kurose et al. (1988). Comparisons to response quantities such as overall force transfer mechanisms and hysteretic response in both directions under unidirectional and bidirectional loads, comparison of local strain development of reinforcing bars at various locations, and crack patterns at different stages of the loading history indicate satisfactory performance from the finite element models.

3. The nonlinear truss element methodology was also evaluated through the results of the experiments on one-way joints. The ability of the truss models to in capture the complex shear-flexure interaction in interior BC joint is proven. The truss model is an efficient supplement to finite element analysis as its model setup is simple and the computation cost low.

4. A parametric study of a prototype interior beam-column-slab joint based on a Type 2 design from ACI 352-02 utilizing the 3D finite element methodology mentioned above shows:

3) Satisfactory performance for connections which meet all the requirements of ACI352R-02 under unidirectional monotonic and cyclic loading. Similar connections designed with a high shear ratio (ie., not meeting ACI352-02 criteria) showed severe joint damage.

4) Inferior performance for connections subjected to simultaneous bidirectional monotonic loading. The shear force predicted by ACI352R-02 overestimated capacity by 10%~26% when compared with that from unidirectional monotonic cases, which result in substantial strength degradation. For these cases damage due to shear cracking and

associated strength and stiffness deterioration dominated performance and were far more important than bond-slip behavior.

5) The ACI352R-02 requirements are less accurate when applied to larger column sizes and shallower beams, even though the shear stress is not significantly higher when compared to cases involving smaller column size.

6.3 Recommendations for Future Research

The models developed herein need to be used to conduct further parametric studies. In particular, extension to exterior and corner beam-columns joints require a new bond-slip model to account for hooks and T-headed bars. In addition, extension to different slab depth and beam width values will require a careful consideration of torsional effects. For the individual models, the following improvements are desirable.

6.3.1 Analysis by Nonlinear Truss Model

1. The truss methodology should be extended to exterior and knee BC joints, to investigate different failure modes.
2. The nonlinear truss methodology should be enhanced to account for the effect of floor slabs.
3. The nonlinear truss methodology should be extended into three dimensions to allow the simulation of two-way joints.
4. The reasons that the ultimate strength was consistently underestimated, especially with large lateral loads. The peak compressive strength of the confined concrete has been found to

significantly affect the obtained peak strength of the joint models. A more accurate model for the peak stress of concrete with confinement is needed.

6.3.2 Finite Element Analysis

1. The finite element analysis can be further developed to better capture the diagonal shear cracks, through addition of, e.g., discrete cohesive crack interface elements in the models. This approach has already been used for three-dimensional analysis of other RC components, such as bridge shear keys (Kottari 2016).

2. The finite element model should be extended to exterior and knee BC joints, to investigate different failure modes.

3. The simulation of interior BC joint should be extended into a frame by adding simplified beam elements to represent beam and columns in other stories, to investigate the behavior of the joint in a true frame structure. This strategy applies for both finite element analogies in 3D analysis and nonlinear truss methodology in 2D analysis.

4. A more refined bond-slip model can be implemented to account for the confinement of concrete (Murcia-Delso and Shing, 2014), the dilatant effect of reinforcement (Murcia-Delso and Shing, 2015) and dowel-action behavior of reinforcement (Kottari et al. 2017).

5. The collapse analysis could be launched for the prototype by FE model, to find out the key factors trigger the collapse.

6. Accounting for bond-slip in the columns has a bigger effect than accounting for bond-slip in the beams. The reasons for this observation should be investigated in the future.

7. Launch more simulations on two-way beam-column-slab joints, for example, Leon 1985.

8. Launch a probability analysis to give wider prediction on different loading curves and develop robust fragility curves.

Appendix A Design Example of A Prototype Type 2 Connection

The connection P1-3 with a column dimension of 20*20 inch from Chapter 5 is set as an example herein for the detailed design calculation summarized in ACI352R-02.

As shown in Figure A-1, the connection is assumed to be located in the middle of a typical building floor plan, with a 20 feet span in all four directions and a 12 feet story height on both adjacent floors. The column is surrounded by four identical beams in four directions.

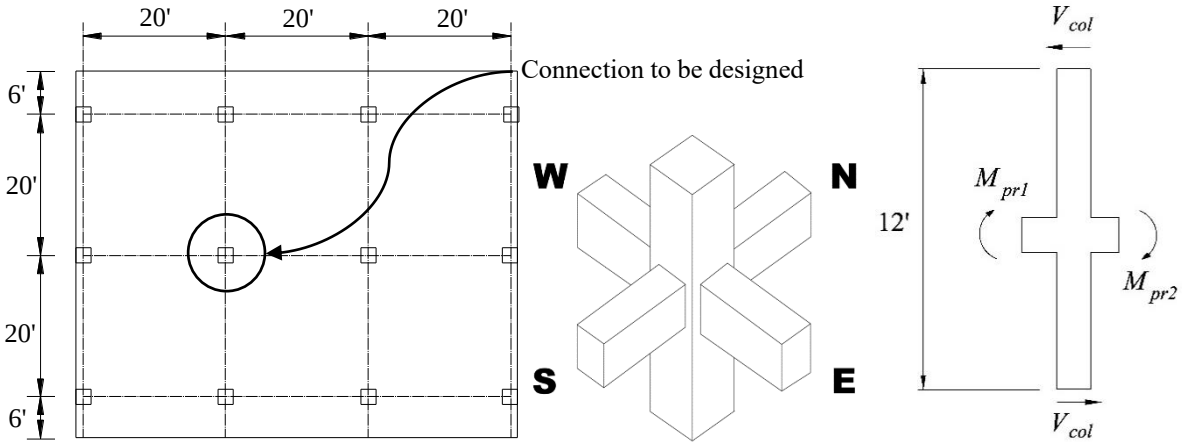

Figure A-1 (a) Floor plan (b) Joint outline (c) Column side view

A.1 Column Longitudinal Reinforcement

Column reinforcement need to be well distributed around the perimeter. The arrangement of 12 No. 9 bars shown in Figure A-2 is applied to give a more uniform distribution. The spacing between supported bars is 4.96 inch (with 1.5” of cover, 1.128” the longitudinal reinforcing bar diameter and 0.5” the hoop diameter), and it’s smaller than the allowable maximum spacing 8” or 1/3 the column dimension (6.67”). Based on the development length of beam longitudinal reinforcement, a 24 inch deep and 16 inch wide beam size will be considered.

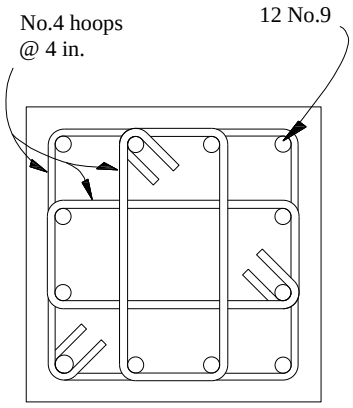

Figure A-2 Column section layout

A.2 Transverse Reinforcement

Provide A_{sh}=4 legs (0.2 in.^{2}/leg) = 0.8 in.^{2} (in each direction).

The spacing s_h is calculated based on Section 4.2.2.3 from ACI352R-02:

$$s_h \le \begin{cases} b_c / 4 = 5\,in. \ (governs) \\ 6d_b = 6(1.128\,in.) = 6.8\,in. \\ 6\,in. \end{cases} \quad \textbf{(A-1)}$$

The total cross-sectional area in each direction of hoops should be at least the larger of:

$$0.3\frac{s_h b_c'' f_c'}{f_{yh}}\left(\frac{A_g}{A_c}-1\right) = 0.3\frac{(5\,in.)(17\,in.)(10\,ksi)}{60\,ksi}\left(\frac{20^2}{17^2}-1\right) = 1.63\,in^2 \quad (governs)$$

$$0.09\frac{s_h b_c'' f_c'}{f_{yh}} = 0.09\frac{(5\,in.)(17\,in.)(10\,ksi)}{60\,ksi} = 1.28\,in^2 \quad \textbf{(A-2)}$$

Because the joint is confined on all sides by beam members, the value of A_{sh} obtained from Equation is reduced by 50%. The required A_{sh} = 0.5(1.63 in.^{2}) =0.82 in.^{2} > 0.8 in.^{2} (inadequate). Thus a 4 in. spacing will be used for the No.4 hoop reinforcement.

A_{sh} = 0.5(1.63 in.^{2}) 4/5=0.65 in.^{2} < 0.8 in.^{2} (OK)

A.3 Joint Shear

To calculate the beam flexural strength, it is necessary to include slab participation under negative bending moment. According to section 6.3.2 of ACI 318-14, the slab effective as a T-beam flange should not exceed:

a) One-eighth of span length on each side = 20 ft./8*2 + 16 in. = 76 in. (governs)
b) 8 times the slab thickness on each side = 16 in. + 8*6 in. *2 = 112 in.
c) One-half the clear distance to the next web on each side = 16 in. + 0.5*(20 ft.−16 in.) = 240 in.

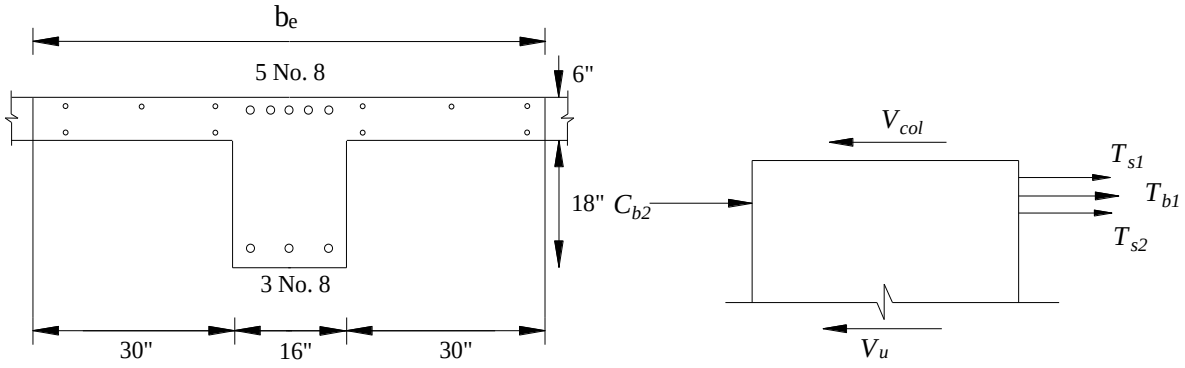

Figure A-3 (a) Effective width of slab (b) Shear force in the joint

For the bending moment calculation that follows, a total of 10 No.3 slab bars (6 on the top and 4 in the bottom) should be considered within the effective width of 76 in.; the effect of compressive reinforcement is ignored; assume $d = h$-2.7 in. in most locations; assume $d = h$-3.7 in. in locations where there is interference between bars from the normal and spandrel beams. Assume inflection point at the midheight of the column (Figure A-1c), the moment capacity of beam = $A_s \alpha f_y \left(d - \frac{a}{2} \right)$, $a = \frac{A_s \alpha f_y}{0.85 f_c' b}$. For positive bending moment:

$$a = \frac{3(0.79\ in.^2)(1.25)(60\ ksi)}{0.85(10\ ksi)(76\ in.)} = 0.28\ in. \quad \textbf{(A-3)}$$

$$M_{pr1} = 3(0.79\ in.^2)(1.25)(60\ ksi)(24 - 3.7 - \frac{0.28}{2}) = 3584\ k-in. = 298.7\ k-ft \quad \textbf{(A-4)}$$

For negative bending moment:

$$a = \frac{(5\times 0.79\ in.^2 + 10\times 0.11\ in.^2)(1.25)(60\ ksi)}{0.85(10\ ksi)(16\ in.)} = 2.78\ in. \quad \textbf{(A-5)}$$

$$\begin{aligned} M_{pr2} &= (5\times 0.79\ in.^2 + 10\times 0.11\ in.^2)(1.25)(60\ ksi)(24 - 2.7 - \frac{2.78}{2}) \\ &= 7540k-in. = 628.3\ k-ft \end{aligned} \quad \textbf{(A-6)}$$

Therefore, the column shear in Figure A-1c is:

$$V_{col} = \frac{M_{pr1} + M_{pr2}}{12\ ft} = \frac{298.7 + 628.3\ k-ft}{12\ ft} = 77.3\ kips \quad \textbf{(A-7)}$$

The required joint shear force based on beam flexural capacity is:

$$\begin{aligned} V_u &= T_{b1} + T_{s,s1} + T_{s,s2} + C_{b2} - V_{col} \\ &= \alpha f_y (A_{s1} + A_{slab} + A_{s2}) - V_{col} \\ &= 1.25\ (60\ ksi)(3.95 + 1.1 + 2.37)\ in.^2 - 77.3 = 479.2\ kips \end{aligned} \quad \textbf{(A-8)}$$

For the joint strength based on the capacity of column:

$$V_n = \gamma\sqrt{f_c'}\, b_j h_c \quad \textbf{(A-9)}$$

Based on Figure 2-4, γ=20 for the current case that "joint effectively confined on all four vertical faces". Based on Section 2.2, $(m\cdot h_c)/2 \leq$extension of the column beyond the edge of the beam. Since $\frac{0.5(20\ in.)}{2} = 5\ in.$, and the extension of column beyond the edge of the beam=2 in., then $(m\cdot h_c)/2$=2 in.

$$b_j \le \begin{cases} \dfrac{b_c + b_b}{2} = \dfrac{20+16}{2} = 18\ in.\ (governs) \\ b_b + \sum \dfrac{m \cdot h_c}{2} = 16 + 2 \times 2 = 20\ in. \\ b_c = 20\ in. \end{cases} \quad \textbf{(A-10)}$$

$$\varphi V_n = 0.85(20)\sqrt{10000\ psi}(18\ in.)(20\ in.)\frac{1\ kip}{1000\ lbs} = 612\ kips > 479.2\ kips\ (OK)$$

A.4 Flexural Strength Ratio

The beam flexural strengths have been found in the previous section using α=1.25. Those beam strengths will be divided by 1.25 to obtain an approximate beam flexural strength when α=1.0 as the column strength calculations will be based on nominal values.

$$\sum M_{beam} = M_{pr1}/1.25 + M_{pr2}/1.25 = 298.7/1.25 + 628.3/1.25 = 741.6\ k-ft \quad \textbf{(A-11)}$$

When determining the column flexural strength, the axial load is assumed to be 20% P_0, where P_0 is the nominal axial strength of column section:

$$P_0 = 0.85 f_c^{'} A_{cc} + f_y A_{cs} = 0.85(10\ ksi)(20 \times 20 - 12 \times 1)in.^2 + (60\ ksi)(12 \times 1)in.^2 = 4018\ kips \quad \textbf{(A-12)}$$

where A_{cc} is the area of concrete in the column section, and A_{cs} is the total area of column longitudinal reinforcement. The assumed axial force P is 20% P_0 = 803.6 kips. The forces applied on column section is illustrated in Figure A-4, with the color of red represents compressive forces and blue for tensile forces.

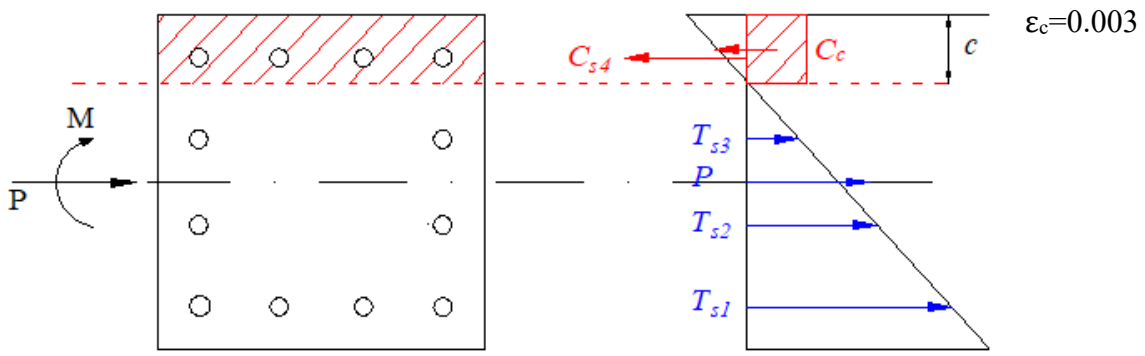

Figure A-4 Forces on the column section

The equilibrium is then accomplished by the tensile forces equal to compressive forces, when the strain of the most extreme concrete cover in tension equals to 0.003:

$$P + T_{s1} + T_{s2} + T_{s3} - C_c - C_{s4} = 0 \qquad \textbf{(A-13)}$$

The value of *c* is solved from Equation (A-13, which equals to 7.27 in. herein. The moment M can be calculated by summing the moments about the center of the section, which results in a moment of 742.1 k-ft. The flexural strength ratio =

$$\frac{\sum M_{column}}{\sum M_{beam}} = \frac{854.6 \times 2}{741.6} = 2.30 > 1.2 \text{ (OK)} \qquad \textbf{(A-14)}$$

A.5 Beam and Column Bars Passing Through the Joint

The plan view and elevation cut are shown in Figure A-5.

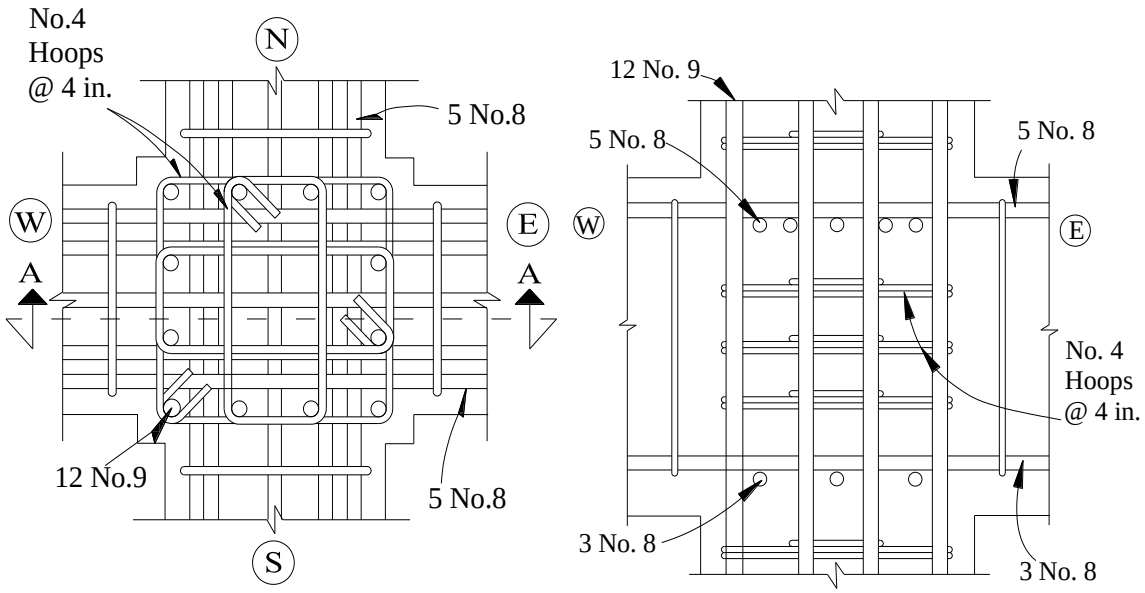

Figure A-5 (a) Plan view of joint (top beam bars) (b) Elevation (section A-A)

To ensure an adequate development length, the column dimension is governed by the largest beam bar diameter. From Equation 2-5:

h_c=20 in. ≥ 20(60000/60000) (1.00 in.) =20.0 in. (OK)

And beam depth is controlled by the column bar diameter. From Equation 2-6:

h_b=24 in. ≥ 20(60000/60000) (1.128in.) =22.6 in. (OK)

Appendix B Detailed Design Parameters of Connections in Chapter 5

No.	if pass ACI rules	Moment ratio: Mc/Mb	Development lengh/top bar diameter	Shear ratio: Vu/Vn	α	Material Property		Column												
								Column section									Column longitudinal reinforcement(352R §4.1)			
						fy/ksi	f'c/ksi	column cover/in	column size/in	column area/in^2	column bar diameter	column bar No.	column bar size	each column bar area	Total column bar area	352R §4.3.2 3/4 width of column	spacing c to c	spacing not exceed 8 & dimension/3	ACI318-14 §18.7.4.1 0.01~0.06Ag	ACI318-14 §18.7.4.2 min 6 bars
P1.1	PASS	1.83	26.67	0.73	1.25	60	10	1.5	20	400	1.128	12	9	1	12	OK	4.9573	OK	OK	OK
P1.2	PASS	2.12	32.00	0.63	1.25	60	10	1.5	20	400	1.128	12	9	1	12	OK	4.9573	OK	OK	OK
P1.3	PASS	2.00	20.00	0.67	1.25	60	10	1.5	20	400	1.128	12	9	1	12	OK	4.9573	OK	OK	OK
P1.4	NO	1.59	26.67	0.85	1.25	70	10	1.5	20	400	1.128	12	9	1	12	OK	4.9573	OK	OK	OK
P1.5	PASS	1.65	26.67	0.82	1.25	60	8	1.5	20	400	1.128	12	9	1	12	OK	4.9573	OK	OK	OK
P1.6	NO	2.14	20.00	1.62	1.25	60	6	1.5	20	400	2.257	12	18	4	48	OK	4.581	OK	NO	OK
P2.1	PASS	1.69	24.00	0.84	1.25	60	10	1.5	24	576	1.128	12	9	1	12	OK	6.2907	OK	OK	OK
P2.2	PASS	1.91	32.00	0.74	1.25	60	10	1.5	24	576	1.128	12	9	1	12	OK	6.2907	OK	OK	OK
P2.3	PASS	1.76	21.28	0.80	1.25	60	10	1.5	24	576	1.128	12	9	1	12	OK	6.2907	OK	OK	OK
P2.4	NO	1.47	24.00	0.99	1.25	70	10	1.5	24	576	1.128	12	9	1	12	OK	6.2907	OK	OK	OK
P2.5	NO	1.51	24.00	0.95	1.25	60	8	1.5	24	576	1.128	12	9	1	12	OK	6.2907	OK	OK	OK
P2.6	NO	2.22	21.28	1.62	1.25	60	6	1.5	24	576	2.257	12	18	4	48	OK	5.9143	OK	NO	OK
P3.1	NO	1.70	24.82	0.90	1.25	60	10	1.5	28	784	1.128	12	9	1	12	OK	7.624	OK	OK	OK
P3.2	NO	1.77	32.00	0.85	1.25	60	10	1.5	28	784	1.128	12	9	1	12	OK	7.624	OK	OK	OK
P3.3	NO	1.69	22.05	0.90	1.25	60	10	1.5	28	784	1.128	12	9	1	12	OK	7.624	OK	OK	OK
P3.4	NO	1.48	24.82	1.05	1.25	70	10	1.5	28	784	1.128	12	9	1	12	OK	7.624	OK	OK	OK
P3.5	NO	1.51	24.82	1.01	1.25	60	8	1.5	28	784	1.128	12	9	1	12	OK	7.624	OK	OK	OK
P3.6	NO	2.22	22.05	1.63	1.25	60	6	1.5	28	784	2.257	12	18	4	48	OK	7.2477	OK	NO	OK
P4.1	NO	1.72	25.20	0.94	1.25	60	10	1.5	32	1024	1.128	12	9	1	12	OK	8.874	OK	OK	OK
P4.2	NO	1.55	28.37	1.06	1.25	60	10	1.5	32	1024	1.128	12	9	1	12	OK	8.874	OK	OK	OK
P4.3	NO	1.40	22.70	1.21	1.25	60	10	1.5	32	1024	1.128	12	9	1	12	OK	8.874	OK	OK	OK
P4.4	NO	1.51	25.20	1.10	1.25	70	10	1.5	32	1024	1.128	12	9	1	12	OK	8.874	OK	OK	OK
P4.5	NO	1.52	25.20	1.06	1.25	60	8	1.5	32	1024	1.128	12	9	1	12	OK	8.874	OK	OK	OK
P4.6	NO	2.20	18.90	1.66	1.25	60	6	1.5	32	1024	2.257	12	18	4	48	OK	8.4977	OK	OK	OK

No.	if pass ACI rules	Moment ratio: Mc/Mb	Development lengh/top bar diameter	Shear ratio: Vu/Vn	Beam															
					Beam section		Top beam bar								Bottom beam bar					
					beam width	beam height	Top beam bar number	Top beam bar size	Top bar area	Top bar diameter	Anchorage lengh/top bar diameter	Top beam bar spacing	clear spacing of two layers	ACI318-14§25.2.1	Bottom beam bar No	Bottom beam bar size	Bottom bar area	Bottom bar diameter	bottom clear spacing in 1 layer	ACI318-14§25.2.1
P1.1	PASS	1.83	26.67	0.73	16	24	10	6	4.40	0.75	22.67	1.13	2.06	OK	6	6	2.64	0.75	1.5	OK
P1.2	PASS	2.12	32.00	0.63	16	24	12	5	3.72	0.625	27.20	1.03	1.65	OK	7	5	2.17	0.625	1.27083	OK
P1.3	PASS	2.00	20.00	0.67	16	24	5	8	3.95	1	17.00	2.75	6.33	OK	3	8	2.37	1	4.5	OK
P1.4	NO	1.59	26.67	0.85	16	24	10	6	4.40	0.75	22.67	1.25	2.06	OK	6	6	2.64	0.75	1.5	OK
P1.5	PASS	1.65	26.67	0.82	16	24	10	6	4.40	0.75	22.67	1.25	2.06	OK	6	6	2.64	0.75	1.5	OK
P1.6	NO	2.14	20.00	1.62	16	24	10	8	7.90	1	17.00	1.22	1.75	OK	6	8	4.74	1	1.2	OK
P2.1	PASS	1.69	24.00	0.84	20	24	10	8	7.90	1	21.00	1.67	2.75	OK	6	8	4.74	1	2	OK
P2.2	PASS	1.91	32.00	0.74	20	24	16	6	7.04	0.75	28.00	1.02	1.43	OK	9	6	3.96	0.75	1.15625	OK
P2.3	PASS	1.76	21.28	0.80	20	24	7	9	7.00	1.128	18.62	2.48	4.82	OK	5	9	5	1.128	2.59	OK
P2.4	NO	1.47	24.00	0.99	20	24	10	8	7.90	1	21.00	1.67	2.75	OK	6	8	4.74	1	2	OK
P2.5	NO	1.51	24.00	0.95	20	24	10	8	7.90	1	21.00	1.67	2.75	OK	6	8	4.74	1	2	OK
P2.6	NO	2.22	21.28	1.62	20	24	12	9	12.00	1.128	18.62	1.35	1.85	OK	7	9	7	1.128	1.35067	OK
P3.1	NO	1.70	24.82	0.90	24	24	12	9	12.00	1.128	22.16	1.72	2.65	OK	7	9	7	1.128	2.01733	OK
P3.2	NO	1.77	32.00	0.85	24	24	18	7	10.80	0.875	28.57	1.13	1.52	OK	12	7	7.2	0.875	0.86364	NO
P3.3	NO	1.69	22.05	0.90	24	24	9	10	11.43	1.27	19.69	2.34	4.08	OK	6	10	7.62	1.27	2.476	OK
P3.4	NO	1.48	24.82	1.05	24	24	12	9	12.00	1.128	22.16	1.72	2.65	OK	7	9	7	1.128	2.01733	OK
P3.5	NO	1.51	24.82	1.01	24	24	12	9	12.00	1.128	22.16	1.72	2.65	OK	7	9	7	1.128	2.01733	OK
P3.6	NO	2.22	22.05	1.63	24	24	13	10	16.51	1.27	19.69	1.56	2.14	OK	8	10	10.16	1.27	1.40571	OK
P4.1	NO	1.72	25.20	0.94	28	24	13	10	16.51	1.27	22.83	1.87	2.82	OK	8	10	10.16	1.27	1.94143	OK
P4.2	NO	1.55	28.37	1.06	28	24	18	9	18.00	1.128	25.71	1.33	1.70	OK	12	9	12	1.128	0.92855	NO
P4.3	NO	1.40	22.70	1.21	28	24	14	11	21.84	1.41	20.57	1.72	2.31	OK	8	11	12.48	1.41	1.78143	OK
P4.4	NO	1.51	25.20	1.10	28	24	13	10	16.51	1.27	22.83	1.87	2.82	OK	8	10	10.16	1.27	1.94143	OK
P4.5	NO	1.52	25.20	1.06	28	24	13	10	16.51	1.27	22.83	1.87	2.82	OK	8	10	10.16	1.27	1.94143	OK
P4.6	NO	2.20	18.90	1.66	28	24	10	14	22.50	1.693	17.13	2.45	3.82	OK	6	14	13.5	1.693	2.7184	OK

No.	Transverse reinforcement in the joint (352R §4.2.2)									Transverse reinforcement into the beam										Transverse reinforcement into the column					
	Spacing						Area			spacing in beam						length lo in beam				spacing in column			length lo in column		
	sh/in	layout of ties	Tie diameter	Provide Ash	fyh,yield stress of tie	§4.2.2.3	Eq. (4.4), Ash	Eq. (4.5), Ash	If adequate	spacing	diameter	ACI318-14 18.6.4.4	ACI318-14 18.6.4.6	ACI318-14 18.6.4.2	ACI318-14 9.7.6.4.3	lo	clear span of column	ACI318-14 18.6.4.1	spacing	diameter	ACI318-14 25.7.2.1	lo	clear span of column	ACI318-14 18.7.5.1
P1.1	4	4No.4@4	0.5	0.8	60	OK	1.31	1.02	OK	4	0.5	OK	OK	OK	OK	110	120	OK	4	0.5	OK	20	120	OK
P1.2	4	4No.4@4	0.5	0.8	60	OK	1.31	1.02	OK	4	0.5	OK	OK	OK	OK	110	120	OK	4	0.5	OK	20	120	OK
P1.3	4	4No.4@4	0.5	0.8	60	OK	1.31	1.02	OK	4	0.5	OK	OK	OK	OK	110	120	OK	4	0.5	OK	20	120	OK
P1.4	4	4No.4@4	0.5	0.8	60	OK	1.31	1.02	OK	4	0.5	OK	OK	OK	OK	110	120	OK	4	0.5	OK	20	120	OK
P1.5	4	4No.4@4	0.5	0.8	60	OK	1.04	0.82	OK	4	0.5	OK	OK	OK	OK	110	120	OK	4	0.5	OK	20	120	OK
P1.6	4	4No.4@4	0.5	0.8	60	OK	0.78	0.61	OK	4	0.5	OK	OK	OK	OK	110	120	OK	4	0.5	OK	20	120	OK
P2.1	4	4No.4@4	0.5	0.8	60	OK	1.29	1.26	OK	4	0.5	OK	OK	OK	OK	110	120	OK	4	0.5	OK	24	120	OK
P2.2	4	4No.4@4	0.5	0.8	60	OK	1.29	1.26	OK	4	0.5	OK	OK	OK	OK	110	120	OK	4	0.5	OK	24	120	OK
P2.3	4	4No.4@4	0.5	0.8	60	OK	1.29	1.26	OK	4	0.5	OK	OK	OK	OK	110	120	OK	4	0.5	OK	24	120	OK
P2.4	4	4No.4@4	0.5	0.8	60	OK	1.29	1.26	OK	4	0.5	OK	OK	OK	OK	110	120	OK	4	0.5	OK	24	120	OK
P2.5	4	4No.4@4	0.5	0.8	60	OK	1.03	1.01	OK	4	0.5	OK	OK	OK	OK	110	120	OK	4	0.5	OK	24	120	OK
P2.6	4	4No.4@4	0.5	0.8	60	OK	0.77	0.76	OK	4	0.5	OK	OK	OK	OK	110	120	OK	4	0.5	OK	24	120	OK
P3.1	4	4No.4@4	0.5	0.8	60	OK	1.27	1.50	OK	4	0.5	OK	OK	OK	OK	110	120	OK	4	0.5	OK	28	120	OK
P3.2	4	4No.4@4	0.5	0.8	60	OK	1.27	1.50	OK	4	0.5	OK	OK	OK	OK	110	120	OK	4	0.5	OK	28	120	OK
P3.3	4	4No.4@4	0.5	0.8	60	OK	1.27	1.50	OK	4	0.5	OK	OK	OK	OK	110	120	OK	4	0.5	OK	28	120	OK
P3.4	4	4No.4@4	0.5	0.8	60	OK	1.27	1.50	OK	4	0.5	OK	OK	OK	OK	110	120	OK	4	0.5	OK	28	120	OK
P3.5	4	4No.4@4	0.5	0.8	60	OK	1.02	1.20	OK	4	0.5	OK	OK	OK	OK	110	120	OK	4	0.5	OK	28	120	OK
P3.6	4	4No.4@4	0.5	0.8	60	OK	0.76	0.90	OK	4	0.5	OK	OK	OK	OK	110	120	OK	4	0.5	OK	28	120	OK
P4.1	4	4No.5@4	0.625	1.24	60	OK	1.26	1.74	OK	4	0.5	OK	OK	OK	OK	110	120	OK	4	0.5	OK	32	120	OK
P4.2	4	4No.5@4	0.625	1.24	60	OK	1.26	1.74	OK	4	0.5	OK	OK	OK	OK	110	120	OK	4	0.5	OK	32	120	OK
P4.3	4	4No.5@4	0.625	1.24	60	OK	1.26	1.74	OK	4	0.5	OK	OK	OK	OK	110	120	OK	4	0.5	OK	32	120	OK
P4.4	4	4No.5@4	0.625	1.24	60	OK	1.26	1.74	OK	4	0.5	OK	OK	OK	OK	110	120	OK	4	0.5	OK	32	120	OK
P4.5	4	4No.5@4	0.625	1.24	60	OK	1.01	1.39	OK	4	0.5	OK	OK	OK	OK	110	120	OK	4	0.5	OK	32	120	OK
P4.6	4	4No.5@4	0.625	1.24	60	OK	0.76	1.04	OK	4	0.5	OK	OK	OK	OK	110	120	OK	4	0.5	OK	32	120	OK

No.	if pass ACI rules	Moment ratio: Mc/Mb	Development lengh/top bar diameter	Shear ratio: Vu/Vn	Joint shear																
					Slab					E-W beam				Required shear		Shear strength					
					Slab effective width	slab thickness	ACI 318-14 §6.3.2	slab bar included	slab bar area	a for Positive moment	Positive bending moment/k-in	a for Negative moment	Negative bending moment/k-in	Column shear/ kips	Required shear Vu/ kips	γ	m*hc/2	Effective joint width bj, §4.3.1	shear capacity Vn/ kips	If Vu/Vn <0.85
P1.1	PASS	1.83	26.67	0.73	76	6	OK	10No.3	1.1	0.31	3989.06	3.03	8160.68	84.37	526.13	20	2	18	720	OK
P1.2	PASS	2.12	32.00	0.63	76	6	OK	10No.3	1.1	0.25	3283.32	2.66	7219.50	72.94	451.31	20	2	18	720	OK
P1.3	PASS	2.00	20.00	0.67	76	6	OK	10No.3	1.1	0.28	3583.87	2.78	7539.98	77.25	479.25	20	2	18	720	OK
P1.4	NO	1.59	26.67	0.85	76	6	OK	10No.3	1.1	0.36	4648.00	3.54	9399.15	97.55	614.70	20	2	18	720	NO
P1.5	PASS	1.65	26.67	0.82	76	6	OK	10No.3	1.1	0.38	3981.47	3.79	8004.28	83.23	527.27	20	2	18	643.988	OK
P1.6	NO	2.14	20.00	1.62	76	6	OK	10No.3	1.1	0.92	7053.62	8.27	11585.68	129.44	901.06	20	2	18	557.71	NO
P2.1	PASS	1.69	24.00	0.84	76	6	OK	10No.3	1.1	0.55	7118.83	3.97	13037.43	139.97	890.53	20	2	22	1056	OK
P2.2	PASS	1.91	32.00	0.74	76	6	OK	10No.3	1.1	0.46	5960.83	3.59	11907.44	124.09	783.41	20	2	22	1056	OK
P2.3	PASS	1.76	21.28	0.80	76	6	OK	10No.3	1.1	0.58	7503.66	3.57	11854.29	134.43	848.07	20	2	22	1056	OK
P2.4	NO	1.47	24.00	0.99	76	6	OK	10No.3	1.1	0.64	8286.28	4.63	14949.76	161.36	1040.89	20	2	22	1056	NO
P2.5	NO	1.51	24.00	0.95	76	6	OK	10No.3	1.1	0.69	7094.38	4.96	12702.41	137.48	893.02	20	2	22	944.515	NO
P2.6	NO	2.22	21.28	1.62	76	6	OK	10No.3	1.1	1.35	10301.95	9.63	16195.36	184.01	1323.49	20	2	22	817.974	NO
P3.1	NO	1.70	24.82	0.90	76	6	OK	10No.3	1.1	0.81	10444.17	4.82	18561.30	201.43	1306.07	20	2	26	1456	NO
P3.2	NO	1.77	32.00	0.85	76	6	OK	10No.3	1.1	0.84	10736.30	4.38	17057.91	193.02	1239.48	20	2	26	1456	NO
P3.3	NO	1.69	22.05	0.90	76	6	OK	10No.3	1.1	0.88	11348.65	4.61	17852.14	202.78	1308.47	20	2	26	1456	NO
P3.4	NO	1.48	24.82	1.05	76	6	OK	10No.3	1.1	0.95	12143.38	5.62	21194.81	231.52	1527.23	20	2	26	1456	NO
P3.5	NO	1.51	24.82	1.01	76	6	OK	10No.3	1.1	1.02	10390.83	6.02	17969.82	196.95	1310.55	20	2	26	1302.29	NO
P3.6	NO	2.22	22.05	1.63	76	6	OK	10No.3	1.1	1.97	14719.58	10.79	21006.24	248.10	1834.65	20	2	26	1127.81	NO
P4.1	NO	1.72	25.20	0.94	76	6	OK	10No.3	1.1	1.18	15019.19	5.55	24467.31	274.21	1808.54	20	2	30	1920	NO
P4.2	NO	1.55	28.37	1.06	76	6	OK	10No.3	1.1	1.39	17643.07	6.02	26201.21	304.47	2028.03	20	2	30	1920	NO
P4.3	NO	1.40	22.70	1.21	76	6	OK	10No.3	1.1	1.45	18322.71	7.23	30427.91	338.55	2317.95	20	2	30	1920	NO
P4.4	NO	1.51	25.20	1.10	76	6	OK	10No.3	1.1	1.38	17435.00	6.47	27832.62	314.36	2115.52	20	2	30	1920	NO
P4.5	NO	1.52	25.20	1.06	76	6	OK	10No.3	1.1	1.47	14906.83	6.94	23551.14	267.07	1815.68	20	2	30	1717.3	NO
P4.6	NO	2.20	18.90	1.66	76	6	OK	10No.3	1.1	2.61	19231.31	12.39	26731.46	319.19	2463.31	20	2	30	1487.23	NO

No.	if pass ACI rules	Moment ratio: Mc/Mb	Development lengh/top bar diameter	Shear ratio: Vu/Vn	Flexture §352R4.4														352R §4.4.2
					Calculate Mn														
					Po/kip	Pn Axial load on column/ kips	β1	c/in	1st layer bar center to top	e4	e3	e2	e1	equation solver objective "0"	Mn about center	φ	φMn	largest tensile strain	If Moment ration>1.2
P1.1	PASS	2.11	26.67	0.73	4018	803.60	0.65	8.35	2.56	0.002069	0.0002991	-0.00148	-0.002069	8E-06	10255.32	0.75	7708.81	0.0033	OK
P1.2	PASS	2.44	32.00	0.63	4018	803.60	0.65	8.35	2.56	0.002069	0.0002991	-0.00148	-0.002069	8E-06	10255.32	0.75	7708.81	0.0033	OK
P1.3	PASS	2.30	20.00	0.67	4018	803.60	0.65	8.35	2.56	0.002069	0.0002991	-0.00148	-0.002069	8E-06	10255.32	0.75	7708.81	0.0033	OK
P1.4	NO	1.84	26.67	0.85	4138	827.60	0.65	8.50	2.56	0.002069	0.0003469	-0.0014	-0.002069	3E-05	10325.97	0.74	7664.33	0.0032	OK
P1.5	PASS	1.89	26.67	0.82	3358	671.68	0.65	8.67	2.56	0.002069	0.0003962	-0.00132	-0.002069	3E-06	9083.153	0.73	6653.33	0.003	OK
P1.6	NO	2.29	20.00	1.62	4675	935.04	0.75	10.68	3.13	0.002069	0.0008338	-0.00045	-0.00174	8E-06	17073.67	0.65	11097.89	0.0017	OK
P2.1	PASS	1.95	24.00	0.84	5514	1102.80	0.65	9.42	2.56	0.002069	0.0001801	-0.00182	-0.002069	1E-06	15685.63	0.80	12547.26	0.0038	OK
P2.2	PASS	2.19	32.00	0.74	5514	1102.80	0.65	9.42	2.56	0.002069	0.0001801	-0.00182	-0.002069	1E-06	15685.63	0.80	12547.26	0.0038	OK
P2.3	PASS	2.03	21.28	0.80	5514	1102.80	0.65	9.42	2.56	0.002069	0.0001801	-0.00182	-0.002069	1E-06	15685.63	0.80	12547.26	0.0038	OK
P2.4	NO	1.70	24.00	0.99	5634	1126.80	0.65	9.55	2.56	0.002069	0.0002196	-0.00176	-0.002069	1E-06	15784.21	0.79	12497.14	0.0037	OK
P2.5	NO	1.73	24.00	0.95	4555	911.04	0.65	9.74	2.56	0.002069	0.0002715	-0.00167	-0.002069	1E-06	13708.99	0.78	10707.27	0.0036	OK
P2.6	NO	2.39	21.28	1.62	5573	1114.56	0.75	12.52	3.13	0.002069	0.0008324	-0.00059	-0.002	9E-06	25284.35	0.65	16434.83	0.002	OK
P3.1	NO	1.96	24.82	0.90	7282	1456.40	0.65	10.49	2.56	0.002069	8.57E-05	-0.002069	-0.002069	-4E-07	22696.17	0.84	19025.03	0.0043	OK
P3.2	NO	2.04	32.00	0.85	7282	1456.40	0.65	10.49	2.56	0.002069	8.57E-05	-0.002069	-0.002069	-4E-07	22696.17	0.84	19025.03	0.0043	OK
P3.3	NO	1.94	22.05	0.90	7282	1456.40	0.65	10.49	2.56	0.002069	8.57E-05	-0.002069	-0.002069	-4E-07	22696.17	0.84	19025.03	0.0043	OK
P3.4	NO	1.71	24.82	1.05	7402	1480.40	0.65	10.62	2.56	0.002069	0.000121	-0.00203	-0.002069	-4E-05	22838.16	0.83	18972.39	0.0042	OK
P3.5	NO	1.73	24.82	1.01	5970	1193.92	0.65	10.81	2.56	0.002069	0.0001719	-0.00194	-0.002069	4E-05	19621.78	0.82	16087.59	0.0041	OK
P3.6	NO	2.39	22.05	1.63	6634	1326.72	0.75	13.76	3.13	0.002069	0.0007375	-0.00084	-0.002069	3E-05	34194.2	0.68	23259.06	0.0024	OK
P4.1	NO	1.98	25.20	0.94	9322	1864.40	0.65	11.43	2.69	0.002069	-3.55E-05	-0.002069	-0.002069	9E-08	31283.33	0.87	27340.01	0.0047	OK
P4.2	NO	1.78	28.37	1.06	9322	1864.40	0.65	11.43	2.69	0.002069	-3.55E-05	-0.002069	-0.002069	9E-08	31283.33	0.87	27340.01	0.0047	OK
P4.3	NO	1.60	22.70	1.21	9322	1864.40	0.65	11.43	2.69	0.002069	-3.55E-05	-0.002069	-0.002069	9E-08	31283.33	0.87	27340.01	0.0047	OK
P4.4	NO	1.74	25.20	1.10	9442	1888.40	0.65	11.64	2.69	0.002069	2.024E-05	-0.002069	-0.002069	1E-06	31543.37	0.86	27187.37	0.0046	OK
P4.5	NO	1.75	25.20	1.06	7602	1520.32	0.65	11.86	2.69	0.002069	7.4E-05	-0.002069	-0.002069	-1E-05	26886.91	0.85	22861.48	0.0044	OK
P4.6	NO	2.39	18.90	1.66	7858	1571.52	0.75	14.78	3.25	0.002069	0.0006146	-0.00111	-0.002069	3E-05	43878.26	0.72	31388.90	0.0028	OK

No.	if pass ACI rules	Moment ratio: Mc/Mb	Development lengh/top bar diameter	Shear ratio: Vu/Vn	Development of reinforcement 352R §4.5						
					352R §4.5.2					352R §4.5.5	
					Development length/in	ldh Eq(4.10) Top bar	if OK	ldh Eq(4.10) Bottom bar	if OK	h of column/ db-beam bar	h of beam/d of column bar
P1.1	PASS	1.83	26.67	0.73	17	7.50	OK	7.50	OK	OK	OK
P1.2	PASS	2.12	32.00	0.63	17	6.25	OK	6.25	OK	OK	OK
P1.3	PASS	2.00	20.00	0.67	17	10.00	OK	10.00	OK	OK	OK
P1.4	NO	1.59	26.67	0.85	17	8.75	OK	8.75	OK	OK	NO
P1.5	PASS	1.65	26.67	0.82	17	8.39	OK	8.39	OK	OK	OK
P1.6	NO	2.14	20.00	1.62	17	12.91	OK	12.91	OK	OK	NO
P2.1	PASS	1.69	24.00	0.84	21	10.00	OK	10.00	OK	OK	OK
P2.2	PASS	1.91	32.00	0.74	21	7.50	OK	7.50	OK	OK	OK
P2.3	PASS	1.76	21.28	0.80	21	11.28	OK	11.28	OK	OK	OK
P2.4	NO	1.47	24.00	0.99	21	11.67	OK	11.67	OK	OK	NO
P2.5	NO	1.51	24.00	0.95	21	11.18	OK	11.18	OK	OK	OK
P2.6	NO	2.22	21.28	1.62	21	14.56	OK	14.56	OK	OK	NO
P3.1	NO	1.70	24.82	0.90	25	11.28	OK	11.28	OK	OK	OK
P3.2	NO	1.77	32.00	0.85	25	8.75	OK	8.75	OK	OK	OK
P3.3	NO	1.69	22.05	0.90	25	12.70	OK	12.70	OK	OK	OK
P3.4	NO	1.48	24.82	1.05	25	13.16	OK	13.16	OK	OK	NO
P3.5	NO	1.51	24.82	1.01	25	12.61	OK	12.61	OK	OK	OK
P3.6	NO	2.22	22.05	1.63	25	16.40	OK	16.40	OK	OK	NO
P4.1	NO	1.72	25.20	0.94	29	12.70	OK	12.70	OK	OK	OK
P4.2	NO	1.55	28.37	1.06	29	11.28	OK	11.28	OK	OK	OK
P4.3	NO	1.40	22.70	1.21	29	14.10	OK	14.10	OK	OK	OK
P4.4	NO	1.51	25.20	1.10	29	14.82	OK	14.82	OK	OK	NO
P4.5	NO	1.52	25.20	1.06	29	14.20	OK	14.20	OK	OK	OK
P4.6	NO	2.20	18.90	1.66	29	21.86	OK	21.86	OK	NO	NO

Appendix C Detailed Design Parameters of Connections in Table 5-1

No.	if pass ACI rules	Moment ratio: Mc/Mb	Development lengh/top bar diameter	Shear ratio: Vu/Vn	α	Material Property		Column												
								Column section									Column longitudinal reinforcement(352R §4.1)			
						fy/ksi	f'c/ksi	column cover/in	column size/in	column area/in^2	column bar diameter	column bar No.	column bar size	each column bar area	Total column bar area	352R§4.3.2 3/4 width of column	spacing c to c	spacing not exceed 8 & dimension/3	ACI318-14§18.7.4.1 0.01~0.06Ag	ACI318-14§18.7.4.2 min 6 bars
1	PASS	1.67	26.67	0.81	1.25	60	10	1.5	20	400	1.128	12	9	1	12	OK	4.96	OK	OK	OK
2	PASS	1.89	32.00	0.71	1.25	60	10	1.5	20	400	1.128	12	9	1	12	OK	4.96	OK	OK	OK
3	PASS	1.68	20.00	0.81	1.25	60	10	1.5	20	400	1.128	12	9	1	12	OK	4.96	OK	OK	OK
4	PASS	1.82	20.00	0.74	1.25	60	10	1.5	20	400	1.128	12	9	1	12	OK	4.96	OK	OK	OK
5	PASS	1.90	32.00	0.71	1.25	60	10	1.5	20	400	1.128	12	9	1	12	OK	4.96	OK	OK	OK
6	PASS	1.85	26.67	0.73	1.25	60	10	1.5	20	400	1.128	12	9	1	12	OK	4.96	OK	OK	OK
7	PASS	1.68	26.67	0.81	1.25	60	10	1.5	20	400	1.128	12	9	1	12	OK	4.96	OK	OK	OK
8	PASS	1.95	26.67	0.69	1.25	60	10	1.5	20	400	1.128	12	9	1	12	OK	4.96	OK	OK	OK
9	PASS	1.66	26.67	0.81	1.25	60	10	1.5	20	400	1.128	12	9	1	12	OK	4.96	OK	OK	OK
10	PASS	1.69	22.86	0.80	1.25	60	10	1.5	20	400	1.128	12	9	1	12	OK	4.96	OK	OK	OK
1	PASS	1.69	24.00	0.84	1.25	60	10	1.5	24	576	1.128	12	9	1	12	OK	6.29	OK	OK	OK
2	PASS	1.91	32.00	0.74	1.25	60	10	1.5	24	576	1.128	12	9	1	12	OK	6.29	OK	OK	OK
3	PASS	1.76	21.28	0.80	1.25	60	10	1.5	24	576	1.128	12	9	1	12	OK	6.29	OK	OK	OK
4	PASS	1.95	27.43	0.73	1.25	60	10	1.5	24	576	1.128	12	9	1	12	OK	6.29	OK	OK	OK
5	PASS	1.90	24.00	0.75	1.25	60	10	1.5	24	576	1.128	12	9	1	12	OK	6.29	OK	OK	OK
6	PASS	1.98	32.00	0.71	1.25	60	10	1.5	24	576	1.128	12	9	1	12	OK	6.29	OK	OK	OK
7	PASS	1.78	21.28	0.80	1.25	60	10	1.5	24	576	1.128	12	9	1	12	OK	6.29	OK	OK	OK
8	PASS	1.94	27.43	0.73	1.25	60	10	1.5	24	576	1.128	12	9	1	12	OK	6.29	OK	OK	OK
9	PASS	1.91	24.00	0.75	1.25	60	10	1.5	24	576	1.128	12	9	1	12	OK	6.29	OK	OK	OK
10	PASS	1.78	21.28	0.80	1.25	60	10	1.5	24	576	1.128	12	9	1	12	OK	6.29	OK	OK	OK
1	PASS	1.88	24.82	0.81	1.25	60	10	1.5	28	784	1.128	12	9	1	12	OK	7.62	OK	OK	OK
2	PASS	1.95	32.00	0.77	1.25	60	10	1.5	28	784	1.128	12	9	1	12	OK	7.62	OK	OK	OK
3	PASS	1.80	22.05	0.84	1.25	60	10	1.5	28	784	1.128	12	9	1	12	OK	7.62	OK	OK	OK
4	PASS	1.97	24.82	0.76	1.25	60	10	1.5	28	784	1.128	12	9	1	12	OK	7.62	OK	OK	OK
5	PASS	1.96	32.00	0.77	1.25	60	10	1.5	28	784	1.128	12	9	1	12	OK	7.62	OK	OK	OK
6	PASS	1.80	22.05	0.84	1.25	60	10	1.5	28	784	1.128	12	9	1	12	OK	7.62	OK	OK	OK
7	PASS	1.92	28.00	0.79	1.25	60	10	1.5	28	784	1.128	12	9	1	12	OK	7.62	OK	OK	OK
8	PASS	1.83	32.00	0.82	1.25	60	10	1.5	28	784	1.128	12	9	1	12	OK	7.62	OK	OK	OK
9	PASS	1.84	28.00	0.82	1.25	60	10	1.5	28	784	1.128	12	9	1	12	OK	7.62	OK	OK	OK
10	PASS	1.88	24.82	0.81	1.25	60	10	1.5	28	784	1.128	12	9	1	12	OK	7.62	OK	OK	OK
1	PASS	1.99	25.20	0.81	1.25	60	10	1.5	32	1024	1.128	12	9	1	12	OK	8.87	OK	OK	OK
2	PASS	1.97	28.37	0.82	1.25	60	10	1.5	32	1024	1.128	12	9	1	12	OK	8.87	OK	OK	OK
3	PASS	1.93	22.70	0.83	1.25	60	10	1.5	32	1024	1.128	12	9	1	12	OK	8.87	OK	OK	OK
4	PASS	1.97	32.00	0.81	1.25	60	10	1.5	32	1024	1.128	12	9	1	12	OK	8.87	OK	OK	OK
5	PASS	1.98	32.00	0.81	1.25	60	10	1.5	32	1024	1.128	12	9	1	12	OK	8.87	OK	OK	OK
6	PASS	1.97	28.37	0.82	1.25	60	10	1.5	32	1024	1.128	12	9	1	12	OK	8.87	OK	OK	OK
7	PASS	1.99	25.20	0.81	1.25	60	10	1.5	32	1024	1.128	12	9	1	12	OK	8.87	OK	OK	OK
8	PASS	1.97	28.37	0.82	1.25	60	10	1.5	32	1024	1.128	12	9	1	12	OK	8.87	OK	OK	OK
9	PASS	1.95	22.70	0.83	1.25	60	10	1.5	32	1024	1.128	12	9	1	12	OK	8.87	OK	OK	OK
10	PASS	1.99	25.20	0.81	1.25	60	10	1.5	32	1024	1.128	12	9	1	12	OK	8.87	OK	OK	OK

No.	if pass ACI rules	Moment ratio: Mc/Mb	Development lengh/top bar diameter	Shear ratio: Vu/Vn	α	Material Property		Beam																	
								Beam section		Top beam bar									Bottom beam bar						
						fy/ksi	f'c/ksi	beam width	beam height	Top beam bar number	Top beam bar size	Top bar area	Top bar diameter	Anchorage lengh/top bar	Top beam bar spacing	clear spacing of two layers	ACI318-14§25.2.1	Bottom beam bar No	Bottom beam bar size	Bottom bar area	Bottom bar diameter	bottom clear spacing in 1	ACI318-14§25.2.1
1	PASS	1.67	26.67	0.81	1.25	60	10	16	24	12	6	5.28	0.75	22.67	1.13	1.50	OK	6	6	2.64	0.75	1.50	OK
2	PASS	1.89	32.00	0.71	1.25	60	10	16	24	15	5	4.65	0.625	27.20	0.81	1.13	OK	7	5	2.17	0.625	1.27	OK
3	PASS	1.68	20.00	0.81	1.25	60	10	16	24	7	8	5.53	1	17.00	1.83	3.40	OK	3	8	2.37	1	4.50	OK
4	PASS	1.82	20.00	0.74	1.25	60	10	16	24	6	8	4.74	1	17.00	2.20	4.50	OK	3	8	2.37	1	4.50	OK
5	PASS	1.90	32.00	0.71	1.25	60	10	16	24	16	5	4.96	0.625	27.20	0.76	1.00	OK	6	5	1.86	0.625	1.65	OK
6	PASS	1.85	26.67	0.73	1.25	60	10	16	24	12	6	5.28	0.75	22.67	1.02	1.50	OK	4	6	1.76	0.75	3.00	OK
7	PASS	1.68	26.67	0.81	1.25	60	10	16	24	13	6	5.72	0.75	22.67	0.94	1.30	OK	5	6	2.2	0.75	2.06	OK
8	PASS	1.95	26.67	0.69	1.25	60	10	16	24	11	6	4.84	0.75	22.67	1.13	1.75	OK	4	6	1.76	0.75	3.00	OK
9	PASS	1.66	26.67	0.81	1.25	60	10	16	24	11	6	4.84	0.75	22.67	1.13	1.75	OK	7	6	3.08	0.75	1.13	OK
10	PASS	1.69	22.86	0.80	1.25	60	10	16	24	9	7	5.40	0.875	19.43	1.39	2.30	OK	4	7	2.4	0.875	2.83	OK
1	PASS	1.69	24.00	0.84	1.25	60	10	20	24	10	8	7.90	1	21.00	1.67	2.75	OK	6	8	4.74	1	2.00	OK
2	PASS	1.91	32.00	0.74	1.25	60	10	20	24	16	6	7.04	0.75	28.00	1.02	1.43	OK	9	6	3.96	0.75	1.16	OK
3	PASS	1.76	21.28	0.80	1.25	60	10	20	24	7	9	7.00	1.128	18.62	2.48	4.82	OK	5	9	5	1.128	2.59	OK
4	PASS	1.95	27.43	0.73	1.25	60	10	20	24	13	7	7.80	0.875	24.00	1.26	1.88	OK	5	7	3	0.875	2.91	OK
5	PASS	1.90	24.00	0.75	1.25	60	10	20	24	9	8	7.11	1	21.00	1.88	3.29	OK	5	8	3.95	1	2.75	OK
6	PASS	1.98	32.00	0.71	1.25	60	10	20	24	16	6	7.04	0.75	28.00	1.02	1.43	OK	8	6	3.52	0.75	1.43	OK
7	PASS	1.78	21.28	0.80	1.25	60	10	20	24	8	9	8.00	1.128	18.62	2.12	3.83	OK	4	9	4	1.128	3.83	OK
8	PASS	1.94	27.43	0.73	1.25	60	10	20	24	12	7	7.20	0.875	24.00	1.38	2.15	OK	6	7	3.6	0.875	2.15	OK
9	PASS	1.91	24.00	0.75	1.25	60	10	20	24	10	8	7.90	1	21.00	1.67	2.75	OK	4	8	3.16	1	4.00	OK
10	PASS	1.78	21.28	0.80	1.25	60	10	20	24	8	9	8.00	1.128	18.62	2.12	3.83	OK	4	9	4	1.128	3.83	OK
1	PASS	1.88	24.82	0.81	1.25	60	10	24	24	11	9	11.00	1.128	22.16	1.89	3.07	OK	6	9	6	1.128	2.65	OK
2	PASS	1.95	32.00	0.77	1.25	60	10	24	24	17	7	10.20	0.875	28.57	1.20	1.68	OK	10	7	6	0.875	1.25	OK
3	PASS	1.80	22.05	0.84	1.25	60	10	24	24	9	10	11.43	1.27	19.69	2.34	4.08	OK	5	10	6.35	1.27	3.41	OK
4	PASS	1.97	24.82	0.76	1.25	60	10	24	24	10	9	10.00	1.128	22.16	2.10	3.59	OK	6	9	6	1.128	2.65	OK
5	PASS	1.96	32.00	0.77	1.25	60	10	24	24	18	7	10.80	0.875	28.57	1.13	1.52	OK	9	7	5.4	0.875	1.52	OK
6	PASS	1.80	22.05	0.84	1.25	60	10	24	24	9	10	11.43	1.27	19.69	2.34	4.08	OK	5	10	6.35	1.27	3.41	OK
7	PASS	1.92	28.00	0.79	1.25	60	10	24	24	14	8	11.06	1	25.00	1.46	2.17	OK	7	8	5.53	1	2.17	OK
8	PASS	1.83	32.00	0.82	1.25	60	10	24	24	18	7	10.80	0.875	28.57	1.13	1.52	OK	11	7	6.6	0.875	1.04	OK
9	PASS	1.84	28.00	0.82	1.25	60	10	24	24	14	8	11.06	1	25.00	1.46	2.17	OK	8	8	6.32	1	1.71	OK
10	PASS	1.88	24.82	0.81	1.25	60	10	24	24	11	9	11.00	1.128	22.16	1.89	3.07	OK	6	9	6	1.128	2.65	OK
1	PASS	1.99	25.20	0.81	1.25	60	10	28	24	12	10	15.24	1.27	22.83	2.04	3.23	OK	6	10	7.62	1.27	3.23	OK
2	PASS	1.97	28.37	0.82	1.25	60	10	28	24	15	9	15.00	1.128	25.71	1.62	2.35	OK	8	9	8	1.128	2.10	OK
3	PASS	1.93	22.70	0.83	1.25	60	10	28	24	9	11	14.04	1.41	20.57	2.79	4.97	OK	6	11	9.36	1.41	3.06	OK
4	PASS	1.97	32.00	0.81	1.25	60	10	28	24	18	8	14.22	1	29.00	1.34	1.84	OK	11	8	8.69	1	1.28	OK
5	PASS	1.98	32.00	0.81	1.25	60	10	28	24	19	8	15.01	1	29.00	1.26	1.68	OK	10	8	7.9	1	1.53	OK
6	PASS	1.97	28.37	0.82	1.25	60	10	28	24	15	9	15.00	1.128	25.71	1.62	2.35	OK	8	9	8	1.128	2.10	OK
7	PASS	1.99	25.20	0.81	1.25	60	10	28	24	12	10	15.24	1.27	22.83	2.04	3.23	OK	6	10	7.62	1.27	3.23	OK
8	PASS	1.97	28.37	0.82	1.25	60	10	28	24	15	9	15.00	1.128	25.71	1.62	2.35	OK	8	9	8	1.128	2.10	OK
9	PASS	1.95	22.70	0.83	1.25	60	10	28	24	10	11	15.60	1.41	20.57	2.48	4.18	OK	5	11	7.8	1.41	4.18	OK
10	PASS	1.99	25.20	0.81	1.25	60	10	28	24	12	10	15.24	1.27	22.83	2.04	3.23	OK	6	10	7.62	1.27	3.23	OK

Transverse reinforcement in the joint (352R §4.2.2)									Transverse reinforcement into the beam									Transverse reinforcement into the column					
Spacing						Area			spacing in beam						length lo in beam			spacing in column			length lo in column		
sh/in	layout of ties	Tie diameter	Provide Ash	fyh,yield stress of tie	§4.2.2.3	Eq. (4.4), Ash	Eq. (4.5), Ash	If adequate	spacing	diameter	ACI318-14 18.6.4.4	ACI318-14 18.6.4.6	ACI318-14 18.6.4.2	ACI318-14 9.7.6.4.3	lo	clear span of column	ACI318-14 18.6.4.1	spacing	diameter	ACI318-14 25.7.2.1	lo	clear span of column	ACI318-14 18.7.5.1
4	4No.4@	0.5	0.8	60	OK	1.3058824	1.02	OK	4	0.5	OK	OK	OK	OK	110	120	OK	4	0.5	OK	20	120	OK
4	4No.4@	0.5	0.8	60	OK	1.3058824	1.02	OK	4	0.5	OK	OK	OK	OK	110	120	OK	4	0.5	OK	20	120	OK
4	4No.4@	0.5	0.8	60	OK	1.3058824	1.02	OK	4	0.5	OK	OK	OK	OK	110	120	OK	4	0.5	OK	20	120	OK
4	4No.4@	0.5	0.8	60	OK	1.3058824	1.02	OK	4	0.5	OK	OK	OK	OK	110	120	OK	4	0.5	OK	20	120	OK
4	4No.4@	0.5	0.8	60	OK	1.3058824	1.02	OK	4	0.5	OK	OK	OK	OK	110	120	OK	4	0.5	OK	20	120	OK
4	4No.4@	0.5	0.8	60	OK	1.3058824	1.02	OK	4	0.5	OK	OK	OK	OK	110	120	OK	4	0.5	OK	20	120	OK
4	4No.4@	0.5	0.8	60	OK	1.3058824	1.02	OK	4	0.5	OK	OK	OK	OK	110	120	OK	4	0.5	OK	20	120	OK
4	4No.4@	0.5	0.8	60	OK	1.3058824	1.02	OK	4	0.5	OK	OK	OK	OK	110	120	OK	4	0.5	OK	20	120	OK
4	4No.4@	0.5	0.8	60	OK	1.3058824	1.02	OK	4	0.5	OK	OK	OK	OK	110	120	OK	4	0.5	OK	20	120	OK
4	4No.4@	0.5	0.8	60	OK	1.3058824	1.02	OK	4	0.5	OK	OK	OK	OK	110	120	OK	4	0.5	OK	20	120	OK
4	4No.4@	0.5	0.8	60	OK	1.2857143	1.26	OK	4	0.5	OK	OK	OK	OK	110	120	OK	4	0.5	OK	24	120	OK
4	4No.4@	0.5	0.8	60	OK	1.2857143	1.26	OK	4	0.5	OK	OK	OK	OK	110	120	OK	4	0.5	OK	24	120	OK
4	4No.4@	0.5	0.8	60	OK	1.2857143	1.26	OK	4	0.5	OK	OK	OK	OK	110	120	OK	4	0.5	OK	24	120	OK
4	4No.4@	0.5	0.8	60	OK	1.2857143	1.26	OK	4	0.5	OK	OK	OK	OK	110	120	OK	4	0.5	OK	24	120	OK
4	4No.4@	0.5	0.8	60	OK	1.2857143	1.26	OK	4	0.5	OK	OK	OK	OK	110	120	OK	4	0.5	OK	24	120	OK
4	4No.4@	0.5	0.8	60	OK	1.2857143	1.26	OK	4	0.5	OK	OK	OK	OK	110	120	OK	4	0.5	OK	24	120	OK
4	4No.4@	0.5	0.8	60	OK	1.2857143	1.26	OK	4	0.5	OK	OK	OK	OK	110	120	OK	4	0.5	OK	24	120	OK
4	4No.4@	0.5	0.8	60	OK	1.2857143	1.26	OK	4	0.5	OK	OK	OK	OK	110	120	OK	4	0.5	OK	24	120	OK
4	4No.4@	0.5	0.8	60	OK	1.2857143	1.26	OK	4	0.5	OK	OK	OK	OK	110	120	OK	4	0.5	OK	24	120	OK
4	4No.4@	0.5	0.8	60	OK	1.2857143	1.26	OK	4	0.5	OK	OK	OK	OK	110	120	OK	4	0.5	OK	24	120	OK
4	4No.4@	0.5	0.8	60	OK	1.272	1.5	OK	4	0.5	OK	OK	OK	OK	110	120	OK	4	0.5	OK	28	120	OK
4	4No.4@	0.5	0.8	60	OK	1.272	1.5	OK	4	0.5	OK	OK	OK	OK	110	120	OK	4	0.5	OK	28	120	OK
4	4No.4@	0.5	0.8	60	OK	1.272	1.5	OK	4	0.5	OK	OK	OK	OK	110	120	OK	4	0.5	OK	28	120	OK
4	4No.4@	0.5	0.8	60	OK	1.272	1.5	OK	4	0.5	OK	OK	OK	OK	110	120	OK	4	0.5	OK	28	120	OK
4	4No.4@	0.5	0.8	60	OK	1.272	1.5	OK	4	0.5	OK	OK	OK	OK	110	120	OK	4	0.5	OK	28	120	OK
4	4No.4@	0.5	0.8	60	OK	1.272	1.5	OK	4	0.5	OK	OK	OK	OK	110	120	OK	4	0.5	OK	28	120	OK
4	4No.4@	0.5	0.8	60	OK	1.272	1.5	OK	4	0.5	OK	OK	OK	OK	110	120	OK	4	0.5	OK	28	120	OK
4	4No.4@	0.5	0.8	60	OK	1.272	1.5	OK	4	0.5	OK	OK	OK	OK	110	120	OK	4	0.5	OK	28	120	OK
4	4No.4@	0.5	0.8	60	OK	1.272	1.5	OK	4	0.5	OK	OK	OK	OK	110	120	OK	4	0.5	OK	28	120	OK
4	4No.4@	0.5	0.8	60	OK	1.272	1.5	OK	4	0.5	OK	OK	OK	OK	110	120	OK	4	0.5	OK	28	120	OK
4	4No.5@	0.625	1.24	60	OK	1.262069	1.74	OK	4	0.5	OK	OK	OK	OK	110	120	OK	4	0.5	OK	32	120	OK
4	4No.5@	0.625	1.24	60	OK	1.262069	1.74	OK	4	0.5	OK	OK	OK	OK	110	120	OK	4	0.5	OK	32	120	OK
4	4No.5@	0.625	1.24	60	OK	1.262069	1.74	OK	4	0.5	OK	OK	OK	OK	110	120	OK	4	0.5	OK	32	120	OK
4	4No.5@	0.625	1.24	60	OK	1.262069	1.74	OK	4	0.5	OK	OK	OK	OK	110	120	OK	4	0.5	OK	32	120	OK
4	4No.5@	0.625	1.24	60	OK	1.262069	1.74	OK	4	0.5	OK	OK	OK	OK	110	120	OK	4	0.5	OK	32	120	OK
4	4No.5@	0.625	1.24	60	OK	1.262069	1.74	OK	4	0.5	OK	OK	OK	OK	110	120	OK	4	0.5	OK	32	120	OK
4	4No.5@	0.625	1.24	60	OK	1.262069	1.74	OK	4	0.5	OK	OK	OK	OK	110	120	OK	4	0.5	OK	32	120	OK
4	4No.5@	0.625	1.24	60	OK	1.262069	1.74	OK	4	0.5	OK	OK	OK	OK	110	120	OK	4	0.5	OK	32	120	OK
4	4No.5@	0.625	1.24	60	OK	1.262069	1.74	OK	4	0.5	OK	OK	OK	OK	110	120	OK	4	0.5	OK	32	120	OK
4	4No.5@	0.625	1.24	60	OK	1.262069	1.74	OK	4	0.5	OK	OK	OK	OK	110	120	OK	4	0.5	OK	32	120	OK

No.	if pass ACI rules	Moment ratio: Mc/Mb	Development lengh/top bar diameter	Shear ratio: Vu/Vn	Joint shear															
					Slab					E-W beam				Required shear		Shear strength				
					Slab effective width	slab thickness	ACI 318-14 §6.3.2	slab bar included	slab bar area	a for Positive moment	Positive bending moment/k-in	a for Negative moment	Negative bending moment/k-in	Column shear/ kips	Required shear Vu/ kips	γ	m*hc/2	Effective joint width	shear capacity Vn/ kips	If Vu/Vn<0.85
1	PASS	1.67	26.67	0.81	76	6	OK	10No.3	1.1	0.31	3989.06	3.52	9350.28	92.63	583.87	20	2	18	720	OK
2	PASS	1.89	32.00	0.71	76	6	OK	10No.3	1.1	0.25	3283.32	3.17	8501.89	81.84	512.16	20	2	18	720	OK
3	PASS	1.68	20.00	0.81	76	6	OK	10No.3	1.1	0.28	3583.87	3.66	9682.39	92.13	582.87	20	2	18	720	OK
4	PASS	1.82	20.00	0.74	76	6	OK	10No.3	1.1	0.28	3583.87	3.22	8624.09	84.78	530.97	20	2	18	720	OK
5	PASS	1.90	32.00	0.71	76	6	OK	10No.3	1.1	0.22	2816.79	3.34	8921.40	81.52	512.48	20	2	18	720	OK
6	PASS	1.85	26.67	0.73	76	6	OK	10No.3	1.1	0.20	2666.11	3.52	9350.28	83.45	527.05	20	2	18	720	OK
7	PASS	1.68	26.67	0.81	76	6	OK	10No.3	1.1	0.26	3328.43	3.76	9933.07	92.09	584.41	20	2	18	720	OK
8	PASS	1.95	26.67	0.69	76	6	OK	10No.3	1.1	0.20	2666.11	3.28	8759.48	79.34	498.16	20	2	18	720	OK
9	PASS	1.66	26.67	0.81	76	6	OK	10No.3	1.1	0.36	4648.00	3.28	8759.48	93.11	583.39	20	2	18	720	OK
10	PASS	1.69	22.86	0.80	76	6	OK	10No.3	1.1	0.28	3628.92	3.58	9510.01	91.24	576.26	20	2	18	720	OK
1	PASS	1.69	24.00	0.84	76	6	OK	10No.3	1.1	0.55	7118.83	3.97	13037.43	139.97	890.53	20	2	22	1056	OK
2	PASS	1.91	32.00	0.74	76	6	OK	10No.3	1.1	0.46	5960.83	3.59	11907.44	124.09	783.41	20	2	22	1056	OK
3	PASS	1.76	21.28	0.80	76	6	OK	10No.3	1.1	0.58	7503.66	3.57	11854.29	134.43	848.07	20	2	22	1056	OK
4	PASS	1.95	27.43	0.73	76	6	OK	10No.3	1.1	0.35	4528.32	3.93	12907.29	121.08	771.42	20	2	22	1056	OK
5	PASS	1.90	24.00	0.75	76	6	OK	10No.3	1.1	0.46	5945.95	3.62	12000.33	124.63	787.37	20	2	22	1056	OK
6	PASS	1.98	32.00	0.71	76	6	OK	10No.3	1.1	0.41	5305.26	3.59	11907.44	119.53	754.97	20	2	22	1056	OK
7	PASS	1.78	21.28	0.80	76	6	OK	10No.3	1.1	0.46	6020.34	4.01	13167.23	133.25	849.25	20	2	22	1056	OK
8	PASS	1.94	27.43	0.73	76	6	OK	10No.3	1.1	0.42	5424.58	3.66	12119.53	121.83	770.67	20	2	22	1056	OK
9	PASS	1.91	24.00	0.75	76	6	OK	10No.3	1.1	0.37	4767.63	3.97	13037.43	123.65	788.35	20	2	22	1056	OK
10	PASS	1.78	21.28	0.80	76	6	OK	10No.3	1.1	0.46	6020.34	4.01	13167.23	133.25	849.25	20	2	22	1056	OK
1	PASS	1.88	24.82	0.81	76	6	OK	10No.3	1.1	0.70	8978.27	4.45	17311.23	182.57	1174.93	20	2	26	1456	OK
2	PASS	1.95	32.00	0.77	76	6	OK	10No.3	1.1	0.70	8978.27	4.15	16291.32	175.48	1122.02	20	2	26	1456	OK
3	PASS	1.80	22.05	0.84	76	6	OK	10No.3	1.1	0.74	9492.32	4.61	17852.14	189.89	1226.11	20	2	26	1456	OK
4	PASS	1.97	24.82	0.76	76	6	OK	10No.3	1.1	0.70	8978.27	4.08	16033.58	173.69	1108.81	20	2	26	1456	OK
5	PASS	1.96	32.00	0.77	76	6	OK	10No.3	1.1	0.63	8094.55	4.38	17057.91	174.67	1122.83	20	2	26	1456	OK
6	PASS	1.80	22.05	0.84	76	6	OK	10No.3	1.1	0.74	9492.32	4.61	17852.14	189.89	1226.11	20	2	26	1456	OK
7	PASS	1.92	28.00	0.79	76	6	OK	10No.3	1.1	0.64	8286.28	4.47	17387.01	178.29	1148.46	20	2	26	1456	OK
8	PASS	1.83	32.00	0.82	76	6	OK	10No.3	1.1	0.77	9858.85	4.38	17057.91	186.92	1200.58	20	2	26	1456	OK
9	PASS	1.84	28.00	0.82	76	6	OK	10No.3	1.1	0.73	9448.30	4.47	17387.01	186.36	1199.64	20	2	26	1456	OK
10	PASS	1.88	24.82	0.81	76	6	OK	10No.3	1.1	0.70	8978.27	4.45	17311.23	182.57	1174.93	20	2	26	1456	OK
1	PASS	1.99	25.20	0.81	76	6	OK	10No.3	1.1	0.88	11348.65	5.15	22948.00	238.17	1558.83	20	2	30	1920	OK
2	PASS	1.97	28.37	0.82	76	6	OK	10No.3	1.1	0.93	11901.36	5.07	22656.61	239.99	1567.51	20	2	30	1920	OK
3	PASS	1.93	22.70	0.83	76	6	OK	10No.3	1.1	1.09	13869.17	4.77	21477.41	245.46	1592.04	20	2	30	1920	OK
4	PASS	1.97	32.00	0.81	76	6	OK	10No.3	1.1	1.01	12901.75	4.83	21700.17	240.29	1560.46	20	2	30	1920	OK
5	PASS	1.98	32.00	0.81	76	6	OK	10No.3	1.1	0.92	11756.03	5.08	22668.78	239.06	1561.69	20	2	30	1920	OK
6	PASS	1.97	28.37	0.82	76	6	OK	10No.3	1.1	0.93	11901.36	5.07	22656.61	239.99	1567.51	20	2	30	1920	OK
7	PASS	1.99	25.20	0.81	76	6	OK	10No.3	1.1	0.88	11348.65	5.15	22948.00	238.17	1558.83	20	2	30	1920	OK
8	PASS	1.97	28.37	0.82	76	6	OK	10No.3	1.1	0.93	11901.36	5.07	22656.61	239.99	1567.51	20	2	30	1920	OK
9	PASS	1.95	22.70	0.83	76	6	OK	10No.3	1.1	0.91	11610.62	5.26	23382.54	243.01	1594.49	20	2	30	1920	OK
10	PASS	1.99	25.20	0.81	76	6	OK	10No.3	1.1	0.88	11348.65	5.15	22948.00	238.17	1558.83	20	2	30	1920	OK

Flexture §352R4.4															Development of reinforcement 352R §4.5						
Calculate Mn														352R §4.4.2	352R §4.5.2					352R §4.5.5	
Po/kip	Pn Axial load on column/ kips	β1	c/in	1st layer bar center	e4	e3	e2	e1	equation solver objective "0"	Mn about center	φ	φMn	largest tensile strain	If Moment ration>1.2	Development length/in	ldh Eq(4.10) Top bar	if OK	ldh Eq(4.10) Botto	if OK	h of column/db-beam bar	h of beam/d of column bar
4018	803.6	0.65	8.35	2.56	0.002069	0.00030	-0.00148	-0.002069	0.00	8905.67	0.81	7222.61	0.0032612	OK	17	7.50	OK	7.50	OK	OK	OK
4018	803.6	0.65	8.35	2.56	0.002069	0.00030	-0.00148	-0.002069	0.00	8905.67	0.81	7222.61	0.0032612	OK	17	6.25	OK	6.25	OK	OK	OK
4018	803.6	0.65	8.35	2.56	0.002069	0.00030	-0.00148	-0.002069	0.00	8905.67	0.81	7222.61	0.0032612	OK	17	10.00	OK	10.00	OK	OK	OK
4018	803.6	0.65	8.35	2.56	0.002069	0.00030	-0.00148	-0.002069	-0.69	8905.01	0.81	7223.56	0.0032644	OK	17	10.00	OK	10.00	OK	OK	OK
4018	803.6	0.65	8.35	2.56	0.002069	0.00030	-0.00148	-0.002069	0.00	8905.67	0.81	7222.61	0.0032612	OK	17	6.25	OK	6.25	OK	OK	OK
4018	803.6	0.65	8.35	2.56	0.002069	0.00030	-0.00148	-0.002069	0.00	8905.67	0.81	7222.61	0.0032612	OK	17	7.50	OK	7.50	OK	OK	OK
4018	803.6	0.65	8.35	2.56	0.002069	0.00030	-0.00148	-0.002069	0.00	8905.67	0.81	7222.61	0.0032612	OK	17	7.50	OK	7.50	OK	OK	OK
4018	803.6	0.65	8.35	2.56	0.002069	0.00030	-0.00148	-0.002069	0.00	8905.67	0.81	7222.61	0.0032612	OK	17	7.50	OK	7.50	OK	OK	OK
4018	803.6	0.65	8.35	2.56	0.002069	0.00030	-0.00148	-0.002069	0.00	8905.67	0.81	7222.61	0.0032612	OK	17	7.50	OK	7.50	OK	OK	OK
4018	803.6	0.65	8.35	2.56	0.002069	0.00030	-0.00148	-0.002069	0.00	8905.67	0.81	7222.61	0.0032612	OK	17	8.75	OK	8.75	OK	OK	OK
5514	1102.8	0.65	9.42	2.56	0.002069	0.00018	-0.00182	-0.002069	0.00	13626.45	0.84	11445.57	0.0038267	OK	21	10.00	OK	10.00	OK	OK	OK
5514	1102.8	0.65	9.42	2.56	0.002069	0.00018	-0.00182	-0.002069	0.00	13626.45	0.84	11445.57	0.0038267	OK	21	7.50	OK	7.50	OK	OK	OK
5514	1102.8	0.65	9.42	2.56	0.002069	0.00018	-0.00182	-0.002069	0.00	13626.45	0.84	11445.57	0.0038267	OK	21	11.28	OK	11.28	OK	OK	OK
5514	1102.8	0.65	9.42	2.56	0.002069	0.00018	-0.00182	-0.002069	0.00	13626.45	0.84	11445.57	0.0038267	OK	21	8.75	OK	8.75	OK	OK	OK
5514	1102.8	0.65	9.42	2.56	0.002069	0.00018	-0.00182	-0.002069	0.00	13626.45	0.84	11445.57	0.0038267	OK	21	10.00	OK	10.00	OK	OK	OK
5514	1102.8	0.65	9.42	2.56	0.002069	0.00018	-0.00182	-0.002069	0.00	13626.45	0.84	11445.57	0.0038267	OK	21	7.50	OK	7.50	OK	OK	OK
5514	1102.8	0.65	9.42	2.56	0.002069	0.00018	-0.00182	-0.002069	0.00	13626.45	0.84	11445.57	0.0038267	OK	21	11.28	OK	11.28	OK	OK	OK
5514	1102.8	0.65	9.42	2.56	0.002069	0.00018	-0.00182	-0.002069	0.00	13626.45	0.84	11445.57	0.0038267	OK	21	8.75	OK	8.75	OK	OK	OK
5514	1102.8	0.65	9.42	2.56	0.002069	0.00018	-0.00182	-0.002069	0.00	13626.45	0.84	11445.57	0.0038267	OK	21	10.00	OK	10.00	OK	OK	OK
5514	1102.8	0.65	9.42	2.56	0.002069	0.00018	-0.00182	-0.002069	0.00	13626.45	0.84	11445.57	0.0038267	OK	21	11.28	OK	11.28	OK	OK	OK
7282	1456.4	0.65	10.49	2.56	0.002069	0.00009	-0.002069	-0.002069	0.00	19718.47	0.86	17016.04	0.004276	OK	25	11.28	OK	11.28	OK	OK	OK
7282	1456.4	0.65	10.49	2.56	0.002069	0.00009	-0.002069	-0.002069	0.00	19718.47	0.86	17016.04	0.004276	OK	25	8.75	OK	8.75	OK	OK	OK
7282	1456.4	0.65	10.49	2.56	0.002069	0.00009	-0.002069	-0.002069	0.00	19718.47	0.86	17016.04	0.004276	OK	25	12.70	OK	12.70	OK	OK	OK
7282	1456.4	0.65	10.49	2.56	0.002069	0.00009	-0.002069	-0.002069	0.00	19718.47	0.86	17016.04	0.004276	OK	25	11.28	OK	11.28	OK	OK	OK
7282	1456.4	0.65	10.49	2.56	0.002069	0.00009	-0.002069	-0.002069	0.00	19718.47	0.86	17016.04	0.004276	OK	25	8.75	OK	8.75	OK	OK	OK
7282	1456.4	0.65	10.49	2.56	0.002069	0.00009	-0.002069	-0.002069	0.00	19718.47	0.86	17016.04	0.004276	OK	25	12.70	OK	12.70	OK	OK	OK
7282	1456.4	0.65	10.49	2.56	0.002069	0.00009	-0.002069	-0.002069	0.00	19718.47	0.86	17016.04	0.004276	OK	25	10.00	OK	10.00	OK	OK	OK
7282	1456.4	0.65	10.49	2.56	0.002069	0.00009	-0.002069	-0.002069	0.00	19718.47	0.86	17016.04	0.004276	OK	25	8.75	OK	8.75	OK	OK	OK
7282	1456.4	0.65	10.49	2.56	0.002069	0.00009	-0.002069	-0.002069	0.00	19718.47	0.86	17016.04	0.004276	OK	25	10.00	OK	10.00	OK	OK	OK
7282	1456.4	0.65	10.49	2.56	0.002069	0.00009	-0.002069	-0.002069	0.00	19718.47	0.86	17016.04	0.004276	OK	25	11.28	OK	11.28	OK	OK	OK
9322	1864.4	0.65	11.43	2.69	0.002069	-0.00004	-0.002069	-0.002069	0.00	27242.64	0.88	24092.54	0.0046946	OK	29	12.70	OK	12.70	OK	OK	OK
9322	1864.4	0.65	11.43	2.69	0.002069	-0.00004	-0.002069	-0.002069	0.00	27242.64	0.88	24092.54	0.0046946	OK	29	11.28	OK	11.28	OK	OK	OK
9322	1864.4	0.65	11.43	2.69	0.002069	-0.00004	-0.002069	-0.002069	0.00	27242.64	0.88	24092.54	0.0046946	OK	29	14.10	OK	14.10	OK	OK	OK
9322	1864.4	0.65	11.43	2.69	0.002069	-0.00004	-0.002069	-0.002069	0.00	27242.64	0.88	24092.54	0.0046946	OK	29	10.00	OK	10.00	OK	OK	OK
9322	1864.4	0.65	11.43	2.69	0.002069	-0.00004	-0.002069	-0.002069	0.00	27242.64	0.88	24092.54	0.0046946	OK	29	10.00	OK	10.00	OK	OK	OK
9322	1864.4	0.65	11.43	2.69	0.002069	-0.00004	-0.002069	-0.002069	0.00	27242.64	0.88	24092.54	0.0046946	OK	29	11.28	OK	11.28	OK	OK	OK
9322	1864.4	0.65	11.43	2.69	0.002069	-0.00004	-0.002069	-0.002069	0.00	27242.64	0.88	24092.54	0.0046946	OK	29	12.70	OK	12.70	OK	OK	OK
9322	1864.4	0.65	11.43	2.69	0.002069	-0.00004	-0.002069	-0.002069	0.00	27242.64	0.88	24092.54	0.0046946	OK	29	11.28	OK	11.28	OK	OK	OK
9322	1864.4	0.65	11.43	2.69	0.002069	-0.00004	-0.002069	-0.002069	0.00	27242.64	0.88	24092.54	0.0046946	OK	29	14.10	OK	14.10	OK	OK	OK
9322	1864.4	0.65	11.43	2.69	0.002069	-0.00004	-0.002069	-0.002069	0.00	27242.64	0.88	24092.54	0.0046946	OK	29	12.70	OK	12.70	OK	OK	OK

Bibliography:

ACI318-14 (2014)."Building code requirements for structural concrete (ACI 318-14) and commentary." *ACI 318-14*. American Concrete Institute.

ACI352R-02 (2002)."Recommendations for Design of Beam-Column Connections in Monolithic Reinforced Concrete Structures.". *ACI352R-02*. Farmington Hills, Michigan, ACI-ASCE Committee 352, American Concrete Institute.

ACI408.2R-12 (2012)."Development and Splicing of Deformed Bars." ACI-ASCE Committee 408.

Al-Nahlawi, K. A. and J. K. Wight (1992). "Beam analysis using concrete tensile strength in truss models." *Structural Journal*, 89(3): 284-290.

Alaee, P., B. Li and P. P. C. Cheung (2015). "Parametric investigation of 3D RC beam-column joint mechanics." *Magazine of Concrete Research*, 67(19): 1054-1069.

Alath, S. (1995). "Modeling inelastic shear deformation in reinforced concrete beam-column joints." University of Central Florida, Master Degree.

Altoontash, A. and G. G. Deierlein (2003). "A Versatile Model for Beam-Column Joints." *ASCE Structures Congress Proceedings*, Seattle, Washington.

Anderson, M., D. Lehman and J. Stanton (2008). "A cyclic shear stress-strain model for joints without transverse reinforcement." *Engineering Structures*, 30(4): 941-954.

Ayoub, A. and F. C. Filippou (1999). "Mixed formulation of bond-slip problems under cyclic loads." *Journal of Structural Engineering*, 125(6): 661-671.

Bao, Y., H. S. Lew and S. K. Kunnath (2014). "Modeling of Reinforced Concrete Assemblies under Column-Removal Scenario." *Journal of Structural Engineering*, 140(1): 04013026.

Bartelletti, R., M. L. Beconcini, A. Favilli, P. Formichi, M. Froli and R. Nicotera (2004). "Ricerca sperimentale su nodi di telai in cemento armato sotto azioni cicliche." *Atti 11° Congr. Naz." L'Ingegneria Sismica in Italia"*, Genova, Gennaio.

Bažant, Z. P. (1991). "Why continuum damage is nonlocal: Micromechanics arguments." *Journal of Engineering Mechanics*, 117(5): 1070-1087.

Bažant, Z. P. (2002). "Concrete fracture models: testing and practice." *Engineering fracture mechanics*, 69(2): 165-205.

Bažant, Z. P. and B. H. Oh (1983). "Crack band theory for fracture of concrete." *Matériaux et construction*, 16(3): 155-177.

Bazant, Z. P. and J. Planas (1997). "Size effect in concrete specimens and structures: New problems and progress." *Fracture Mechanics of Concrete Structures (Proc., FraMCoS-5, 5th Int. Conf. on Fracture Mech. of Concrete and Concr. Structures, Vail, Colo.)*, CRC press, 1.

Beckingsale, C. W. (1980). "Post elastic behaviour of reinforced concrete beam-column joints." University of Canterbury, Ph.D. Degree.

Belytschko, T. and L. P. Bindeman (1993). "Assumed strain stabilization of the eight node hexahedral element." *Computer Methods in Applied Mechanics and Engineering*, 105(2): 225-260.

Beres, A., S. P. Pessiki, R. N. White and P. Gergely (1996). "Implications of experiments on the seismic behavior of gravity load designed RC beam-to-column connections." *Earthquake Spectra*, 12(2): 185-198.

Bertero, V. V. and S. A. Mahin (1978). "Earthquake-resistant reinforced concrete building construction. Volume 2: Technical Papers." *Proceedings of a Workshop*, University of California: Berkeley, June 11-15.

Biddah, A. and A. Ghobarah (1999). "Modelling of shear deformation and bond slip in reinforced concrete joints." *Structural Engineering and Mechanics*, 7(4): 413-432.

Bonacci, J. and S. Pantazopoulou (1993). "Parametric investigation of joint mechanics." *ACI structural journal*, 90: 61-61.

Bowers, J. T. (2014). "Nonlinear cyclic truss model for beam-column joints of non-ductile RC frames." Virginia Tech, Master Degree.

Caner, F. C. and Z. P. Bažant (2012). "Microplane model M7 for plain concrete. I: Formulation." *Journal of Engineering Mechanics*, 139(12): 1714-1723.

Cofer, W. F. (1999)."Documentation of strengths and weaknesses of current computer analysis methods for seismic performance of reinforced concrete members." University of California, Berkeley**:** 39.

Conley, C. (1993). " "Chapter 9 - specific applications," in Finite Element Analysis of Reinforced Concrete Structures II." *Proceedings of the Int'l Workshop*, New York, NY, Isenberg, J., ed. ASCE.

Cox, J. V. and L. R. Herrmann (1998). "Development of a plasticity bond model for steel reinforcement." *Mechanics of Cohesive‐frictional Materials: An International Journal on Experiments, Modelling and Computation of Materials and Structures*, 3(2): 155-180.

Daoud, A., O. Maurel and C. Laborderie (2012). "Mesoscopic modeling of the interaction between steel reinforcement and the early-age cracking during cement hydration." *Bond in Concrete*.

Darwin, D. and D. A. Pecknold (1977). "Nonlinear biaxial stress-strain law for concrete." *Journal of the Engineering Mechanics Division*, 103(2): 229-241.

Deaton, J. B. (2013). "Nonlinear finite element analysis of reinforced concrete exterior beam-column joints with nonseismic detailing." Georgia Institute of Technology, Ph.D. Degree.

Dodd, L. and J. Restrepo-Posada (1995). "Model for predicting cyclic behavior of reinforcing bar." *Journal of Structural Engineering*, 121(3): 433-445.

Durrani, A. J. and J. K. Wight (1982). "Experimental and analytical study of internal beam to column connections subjected to reversed cyclic loading." Michigan University, Ann Arbor, Ph.D. Degree.

Eligehausen, R., G. Genesio, J. Ozbolt and S. Pampanin (2008). "3D analysis of seismic response of RC beam-column exterior joints before and after retrofit." *Concrete Repair, Rehabilitation and Retrofitting II; CRC Press*, Boca Raton, FL, USA.

Eligehausen, R., J. Ozbolt, G. Genesio, M. Hoehler and S. Pampanin (2006). "Three-dimensional modelling of poorly detailed RC frame joints." *NZSEE conference: Remembering Napier 1931 - Building on 75 Years of Earthquake Engineering*, NZ. OAI.

Eligehausen, R., E. Popov and V. Bertero (1983)."Local bond stress-slip relationships of deformed bars under generalized excitations." University of California, Berkeley, CA, USA, Report No. UCB/EERC-83/23 27.

Elmorsi, S. E. M. (1998). "Analytical modeling of reinforced concrete beam column connections for seismic loading." Ph.D. Degree.

Eurocode8 (2004)."Eurocode 8: Design of structures for earthquake resistance-Part 1: General rules, seismic actions and rules for buildings." *BS EN 1998-1:2004*.

Feng, D.-C. and J. Xu (2018). "An efficient fiber beam-column element considering flexure-shear interaction and anchorage bond-slip effect for cyclic analysis of RC structures." *Bulletin of Earthquake Engineering*: 1-28.

fib (2000)."State of the art Bulletin 10: Bond of reinforcement in concrete." International Federation for Structural Concrete (fib).

Filippou, F. C., E. P. Popov and V. V. Bertero (1983). "Modeling of R/C joints under cyclic excitations." *Journal of Structural Engineering*, 109(11): 2666-2684.

Flanagan, D. and T. Belytschko (1981). "A uniform strain hexahedron and quadrilateral with orthogonal hourglass control." *International journal for numerical methods in engineering*,

17(5): 679-706.

Fleury, F., J. Reynouard and O. Merabet (1999). "Finite element implementation of a steel-concrete bond law for nonlinear analysis of beam-column joints subjected to earthquake type loading." *Structural Engineering and Mechanics*, 7(1): 35-52.

Fujii, S. and S. Morita (1991). "Comparison Between Interior and Exterior R/C Beam-Column Joint Behavior." *Special Publication*, 123: 145-166.

GB50011- (2010). "GB50011-2010: Code for seismic design of buildings (edition of 2016)."

Goto, Y. and O. Joh (2004). "Shear resistance of RC interior eccentric beam-column joints." *13 th World Conference on Earthquake Engineering*, Vancouver, B.C., Canada, Paper No. 649, August 1-6.

Goto, Y., O. Joh and S. T (1997). "An experimental study of shear failure mechanism of RC interior beamcolumn joints." *Concrete Research & Technology*, 8(2): 39-49.

H. Sezen, J. E., A. Whittaker, K. Mosalam, J. Wallace, J. Stanton (2000)."Structural Engineering Reconnaissance of the August 17, 1999 Earthquake: Kocaeli (Izmit), Turkey." 2000/09.

Hanson, N. W. and H. W. Conner (1967). "Seismic resistance of reinforced concrete beam-column joints." *Journal of the Structural Division*, 93(5): 533-560.

Hawileh, R., A. Rahman and H. Tabatabai (2010). "Nonlinear finite element analysis and modeling of a precast hybrid beam-column connection subjected to cyclic loads." *Applied Mathematical Modelling*, 34(9): 2562-2583.

Hegger, J., A. Sherif and W. Roeser (2004). "Nonlinear finite element analysis of reinforced concrete beam-column connections." *Structural Journal*, 101(5): 604-614.

Hiraishi, H. (1984). "Evaluation of shear and flexural deformations of flexural type shear walls." *Bulletin of the New Zealand National Society for Earthquake Engineering*, 17(2): 135-144.

Hoshikuma, J., K. Kawashima, K. Nagaya and A. Taylor (1997). "Stress-strain model for confined reinforced concrete in bridge piers." *Journal of Structural Engineering*, 123(5): 624-633.

Hsu, T. T. (1996). "Toward a unified nomenclature for reinforced-concrete theory." *Journal of Structural Engineering*, 122(3): 275-283.

Hughes, T. J. and W. K. Liu (1981). "Nonlinear finite element analysis of shells: Part I. Three-dimensional shells." *Computer Methods in Applied Mechanics and Engineering*, 26(3): 331-362.

Ihzuka, T. (1992). "Nonlinear finite element analysis of reinforced concrete members with normal to high strength materials." *Proceedings of the JCI*, 14(2): 9-14.

Jirsa, J. O. (1991). "Design of Beam-Column Joints for Seismic Resistance." *American Concrete Institute*, Detroit, USA, SP-123.

Joh, O., Y. Goto and T. Shibata (1991). "Influence of Transverse Joint and Beam Reinforcement and Relocation of Plastic Hinge Region onBeam Column Joint Stiffness Deterioration." *Special Publication*, 123: 187-224.

Kamimura, T., S. Takeda and M. Tochio (2000). "Influence of joint reinforcement on strength and deformation of interior beam-column subassemblages." *12th World Conference on Earthquake Engineering*.

Kang, H. D., K. Willam, B. Shing and E. Spacone (2000). "Failure analysis of R/C columns using a triaxial concrete model." *Computers & structures*, 77(5): 423-440.

Kashiwazaki, T. and H. Noguchi (2004). "Seismic performance evaluation of RC eccentric beam-column joints using three-dimensional FEM analysis." *13th World Conference on Earthquake Engineering*, Vancouver, B.C., Canada Paper No. 1354, August 1-6.

Kazuhiro, K., O. Shunsuke and A. Hiroyuki (1991). "Development of design criteria for RC interior beam-column joints." *Special Publication*, 123: 97-124.

Kim, J. and J. M. LaFave (2007). "Key influence parameters for the joint shear behaviour of reinforced concrete (RC) beam-column connections." *Engineering Structures*, 29(10): 2523-2539.

Kim, S.-W. and F. J. Vecchio (2008). "Modeling of shear-critical reinforced concrete structures repaired with fiber-reinforced polymer composites." *Journal of Structural Engineering*, 134(8): 1288-1299.

Kim, S., F. Kusuhara and H. Shiohara (2017). "Analysis of RC slab-beam-column subassemblages subjected to bidirectional lateral cyclic loading using a new 3 D macroelement." *Earthquake Engineering & Structural Dynamics*, 46(14): 2519-2536.

Kim, S. H. and I. Koutromanos (2016). "Constitutive Model for Reinforcing bar under Cyclic Loading." *Journal of Structural Engineering*, 142(12): 04016133.

Kitayama, K. (1992). "Restoring force characteristics in reinforced concrete beam-column joints." *Trans JCI*, 14: 491-498.

Kitayama, K., S. Otani and H. Aoyama (1987). "Earthquake resistant design criteria for reinforced concrete interior beam-column joints." *Pacific Conference on Earthquake Engineering*, Wairakei, New Zealand.

Kitayama, K., S. OTANI and H. AOYAMA (1988). "Behavior of Reinforced Concrete Beam-Column-Slab Subassemblages Subjected to Bi-directional Load Reversals." *Proceedings of*

Ninth World Conference on Earthquake Engineering, Tokyo-Kyoto, Japan, VIII, August 2-9.

Koutromanos, Ioannis, Stavridis, Andreas, B. Shing, Willam and Kaspar (2011). "Numerical modeling of masonry-infilled RC frames subjected to seismic loads." *Computers & structures*, 89(11): 1026-1037.

Koutromanos, I. and P. B. Shing (2012). "Cohesive Crack Model to Simulate Cyclic Response of Concrete and Masonry Structures." *ACI Structural Journal*, 109(3): 349-358.

Kurose, Y., G. N. Guimaraes, Z. Liu, M. E. Kreger and J. O. Jirsa (1988). "Study of Reinforced Concrete Beam-Column Joints Under Uniaxial and Biaxial Loading." *PMFSEL report*.

Kwak, H.-G. and F. C. Filippou (1990). "Finite element analysis of reinforced concrete structures under monotonic loads." Department of Civil Engineering, University of California Berkeley, CA.

Lee, J. and G. L. Fenves (1998). "Plastic-damage model for cyclic loading of concrete structures." *Journal of Engineering Mechanics*, 124(8): 892-900.

Leon, R. and J. O. Jirsa (1986). "Bidirectional loading of RC beam-column joints." *Earthquake Spectra*, 2(3): 537-564.

Leon, R. T. (1985). "The influence of floor members on the behavior of reinforced concrete beam-column joints subjected to severe cyclic loading." University of Texas, Ph.D. Degree.

Leon, R. T. (1989). "Interior joints with variable anchorage lengths." *Journal of Structural Engineering*, 115(9): 2261-2275.

Leon, R. T. (1990). "Shear strength and hysteretic behavior of interior beam-column joints." *Structural Journal*, 87(1): 3-11.

Leon, R. T., W. Y. Kam and S. Pampanin (2014). "Performance of Beam-Column Joints in the 2010-2012 Christchurch Earthquakes." *Special Publication*, 296: 1-20.

Li, B., C. T. N. Tran and T.-C. Pan (2009). "Experimental and numerical investigations on the seismic behavior of lightly reinforced concrete beam-column joints." *Journal of Structural Engineering*, 135(9): 1007-1018.

Li, B., Y. Wu and T. C. Pan (2003). "Seismic behavior of nonseismically detailed interior beam-wide column joints Part II: Theoretical comparisons and analytical studies." *ACI Structural Journal*, 100(1): 56.

Lotfi, H. and P. Shing (1991). "An appraisal of smeared crack models for masonry shear wall analysis." *Computers & structures*, 41(3): 413-425.

Lotfi, H. R. and P. B. Shing (1994). "Interface model applied to fracture of masonry structures."

Journal of Structural Engineering, 120(1): 63-80.

Lowes, L. N. and A. Altoontash (2003). "Modeling reinforced-concrete beam-column joints subjected to cyclic loading." *Journal of Structural Engineering*, 129(12): 1686-1697.

Lowes, L. N., J. P. Moehle and S. Govindjee (2004). "Concrete-steel bond model for use in finite element modeling of reinforced concrete structures." *Structural Journal*, 101(4): 501-511.

Lu, Y. and M. Panagiotou (2014). "Three-Dimensional Cyclic Beam-Truss Model for Nonplanar Reinforced Concrete Walls." *Journal of Structural Engineering*, 140(3): 04013071.

Lu, Y., M. Panagiotou and I. Koutromanos (2016). "Three‐dimensional beam‐truss model for reinforced concrete walls and slabs-part 1: modeling approach, validation, and parametric study for individual reinforced concrete walls." *Earthquake Engineering & Structural Dynamics*, 45(9): 1495-1513.

Lu, Y. J. (2014). "Three-dimensional Seismic Analysis of Reinforced Concrete Wall Buildings at Near-fault Sites." University of California, Berkeley.

Lubliner, J., J. Oliver, S. Oller and E. Onate (1989). "A plastic-damage model for concrete." *International Journal of Solids and Structures*, 25(3): 299-326.

Malvar, L. J., J. E. Crawford, J. W. Wesevich and D. Simons (1997). "A plasticity concrete material model for DYNA3D." *International journal of impact engineering*, 19(9-10): 847-873.

Mander, J. B., M. J. Priestley and R. Park (1988). "Theoretical stress-strain model for confined concrete." *Journal of Structural Engineering*, 114(8): 1804-1826.

Mazars, J., P. Kotronis and L. Davenne (2002). "A new modelling strategy for the behaviour of shear walls under dynamic loading." *Earthquake Engineering & Structural Dynamics*, 31(4): 937-954.

Mazars, J., G. Pijaudier-Cabot and J. Clement (1992). "Analysis of steel-concrete bond with damage mechanics: non linear behaviour and size effect." *Applications of Fracture Mechanics to Reinforced Concrete*: 307-331.

Meinheit, D. and J. O. Jirsa (1977)."The shear strength of beam-column joints." CERSL Report No. 77.

Menengotto, M. (1973). "Method of Analysis for Cyclically Loaded Reinforced Concrete Plane Frames Including Changes in Geometry and Nonelastic Behavior of Elements under Combined Normal Force and Bending." *IABSE Symposium on Resistance and Ultimate Deformability of Structures*.

Miki, T. and J. Niwa (2004). "Nonlinear analysis of RC structural members using 3D lattice model." *Journal of Advanced Concrete Technology*, 2(3): 343-358.

Mitra, N. and L. N. Lowes (2007). "Evaluation, calibration, and verification of a reinforced concrete beam-column joint model." *Journal of Structural Engineering*, 133(1): 105-120.

Moharrami, M. and I. Koutromanos (2016). "Triaxial Constitutive Model for Concrete under Cyclic Loading." *Journal of Structural Engineering*, 142(7): 04016039.

Moharrami, M. and I. Koutromanos (2017). "Finite element analysis of damage and failure of reinforced concrete members under earthquake loading." *Earthquake Engineering & Structural Dynamics*, 46(15): 2811-2829.

Moharrami, M., I. Koutromanos and M. Panagiotou (2015). "Nonlinear Truss Modeling Method for the Analysis of Shear Failures in Reinforced Concrete and Masonry Structures." Improving the Seismic Performance of Existing Buildings and Other Structures 2015. 74-85.

Moharrami, M., I. Koutromanos, M. Panagiotou and S. C. Girgin (2015). "Analysis of shear‐dominated RC columns using the nonlinear truss analogy." *Earthquake Engineering & Structural Dynamics*, 44(5): 677-694.

Moharrami, M. G. (2016). "Development of Novel Computational Simulation Tools to Capture the Hysteretic Response and Failure of Reinforced Concrete Structures under Seismic Loads." Virginia Tech, Ph.D. Degree.

Monti, G., F. C. Filippou and E. Spacone (1997). "Finite element for anchored bars under cyclic load reversals." *Journal of Structural Engineering*, 123(5): 614-623.

Monti, G. and E. Spacone (2000). "Reinforced concrete fiber beam element with bond-slip." *Journal of Structural Engineering*, 126(6): 654-661.

Morita, S. (1975). "Bond-slip relationship under repeated loading." *Trans. Archit Inst. Jpn.*, 229: 15-24.

Murcia-Delso, J. and B. P. Shing (2014). "Bond-Slip Model for Detailed Finite-Element Analysis of Reinforced Concrete Structures." *Journal of Structural Engineering*, 141(4): 04014125.

Murcia-Delso, J., A. Stavridis and P. B. Shing (2013). "Bond strength and cyclic bond deterioration of large-diameter bars." *ACI Structural Journal*, 110(4): 659.

Murray, Y. (2007)."User's manual for LS-DYNA material model 159." McLean, VA.

Naganuma, K. and M. Ohkubo (2000). "An analytical model for reinforced concrete panels under cyclic stresses." *J. Struct. Constr. Eng*, 536: 135-142.

Ngo, D. and A. Scordelis (1967). "Finite element analysis of reinforced concrete beams." *Journal Proceedings*, 64.

Nguyen, G. D. and A. M. Korsunsky (2008). "Development of an approach to constitutive modelling of concrete: isotropic damage coupled with plasticity." *International Journal of Solids and Structures*, 45(20): 5483-5501.

Noguchi, H. (1981). "Nonlinear finite element analysis of reinforced concrete beam-column joints." *Final report of IABSE colloquium*.

Noguchi, H. and T. Kashiwazaki (1992). "Experimental studies on shear performances of RC interior column-beam joints with high-strength materials." *10 th World Conference on Earthquake Engineering*.

Noguchi, H. and T. Kashiwazaki (2004). "FEM analysis of structural performance deterioration of RC elements subjected to seismic reversed cyclic shear." *13th World Conference on Earthquake Engineering*, Vancouver, B.C., Canada, 672, August 1-6.

Noguchi, H., T. Kashiwazaki and J. Hong (2008). "FEM analysis of three-dimensional interaction of RC frames subjected to multi-directional cyclic loading." *The 14th World Conference on Earthquake Engineering*, Beijing, China, October 12-17.

NZS3101:Part1: (2006)."New Zealand Standard Concrete Structures Standard Part 1 The Design of Concrete Structures."

Oka, K. and H. Shiohara (1992). "Tests on high-strength concrete interior beam-column joint subassemblages." *Tenth World Conference on Earthquake Engineering*, Madrid, Spain.

Okamura, H. and A. Pimanmas (2003). "Nonlinear Mechanics of Reinforced Concrete." Taylor & Francis.

Ožbolt, J., Y. Li and I. Kožar (2001). "Microplane model for concrete with relaxed kinematic constraint." *International Journal of Solids and Structures*, 38(16): 2683-2711.

Pagni, C. and L. N. Lowes (2004)."Predicting earthquake damage in older reinforced concrete beam-column joints." University of Berkeley.

Pampanin, S., G. Magenes and A. J. Carr (2003). "Modelling of shear hinge mechanism in poorly detailed RC beam-column joints."

Panagiotou, M., J. I. Restrepo, M. Schoettler and G. Kim (2012). "Nonlinear cyclic truss model for reinforced concrete walls." *ACI Structural Journal*, 109(2): 205.

Pantazopoulou, S. and J. Bonacci (1994). "On earthquake-resistant reinforced concrete frame connections." *Canadian Journal of Civil Engineering*, 21(2): 307-328.

Park, H. and T. Eom (2007). "Truss model for nonlinear analysis of RC members subject to cyclic loading." *Journal of Structural Engineering*, 133(10): 1351-1363.

Park, R., M. Priestley and W. D. Gill (1982). "Ductility of square-confined concrete columns." *Journal of the Structural Division*, 108(4): 929-950.

Park, S. and K. Mosalam (2009). "Shear strength models of exterior beam-column joints without transverse reinforcement." *PEER report*, 106.

Peng, B. H., R. P. Dhakal, R. C. Fenwick and A. J. Carr (2011). "Elongation of plastic hinges in ductile RC members: model development." *Journal of Advanced Concrete Technology*, 9(3): 315-326.

Pochanart, S. and T. Harmon (1989). "Bond-slip model for generalized excitations including fatigue." *Materials Journal*, 86(5): 465-474.

Rehm, G. (1961). "Uber die Grunlagen des Verbundes Zwischen Stahl und Beton." *Deutscher Ausschuss fur Stahl-beton*, 138: 59.

Reinhardt, H., J. Blaauwendraad and E. Vos (1984). "Prediction of bond between steel and concrete by numerical analysis." *Matériaux et construction*, 17(4): 311.

Richart, F. E., A. Brandtzaeg and R. L. Brown (1928)."A study of the failure of concrete under combined compressive stresses."

Ritter, W. (1899). "Die bauweise hennebique." *Schweizerische Bauzeitung*, 33(7): 59-61.

Rots, J. G. and J. Blaauwendraad (1989). "Crack models for concrete, discrete or smeared? Fixed, multi-directional or rotating?" *HERON*, 34(1).

Saenz, L. P. (1964). "discussion of" Equation for the Stress-Strain Curve of Concrete" by Desayi and Krishnan." *Journal of the American Concrete Institute*, 61: 1229-1235.

Sagbas, G., F. Vecchio and C. Christopoulos (2011). "Computational modeling of the seismic performance of beam-column subassemblies." *Journal of Earthquake Engineering*, 15(4): 640-663.

Santos, J. and A. Henriques (2012). "FE modelling of bond-slip response including steel strains." *Proceedings of Bond in Concrete*.

Sato, T. S. "N.(1978): Elasto-Plastic Behavior of RC Shear Walls." *Summaries of Technical Papers of Annual Meeting*, C-2.

Schlaich, J., K. Schäfer and M. Jennewein (1987). "Toward a consistent design of structural concrete." *PCI journal*, 32(3): 74-150.

Selby, R. and F. Vecchio (1997). "A constitutive model for analysis of reinforced concrete solids." *Canadian Journal of Civil Engineering*, 24(3): 460-470.

Serpieri, R. and G. Alfano (2011). "Bond‐slip analysis via a thermodynamically consistent interface model combining interlocking, damage and friction." *International journal for numerical methods in engineering*, 85(2): 164-186.

Sharma, A., R. Eligehausen and G. Reddy (2011). "A new model to simulate joint shear behavior of poorly detailed beam-column connections in RC structures under seismic loads, Part I: Exterior joints." *Engineering Structures*, 33(3): 1034-1051.

Shin, M. and J. M. LaFave (2004). "Modeling of cyclic joint shear deformation contributions in RC beam-column connections to overall frame behavior." *Structural Engineering and Mechanics*, 18(5): 645-669.

Spencer, B. and P. Shing (2002). "Stress Hybrid Embedded Crack Element Analysis for Concrete Fracture." *Special Publication*, 205: 323-346.

Sritharan, S., M. N. Priestley and F. Seible (2000). "Nonlinear finite element analyses of concrete bridge joint systems subjected to seismic actions." *Finite elements in analysis and design*, 36(3-4): 215-233.

Stevens, N. J., S. Uzumeri and G. Will (1991). "Constitutive model for reinforced concrete finite element analysis." *Structural Journal*, 88(1): 49-59.

Supaviriyakit, T., A. Pimanmas and P. Warnitchai (2007). "Cyclic response of non-seismically detailed interior RC beam-column connection with varying column tributary area." *Magazine of Concrete Research*, 59(5): 351-365.

Tajima, K., T. Mishima and N. Shirai (2004). "3-D Finite Element Cyclic Analysis of RC Beam/Column Joint using Special Bond Model." *13th World Conference on Earthquake Engineering*, Vancouver, BC, Canada.

Tajima, Y., K. Kitayama, M. Okuda and S. Kishida (2000). "Influences of beam and column bar bond on failure mechanism in reinforced concrete interior beam-column joints." *Transactions of the Japan Concrete Institute*, 22: 433-440.

Valentini, B. and G. Hofstetter (2013). "Review and enhancement of 3D concrete models for large‐scale numerical simulations of concrete structures." *International Journal for Numerical and Analytical Methods in Geomechanics*, 37(3): 221-246.

Vallenas, J. M., V. V. Bertero and E. P. Popov (1979). "Hysteric behavior of reinforced concrete structural walls." *NASA STI/Recon Technical*, Report NO. 80.

Vecchio, F. (2000). "Disturbed stress field model for reinforced concrete: formulation." *Journal of Structural Engineering*, 126(9): 1070-1077.

Vecchio, F. J. and M. P. Collins (1986). "The modified compression-field theory for reinforced concrete elements subjected to shear." *ACI J.*, 83(2): 219-231.

Viwathanatepa, S., E. P. Popov and V. V. Bertero (1979). "Effects of generalized loadings on bond of reinforcing bars embedded in confined concrete blocks." University of California, Earthquake Engineering Research Center.

Willam, K. J. (1975). "Constitutive model for the triaxial behaviour of concrete." *Proc. Intl. Assoc. Bridge Structl. Engrs*, 19: 1-30.

Youssef, M. and A. Ghobarah (2001). "Modelling of RC beam-column joints and structural walls." *Journal of Earthquake Engineering*, 5(01): 93-111.

Zhang, D., H. Noguchi and T. Kashiwazaki (2002). "Two-dimensional finite element analysis on shear performance of RC interior beam-column joints reinforced by a new reinforcing method." *Finite Elements in Civil Engineering Applications: Third DIANA World Conference*, Tokyo, Japan, Taylor and Francis.

Zhao, J. and S. Sritharan (2007). "Modeling of strain penetration effects in fiber-based analysis of reinforced concrete structures." *ACI Structural Journal*, 104(2): 133-141.